REPAIR OF WOODEN UTILITY POLES USING FIBRE-REINFORCED POLYMERS

by

Jonathan Adam Kell

A Thesis
Submitted to the Graduate Studies
In Partial Fulfillment of the Requirements
for the Degree of

MASTER OF SCIENCE

Department of Civil and Geological Engineering
University of Manitoba
Winnipeg, Manitoba
Canada

THE UNIVERSITY OF MANITOBA

FACULTY OF GRADUATE STUDIES

*****

COPYRIGHT PERMISSION

REPAIR OF WOODEN UTILITY POLES USING FIBRE-REINFORCED POLYMERS

BY

JONATHAN ADAM KELL

A Thesis/Practicum submitted to the Faculty of Graduate Studies of The University of Manitoba in partial fulfillment of the requirement of the degree

of

MASTER OF SCIENCE

ABSTRACT

All wood utility poles require an effective maintenance program to ensure safe and reliable service. The end of a wood utility pole's useful life can be attributed to several factors including decay, mechanical damage, weathering and changing design circumstances that require the pole to be modified. Pole life can be extend through an effective preservative treatment and maintenance program, but at some point, all poles will reach a point when they are no longer suitable for their intend use. With the increasing cost of quality wood for use in poles, and the environmental concerns regarding pole disposal and chemical treatment of existing poles, new methods are required to restore and maintain wood poles.

A research program was initiated at the University of Manitoba's Civil Engineering Composites Facility to develop a repair and restoration technique for wooden poles using fibre-reinforced polymers (FRP) to extend their useful life. Twenty-seven 3050-mm poles were tested as cantilevers under static loading. The experimental results showed that the repair techniques developed for restoring wood poles were successful in restoring fully the original installation strength. The program also included the development of finite element models used to predict the behavior of FRP-rehabilitated utility poles. Equations were also developed to assist in the design of the FRP-repair.

TABLE OF CONTENTS

LIST OF TABLES

LIST OF FIGURES

NOTATION

A	= radius of the pole at ground line
A_{dl}	= bond development area required
A_{FRP}	= cross-sectional area of the FRP spline
B	= radius of pole at the level of the applied load
b	= depth of groove
C	= circumference of pole at ground line
d	= distance of centroid of spline from center of pole
d_{ϕ}	= average diameter of pole at repair loaction
h_{load}	= height of applied load above measured from base of stub
I_{FRP}	= moment of inertia of the FRP spline
L	= distance from ground line to point of load
l_{shear}	= length of the shear layer
l_{spline}	= development length of spline
M_{FRP}	= moment capacity of spline
MOE	= modulus of elasticity
MOR	= modulus of rupture, the maximum stress at ground line
M_{pole}	= ultimate bending moment in pole
$P_{applied}$	= applied load
P_{ult}	= ultimate applied load
Q	= applied load effect

R = load resistance

r = radius of pole

S_H = stub height

S_{pole} = section modulus of pole about the axis of bending

S_s = section modulus of spline

t_{jacket} = thickness of FRP jacket

w = width of groove

w_s = total width of spline

y_{cgs} = centroid of FRP spline

δ_L = lateral deflection at the load point at the maximum load

ε_{ult} = ultimate strain in test pole at failure

ϕ = strength capacity factor that limits R to account for variability of the resistance property

γ = load factor applied to Q greater or equal to one that compensates for uncertainty in the definition of loads and assumptions made in the analysis

σ_{FRP} = ultimate strength FRP splines

σ_{ult} = ultimate stress in test pole at failure

τ_{wood} = maximum allowable shear stress in wood

CHAPTER 1

INTRODUCTION

1.1 GENERAL

Economic concerns and environmental constraints are placing ever-increasing demands on wood utility-line structures. For most utilities, the wood pole infrastructure is one of their largest assets (Goodman, *et al*, 1990). Extending service life, while maintaining reliability is being increasingly emphasized as existing pole infrastructure comes to the end of its useful life. Wood utility poles need to be replaced or repaired for numerous reasons, such as rot, fire damage, insufficient height, or premature failure.

It is estimated that there are in excess of 120 million chemically treated-wood utility poles in the United States. The majority of these poles are treated with Pentachlorophenol (penta), as it has been the dominant preservative used for the treatment of utility poles in the last 25 years. Penta is on the Environmental

Protection Agencies (EPA's) list of constituents that could classify a pole treated with penta as hazardous waste. Additionally, poles can also be treated with chromium and arsenic, which can cause a pole to be classified as hazardous waste. Assuming that 3% of the existing poles (3.6 million) are replaced every year, pole removals potentially constitute a significant volume of material that must be either disposed of or recycled (American Wood Preservers Institute, 2001).

Some areas in the United States classify chemically treated poles as solid waste, and do not allow them to be disposed in municipal landfills. However, the high cost and unnecessary disposal of a limited resource makes this option generally inappropriate. In examining the disposal of penta-treated utility poles alone, the Electric Power Research Institute has estimated that "by avoiding the hazardous waste designation, the utility industry would have saved $15 billion between 1989 and 1993." When expanded to all treated wood, the savings could exceed several billions of dollars each year (American Wood Preservers Institute, 2001).

Manitoba Hydro reports that wood distribution poles currently cost between $350, for the familiar backyard poles, to $3000 for the most common 23-metre-tall transmission line poles. There are more than 600,000 power distribution poles in Manitoba Hydros transmission and distribution system (Manitoba Hydro, 2001). If 3% of these poles need to be replaced annually, the cost could approach $5.4

million per annum. This does not include the cost of installation and removal of the old poles.

Due to the high costs associated with pole replacement, and the environmental concerns, pole restoration systems must offer effective and economical alternatives to replacement.

In recent years, there has been considerable research into the use of fibre-reinforced polymers (FRP) for the strengthening and repair of structures. The main advantages of FRP's are their high strength-to-weight ratio, their corrosion resistance and their design flexibility. Fibre reinforced polymers have been used successfully in restoring both concrete and wood structures at a fraction of the cost of replacement. Due to the lack of feasible solutions for repairing, strengthening and extending the height of wood utility poles, a research program was undertaken at the University of Manitoba, with the support of Manitoba Hydro and ISIS-Canada.

1.2 OBJECTIVES

The main objective of this research project was to develop a rehabilitation strategy using FRP materials to repair, strengthen and increase the height of wooden utility poles. The research focused on developing fabrication processes, installation techniques, and design methodologies for rehabilitating wooden poles. It involved both experimental and analytical work and a number of

parameters which affect the behavior of repaired poles were examined. A new and innovative technique developed as an alternative to pole replacement was developed in this research project. The basis of the proposed technique involved the replacement of a section of the existing pole with a wooden stub. This wooden stub could be used to increase the height of the pole or to replace a broken or damaged section of the pole. The stub was connected to the existing pole through a set of FRP splines placed in grooves machined on the surface pole. These splines were designed to resist the full bending moment capacity of the pole at its original installation capacity. The splines were confined using an FRP jacket, which provided additional strength and stability to the wooden pole. The proposed repair technique is shown in Figure 1.1. Further details related to the design and the manufacturing process of the repair system are given in subsequent sections.

The goal of the rehabilitation project was to develop the necessary materials and procedures needed to implement this system in the field. The repair system was designed to be durable, capable of maintaining or improving the desired strength class of a pole, allow for a live line repair, be relatively simple and be environmentally friendly. Most importantly, the repair had to be achieved at a cost, which was competitive with existing repair methods and was an attractive alternative to pole replacement.

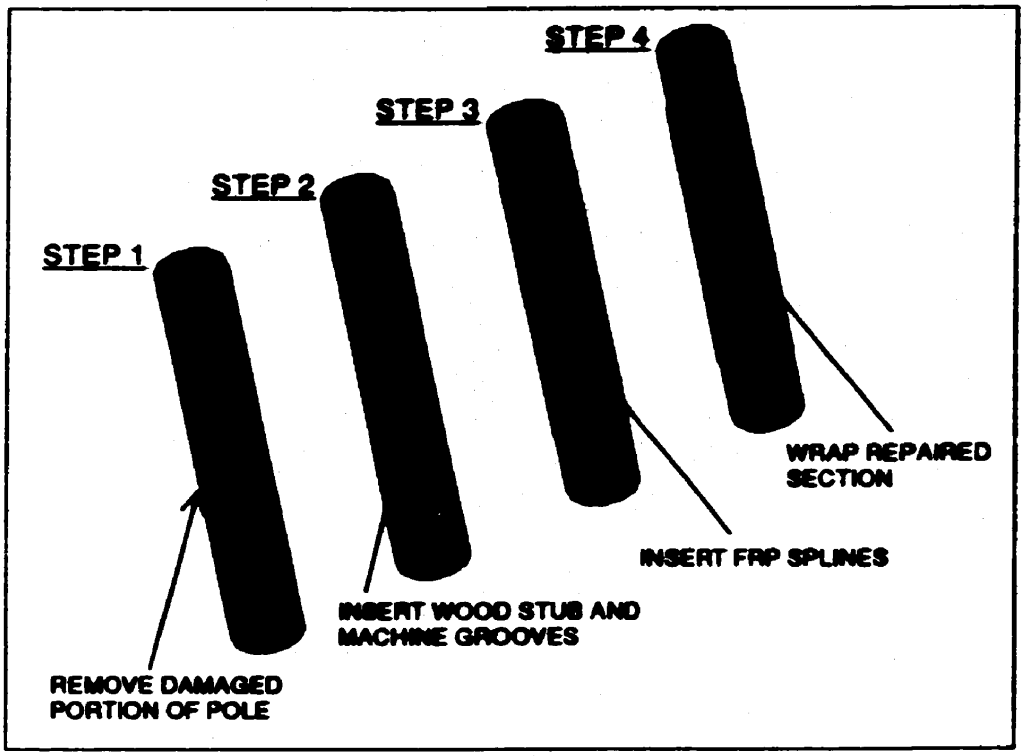

Figure 1.1 - Proposed repair method.

Twenty-seven scaled 3050-mm wooden poles were tested according to ASTM D-1036-99, Standard Test Methods of Static Tests of Wood Poles. The average diameter at ground line was 154-mm and the average diameter at the top of the pole was 135-mm. Seven poles served as control specimens, thirteen poles were cut halfway through their cross-section at a point 610-mm above the ground line and seven of these specimens were reinforced over the cut with varying lengths of FRP splines. The remaining six poles were reinforced with FRP splines and a FRP confinement jacket. The other seven poles were cut into three pieces, with the first cut 610-mm above ground line. The three pieces were then restored using the proposed FRP system. The decision to cut the poles at this level was based on the limitations provided by the repair equipment. In

practice, these limitations would be overcome by designing more flexible repair techniques and equipment. The poles were all fabricated and tested by ISIS Canada at the McQuade Structural Laboratory at the University of Manitoba.

1.3 SCOPE

The introduction to the project and the scope of the research program are given in Chapter 1. A brief description of the project is given, and reasons why this project was initiated are discussed.

The current wood pole design specifications and standards are described in Chapter 2. The challenges facing utility companies with regard to their wood pole inventory are also explored in this chapter, as are the types, characteristics, and properties of the FRP's and their constituents, as well as relevant manufacturing processes. The background of FRP used for structural rehabilitation is given, with particular emphasis on wood rehabilitation.

Details of the manufacturing steps taken to produce the FRP molds needed to complete this project are described in Chapter 3. A description of the fabrication of the test specimens and the testing procedures are also given here. This chapter concludes with a description of the material characterization tests preformed on the FRP.

The results of the experimental program are given in Chapter 4. A detailed description of the structural performance of the tested poles is given and the results are evaluated through comparison with current CSA standards.

The development of finite element models used to analyze repaired wooden poles, as well as new wood poles are described in Chapter 5. Emphasis is placed on comparing the analytical results with the experimental results. Simplified design equations are given in this Chapter.

A summary of the research findings is given in Chapter 6 along with a number of conclusions and recommendations for further work.

1.4 ACKNOWLEDGEMENTS

The author wishes to acknowledge the contibutions of the following individuals and groups without whom this project would not have been a success.

- Dr. Dimos Polyzois, supervisor of the research project, for his support, guidance and the opportunity to work on an exciting and challenging research topics;
- Mr. Vladymir Burachynsky, Ph.D candidate, and owner of Cormorant Advance Composites for his help and support during the design and manufacturing of the equipment and tools used in this project;
- Mr. Dino Philopulos, undergraduate research assistant, for his dedicated help and patience over the course of this project;

- Mr. Moray Mcvey, Mr. Scott Sparrow, Mr. Grant Whiteside and fellow graduate students for their cooperation and assistance during testing;
- Mr. Frank Roberts for his support and encouragement;
- Manitoba Hydro and ISIS-Canada for their financial contribution to the project;
- My wife, Lindsay, for her tremendous support, encouragement and understanding.

CHAPTER 2

BACKGROUD

2.1 POLE DESIGN SPECIFICATIONS AND STANDARDS

The load carrying capacity of a wooden pole structure depends on several factors. These factors include the loading condition, the type and condition of the timber, and the geometric properties. Since the properties of wood are by nature, very inconsistent, national standards and design guidelines have been developed to account for any uncertainties in wood pole design. A brief review of relevant design specifications is given below.

2.1.1 Canadian Standards Association

The Canadian Standards Association (CSA) publishes Standard CAN/CSA-015-090, for "Wood Utility Poles and Reinforcing Stubs". This standard covers material, manufacturing, class dimensional requirements for seasoned wood poles and reinforcing stubs that are primarily intended for the support of either

electrical power or communication lines (CSA, 1990). It classifies poles according to species, length, and minimum circumferential measurements at the top of the pole and 1830-mm from the butt. The minimum circumferences specified in this standard for each species in a given strength class were calculated by the CSA in order to develop ground line stresses approximately equal to the maximum stresses in a given species of wood pole. The classification stresses were determined using a database of tests conducted on wood poles at various locations. In making the calculation, the CSA assumed that pole is used as a simple cantilever and that the maximum stress in the pole would occur at the ground line. The minimum required circumference at the ground line was then calculated using these stresses. This value was then used to calculate the required circumference 1800-mm from the butt of the pole. This circumference must be used in order to ensure that each species in a given class does not exceed the maximum ground line stresses. The assumption that the maximum fibre stress in the pole occurs at the ground line is, theoretically, correct, provided the circumference at ground line is not more than one and a half times the circumference at the point of loading (CSA, 1990).

In the present research project, 3050-mm, air-dried jack-pine poles were used. The classification stress for jack-pine is given by CSA as 44 MPa. However, the CSA Standard classifies only poles that have a minimum height of 6100-mm. In order to determine the class the 3050-mm poles tested, the CSA classification table for jack-pine poles was extrapolated to include 3050-mm long poles. The

information obtained through this extrapolation is shown in Figure 2.1. Additionally, the CSA Standard specifies a minimum top circumference for wooden poles. These minimum circumferences remain constant for individual pole classes, regardless of pole height. These minimum circumferences, with their corresponding class are listed in Table 2.1. The unfactored maximum transverse loads for the various classes are listed in Table 2.2.

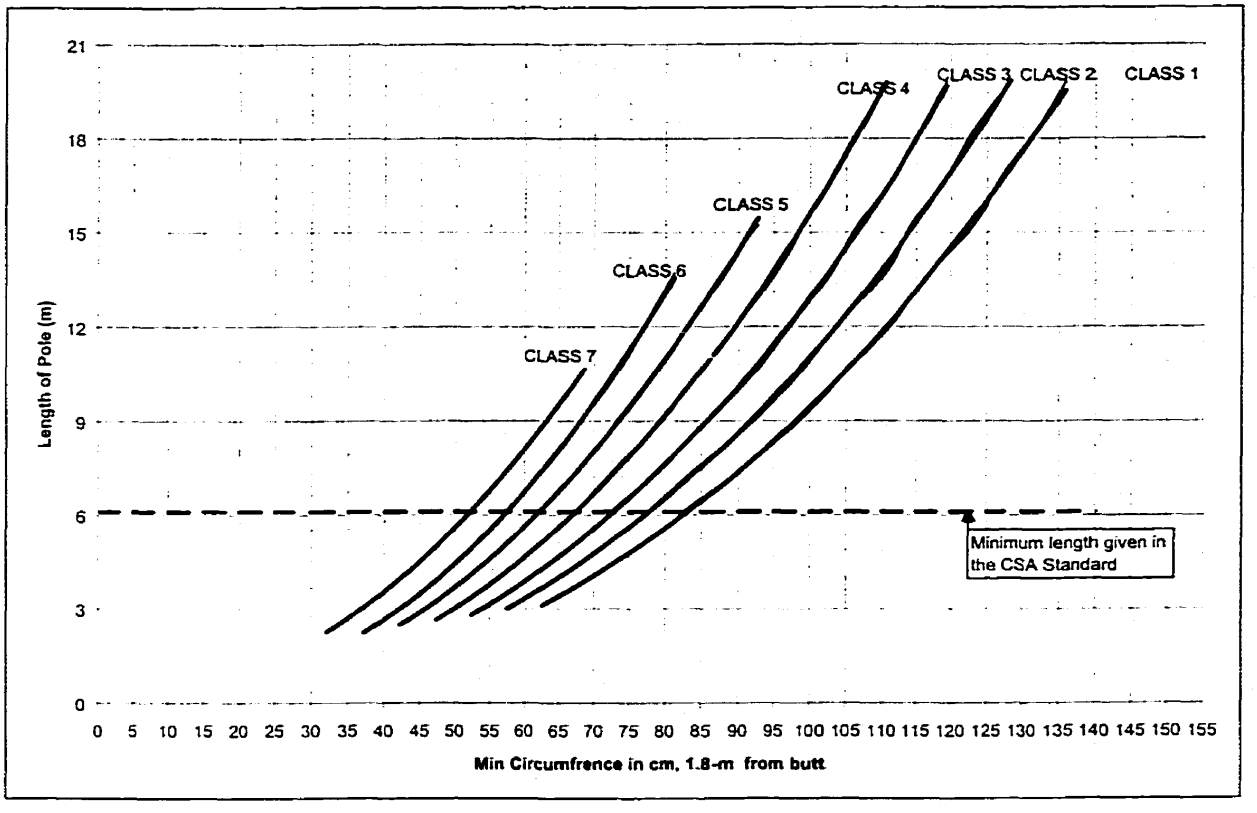

Figure 2.1 – Wooden Pole Classification (values extrapolated from CSA-015-090).

Table 2.1 – Minimum circumferences at top of pole.

Class	1	2	3	4	5	6	7
Minimum circumference at top, cm	69	64	58	53	48	43	38

Table 2.2 – Transverse load capacity of wooden poles according to CAN/CSA 015-090.

Class	Ultimate Horizontal Load (N)
H6	50700
H5	44500
H4	38700
H3	33400
H2	28500
H1	24000
1	20000
2	16500
3	13300
4	10700
5	8500
6	6700
7	5300

2.1.2 American National Standards Institute

The American National Standards Institute (ANSI) has a published standard for wood poles, ANSI 0.5.1-1992. This standard is essentially the same as the CSA standard. Pole classes in this standard are defined such that poles of various species will have approximately equal load carrying capacities. The main difference between the ANSI and CSA Standard as far as the scope of this research project is concerned, is that the classification stress for jack-pine poles according to the ANSI Standard is higher than that given in the CSA Standard. The ANSI Standard gives the classification stress for jack-pine poles as 45.5 MPa while the CSA Standards gives a slightly lower classification stress for jack-pine poles of 44 MPa. The ANSI Standard also includes transverse loads for two additional classes; a class 9 pole, with an ultimate load of 3300 N, and a class 10

pole, with an ultimate load of 1600 N. Additionally, this Standard provides reduction factors for height effects and manufacturing processes, such as the type of drying (kiln versus air-dried).

2.1.3 Institute of Electrical and Electronics Engineers

2.1.3.1 Trial-Use Design Guide for Wood Transmission Structures

The Institute of Electrical and Electronics Engineers (IEEE) addresses wooded poles in a guide titled "Trial-Use Design Guide for Wood Transmission Structures". The purpose of this design guide is to provide the design engineer with proven methods for the design of wood structures for overhead electric transmission lines. The design guidelines were developed using the recommended design strengths published in the ANSI Standards. The main objective of the IEEE design guide is to provide a structure with resistance greater than the maximum load expected during the design lifetime of a pole, with the desired level of safety and reliability and within acceptable economic parameters (IEEE, 1991). The design is thus a reliability-based design, and requires that;

$$\phi R \geq \gamma Q \qquad \textit{Equation 2.1}$$

where, R and Q are the nominal values of the resistance and the load effect, respectively, and ϕ and γ are the strength and overload factors, respectively. The overload factors are specified in the National Electrical Safety Code (IEEE, 1997), and are discussed in the next section. For a wood pole designed for

bending, R is the modulus of rupture (MOR) at the ground line given in the ANSI and CSA standards, and Q is the calculated bending stress at the ground line for a given load.

2.1.3.2 National Electrical Safety Code (NESC)

The Institute of Electrical and Electronics Engineers published the 1997 version of the NESC to safeguard persons during the installation, operation, or maintenance of electrical supply and communication lines and associated equipment (IEEE,1997). In the case of unguyed, single pole structures, this is accomplished through using strength and overload factors. These factors are specified according to the grade of construction that differentiates between the relative degree of strength and expected performance. The NESC gives overload and strength factors for construction grades B and C, with grade B representing the most conservative requirements. The NESC strength factors for wooden poles are 0.65 and 0.85 for grade B and C, respectively. The overload factors for wood poles under transverse loading is given by NESC as 4.00 when installed, and 2.67 at replacement, for Grade B construction. For Grade C construction these values are 2.67 when installed and 1.33 at replacement. Therefore, when the pole strength deteriorates below the level of 2.67 times the loads for Construction Grade B, the structure must be replaced or rehabilitated. When a pole structure is replaced, it shall meet the "when installed" overload factors at replacement. If a pole is rehabilitated, these poles do not have to meet the "at installation" capacities. They are only required to produce a factored

resistance between 2.67 and 4.00 times the service load for Construction Grade B (NESC 1997).

2.1.4 American Society for Testing and Materials

The purpose of the American Society for Testing and Materials (ASTM) Standard, D 1036-99, "Standard Test Methods of Static Tests of Wood Poles", is to cover testing methods in sufficient detail so that the results from tests conducted at different research facilities and in accordance with these test methods are comparable (ASTM, 1999). The standard, however, notes that other test methods can be used, if they are better adapted to a particular investigation. The test methods outlined in the ASTM Standard require the pole to be fixed from the butt to the ground line and the pole be tested in a horizontal position with the load applied near the tip by means of a pulling line. The ASTM Standard specifies the following calculations for determination of the maximum stress at the ground line (the modulus of rupture) and the modulus of elasticity as;

$$MOR = \frac{32\pi^2 P_{ult}(L - \delta_L)}{C^3} \qquad \textit{Equation 2.2}$$

where:

MOR = Modulus of Rupture, the maximum stress at ground line;

P_{ult} = load at failure;

L = distance from ground line to point of load;

δ_L = horizontal deflection of the load point at the maximum load; and,

C = circumference at ground line.

$$MOE = \frac{4L^3P}{3\pi\delta_L A^3 B} \qquad \textit{Equation 2.3}$$

where:

MOE = modulus of elasticity;

$P_{applied}$ = applied load;

A = radius of the pole at ground line; and,

B = radius of pole at point where load is applied.

2.2 INFRASTRUCTURE CHALLENGES

Economic concerns and environmental constraints place ever-increasing demands on wood utility line structures. Extending service life, while maintaining reliability is being increasingly emphasized (Goodman *et al.*, 1990). The average life expectancy for a wood pole varies, depending on location, from 30 to 40 years (Bingell *et al.*, 1995). This useful life of a pole may be shortened due to several factors. One of the most common problems associated with wood utility poles is decay of the wood. New poles receive a preservative treatment to help prevent decay. As a pole ages, the original treatment may become ineffective, and the pole will begin to decay. Decay most often occurs within a region extending about 460-mm above and 460-mm below the ground line. Once decay begins, it is likely to continue until the pole strength is reduced below code requirements (Bingell *et al.*, 1995).

The level at which a pole is expected to perform may change with time and eventually a pole must be replaced if its load carrying capacity falls below acceptable limits. Additionally, as more line clearance is needed to accommodate urban development and as higher voltage requirements are needed, poles often have to be replaced with taller ones. An increase in line-to-ground clearance allows a thermal capacity increase on existing lines or provides space for construction of an additional circuit.

Typically pole replacement is neither easy nor economical. Poles treated with preservatives, creosote and pentachlorophenal, by far the majority, are considered hazardous waste in some states in the United States. This implies some landfills will not accept them, thus other more costly disposal methods must be employed. Depending on the complexity of the system, the replacement price tag for just one pole could be as much as US$10,000 (SPI Composites Institute, 1995). A survey conducted in 1986 by the Electric Power Research Institute (EPRI) produced a figure of US$810, on average, to replace a distribution pole, and US$1,690 per transmission pole (Hayes, 1986). These values are much higher now considering inflation. Present worth analysis indicates that pole restoration is economically justifiable since restoration costs can, generally, be recovered within 5-7 years (EDM,1995).

In recent years, utilities have become more innovative in their approach to pole rehabilitation. The use of FRP materials for wood restoration has been

investigated and found to yield promising results. FRP materials are lightweight, provide a high strength and do not readily corrode. As an innovative alternative, pole owners are taking a hard look at using composite materials to rehabilitate damaged poles for a fraction of the cost of replacement.

2.3 FRP MATERIALS

Fiber reinforced polymers belong in the broad family of composites. The term composite is derived from the Latin compositus, coming from the root word componere, to bring together: com – together + ponere – to put (to put together) (Funk & Wagnalls, 1989). This general definition implies that any material composed of two or more distinct components can be considered a composite, and, in fact, this definition can include both natural and synthetic composites.

Wood is an example of a natural composite material. Wood is a combination of cellulose (a natural fibre) and lignin (a natural polymer). The cellulose fiber provides strength and the lignin is the "glue" that bonds and stabilizes the fiber (Lacovara, 2000). Examples of synthetic composites are: steel reinforced concrete and steel belted radial tires.

This broad definition is too general to describe the form of composites FRP materials come under. In this thesis, FRP's and composites were placed under the definition of "advanced composites". This definition implies that FRP

materials are engineering materials that consist of a polymer–based resin and fibre reinforcement.

2.3.1 Fibres

The physical properties of composites are fibre dominant. When the resin and fibre are combined, their performance depends mostly on the properties of the fibres. For this reason, fibre selection is critical when designing composite structures. In general, the composite designer has a choice of three types of reinforcing materials. These are: glass fibre, carbon fibre and aramid fibre. In this thesis, aramid and carbon fibre will be discussed briefly. Of the three reinforcing options, aramid exhibits the lowest density, highest specific tensile strength and superior toughness. It is priced between glass and carbon. Unfortunately, aramid has a low service temperature, poor compressive properties and is difficult to cut and machine.

Carbon fibre reinforcement is a modern reinforcement characterized by extremely low weight, high tensile strength and high stiffness. The material handles and molds easily. However, some advanced techniques are necessary to achieve the maximum performance of this material. Carbon fibre reinforcement is also the most expensive of the reinforcing fibres. This fact often limits its use to parts needing selective reinforcement or high stiffness with extremely low weight.

2.3.1.1 Glass Fibres

Based on an alumina-lime-borosilicate composition, E-glass produced fibres are considered the predominant reinforcement for polymer matrix composites due to their high electrical insulating properties, low susceptibility to moisture and high mechanical properties.

Glass fibres are amorphous, isotropic and are a long, 3D network of silicon, oxygen and other atoms arranged in a random fashion (Schwartz, 1997). The manufacturing process begins when various ingredients are dry-mixed and melted in a refractory furnace at 1370^{0}C. The molten glass is extruded through a number of orifices and drawn into filaments. A protective coating (called a "size") is then applied on individual filaments before they are gathered together into a strand and wound on a drum. The size is a mixture of lubricants, anti-static agents and a binder. The binder packs the filaments together into a strand.

The basic commercial form of continuous glass fibres is a strand. A roving is a group of untwisted parallel strands wound in a cylindrical forming package. Rovings are used in continuous molding operations such as filament winding and pultrusion, or in some cases as unidirectional reinforcement. Roving is often woven into mats. These mats come in various forms, widths and thickness. Figure 2.2(a) shows roving and Figure 2.2 (c) shows a bi-directional mat.

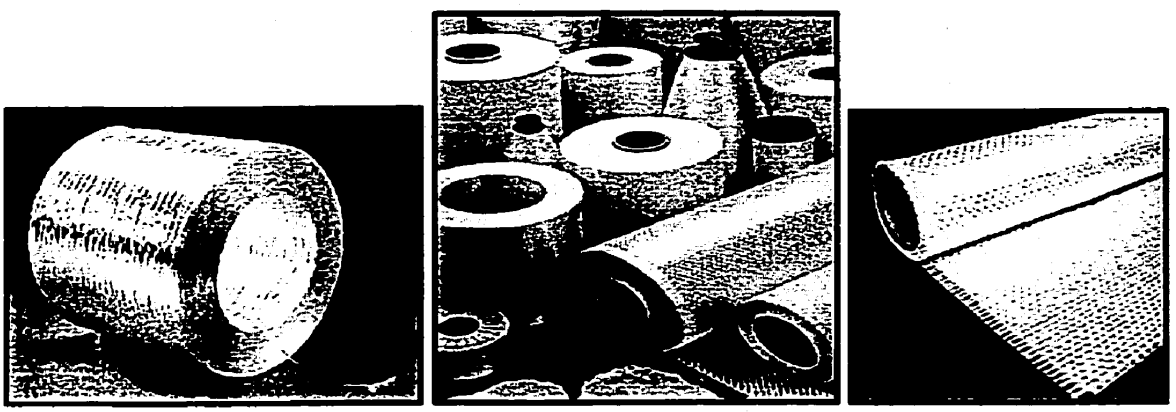

(a) roving *(b) various form of fibre* *(c) matting*

Figure 2.2 - Commercial forms of glass fibre (Owens Corning, 2001)

The physical properties of glass fibres are essentially standard across the industry and can be divided into two broad categories: E-Glass and S-Glass. E-Glass fibres have the lowest cost of all commercially available fibres, which explains their widespread use. S-Glass fibres were originally developed for aerospace applications. They have the highest tensile strength among all fibres in use, but are very cost prohibitive. Typical fibre properties are listed in Table 2.3, along with the properties of steel.

Material	Tensile Modulus, E (Gpa)	Tensile Strength, σ_u (Gpa)	Density, ρ (g/cm^3)	Specific Modulus (E/ρ)	Specific Strength (σ_u/ρ)
E-Glass	72.4	3.5[a]	2.54	28.5	1.38
S-Glass	85.5	4.6[a]	2.48	34.5	1.85
Carbon (high Modulus)	390	2.1	1.9	205	1.1
Carbon (high strength)	240	2.5	1.9	126	1.3
Aramid	130	2.8	1.5	87	1.87
Steel	210	.35	7.8	26.9	.043

[a] *Virgin strength values. Actual Strength after processing much less.*

Table 2.3 Mechanical properties of various reinforcing materials (Agarwal, B.D, et. al., 1980).

2.3.2 Matrix Materials

The primary functions of the resin are to transfer stress between the reinforcing fibers, to act as glue to hold the fibers together, and to protect the fibers from mechanical and environmental damage. Resins are divided into two major groups known as thermoset and thermoplastic. Thermoplastic resins become soft when heated, and may be shaped or molded while in a heated semi-fluid state and become rigid when cooled. Thermoset resins, are usually liquids or low melting point solids in their initial form. When used to produce finished goods, these thermosetting resins are "cured" by the use of a catalyst, heat or a combination of the two. Catalysts are used to polymerize the resin at room temperature. The heat created by this chemical reaction is called the exotherm, and is the heat, which cures the resin. Once cured, solid thermoset resins cannot be converted back to their original liquid form. Unlike thermoplastic resins, cured thermosets will not melt and flow but will soften when heated (and lose hardness) and once formed they cannot be reshaped. The most common thermosetting resins used in the composites industry are polyesters, epoxies, and vinyl esters.

2.3.2.1 Epoxies

Epoxies are named for the epoxide reactive group in which an oxygen atom is joined to each of two carbon atoms already united in some other way. Epoxies are used widely as structural adhesives. The advantages of epoxies are: high strength and modulus, low levels of volatiles, excellent adhesion, low shrinkage,

good chemical resistance and ease of processing (Department of Defense, 1997). All of these qualities make epoxies highly desirable in composite fabrication. The disadvantages of epoxies are their brittleness and their high costs. The processing and curing time of epoxies is also longer than most commercially available resins.

2.3.2.2 Polyesters

Polyester resins are relatively inexpensive and fast processing resins and are used generally for low-cost applications. The curing mechanism for polyesters is relatively straightforward, and small errors in the amount of catalyst will only affect the length of time the system needs to develop full strength. These resins are not suitable in applications where high strength and low weight are desired. They do not develop the high shear-strength levels available from epoxies, and behave poorly as a structural adhesive.

2.3.2.3 Vinyl Esters

Vinyl esters combine the excellent mechanical properties of epoxies with the simple processing characteristics of polyesters. Priced between the epoxies and polyesters, vinyl esters exhibit excellent chemical resistance but have poor characteristics as structural adhesives. Additionally, these resins are very toxic, and need to be handled with caution.

2.3.3 Other Constituents

Other materials relevant to the work presented here are: fillers and graphite powder. Fillers are used to take up volume in the composite and to increase the viscosity of the resin. Common fillers include colloidal silica calcium carbonate, clay, and mica. Unfortunately, fillers tend to reduce the physical properties of the resin, and should be used with caution.

Graphite powder is used in the mold making process to give the tool surface a harder surface and to give the tool a different colour (black) than the part to ensure that the part is properly fabricated. The black color is important when wetting out glass against the mold surface because air bubbles and dry places in the glass are white while the properly wet-out glass is transparent showing the black surface. The high contrast makes it easier to produce high quality parts free of voids. Additionally, the graphite helps with the release of the part from the mold, as an extremely smooth surface can be obtained with this type of tooling surface.

2.4 COMPOSITE MANUFACTURING

2.4.1 Hand Lay-Up

Hand lay-up is, typically, one of the simplest FRP processing techniques. It is descriptive of several procedures used to form a composite shape. There is virtually no limit in the size of the part that can be made. With this method, the molds can be made of wood, sheet metal, plaster, and FRP composites. The

reinforcement, usually a woven mat, is first impregnated with resin and then placed into the mold. Brushes and spreaders are used to remove entrapped air and to compact it against the mold surface. Often, resin needs to be applied to the tool surface to promote proper wetting of the fabric.

2.4.2 Filament Winding

Filament winding is a process in which continuous roving is drawn through a resin impregnation bath and wound over a mandrel. The reinforcements are orientated in the axis of the loads expected on the finished products. Two examples of filament winding are shown in Figure 2.3.

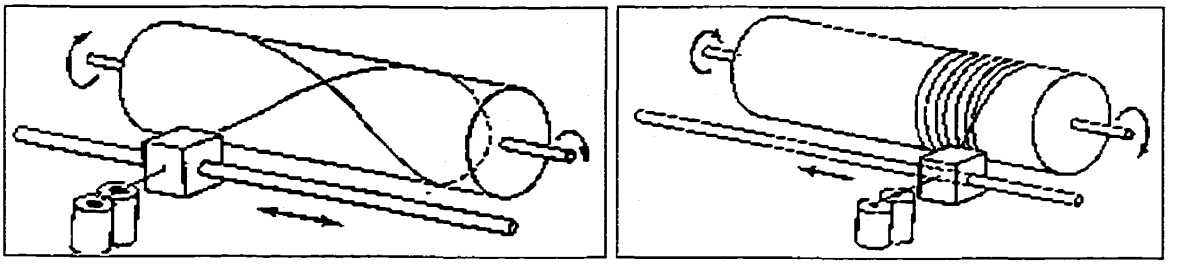

(a) (b)

Figure 2.3 – Filament winding (Richardson, T., 1987).

Another type of filament winding involves filling a female mandrel with continuous roving. The mold is spun, and the fibres are packed into the mold. Very complex, symmetric shapes can be produced in this manner, as the wet bundles of fibre behave like a liquid, can be packed into small spaces, as shown in Figure 2.4.

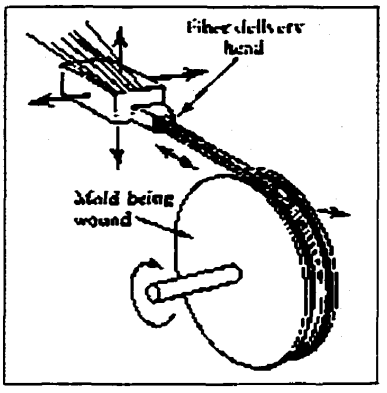

Figure 2.4 – Filament winding in a female mandrel (Richardson, T., 1987).

2.4.3 Mold Making

A significant portion of the present research project was spent on the design and construction of molds. Of all the advantages offered by composite materials, their ability to be molded into complex shapes is, perhaps, the most significant. When a shape need to be reproduced several times, it is most efficient to build a tool or mold within which the part can be fabricated. Once a mold has been perfected, molded parts emerge perfectly shaped every time and require little post-finishing work.

2.4.3.1 Types of Molds

Male and female molds are the only two fundamental types of forms, but they yield significantly different finished parts. The male or positive mold is a form that mimics the final shape of the part, and the part is fabricated over its outer surface. Usually this type of mold is quicker to construct, but each part produced will have a rough outer texture that may require finishing. Also, because the part is being fabricated from the inside, the part will grow during lamination, adding additional complexity to the design. When producing a small quantity of a part,

or if the part is not overly complex, satisfactory parts can be produced using a male mold.

Female or cavity molds are generally more costly, but offer numerous advantages over male molds. Finishing time is significantly reduced because every part emerges with a smooth outer surface as the outside surface of the part typically is directly against the tooling surface.

To make a female mold, the first step is to create a master or plug of the exact shape and surface finish of the final desired part. The plug can be made of virtually anything that can be formed to the desired shape, holding it long enough to make a "splash". The splash is a wet resin surface that is backed up with glass fibres and a full-scale composite structure, so that it becomes the mold after it is cured. Resin selection is important in any mold construction, as it determines the durability of mold.

The most common material used for molds is formulated epoxy systems in which the surface of the tool is made of "surfacing resin". The surfacing resin is placed directly on the plug. The backup structure, made of glass, and saturated with another version of the same resin is applied next. When laying up the splash on the plug, the plug must be properly coated with a mold release so that the tool surface will not be damaged when the splash is removed from the plug. The final step in manufacturing the final tool, is to place the splash onto a backup structure

in the form of a table or flat plate so that it rests flat on the surface on which it will be used (Marshall, 1998).

Molds may be made of wood, wood/FRP, plaster, FRP, or metals. All molds must be properly prepared to prevent the part from sticking to the surface. Metal tooling is used when long production runs are required, and plaster tooling is typically used for prototype creation and short production runs. Wood tooling is used primarily for master patterns, short-run parts, and wet hand lay-up production.

2.5 RELATED RESEARCH

Advanced composite materials were originally used primarily in the aerospace industry where cost was not always an issue. In civil engineering however, price is an issue, as contracts are typically awarded on the basis of cost. With the falling costs of FRP's today, the cost of using FRP to restore structures can be the most cost-effective long-term solution.

There is a large number of papers dealing with the use of FRP to repair and strengthen concrete structures. The focus of the research project was the rehabilitation of wooden poles. The following sections presents a review of related literature and other wooden utility pole restoration techniques.

2.5.1 Wood Strengthening

Worldwide, the source of quality timber to be used as structural lumber is shrinking through over cutting and the introduction of strict environmental regulations. Strengthening techniques for wood can increase the useful service life of existing timber structures, allow low-grade wood to be utilized structurally, and permit a reduction in the size of the cross section of the wood member. In the 1960's and 1970's much attention was focused on strengthening wood using metallic reinforcement. Unfortunately, none of these reinforcement techniques reached full commercialization, as most of them appeared to be very labour-intensive, difficult to apply, and unreliable as far as long-term performance is concerned (Plevris et al, 1992). The availability of low cost FRP materials and the success fibre reinforced polymers had in strengthening concrete structures, made FRP materials an attractive method of reinforcing timber in the last decade. Pelvris and Triantafillou (1992) found that reinforcing wood members with very thin fibre-composite sheets bonded on their tension face was a very promising method of increasing the strength, stiffness, and ductility characteristics of wood structures. The authors concluded that even very small fractions of composite reinforcement resulted in significant improvements in the mechanical behavior of the restored members.

Cheng and Dorey (1996) investigated the potential of glass and carbon fibre reinforcement for glued laminated (glulam) timber beams. In their experimental program, they tested 18 beams, with varying amounts of composite

reinforcement. They recorded an increase in maximum strength of 127% with a fibre to wood area fraction of 8.23%.

Johns and Lacroix (2000) used FRP sheets to reinforce commercial "2x4" lumber. They preformed experiments using matched samples of 25 pairs of beams for three reinforcement strategies. They found that the increase in strength for virtually all the 150 beams tested was greater than that predicted by simple transformed section analysis. They recorded strength increases in the weakest members, which determines the building code strength, of 40% to 100%. They attributed this increase in strength to the local bridging and confining action of composite on the wood.

Gentile (2000) used FRP bars for improving the flexural strength of sawn timber bridge beams. The bars were inserted into cut slits on the tension side of the beam. Fifteen scaled reinforced timber bridge stringers were tested to failure. Additionally, three 40-year-old full-scale reinforced stringers were tested. The test results showed up to 64% increase in the strength of the timber. He concluded that the FRP material in the grooves arrests crack opening, confines local rupture, and bridges local defects in the adjacent timber, allowing the timber to support higher loads.

2.5.2 Traditional Utility Pole Rehabilitation Techniques

One of the most common methods used for restoring the ground line strength of utility poles is the Osmose-C-Truss. With installations in service since the early 1960's, the C-truss has been used to reinforce more poles than any other systems combined (Osmose, 2000). The principle of this system depends on a 3660-mm long steel member, the size of which is determined by the size of the pole being repaired, driven into the ground immediately adjacent to the defective pole. The pole and the steel member are then strapped tightly together using galvanized steel straps. Unfortunately this system is not suitable for all ground types, and the damaged or decayed portion of the pole remains part of the structure.

A similar product offered by Osmose is the Polesplint™. This is a clamp-type steel reinforcer designed to restore adequate strength and prevent further deterioration following localized damage. Similar to the C-Truss system, the Polesplint™ is used to restore the pole above the ground line. The Polesplint™ principle involves strapping steel members to the pole to restore the strength. The splints and bands are constructed from hot dip galvanized AISI 1020 hot rolled steel. Polesplint™ is also utilized as a temporary support for emergency use when poles are damaged.

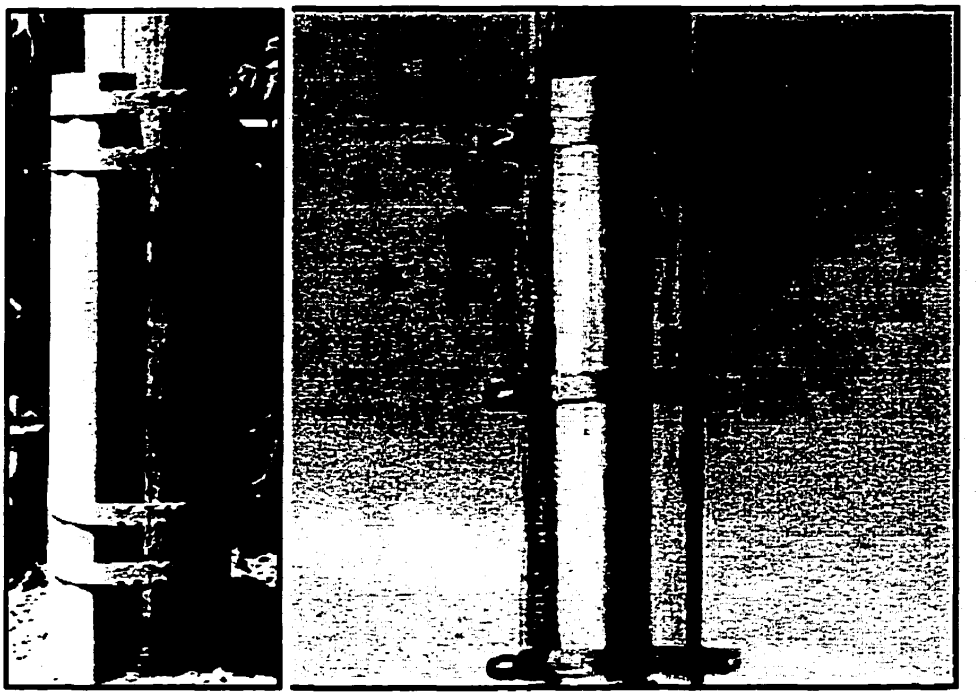

(a) (b)

Figure 2.5 - Osmose-C-Truss (Osmose, 2000).

Laminated Wood Systems, Inc. promotes the Pole Reclassification System which enables utilities to reinforce and reclassify existing poles up to three or more classes. This system is similar to the Osmose-C-Truss, with the main difference being that the pole is strengthened along the entire length. The process involves four steps, as outline in Figure 2.6. First a steel sleeve is driven into the ground next to the pole seen in Figure 2.6(a), and then another sleeve is placed over the bottom unit and rested on the ground seen in Figure 2.6(b). Two high strength galvanized bands are then placed near the bottom to hold the two parts together seen in Figure 2.6(c). Three pairs of cross bolts are driven into the specially tapered upper unit, structurally connecting the units to the pole seen in Figure 2.6(d) (Laminated Wood Systems, 2000).

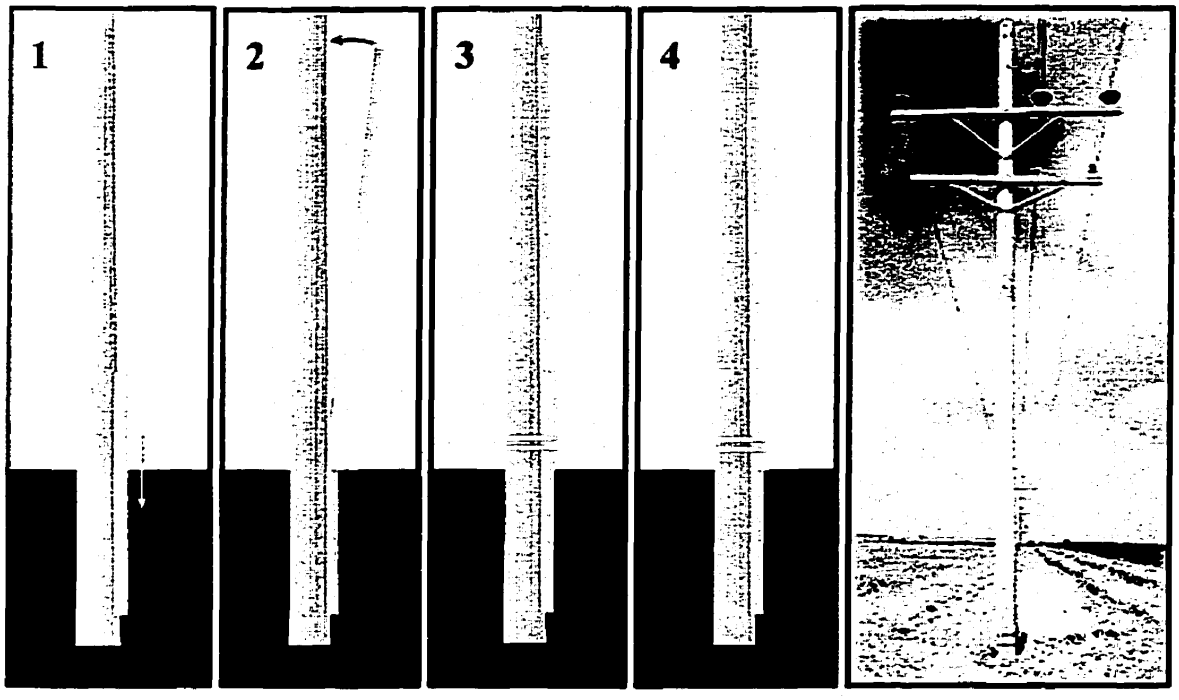

Figure 2.6 - Pole Reclassification System (Laminated Wood Systems, 2000).

Utilitech offers a system called Repol that encapsulates the damaged section of the pole in a layer of high-strength epoxy cement. Earth around the pole is excavated to expose the decayed or damaged portion. Using specialized driving machinery, a split steel casing is fastened around the pole and then screwed into the earth to a depth of 12220-mm. The casing is designed to provide a 51-mm annulus around the pole and to clear the earth from around the pole as the casing is driven to the required depth. After the casing has been installed, the annular space is filled with a pea-gravel and epoxy mix. The mixture sets and bonds to the pole and casing in less than an hour. The resulting rigid structure restores the pole to at least the original strength, and usually much more (Hayes, 1986).

The University of Saskatchewan conducted research in November 1978 to evaluate several designs used to compensate for the limited lengths of jack-pine poles available. Three designs were considered. The first design consisted of joining two jack-pine poles with a steel-connecting device. The second method involved strapping together three or four poles to build up a pole of sufficient height. The final method involved using a concrete base with the wood pole embedded inside (Hosain *et al.,* 1978). Test results showed that the steel jacket was the most favorable of all the designs investigated.

The steel jacket consisted of a steel plate that was rolled into a cylinder with an open overlapping edge. The poles were inserted into each end of the sleeve, and hydraulics was used to create a snug fit. The outside edge was then lapwelded to create a strong tight joint. Two twenty foot poles were spliced and tested as a simply supported beam, subjecting the connection to the same moments and shear forces as produced by cantilever loading. The pole reached an ultimate load of 33 kN, and according to Table 2.2 this pole could be classified as a class H3 pole.

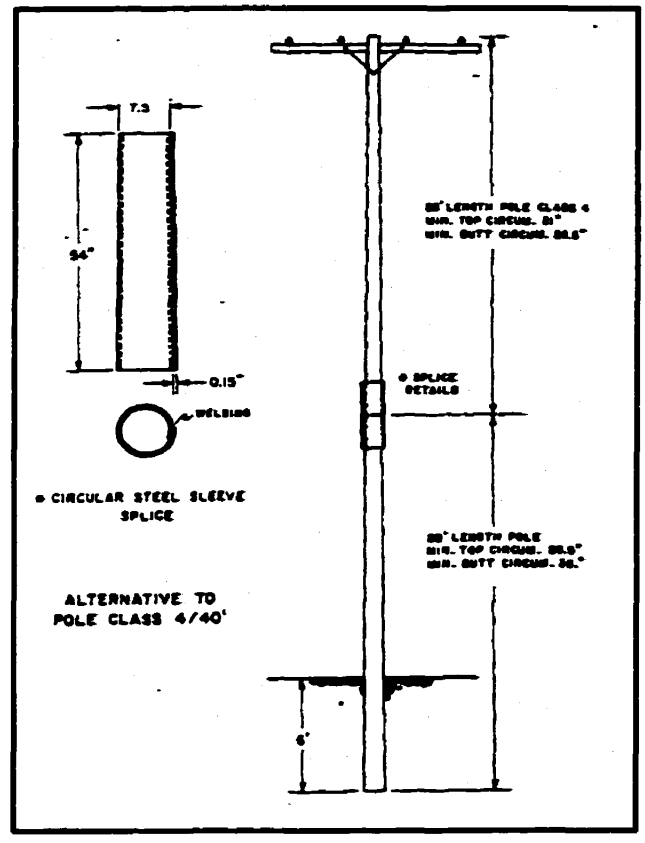

Figure 2.7 – Steel jacketed pole (Hosain et al., *1978).*

Strapped poles, shown in Figure 2.8 is a concept that has been used for several years. The University of Saskatchewan's research showed that this method was susceptible to excessive deflections and premature shear separation. The observed elastic deflection was approximately 50% more than the predicted value for a single pole, and shear separation was observed at a load of only 15% of the ultimate load (Hosain *et al.*, 1978). The strapped pole is shown in Figure 2.8(a) and the test set-up used is shown in Figure 2.8(b).

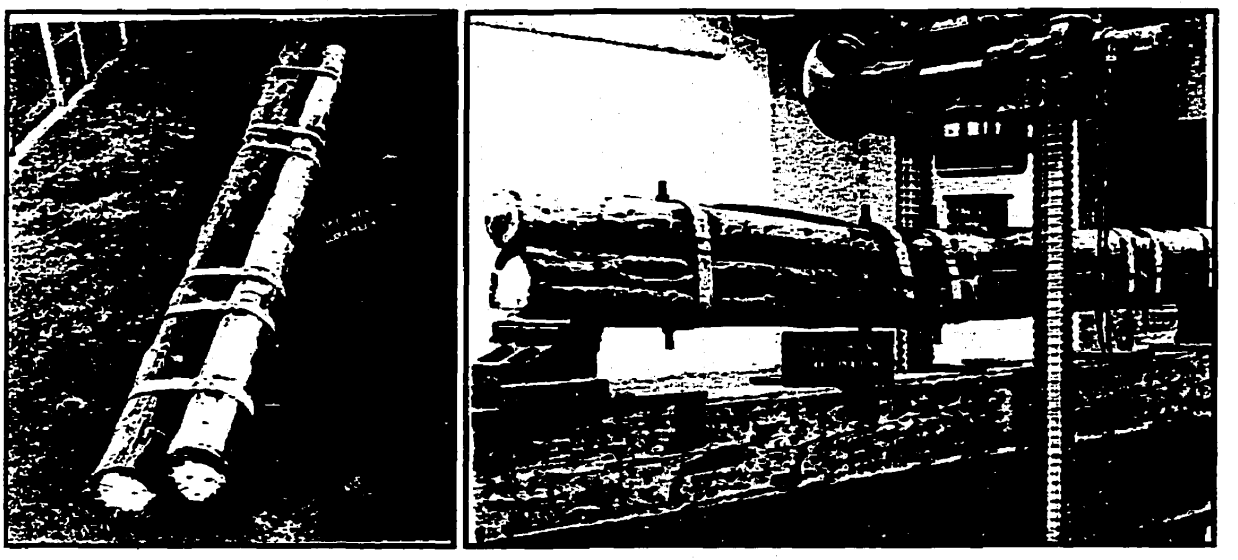

(a) *(b)*

Figure 2.8 – Strapped Poles (Hosain et al., *1978).*

Poles in which the lower half was composed of a pre-cast concrete base was found to be structurally sound. Unfortunately, from a practical standpoint this type of pole is unsuitable due to handling, transportation, and installation problems (Hosain *et al.*, 1978).

The Phaseraiser produced by Laminated Wood Systems, Inc. provides a way to raise existing line structures up to 3660-mm while keeping the line in service. Proprietary tooling is required to install the Phaseraiser, and crews of three people are required. After initial preparation, cross bolts are installed to secure the bottom section of the pole to the steel structure. Once the section is secure, the poles are encased in a steel jacket, and cut through. The pole is then raised either using a crane or specially designed hydraulic cylinders. Once the pole is lifted to the desired height, the top section of the pole is fastened to the jacket.

Phaseraiser is available in two systems, one in which the Phaseraiser steel members are driven into the ground, and the pole is cut 760-mm above the ground. The other system the steel members are set level on top of the soil, not driven into the ground, and the pole is cut at 1980-mm above the ground (Laminated Wood Systems, 2000).

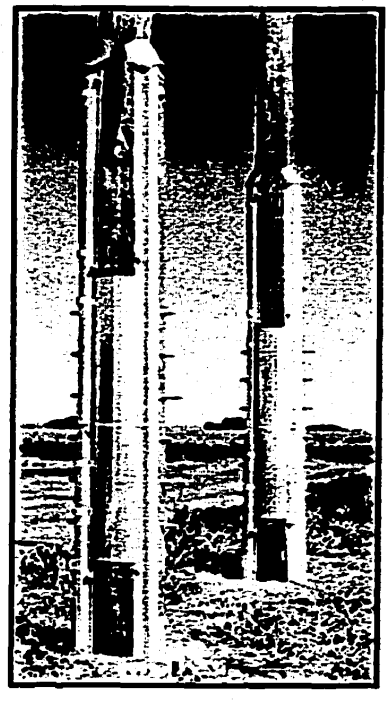

Figure 2.9 – Phaseraiser (Laminated Wood Systems, 2000).

2.5.3 FRP Utility Pole Rehabilitation Techniques

The concept of using fibre-reinforced plastics to strengthen utility poles is not new. In the early 1970's the University of Kentucky laminated poles with reinforced plastics over their entire length, and full-scale dynamic and static tests were preformed. The wood species used in their tests included virginia pine, yellow-poplar, and scarlet oak, which at the time of testing had little commercial

value as pole timber. Ten poles of each type measuring 10058-mm in length, with a 203.2-mm butt diameter were wrapped with a total of six layers of FRP, three axial, and three helical. The poles were then loaded until they reached a deflection of 508-mm at the free end. The test results showed an average of 17% increase in both the dynamic and static bending stiffness. Comparing experimental results to theoretical results, researchers discovered they could not use the elementary bending theory to determine the maximum deflection of the composite beam (Adams *et al.*, 1972).

More recently, several companies have designed composite systems for pole repair. PoleCare Industries have developed FiberTect, as shown in Figure 2.10, a system designed to restore standing utility poles that have been weakened by decay, insect attack or structural damage and allow them to remain in service. After a pole is cleaned and treated to prevent further decay, a fibreglass fabric is wrapped around the pole, in a spiral fashion, starting 900-mm to 1220-mm below the ground up to approximately 900-mm to 1524-mm above the ground. Alternating layers of fabric and phenolic resin are applied to achieve a 10 to 13 mm composite layup. A final pigment layer is applied, and the composite cures on its own in a few hours. PoleCares claims that their system restores poles to their original strength while providing a class A fire rating on the pole wrap and preventing splitting due to seasonal changes in the dimensional structure of the pole (SPI Composites Institute, 1995).

Figure 2.10 – PoleCares Fibertect system (SPI Composites Institute, 1995).

A similar product offered by Fyfe Company LLC. is the Tyfos Fibrwrap System. Figure 2.11 shows a field application of the Tyfos system. To evaluate the structural performance of their system, Fyfe Company contracted Engineering Data Management Inc (EDM) to conduct independent testing of the structural capabilities of the TYFOs Fibrwrap System for restoring wood utility poles. Ten douglas-fir wood poles, 10680-mm to 15250-mm in length, and of varying class size were used in their experiments. The poles were purposely altered by EDM to simulate the effect of severe internal and external damage, see Figure 2.12(a). The poles were coated then wrapped above and below the ground line with vertical and horizontal layers of the Fibrwrap system, a combination of woven fabric made up of fibers of Polyaramide-glass saturated with epoxy, as shown in Figure 2.12(a).

Figure 2.11 – Tyfos Fibrwrap System (Fyfe, 1999).

The poles were then tested according to ASTM D 1036-90 "Standard Methods of Static Tests of Wood Poles", as shown in Figure 2.12(b).

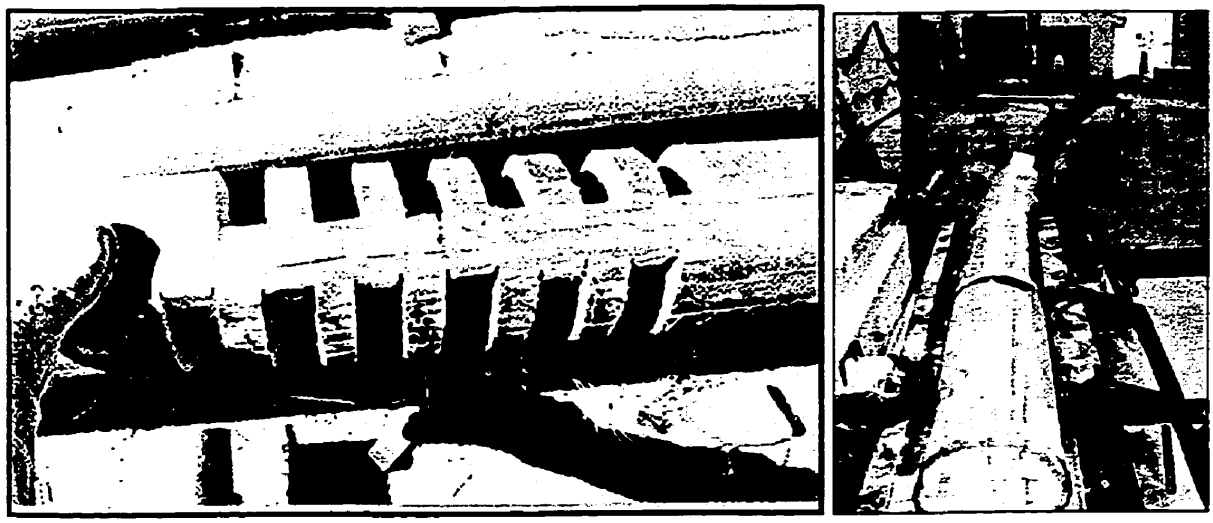

(a) *(b)*

Figure 2.12 – Testing of Tyfos System for wood poles (Fyfe, 1999).

Of the ten poles tested, only one was restored to a point above the original, installation strength. However, as EDM points out and described previously, the National Electrical Safety Code provides an overload capacity factor (OCF) for "new" installations of 4.0 and an OCF for "at replacement" of 2.67. The ratio of these factors, 2.67/4.0 , or 67% of the remaining section modulus has traditionally formed the basis for defining when a wood pole is to be considered non-serviceable. Based on this, nine of the ten poles tested achieved a capacity higher than the "at replacement" capacity (i.e., higher than 67% of the "installation" load capacity). Only one reached a value higher than the "at installation" capacity (EDM, 1995). The summary of the tests conducted on the Tyfos System are shown in Table 2.4.

Table 2.4 – Summary of Tyfos System evaluation (EDM, 1995).

Sample Number	Predicted NESC "At Intallation" Load Capacity (N)	Actual Load (N)	Predicted NESC "At Replacement" Load Capacity (N)	Ratio of Actual to Installation	Ratio of Actual to 67% of Installation Strength
1	15168	14901	10141	.98	1.47
2	9919	11965	6628	1.20	1.81
3	21039	18281	14100	.87	1.30
4	16591	15301	11120	.92	1.35
5	38609	30513	25887	.79	1.18
6	15390	13122	10853	.81	1.21
7	17169	15390	11520	.89	1.34
8	9519	7072	6361	.74	1.11
9	13833	8940	9252	.65	1.00
10	10542	10542	16057	.44	.67

CHAPTER 3

EXPERIMENTAL PROGRAM

3.1 INTRODUCTION

The main objective of the experimental program was to evaluate the performance of FRP rehabilitated poles tested according to the requirements of ANSI/ASTM D1036-99, Standard Methods of Static Tests of Wood Poles. The design of single pole structures is, typically, controlled by their bending capacity; thus, scaled bending tests were performed to evaluate the performance of the proposed restoration system. The rehabilitated poles were expected to resist loads prescribed by CAN/CSA-015-90 specification for Wood Utility Poles and Reinforcing Stubs.

Table 3.1 lists the poles tested in the experimental program along with their corresponding circumferences at ground line, at the top of the pole and 1800-mm above ground line. In total, 27 poles with a height above ground line of 2705-mm were tested in four phases.

Table 3.1 – Geometric properties of tested poles

Specimen	Circumference at Ground line (mm)	Circumference at Top of Pole (mm)	Circumference at 1800-mm above Ground Line (mm)
P1-1	490	405	448
P1-2	484	393	438
P1-3	478	399	438
P1-4	515	424	470
P1-5	509	430	470
P1-6	465	393	429
P1-7	484	430	457
P2-203-1	509	424	467
P2-305-1	484	459	471
P2-305-2	459	418	438
P2-305-3	465	393	429
P2-254-1	522	405	463
P2-406-1	553	440	496
P2-406-2	484	418	451
P3-2-305-1	490	443	467
P3-4-305-1	459	405	432
P3-2-406-1	503	430	467
P3-4-406-2	443	443	443
P3-4-406-3	509	465	487
P3-4-406-4	534	484	509
P4-1	465	399	432
P4-2	471	421	446
P4-3	446	396	421
P4-4	452	380	416
P4-5	462	412	437
P4-6	481	427	454
P4-7	503	456	479

Phase I involved the testing of seven poles to obtain their average ultimate strength, to determine an average value for the modulus of elasticity, and their modulus of rupture. Phase II consisted of testing poles with varying lengths of reinforcement placed over a cut through half the cross-section located 610-mm above the base of the pole. Phase III involved the use of selected reinforcement schemes from Phase II and confining it with bi-directional glass and to develop

the bond between the spline and the pole further. Phase IV involved the testing of seven fully restored scaled poles. FRP coupons were also fabricated and tested in order to determine the material properties of the FRP for use in the theoretical model.

The pole specimens were given an alphanumeric designation. All designations begin with the letter P followed by a number indicating the experimental phase. For example, P1 refers to specimens in Phase I while P3 refers to specimens in Phase III. In Phase I, the poles were designated as P1-z, where z indicates individual test specimens in Phase I. In Phase II, the specimens were designated as P2-y-z, where y indicates the length of the FRP spline in millimeters. For example, P2-305-2 is the second specimen tested in Phase II with a 305-mm long spline. In Phase III, the specimens were designated as P3-w-y-z, where w indicates the number of circumferential layers of the FRP used for the confinement jacket. For example, P3-4-305-2 is the second specimen tested in Phase III with a 305-mm long spline and four layers of circumferential wrap. For the poles tested in the fourth phase, the numbering system is the same as that for the first phase.

3.2 MANUFACTURING THE SPLINES

3.2.1 Design of Splines

The splines were manufactured in two steps. The first step involved building the required molds. The second step required using the molds to fabricate the spline

to be used as reinforcement. The spline molds were designed based on the following requirements of the final product:

a) The moment capacity of a spline had to be, approximately, equivalent to the moment capacity of the poles;

b) The splines had to be designed with flanges so that the FRP reinforcement would anchor in a groove and provide stiffness at the surface of the pole. The radius of the flanges had to match the radius of the poles;

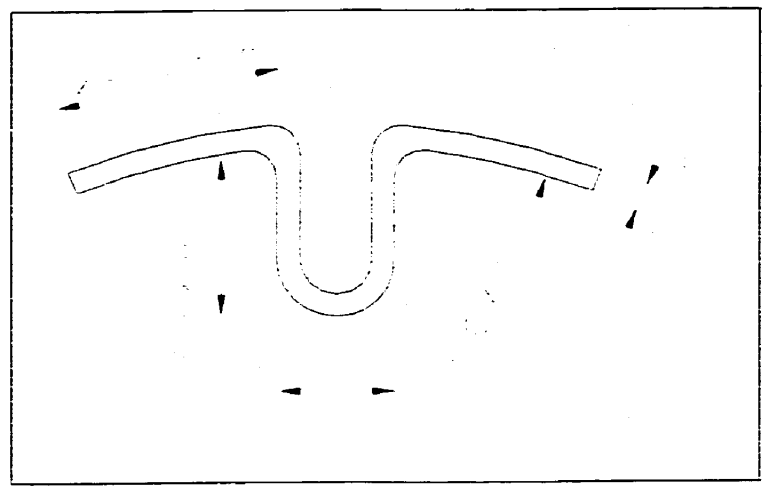

Figure 3.1 – Dimensions of Spline

The basic shape of the spline used in the research program is shown in Figure 3.1. This profile was chosen because of its structural advantages over other shapes, it lends itself to future design changes and its ease of manufacturing. The final dimensions of the splines were determined using the criteria listed above. The calculated moment capacity of the jack-pine poles used in the experimental program is 15.41-kN-m using the maximum fibre stress of 44-MPa given by the CSA (CSA, 1990). The calculated maximum moment capacity of

the spline shown in Figure 3.1 is 14.15-kN-m. The calculations for the moment capacity of both the wood poles and the splines are shown in Appendix A. Although the moment capacity of the spline is lower than the moment capacity of the pole, it was assumed that with the addition of confinement layers and additional splines, the capacity of the FRP system as a whole will be more than adequate to restore the full capacity of the pole.

3.2.1.1 Manufacturing of spline mold

Once the shape of the spline was determined, a mold had to be fabricated to produce the splines. It was decided that four splines would be fabricated at once to save production time. Also, as the flanges of the spline had to match the surface profile of the pole meant that a mold with a curved surface matching the curvature of the surface of the pole had to be fabricated. The manufacturing of the spline mold was done in three main steps: creating a master pattern; making the male plug; making the final mold. The steps are described briefly below.

a) Creating a master pattern.

In order to achieve the 76-mm radius on the flange to match the 76-mm radius of the pole, a female mold had to be fabricated. Using a sheet of baltic-birch wood, a hollow square section (170-mm by 170-mm) was fabricated. This plug was then machined into a round cylinder with a radius of 76-mm. Next, a tooling surface was applied to the machined cylinder. For this, 340-g/m^2 fabric was saturated with a graphite powder/resin mixture and applied to the surface of the

cylinder. After the tooling surface cured, grooves were machined into the cylinder. The grooves were then filled with tooling resin, and allowed to cure. Once the resin cured, the filled grooves were machined again, this time with the final dimensions of the spline. The mold was then polished and waxed. The mold had the final dimensions required to manufacture the FRP splines, and, because it was a female mold, the inside dimensions of the spline would not change, with the inside dimensions being defined as those matching the surface of the pole. Unfortunately, the form of the mold did not lend itself to efficient production, as only one spline could be fabricated at once. Another female mold needed to be made that mimicked the master mold exactly, but with the ability to fabricate four splines at once. In order to do this a "copy" of the mold needed to be made.

b) Making the male plug.

To make the copy of the master mold and translate it to a more workable female mold, another mold was required that could be used to fabricate the final female mold. This mold would use the master mold as its mold and become a male mold. As mentioned in Chapter 2, when a male mold is used and FRP is placed over it the inside dimensions with respect to the spline would increase in size as FRP is added to the mold. For this reason, this mold could not be used to fabricate the final splines. However, the outside dimensions of splines fabricated with the male mold matched perfectly with the inside dimensions of the female mold. Realizing this, another mold was fabricated by placing a tooling surface on

the master mold. Over this tooling surface, a backing structure of 340-g/m^2, 101.6-mm wide tape saturated with tooling resin was applied. Once the male plugs cured and were removed from the master mold, they were arranged and bonded on a flat plate. Figure 3.2 and Figure 3.3 show the master plug with a male mold being removed and Figure 3.4 shows the male molds arranged together to form the final male mold.

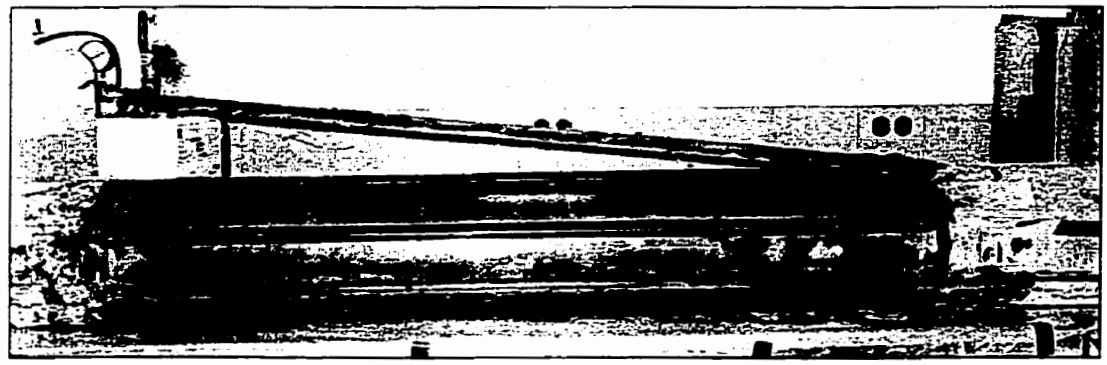

Figure 3.2 – Side view of splash being removed from plug.

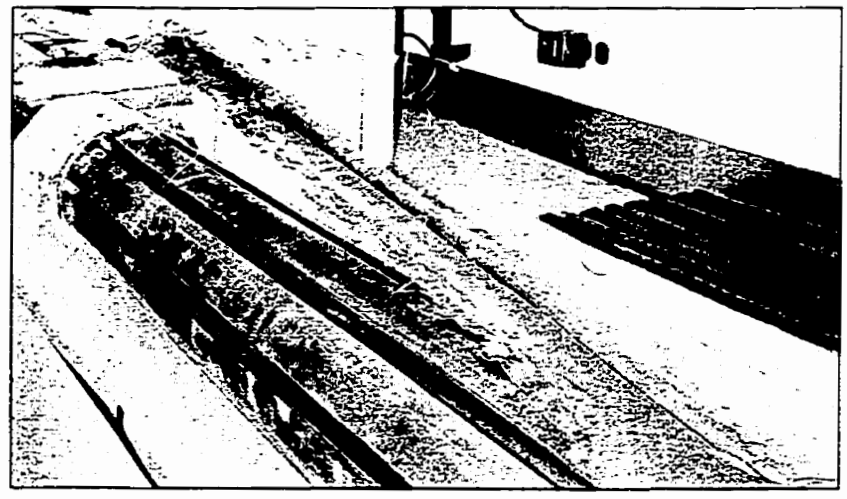

Figure 3.3 – Top view of splash being removed from plug.

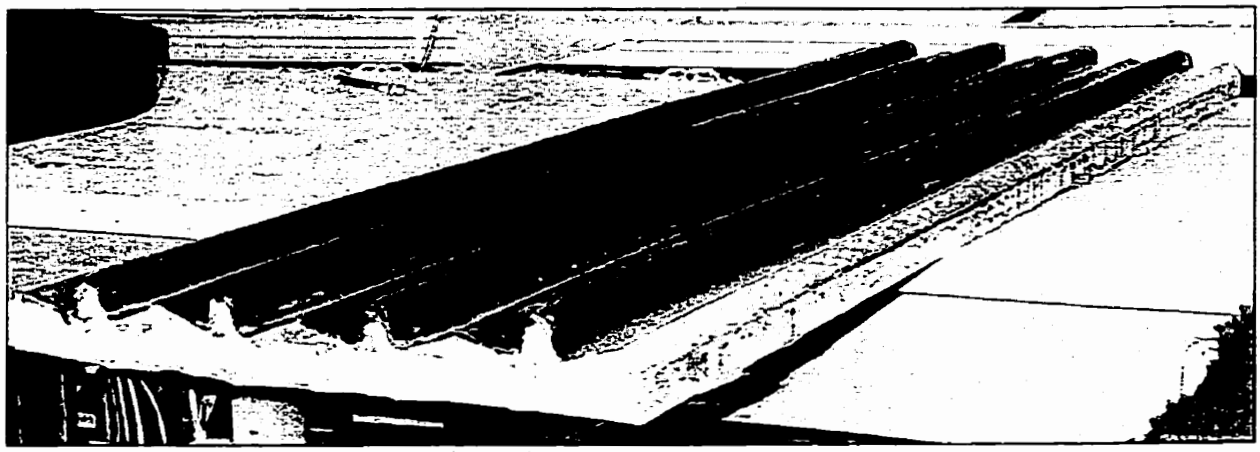

Figure 3.4 – Male mold.

c) Making the final mold.

As mentioned previously, the male molds cannot be used to make the final splines. However, by laying an FRP tooling surface and backing structure over the male mold, the desired female mold was obtained. Figure 3.5(a) shows how the female and male molds fit together, and Figure 3.5(b) shows the female spline mold. Using this mold, parts with the exact inside dimensions could be obtained consistently and allow for additional FRP to be added if needed.

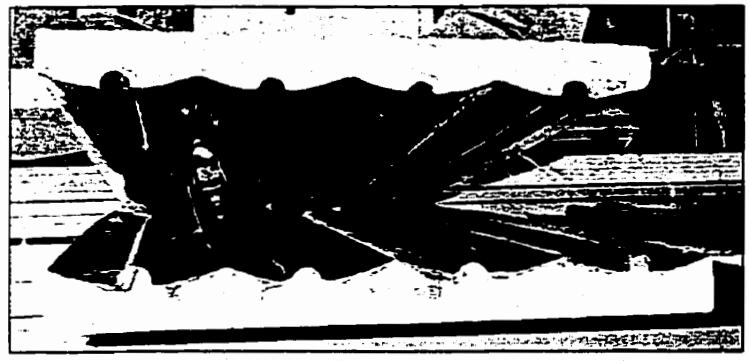

(a) Male and female molds.

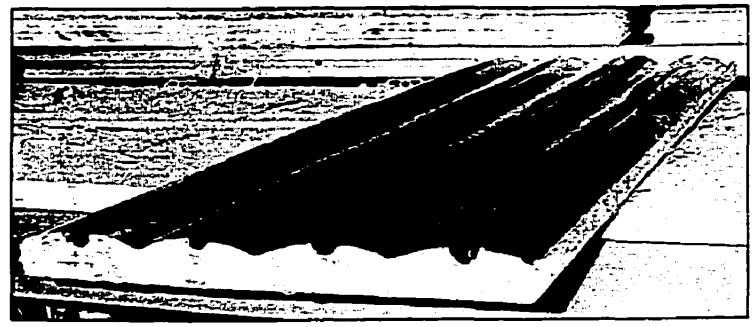

(b) Final production mold

Figure 3.5 – Spline molds.

3.2.1.2 Fabricating Splines.

To fabricate the splines, the mold shown in Figure 3.5(b) was used. The mold was polished and waxed with mold release wax prior to fabrication of any part. Two 900-mm by 630-mm sheets of 1200-g/m^2 uni-directional glass mats were saturated with 500-grams West System 105/205 Epoxy resin. This type of glass mat was chosen because of its capacity to resist the maximum moments developed in the pole. The sheets were saturated on a flat surface because the glass was dense, and it was important that the resin saturate the fabric thoroughly, see Figure 3.6.

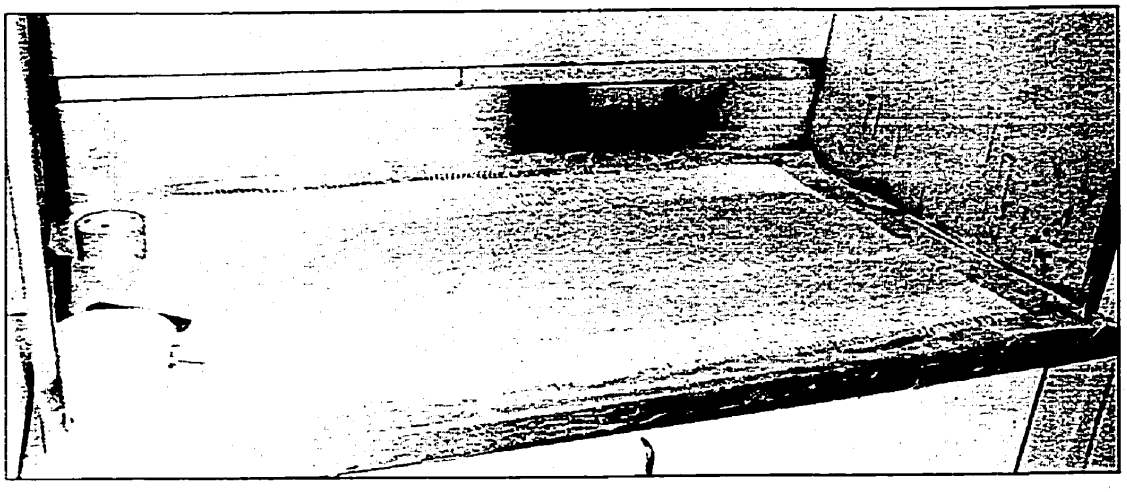

Figure 3.6 – Saturating fabric with West System Epoxy.

Once the fabric was saturated, it was rolled in the long direction, and unrolled into the mold, see Figure 3.7(a). As the wet fabric was rolled into the mold, it was pressed into the grooves of the mold, see Figure 3.7(b). This provided very good compaction against the mold surface.

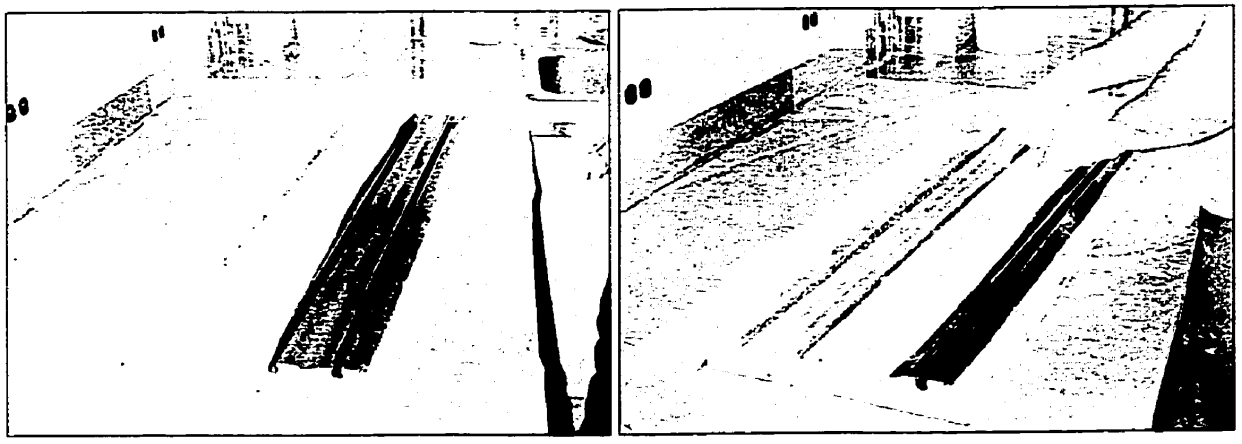

(a) Rolling fabric into mold *(b) Pressing fabric into grooves.*

Figure 3.7 – Rolling fabric into mold.

After the wet fabric was rolled and pressed into the mold, entrapped air was forced out, see Figure 3.8, and the edges were trimmed, see Figure 3.9. It is evident in these figures that the black mold surface can be seen through the wet glass indicating good compaction. Once the part cured, it was removed from the mold, and cut to the desired dimensions.

Figure 3.8 – Removing entrapped air.

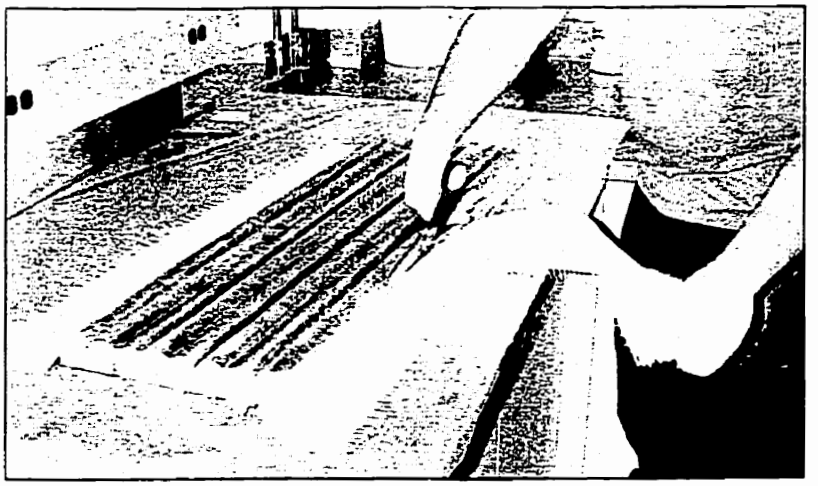

Figure 3.9 – Trimming excess material.

3.3 TEST SPECIMENS

The pole testing program consisted of four phases as described in Section 3.1. A detailed description of the testing in each of these phases is given in subsequent sections. Additionally, a description of tests conducted in order to determine the material properties of the FRP used in the experimental program is given.

3.3.1 Phase I

Phase I involved the testing of seven poles to measure the structural performance of the poles in their "as bought" condition. These poles were used as a benchmark for the remainder of the experimental program.

3.3.1.1 Specimen Fabrication

The specimens tested in Phase I had a measured average height of 2705-mm from the ground line, and an average base diameter of 156-mm. As the cross section of the poles varied, a concrete base was cast at the base of each specimen, as shown in Figure 3.10, to provide a uniform cross-section so that a common test set-up could be used. The dimensions of the concrete base are shown in Figure 3.11. The dimensions of the specimens tested in Phase I are shown in Table 3.1 along with the corresponding class for each specimen defined according to the information shown in Figure 2.1 and Table 2.1.

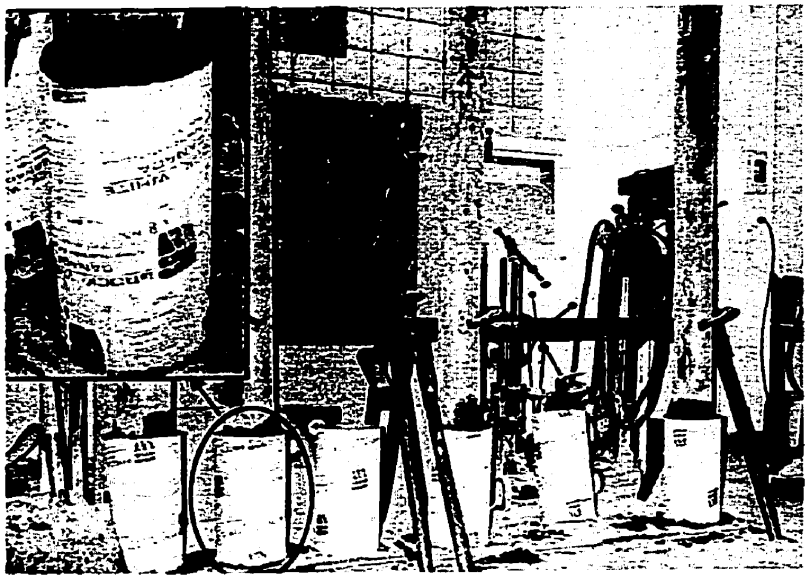

Figure 3.10 - Poles in concrete base.

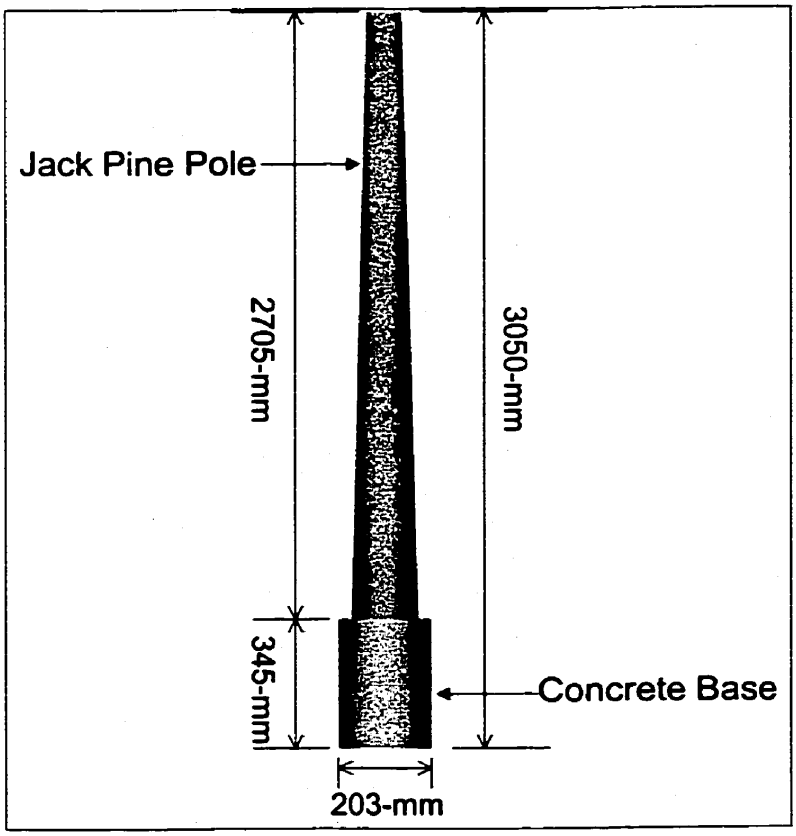

Figure 3.11 – Dimensions for Phase I specimens.

Table 3.2 – Phase I Specimens

Specimen	Circumference at Top of Pole (mm)	Circumference at 1800-mm above Ground Line (mm)	Class
P1-1	405	448	7
P1-2	393	438	7
P1-3	399	438	7
P1-4	424	470	7
P1-5	430	470	6
P1-6	393	429	7
P1-7	430	457	6

3.3.1.2 Test Set-up

All poles were tested using the common test set-up shown in Figure 3.12. A plastic sleeve, with its inner diameter matching the outer diameter of the previously described concrete base, was pressed over the concrete. The specimen was then placed vertically into a reinforced concrete block, which was rigidly attached to the structural floor of the laboratory. The load was applied horizontally through a cable attached to the pole 2440-mm from the base of the pole. The steel cable was attached to a 2500-mm long lever arm, with a lever ratio of 2.5:1. The load was applied using a hydraulic jack with a capacity of 250-kN and a stroke of 168-mm. Through the lever arm, the maximum load that could be applied to the pole was 100-kN, with a maximum stroke length of 420-mm. The hydraulic pressure was provided through a pneumatic hydraulic pump.

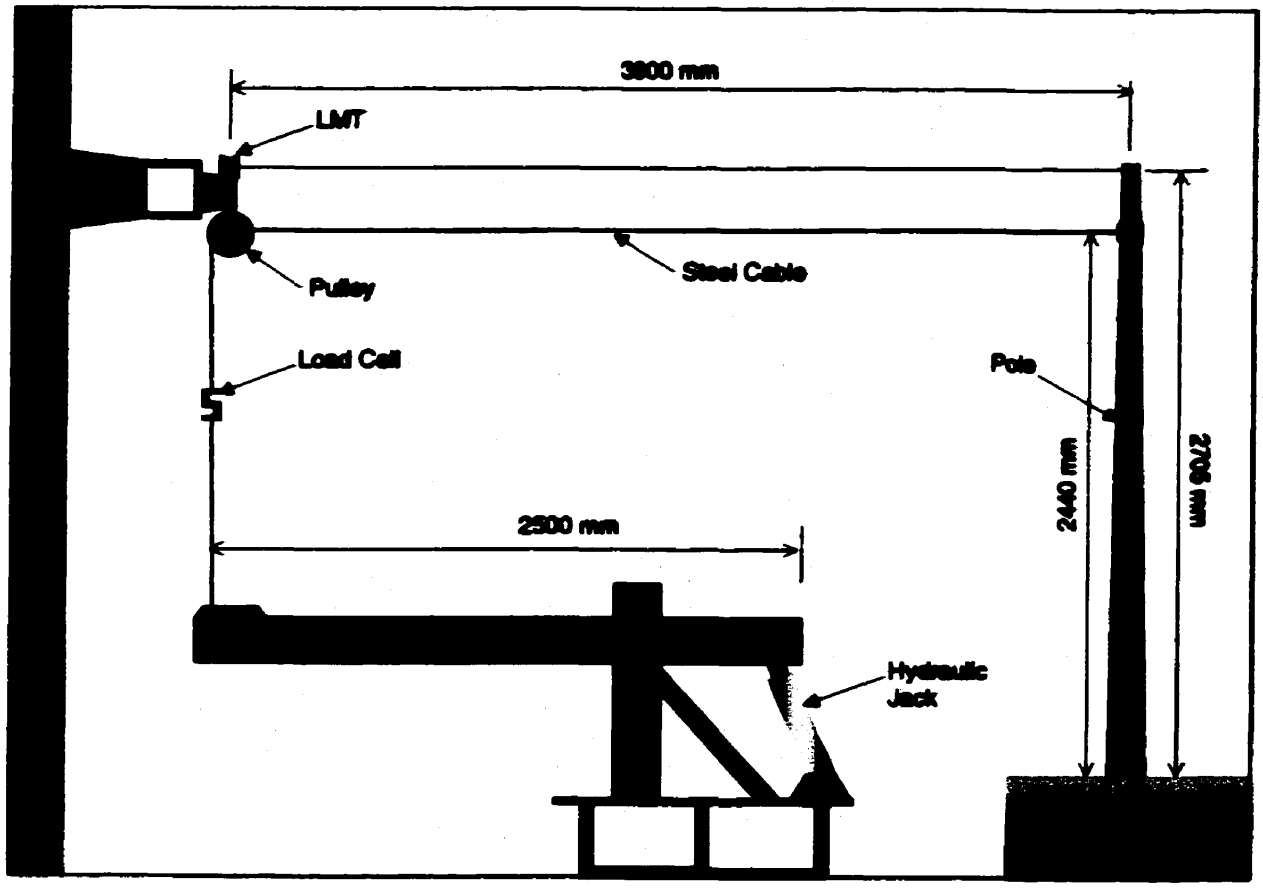

Figure 3.12 – Test set-up.

3.3.1.3 Instrumentation

The instrumentation used in phase I was designed to measure:

a) the applied load at the top of the pole; and,

b) the horizontal displacement of the tip of pole.

The load was measured with a pre-calibrated electronic load cell having a capacity of 44-kN. The lateral deflection was monitored through an electronic linear measurement transducer (LMT) mounted on a fixed steel column 3900-mm away from the specimen, as shown in Figure 3.12. The fixed stroke range for the

LMT was 350-mm but the actual stroke range was modified during the testing by using extension cables. The load was applied 2440-mm from the base of the pole and the deflection was measured 203-mm above the applied load. This testing procedure conforms to the requirements of ANSI/ASTM D1036-99.

3.3.2 Specimens for Phase II

The purpose of this phase was to evaluate different lengths of reinforcement for repairing utility poles. Seven poles were tested in Phase II with spline lengths of 203-mm, 254-mm, 305-mm and 406-mm.

3.3.2.1 Specimen Fabrication

The poles were prepared by cutting a 2-mm wide slot halfway through the cross-section at 610-mm from the ground line of the pole using a horizontal band saw, as shown in Figure 3.13. This location was selected based on the limitations of the rehabilitation process. However, Bingell (Bingell *et al.* 1995) states that pole decay typically occurs 460-mm above and below the ground line. By replacing the wood 610-mm from the ground line to the butt of the pole ensures no decayed wood remains. The decayed portion of the pole could be removed, and a single 1040-mm stub would be used to restore the pole.

Rehabilitation of wooden poles does not always require the removal of the lower 1040-mm of the pole. For example, increasing the height of a pole, or restoring an insect-damage may require a section of the pole to be added or replaced at a

point above 610-mm from the ground line. Assuming all rehabilitation work must occur 610-mm above the ground line the FRP system can be designed for the maximum bending moment of the pole.

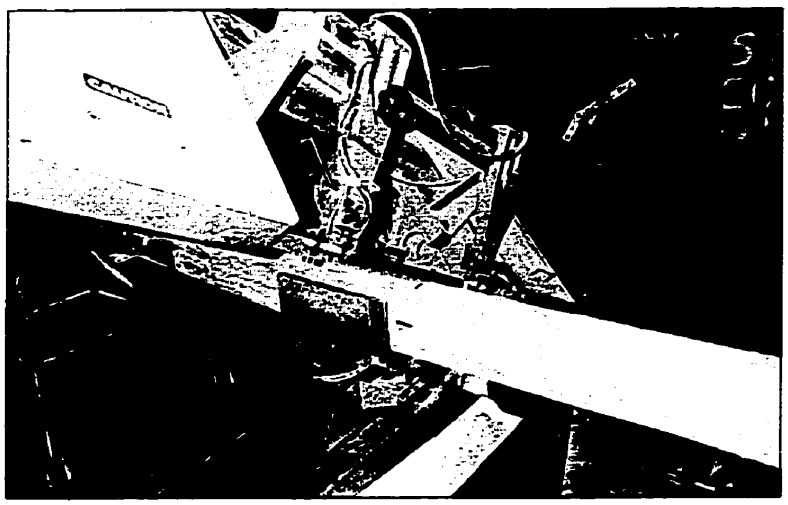

Figure 3.13 – Cutting of gauged crack.

After the poles were cut, grooves of varying lengths where machined into the pole using a Pole Milling Machine (PMM) designed and built for this project. Each pole had a 13-mm wide groove cut into it along the length of the pole and perpendicular to the gauged cut, as is shown Figure 3.14. The depth of the groove was difficult to maintain as all of the poles were tapered. The PMM was set to cut 19-mm deep at the top of the gauged crack. This ensured that the reinforcement would fit along the length of the groove and the groove would not be too shallow at the top of the groove.

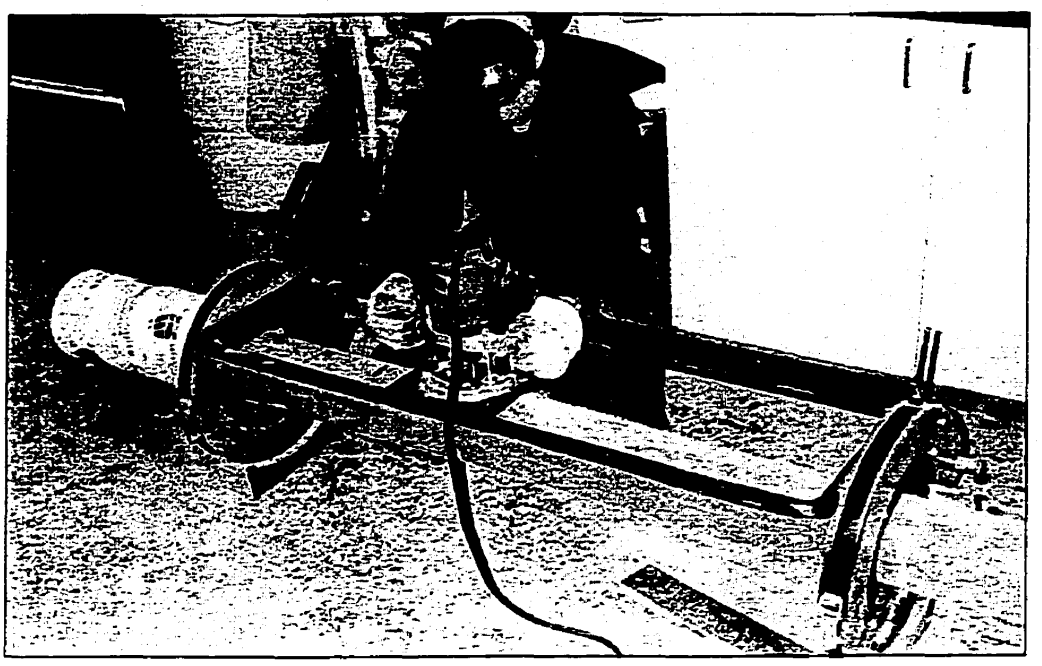

Figure 3.14 – Cutting grooves in pole with the PMM.

Once the grooves were machined and the reinforcement cut to the proper length, the splines were bonded to the pole. As the concept of the pole rehabilitation was to restore the strength of the pole in a vertical position, the adhesive needed to have a viscosity high enough to ensure that it would not run out of the groove while curing. To facilitate this, west system epoxy was thickened with silica powder, a thixotropic agent. The thickened epoxy was used to fill the grooves as well as to coat the inside surface of the spline, as shown in Figure 3.15(a). Once the pole and spline were coated, the spline was pressed into the epoxy filled groove, Figure 3.15(b) and left to cure, see Figure 3.16.

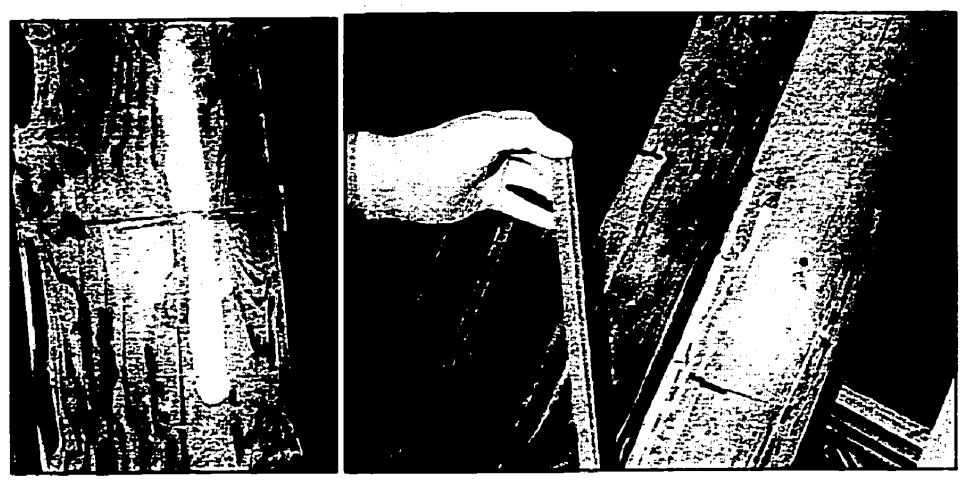

(a) (b)

Figure 3.15 – Filling groove with thickened epoxy and inserting spline.

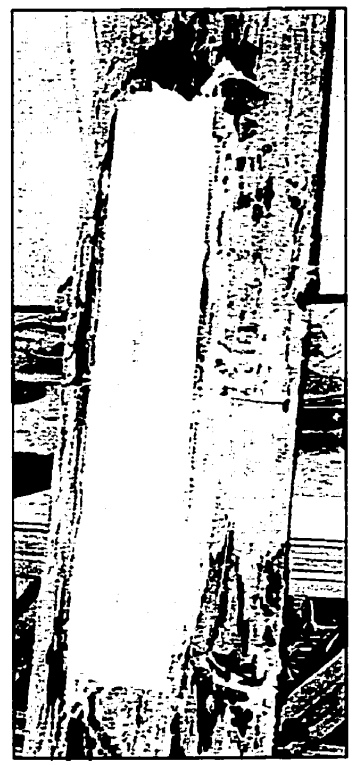

Figure 3.16 – Spline placed in groove.

Seven specimens were fabricated in this manner. The rehabilitation schemes are summarized in Table 3.3 and are shown in Figure 3.17.

Table 3.3 – Rehabilitation schemes for Phase II specimens.

Specimen	Circumference at Top (mm)	Circumference at 1800-mm from Ground line (mm	Spline Length (mm)
P2-203-1	424	467	203
P2-254-1	405	463	254
P2-305-1	459	471	305
P2-305-2	418	438	305
P2-305-3	393	429	305
P2-406-1	440	496	406
P2-406-2	418	451	406

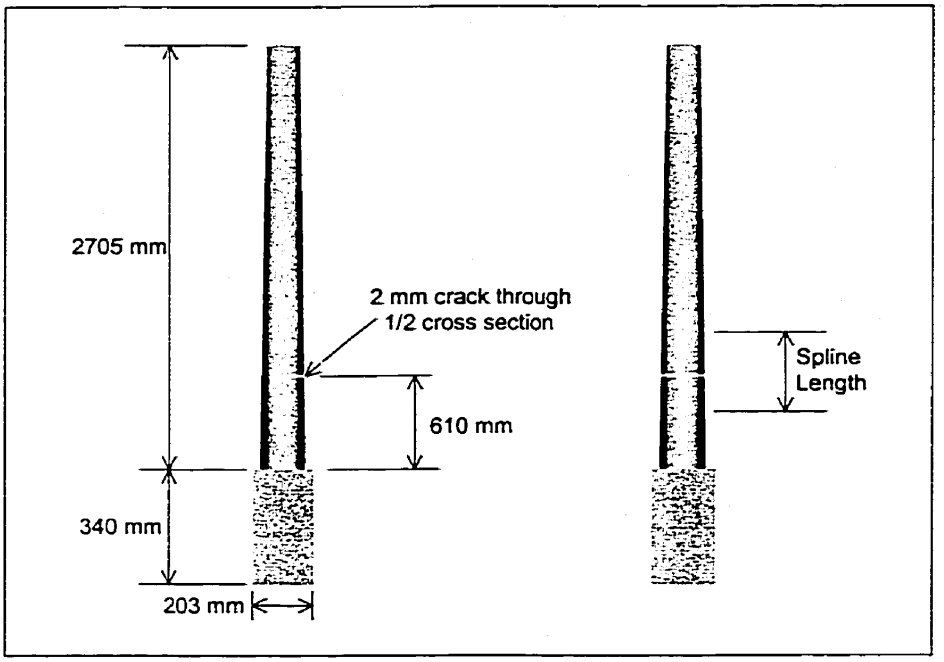

Figure 3.17 – Rehabilitation scheme for Phase II specimens.

3.3.2.2 *Instrumentation*

The instrumentation in this phase was designed to measure:

a) the applied load at the top of the pole;

b) the horizontal displacement of the tip of pole;

c) the strain in the FRP spline;

d) the strain in the wood across the gauged crack; and,

e) the compressive strain in the wood.

The application of the load and measurement of the deflection were done similar to those in Phase I. The strains were measured using pre-calibrated 200-mm PI-gauges. The PI-gauge location on the tension side of the pole is shown in Figure 3.18(a) and (b). The PI-gauge location on the compression side of the pole is shown in Figure 3.19(a) and (b).

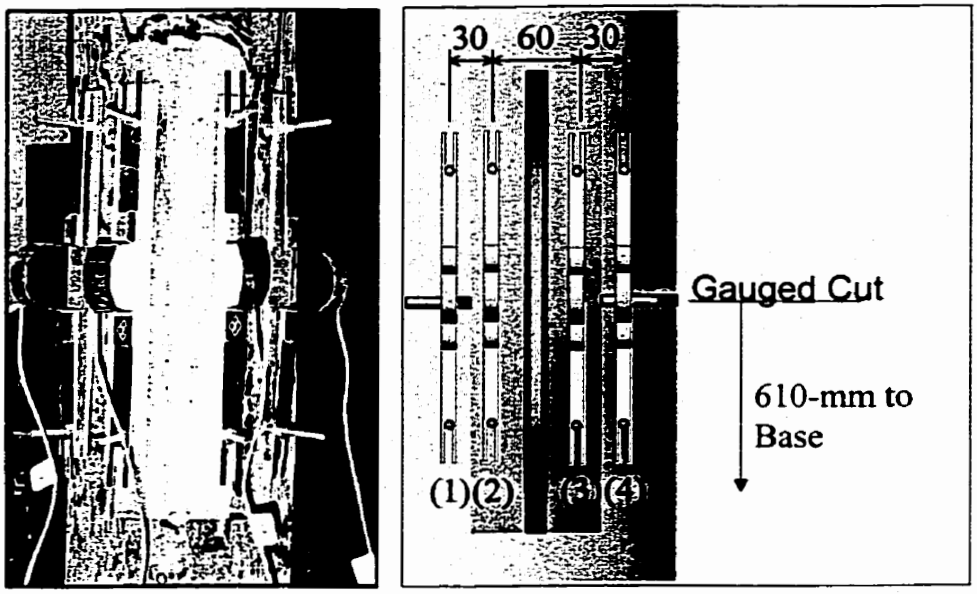

(a) *(b)*

Figure 3.18 – PI-Gauge layout for tension side of Phase II specimens

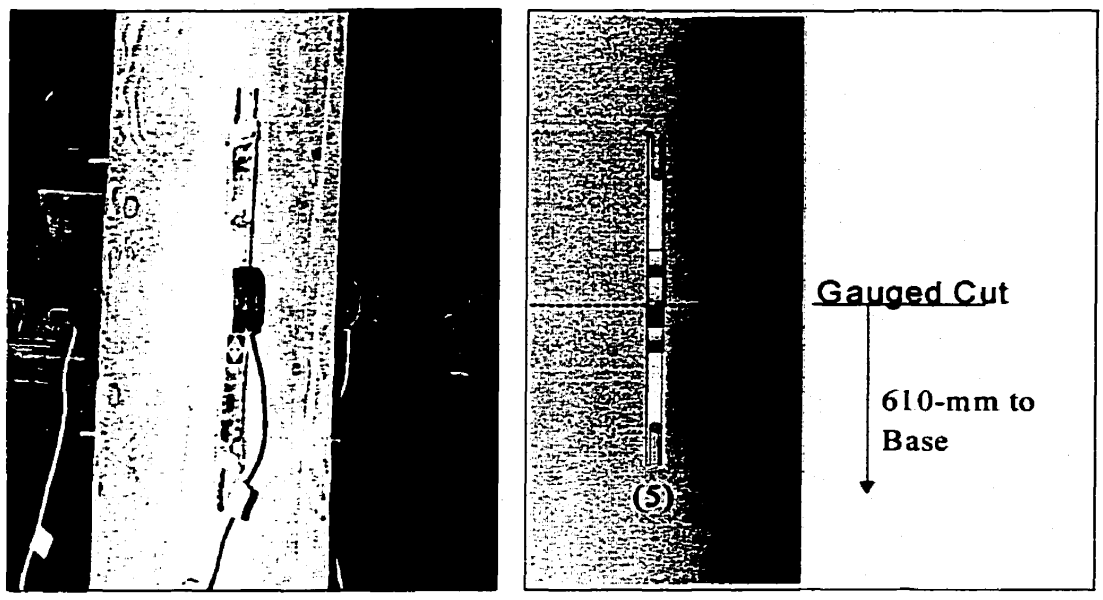

(a) (b)

Figure 3.19.– PI-Gauge layout for compression side of Phase II specimens

3.3.3 Specimens for Phase III

Based on the performance of the 305-mm and the 406-mm splines in the previous phase, these reinforcement lengths were selected, and confined helically with FRP sheets in the third phase. Six specimens were tested in this phase.

3.3.3.1 Specimen Fabrication

Testing in Phase III was sub-divided into three sub-categories, with two specimens being tested in each category. All specimens were fabricated in the same manner as in Phase II but only the 305-mm and 406-mm reinforcement were used. In the first sub-category, one pole was reinforced with a 305-mm spline and one with a 406-mm spline. The specimens were wrapped with two

layers of 340-g/m^3 bi-directional glass tape to confine the reinforcement. In the next subcategory, two specimens, one with a 305-mm spline and one with a 406-mm spline, were wrapped with four layers of 340-g/m^3 tape.

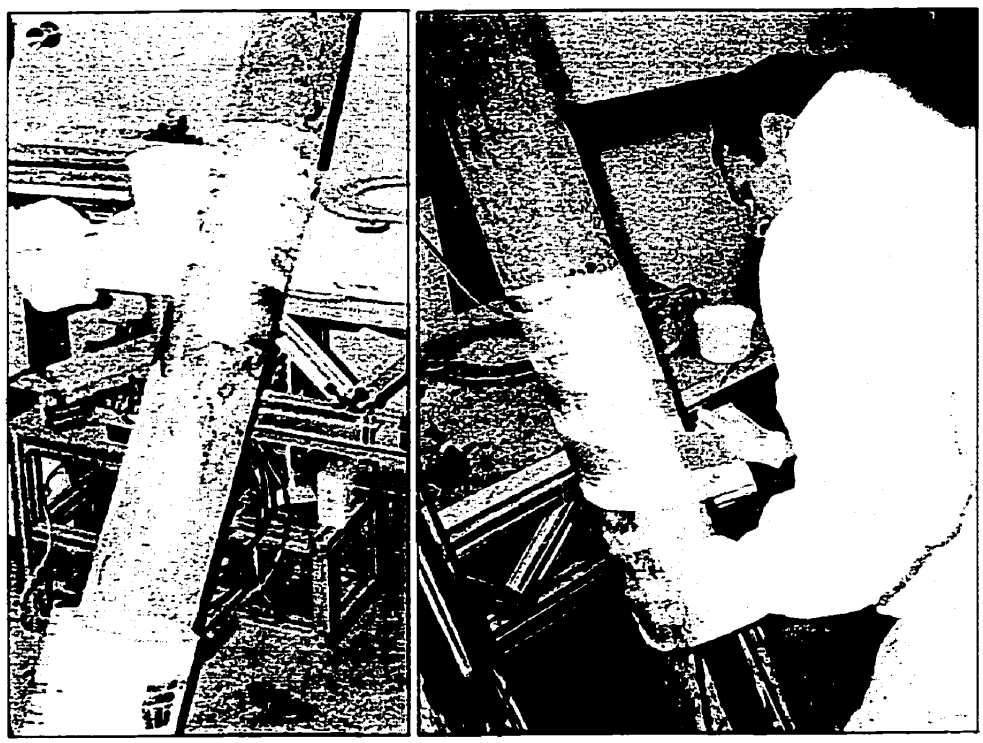

(a) (b)

Figure 3.20 Wrapping poles with bi-directional tape.

The tape was applied by hand, as shown in Figures 3.20(a) and (b). As the tape was wrapped tightly around the pole and the FRP spline, unthickened west system epoxy resin was brushed into the fabric saturating it. The resin was applied continuously until the tape was transparent and the pole and spline could be seen.

The final two specimens were prepared initially in the same manner as those in Phases II and III. However, before the splines were bonded into the pole, a different method of promoting proper bonding was attempted. In order to saturate the wood pole with resin prior to applying the thickened epoxy, a single layer of resin-saturated tape was placed in the groove.

The thixotropic agent that was added to the resin to increase the viscosity also prevented the resin from saturating the wood thoroughly, in effect reducing the bond performance. By placing the wet fabric next to the wood and the thickened epoxy on the wet fabric, it was hoped a stronger bond could be developed. The resin in the fabric would saturate into the wood and bond the fabric to the wood. Then the thickened epoxy would bond to the resin-impregnated fabric. By relying on the fabric to provide the primary bond to the wood, it was hoped that the thickened epoxy would bond to the interface layer better than the wood, as it would essentially be bonding to itself. The pole was then wrapped with bi-directional tape, as before. Figure 3.21(a) shows the fibre interface layer being placed in the groove, Figure 3.21(b) shows the thickened epoxy being placed on the fibre interface layer, and Figure 3.21(c) shows the spline being placed. The wrapped poles are shown in Figure 3.22(a), (b) and (c). The characteristics of each specimen tested in Phase III are listed in Table 3.4.

Table 3.4 – Phase III specimen characteristics

Specimen	Circumference at Top of Pole (mm)	Circumference at 1800-mm above Ground Line (mm)	Spline Length (mm)	Number of Confinement Layers
P3-2-305-1	443	467	305	2
P3-4-305-1	405	432	305	4
P3-2-406-1	430	467	406	2
P3-4-406-2	443	443	406	4
P3-4-406-3	465	487	406	4
P3-4-406-4	484	509	406	4

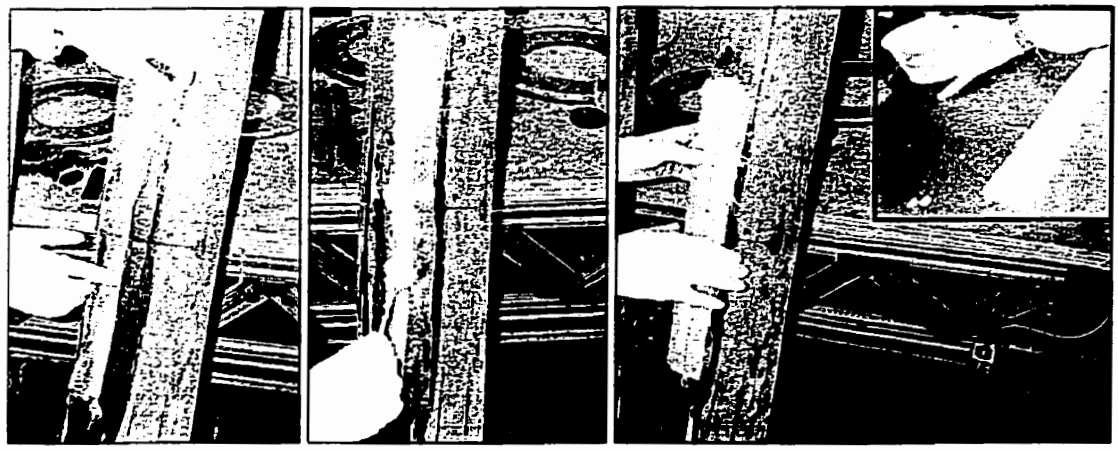

(a) *(b)* *(c)*

Figure 3.21 – Inserting fibre-interface layer.

(a) *(b)* *(c)*

Figure 3.22 Wrapped Poles

3.3.3.2 Instrumentation

The instrumentation in this phase was designed to measure:

a) the applied load at the top of the pole;

b) the horizontal displacement of the tip of pole; and,

c) the strain in the FRP jacket.

The application of the load and measurement of the deflection were done similar to those in Phase I. The strains were measured in specimens P3-2-305-1 and P3-2-406-1 using pre-calibrated 200-mm PI-gauges configured as shown in Figures 3.23 and 3.24. It was found that the PI-gauges would not remain fixed to the specimens for the duration of the testing, so a combination of 200-mm PI-gauges and strain gauges were used for the remaining specimens in Phase III. Figure 3.25 and 3.26 shows the PI-gauge and strain gauge locations for the remaining specimens in Phase III.

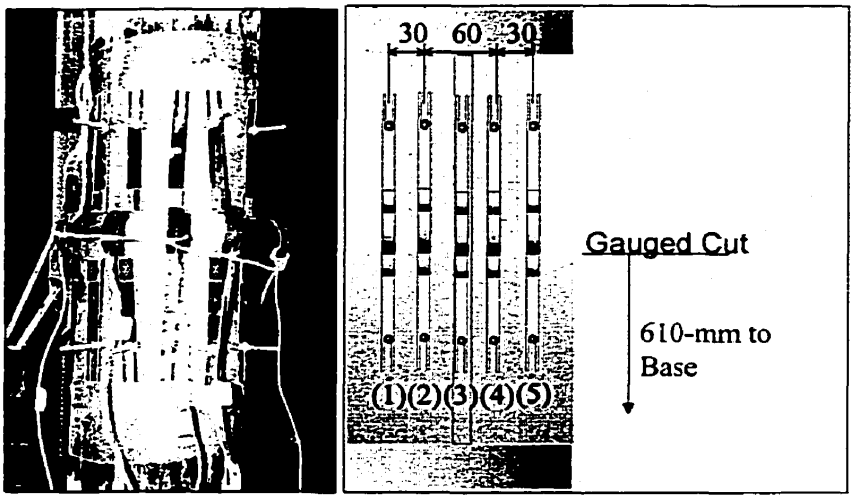

Figure 3.23 – PI-gauge locations of tension side of Phase III specimens P3-2-305-1 and P3-2-406-1.

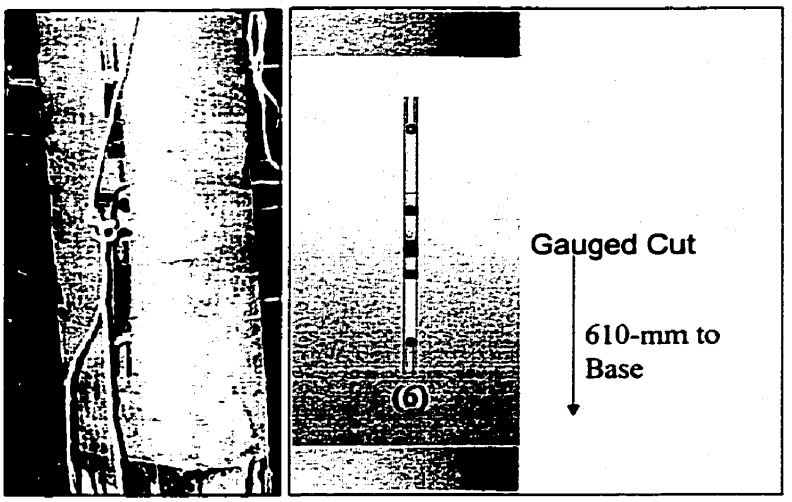

(a) (b)

Figure 3.24 - PI-gauge locations on compression side of Phase III specimens P3-2-305-1 and P3-2-406-1.

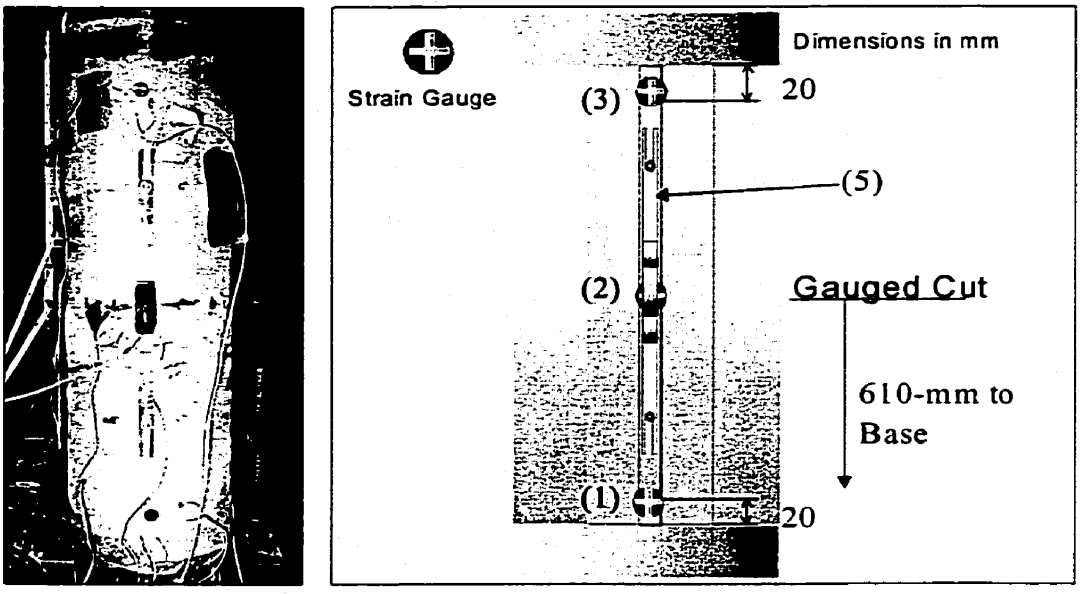

(a) (b)

Figure 3.25 - PI-gauge and strain gauge locations of tension side of Phase III specimens.

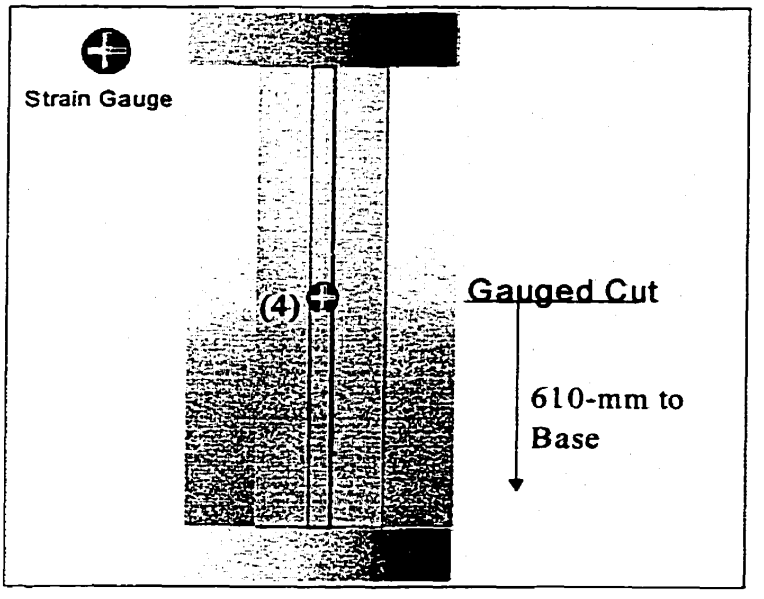

Figure 3.26 –Strain gauge location on compression side of Phase III specimens.

3.3.4 Specimens for Phase IV

Seven specimens were tested in Phase IV. The specimens were modified to simulate poles in which a wood stub was required to increase the height of a pole or to replace a damaged section of a pole.

3.3.4.1 Specimen Fabrication

The specimens in Phase IV were fabricated using three methods and three different reinforcement techniques. The first specimen was repaired to simulate a field installation. Due to some fundamental problems with the PMM the next four specimens were repaired horizontally in order to ensure consistency. The final specimen was fabricated using a combination of the two methods.

Specimen P4-1 was repaired almost entirely in the vertical position. The only process that was not done vertically was cutting the pole in order to incorporate the stub, shown in Figure 3.27. This process was done using the horizontal band saw as shown in Figure 3.13. In these specimens, 13-mm diameter holes were drilled, 75-mm in depth, into matching faces of the pole pieces, and 150-mm FRP alignment keys were placed into the holes. The poles were fitted together, as seen in Figure 3.28.

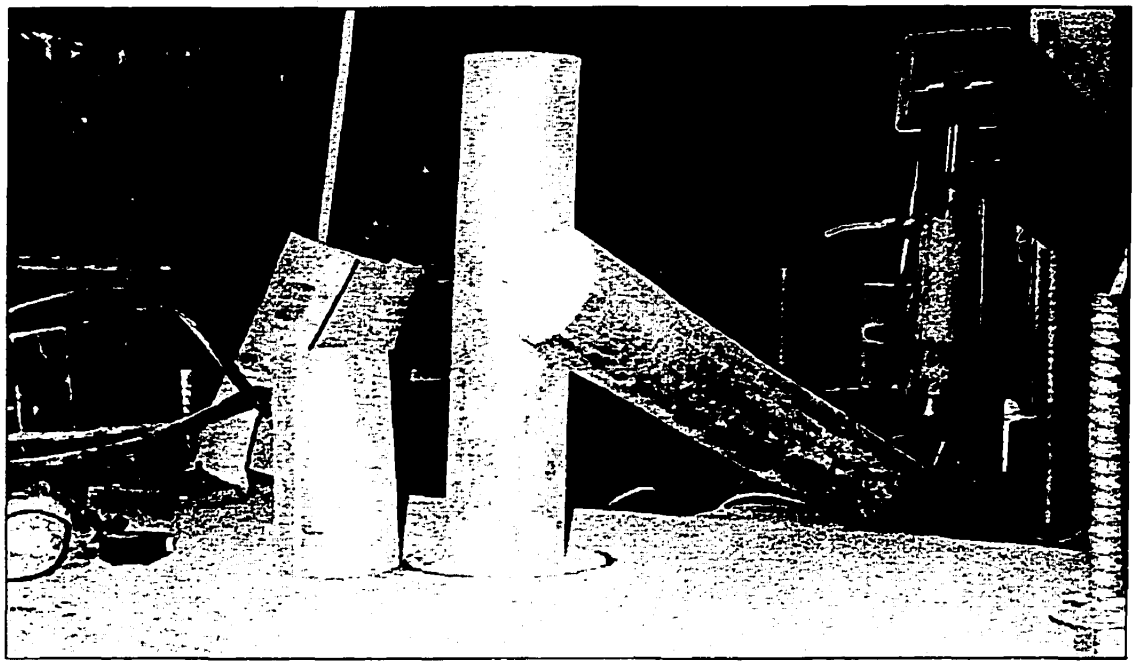

Figure 3.27 – Pole in three pieces.

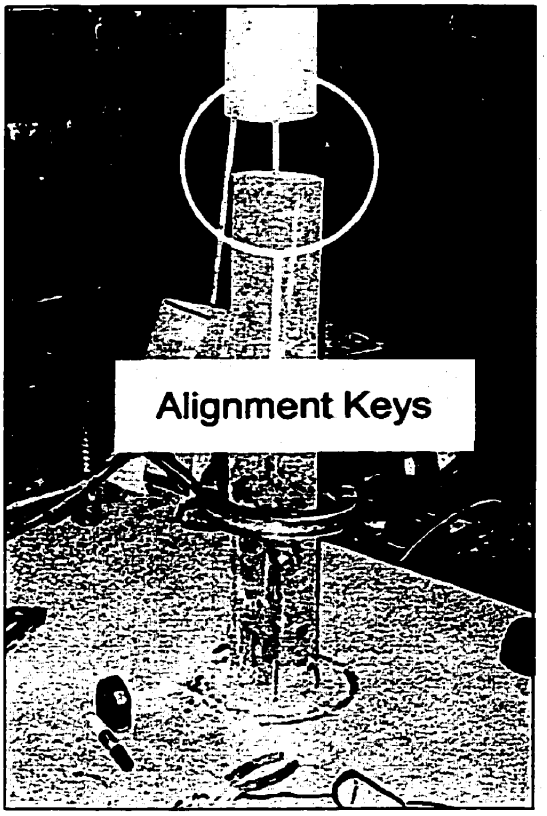

Figure 3.28 – Alignment keys.

The pole was able to support itself with only these alignment keys. However, when the Pole Milling Machine was attached to the pole, there was significant deflection making it impossible to cut straight grooves. In order to provide a stable support, prior to the Pole Milling Machine being attached to the pole, 13 mm glass bars were attached to the outer surface of the pole using duct tape to provide additional stiffness to the pole during machining, as shown in Figure 3.29(a). The bars were removed after the grooves were cut. Additionally, the specimen twisted when the pole-milling machine was machining the grooves, and the grooves did not line up between the pole and the stub. Additional holes were added to prevent this rotation as shown in Figure 3.29(b).

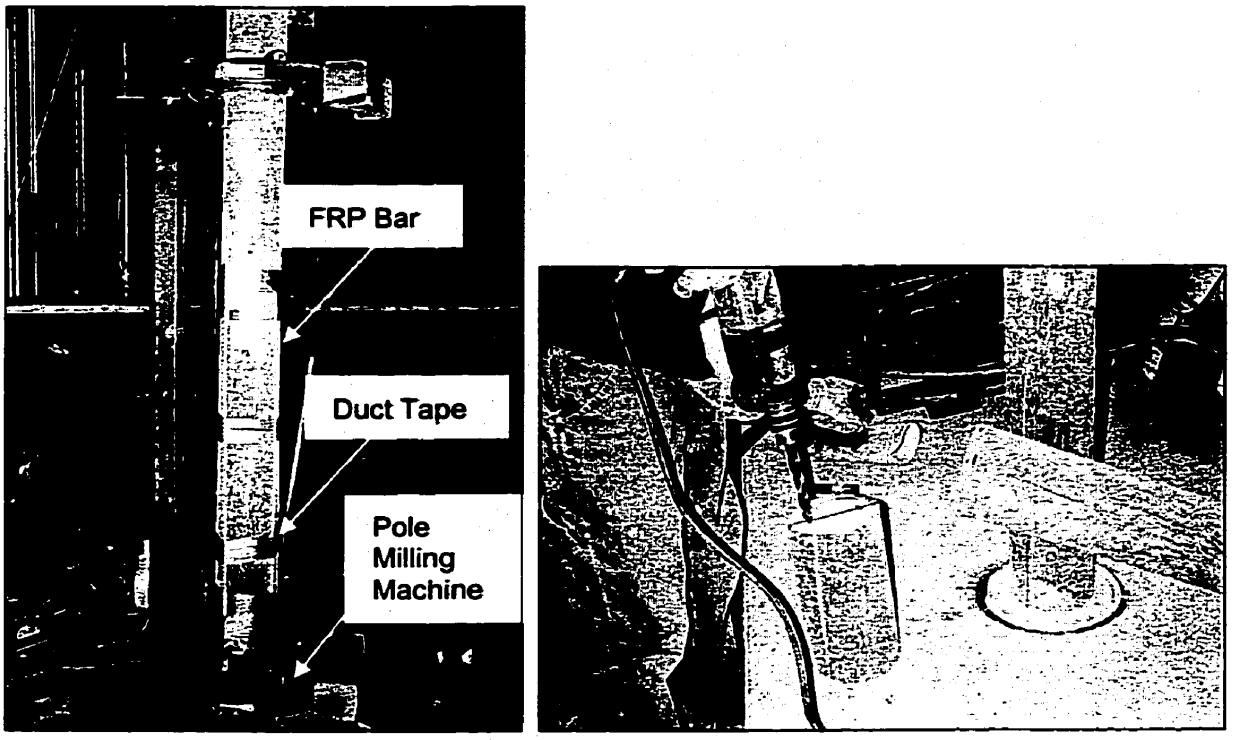

(a) Additional Support *(b) Additional holes to prevent rotation*

Figure 3.29- Specimen P4-1

After the grooves were cut, the saturated fibre interface layers were placed into the grooves, and the grooves were filled with thickened epoxy, as shown in Figure 3.30. The splines then had their flanges coated with thickened epoxy to ensure a good bond and inserted into the grooves of the pole. The restored area was wrapped with four layers of bi-directional glass tape, Figure 3.31(a), then saturated with resin, as shown in Figure 3.31(b). The wrapped pole is shown in Figure 3.31(c).

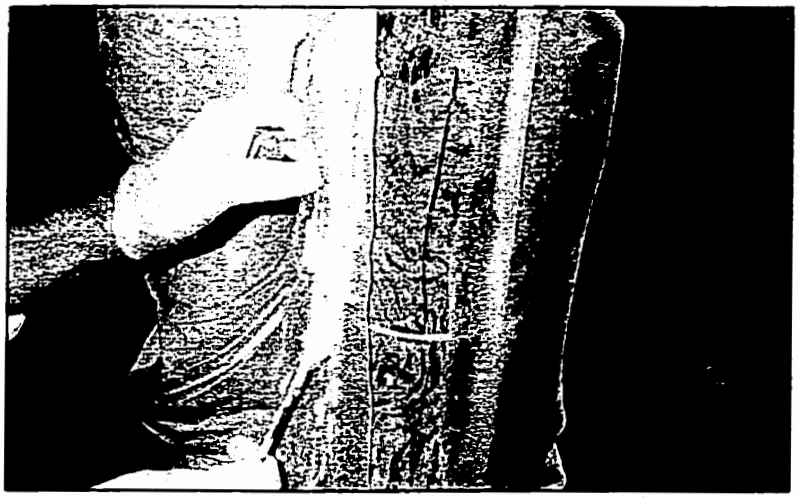

Figure 3.30 – Bond preparation of Phase IV poles.

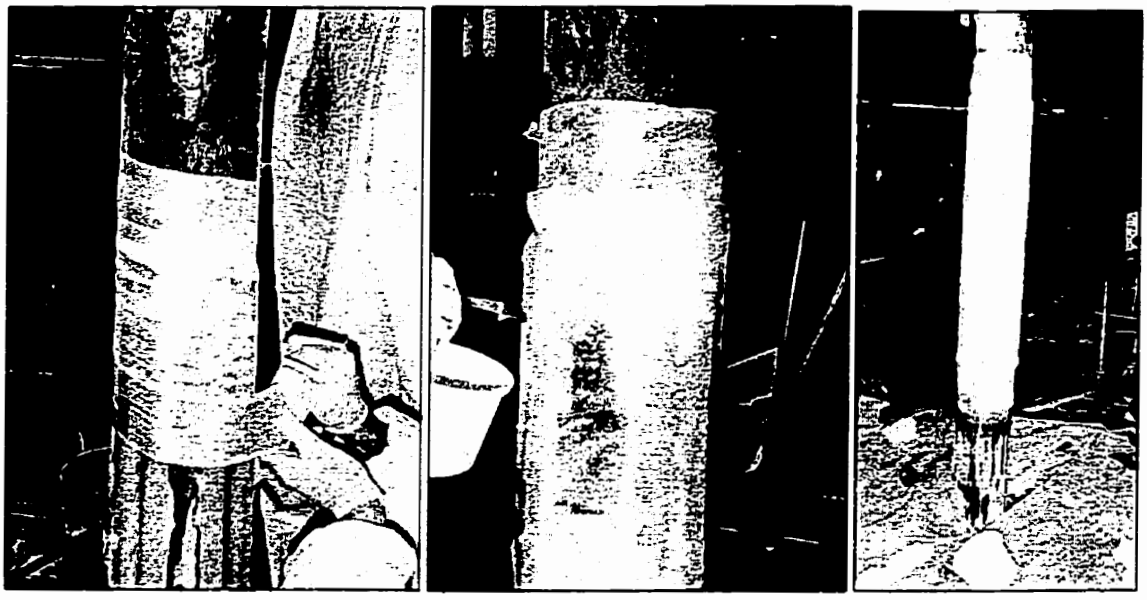

(a) *(b)* *(c)*

Figure 3.31 – Wrapping of specimen P4-1

Due to the difficulty in preparing the first specimen, specimens P4-2, P4-3, P4-4, P4-5 and P4-6 were machined horizontally and repaired vertically. Additionally, the results of specimen P4-1 indicated that having more than one alignment key

resulted in high coupling stress, causing premature failure. To cut the grooves, the pole was placed into the milling machine, as shown in Figure 3.14, and four grooves were cut into the pole at 45^0 intervals. The pole was then cut into three pieces using the horizontal band saw. Thirteen-mm holes were then drilled into the center of the pole pieces on matching faces of the cut pieces to a depth of 75-mm. FRP alignment keys, 150-mm long, were then placed into the holes. The pole pieces were then fitted together and the ribs were bonded to the pole, as in the previous specimen.

Specimen P4-2 experienced shear failure in the wood at the base of the spline and rupture of the composite jacket. The results are discussed in more detail in Chapter 4. In order to avoid a stress concentration at the base of the spline and to force the failure into the base of the pole, modifications were made to both the confinement wrap and the splines. This involved chamfering the ends of the splines to 45^0 and longitudinal fibres were placed near the ends of the splines covering 100 mm of the spline and 150 mm of the pole to transfer the stress from the base spline to the base of the pole. This is represented schematically in Figure 3.32.

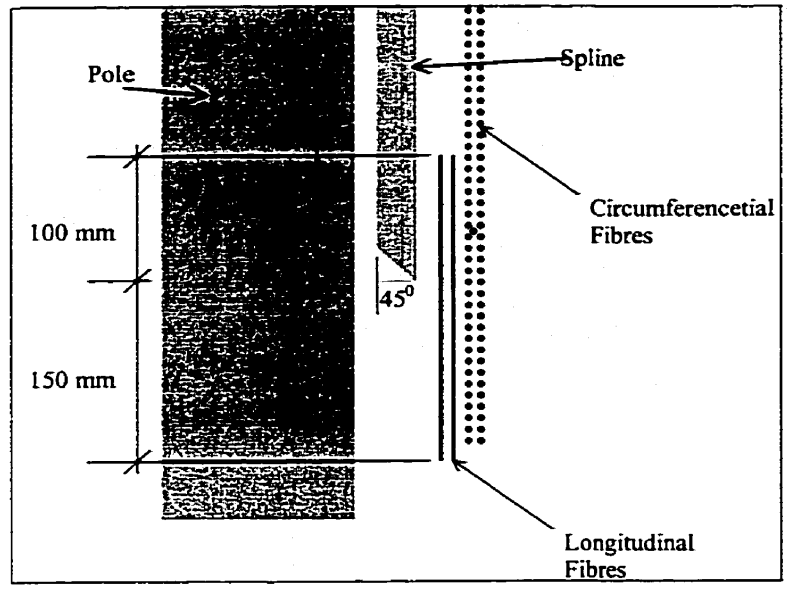

Figure 3.32 – Shear transfer zone.

The confining jacket was made using four layers of the 1200-g/m^2 uni-directional fabric tape for the remaining Phase IV specimens, instead of the four layers of 340-g/m^2 of bi-directional. Using the uni-directional fabric, it was found that the fabric could be placed much more efficiently than the bi-directional tape. The uni-directional fabric measured 813-mm in width while the tape measured 102-mm in width. Using the fabric, the reinforcement could be applied to the pole in long sheets which allowed the confining jacket to be perpendicular to the spline reinforcement, as shown in Figure 3.33(b). With the tape, it was much more difficult to maintain this direction as to advance the tape along the length of the repair, the tape had to be applied at an angle, as shown in Figure 3.33(a). Additionally, more tension could be applied to the fabric than the tape. The fabric was placed onto the pole in sheets and pulled very tightly against the splines. Prior to placement of the FRP sheets, small, 10-mm plastic cinch straps were

used to ensure that the splines remained firmly attach to the pole while the sheets were applied. Finally, a light bi-directional tape was placed on top for a more desirable surface finish.

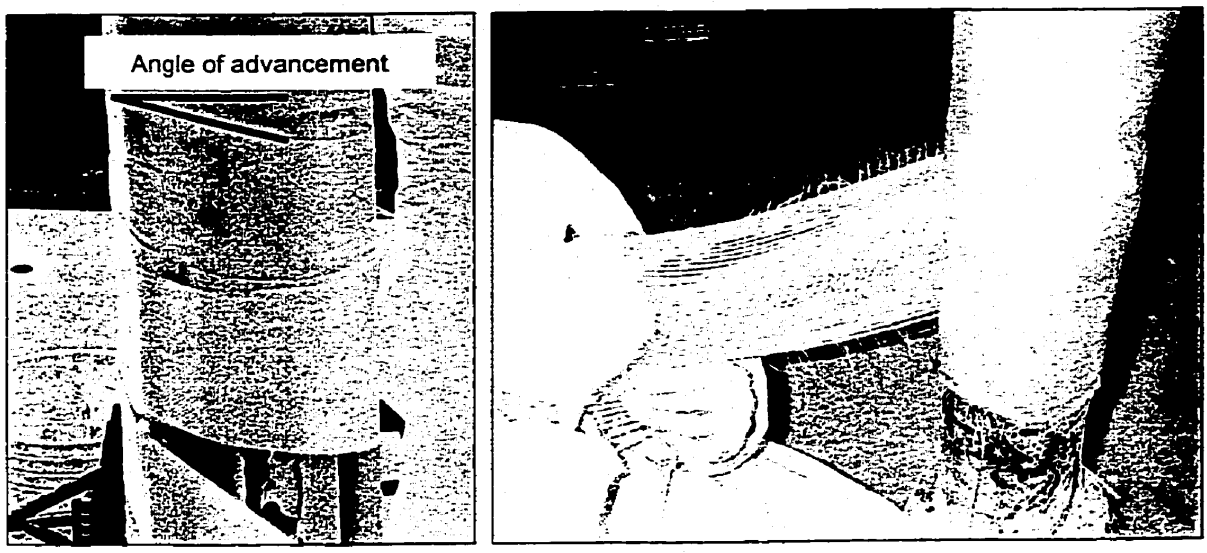

(a) (b)

Figure 3.33 – Phase IV confinement jackets

For the final specimen, P4-7, the grooves were machined with the pole standing vertically prior to cutting it into three pieces. Since the pole was uncut, there was no problem supporting the Pole Milling Machine, and the grooves were successfully cut in the vertical orientation. The pole was then cut into three pieces as shown in Figure 3.27. The materials used in the final repair of the pole are shown in Figure 3.34. The dimensions of the poles tested in Phase IV are shown in Table 3.5 along with their corresponding class based on the information given in Figure 2.1.

Table 3.5 –Summary of Phase IV specimens.

Specimen	Circumference at Top of Pole (mm)	Circumference at 1800-mm above Ground Line (mm)	Class
P4-1	399	432	7
P4-2	421	446	7
P4-3	396	421	7
P4-4	380	416	7
P4-5	412	437	7
P4-6	427	454	7
P4-7	456	479	5

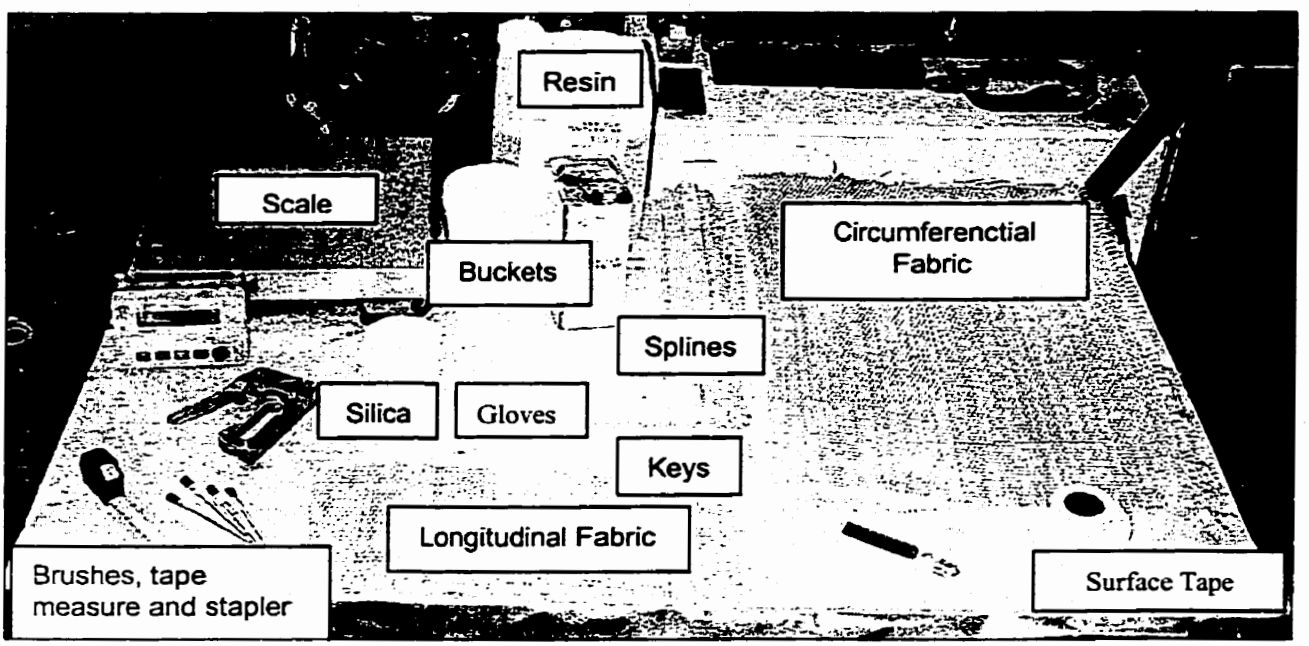

Figure 3.34 – Required materials for pole restoration.

3.3.4.2 Instrumentation

The instrumentation in this phase was designed to measure:

a) the applied load at the top of the pole;

b) the horizontal displacement of the tip of pole; and,

c) the strain in the FRP jacket.

The application of the load and measurement of the deflection were done similar to those in Phase I. The strains were measured using strain gauges configured as shown in Figures 3.35 and 3.36.

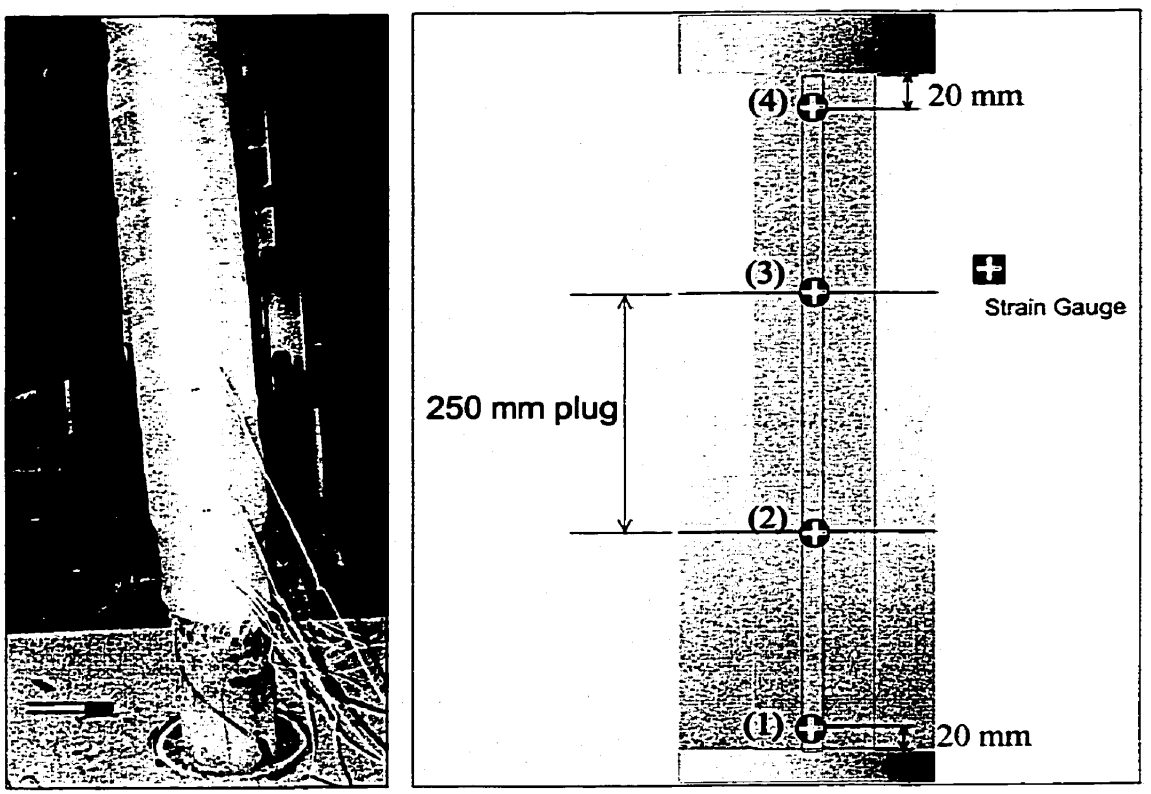

Figure 3.35 – Strain gauge location for tension side of Phase IV specimens.

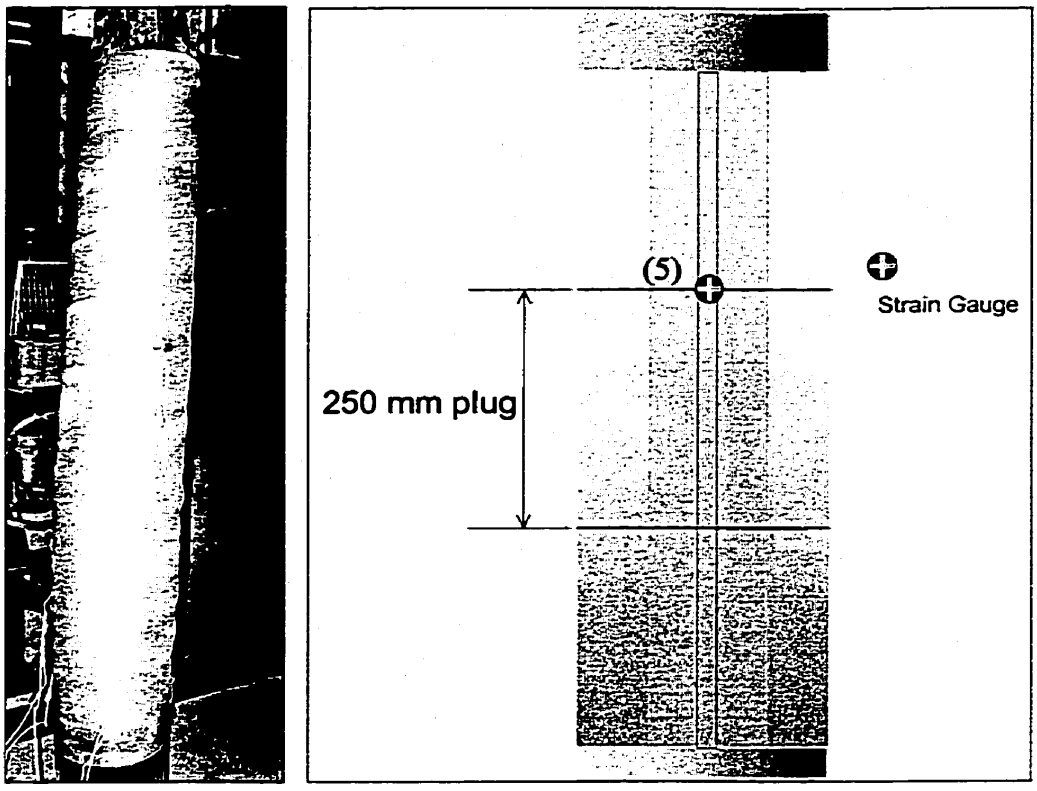

Figure 3.36 – Strain gauge location for compression side of Phase IV specimens.

3.3.5 Material Coupons

To determine the actual material properties of the glass fibre and the epoxy resin, several coupons were fabricated and tested. The physical properties obtained from the coupons were the tensile modulus, the tensile ultimate strength, the compressive modulus, the shear modulus, density of the FRP, and the volume fractions of the fibre and resin matrix. In order to simulate the actual material properties of the FRP used to rehabilitate the poles, flat panels were fabricated using the same manufacturing methods as the splines and confinement wrap, as shown in Figure 3.37.

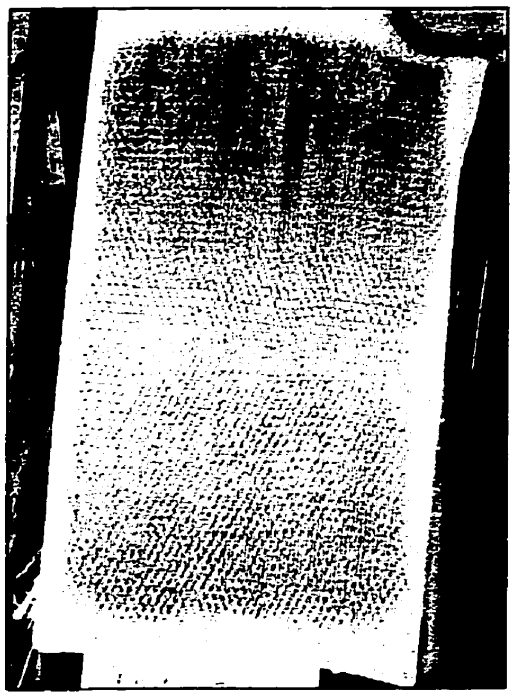

Figure 3.37 – Panel for test coupons

The panel was then cut into four different configurations for various tests. Two configurations were fabricated using the ASTM standards D 3039, Standard Test Methods for Tensile Properties of Polymer Matrix Composite Materials" and, D 3410, "Standard Test Method for Compressive Properties of Polymer Matrix Composite Materials with Unsupported Gage Section by Shear Loading". One configuration was fabricated using shear notches as described by Daniel *et al.* (1994). The final configuration were small coupons of fixed dimensions for determining geometric properties.

The tensile coupons had a gauge length of 150-mm, a width of 13-mm, and a thickness of 2.5 mm. The tensile tests were conducted in order to determine the in-plane tensile properties of the FRP, in accordance with ASTM Standard D

3039. The strains were measured using strain gauges and a strain gauge indicator while the loads were read and recorded using a dial gauge. The tensile coupon set-up is shown in Figure 3.38(a) and the tensile coupon is shown in Figure 3.38(b). All coupons were tested to failure. Unfortunately, the strain gauges could not record the strain to failure, so only the ultimate load was recorded at failure.

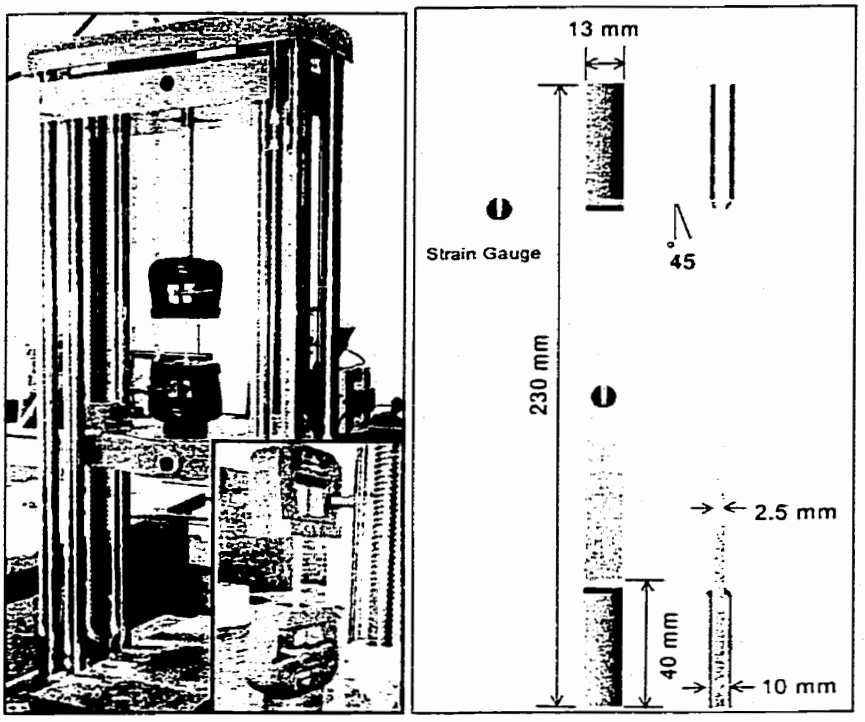

Figure 3.38 - Tensile coupons.

The compression coupons had a gauge length of 13-mm, a width of 13-mm, and a thickness of 1.25-mm. The compression test was conducted using a Modified Celenase Test Fixture, supplied by Wyoming Test fixtures, as shown Figure 3.39(a). The compression coupon is shown in Figure 3.39(b). The strains and

loads were recorded the same way as the tensile coupons. All coupons were tested to failure.

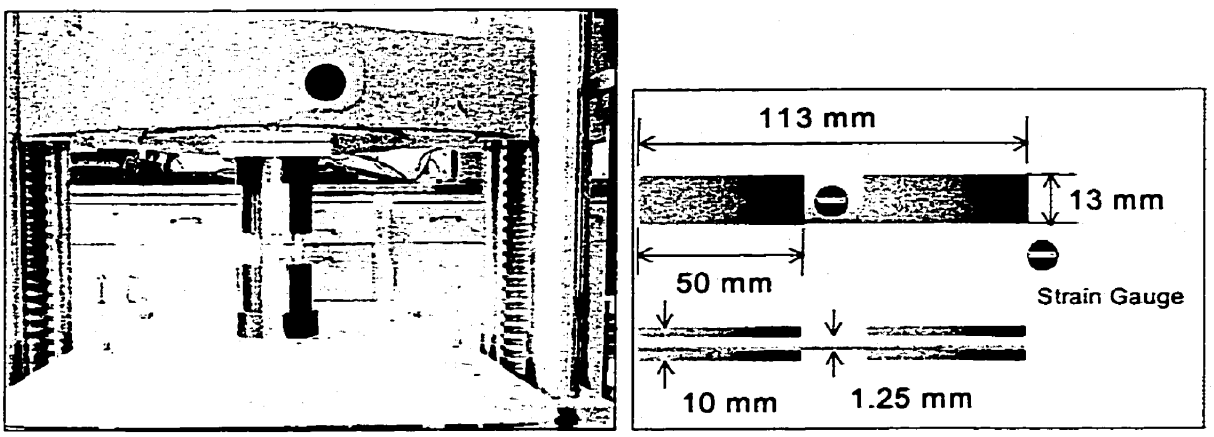

Figure 3.39 – Compression coupons.

The shear coupons had a gauge length of 150-mm, a width of 13-mm, and a thickness of 2.5 mm. An example of the shear coupon is shown in Figure 3.40.

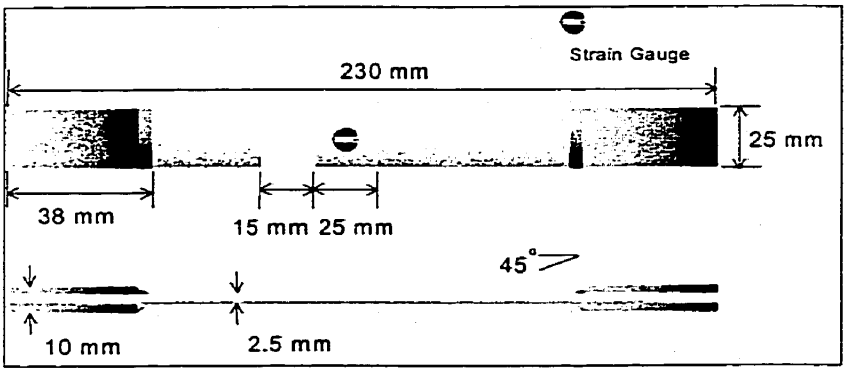

Figure 3.40 – Shear coupon.

3.3.6 Volume Fraction

The volume fractions of the matrix and fibre, as well as the density of the composite material were determined by manufacturing panels using similar techniques as those used for the fabrication of the FRP splines and jacket. These panels were cut to a fixed dimension and weighed. Dry glass cloth was cut to identical dimensions and weighed. The volume of the FRP panels was determined by a displacement test, where the panels were immersed in a beaker containing de-ionized water, and the increase in volume was recorded. The average volume of the panels was found to be 15 000-mm^3, and the average dry weight of the panels was measured to be 25.45-grams. This gives a FRP density of 1.7 x 10^{-3}-grams/mm^3. The differences between the dry glass cloth and the FRP panels gives the mass of the resin in the FRP and this was measured to be 9.76-grams. Using the manufacturer's specific gravity of the epoxy resin, 1.18, as shown in Appendix E, the volume of the resin was calculated to be 8271-mm^3. Using this value and the volume of the FRP, the volume fraction of the matrix resin and glass fibre were 55% and 45% respectively. Using these values and the manufactured material properties, the theoretical FRP properties were computed. The material properties for glass fibre were obtained from Table 2.3, and the properties of resin were obtained from the west system epoxy material properties data sheet (Gougen, 2001). The values are summarized in Table 3.6. The results show that the measured density of the FRP and the density calculated using the manufacturers data are comparable.

Table 3.6 - Calculated material properties.

Property (Vf = 45%, Vm = 55%)	West System Epoxy Resin	Glass Fibre	FRP
Density (g/cm^3)	1.18	2.54	1.79
Longitudinal Modulus (GPa)	3.2	72.4	34.34
Transverse Modulus (GPa)	3.2	72.4	5.62
In-Plane Shear Modulus (MPa)	*no values*	*no values*	###
Longitudinal Tensile Strength (MPa)	50.5	3450	1580.28
Transverse Tensile Strength (MPa)	50.5	3450	90.73
In-Plane Shear Tensile Strength (MPa)	*no values*	*no values*	###

CHAPTER 4

EXPERIMENTAL RESULTS AND ANALYSIS

4.1 GENERAL

The results from the four phases of the pole testing are presented and discussed in this chapter. The data is presented in the form of Load versus Deflection and Load versus Strain graphs, tables and figures. The results for each phase are presented separately.

4.2 PHASE I POLES

Seven specimens were loaded monotonically until failure to determine the virgin ultimate load of the poles used in the experimental program. The load-deflection curves for all seven specimens are shown in Figure 4.1. The ultimate loads and the deflections at ultimate loads are listed in Table 4.1.

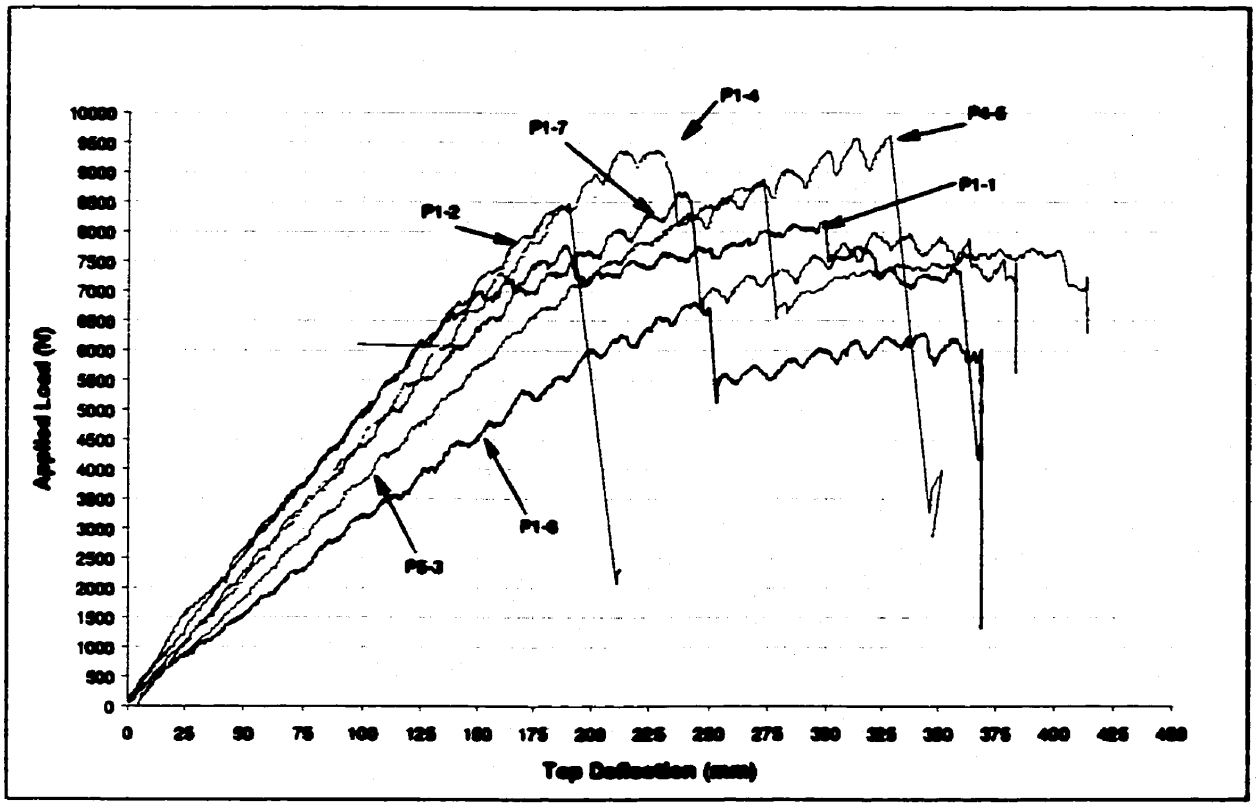

Figure 4.1 – Load-deflection curves for Control Poles

All specimens failed in a combination of tension failure at the base and shear failure through the geometric center of the pole in the butt. The ultimate load varied between 6800-N and 9400-N. The average ultimate load capacity was 8460-N. The test results showed a large variation in both the ultimate strength and stiffness in the specimens tested. The standard deviation was 910-N, which is to be expected in wood. The tip deflection varied from 190-mm (7% of pole height above ground line) to 273-mm (10% of pole height above ground line). Typical failures observed in the control specimens are shown in Figure 4.2(a) and (b).

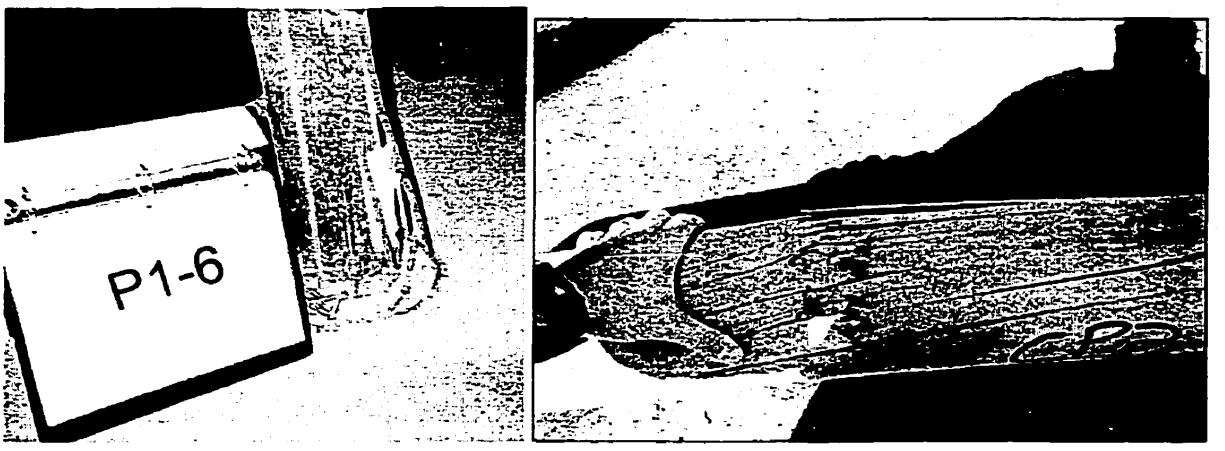

(a) (b)

Figure 4.2 - Typical tension failure in base of Phase I specimens.

The modulus of elasticity (MOE) and the modulus of rupture (MOR), as well as the corresponding pole class, are listed for each specimen in Table 4.1. Failure was defined as the load at which the specimens showed a significant drop in load capacity. The MOR and the MOE were calculated using Equations 1.1 and 1.2, as specified by the ASTM Standard D 1036 using the measured deflection and the corresponding applied load. Comparing the class of the pole obtained using the CSA standards, as shown in Table 3.2 for Phase I specimens, to the actual class of the pole obtained through testing, it is shown that all of the specimens met or exceeded their CSA predicted load capacity.

As was mentioned previously, the CSA standard classifies poles into strength classes based on species, length, and specified minimum circumferential measurements. The IEEE in its Design Guide for Wood Transmission Structures gives a modulus of elasticity for jack-pine poles of 8400 MPa, which is higher

than the average calculated value shown in Table 4.1. The difference in the modulus of elasticity may be attributed to the small sample number of specimens. The CSA gives the modulus of rupture for air-seasoned jack-pine poles as 44 MPa. Using the circumferential measurements at the ground line of the poles tested and the modulus of rupture given by the CSA, the ultimate strength of the specimens was calculated, as shown in Table 4.2. These calculated values give a higher predicted capacity of the poles than the predicted capacity using the circumference measured 1800-mm from the ground line, and the circumference at the top of the pole. The CSA takes a conservative approach in pole classification, as poles are required to meet a minimum standard in order to be classified for a certain load level, and it ignores the strength levels in between the classes. Table 4.2 shows the actual, theoretical capacity, without regard to class.

Table 4.1 - Control specimen results summary.

Specimen	Failure Load (N)	Deflection at Failure (mm)	MOR (MPa)	MOE (MPa)	Class
P1-1	7700	190	46.8	8181	6
P1-2	8490	190	60.5	10928	5
P1-3	8890	273	58.6	7336	5
P1-4	9260	218	47.7	7044	5
P1-5	9370	228	49.9	6962	5
P1-6	6810	244	47.4	6825	6
P1-7	8700	237	53.8	7254	5
Average	*8460*	*226*	*52.1*	*7790*	*5*
Standard Deviation	*910*	*30*	*5.6*	*1453*	*n/a*

Table 4.2 - Ultimate load and Deflection at failure of control specimens.

Specimen Number	Experimental Load (N)	CAN/CSA-015-90 (N)
P1-1	7700	6700
P1-2	8490	5700
P1-3	8890	5900
P1-4	9260	7800
P1-5	9370	7500
P1-6	6810	5700
P1-7	8700	6400
Average Values	*8460*	*6500*

The CSA standard bases the value of the MOR on the assumption that the pole is used as a simple cantilever and that the maximum bending stress will occur at the ground level. The assumption that the maximum stress in the pole occurs at the ground level is theoretically correct providing the circumference at the ground line is not more than 1.5 times the circumference at the point of loading. This is the case with the poles tested in Phase I where the average circumference at ground level is 1.16 times the circumference of the pole at the point of loading (CSA, 1990). The CSA standard specifies a coefficient of variation (COV) that can be used to predict the strength of wood poles. For jack-pine poles, the CSA standard gives a COV of 20%. Increasing the CSA predicted load by the COV in Table 4.2, it can be seen that all control specimens tested failed within the range of values calculated according to the CSA standards.

4.3 PHASE II POLES

4.3.1 Load Deflection Characteristics

Seven specimens with a gauged cut and reinforced with splines of varying lengths were loaded to failure to determine the effectiveness of splines having different lengths. Typical Load-Deflection curves are shown in Figure 4.3. The load-deflection curves were linear until failure. In all cases, failure was due to debonding of the spline from the wood. Once debonding occurred, splitting occurred beginning at the base of the cut and continuing through the pole. This was observed in all tests with the exception of specimens P2-203-1 and P2-305-2. This failure was similar to the shear failure in the control specimens. The experimental results are summarized in Table 4.3, along with the calculated capacity obtained using the CSA standard.

Table 4.3 - Phase II summary

Specimen	Spline Length (mm)	Experimental Load (N)	Deflection at Experimental Load (mm)	CAN/CSA-015-90 (N)
P2-203-1	203	3440	79	7500
P2-254-1	254	4570	101	8100
P2-305-1	305	4900	116	6500
P2-305-2	305	1880	55	5500
P2-305-3	305	3700	146	5700
P2-406-1	406	5480	141	9650
P2-406-2	406	4880	161	6500

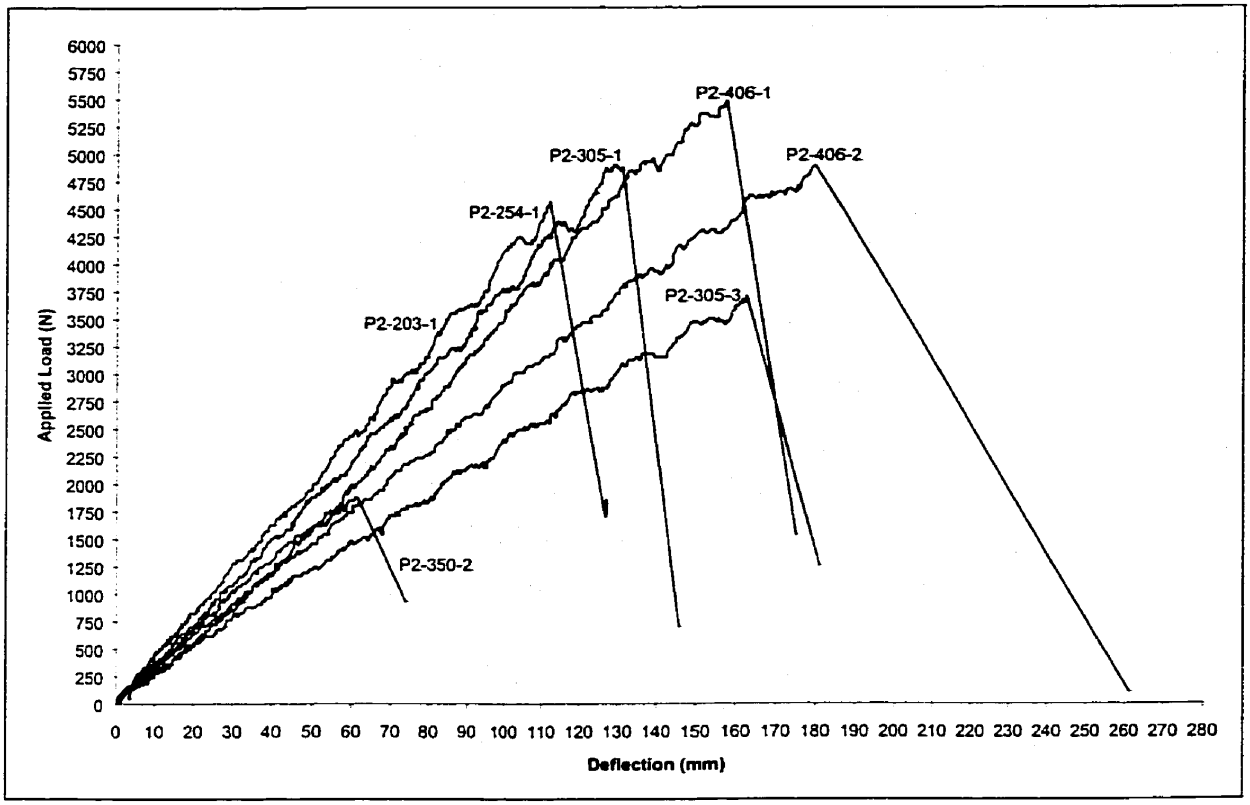

Figure 4.3 - Load-deflection curves for Phase II specimens.

Specimen P2-305-2 repaired with a 305-mm spline failed at a very low load. This is attributed to low bond strength due to a documented error in fabrication. With the exception of specimen P2-305-2, the 305-mm and 406-mm splines performed well, and the specimens achieved high capacities. Specimens P2-406-1 and P2-406-2 exhibited well developed bonds as was evident by the large portions of wood that seperated from the pole next to the spline at failure. Test results showed a large variation in the measured stiffness and ultimate strength for all specimens. Figures 4.4(a), and (b) as well as Figure 4.5 show typical failures in the specimens tested.

(a) (b) (c)

Figure 4.4 – Typical Phase II failures

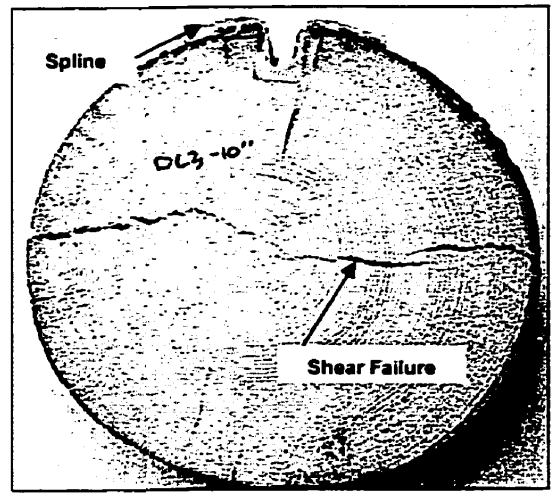

Figure 4.5 - Typical cross-section failure of Phase II specimens.

4.3.2 Strain Distribution and Bond Performance

In Phase II, the strain in the wood was monitored at three locations, and the strain in the FRP spline was monitored in two locations. All strains were measured using PI-gauges with a gauge length of 200-mm, as was shown in Figures 3.18 and 3.19. Strains are plotted in Figures 4.7 through 4.13. The strains at failure are listed in Table 4.4. The majority of the poles were characterized by long helical cracks along the length of the pole. With the application of a load, these cracks were forced to close, and the pole twisted about their longitudinal axes. The twisting produced additional strains resulting in a non-linear load-strain diagram. In comparing the load-strain curves to the load-deflection curves, an increase in strain without an increase in deflection indicates twisting of the pole. An increase in strain with a comparable increase in deflection indicates either shear failure in the pole or debonding of the spline.

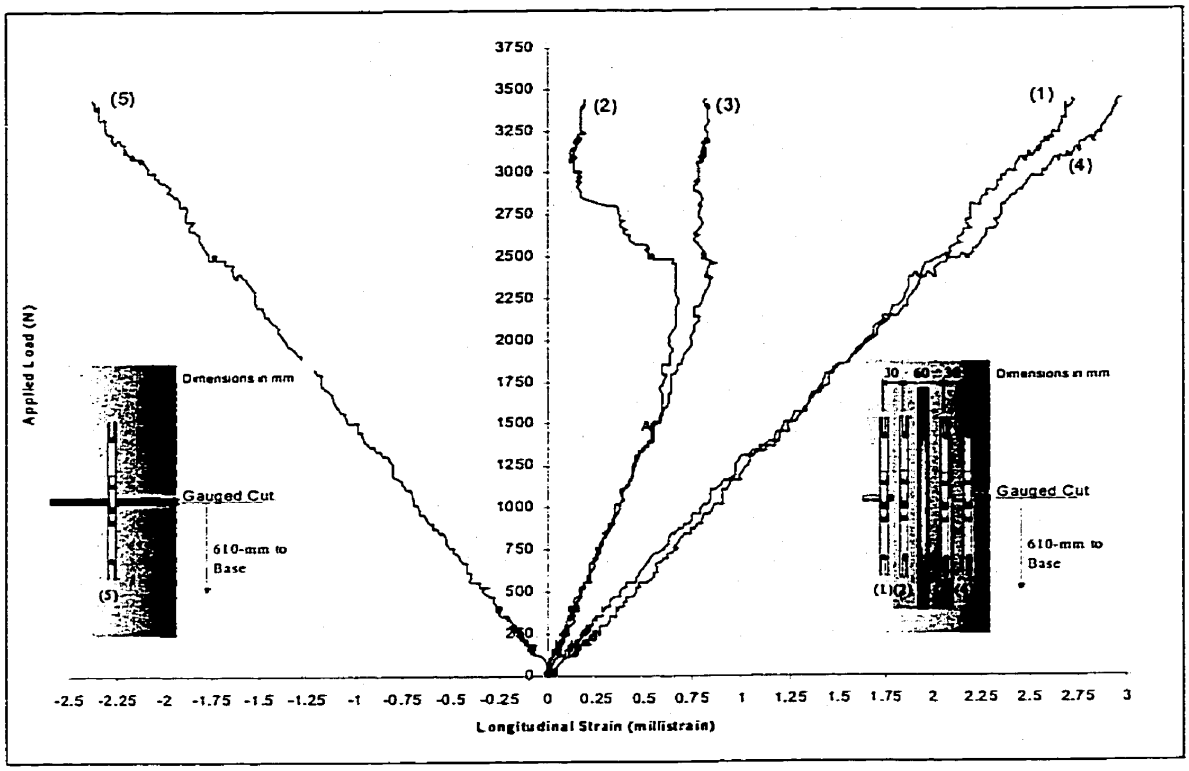

Figure 4.6 – Load-Longitudinal Strain curves for specimen P2-203-1

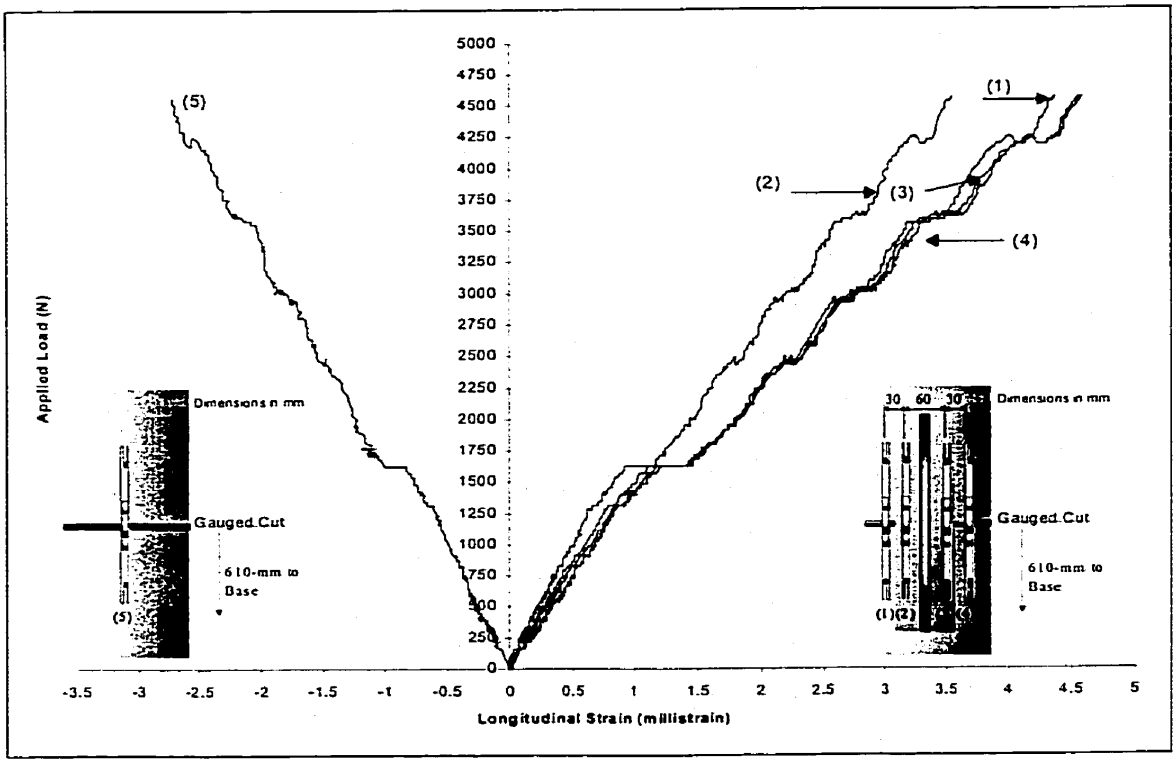

Figure 4.7 - Load- Longitudinal strain curve for specimen P2-254-1

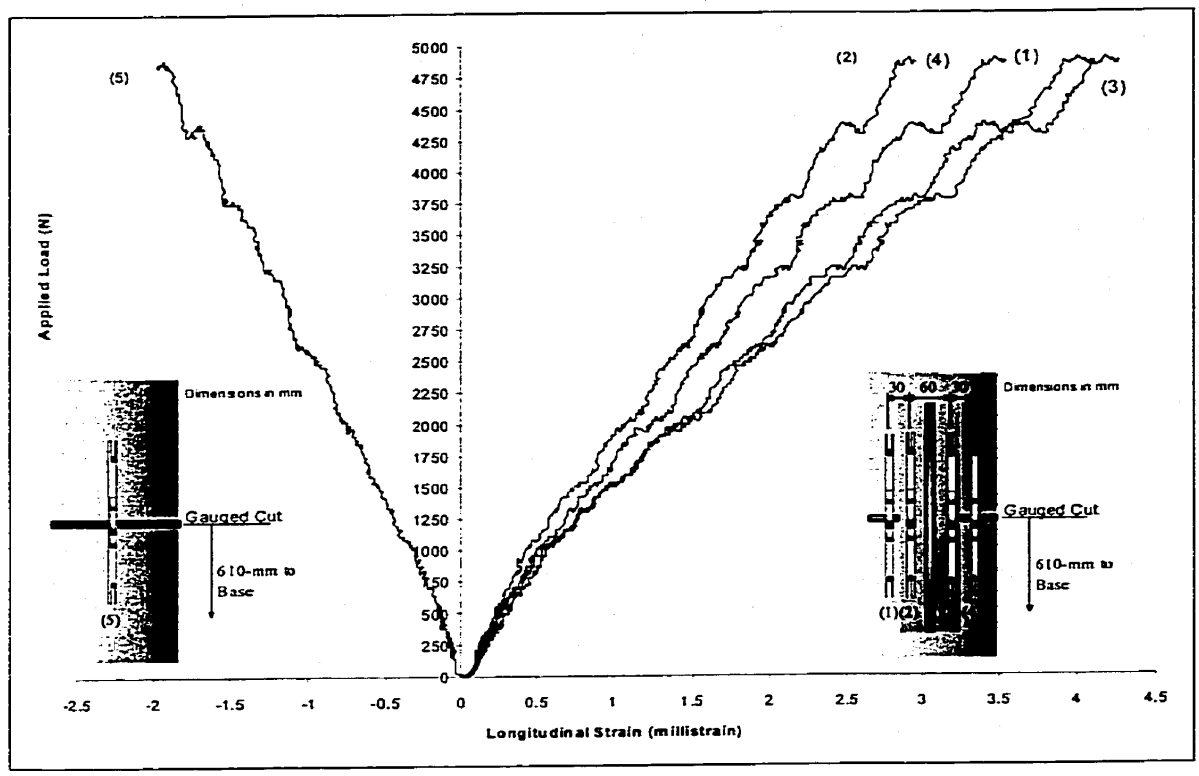

Figure 4.8 - Load-Longitudinal Strain curve for specimen P2-305-1

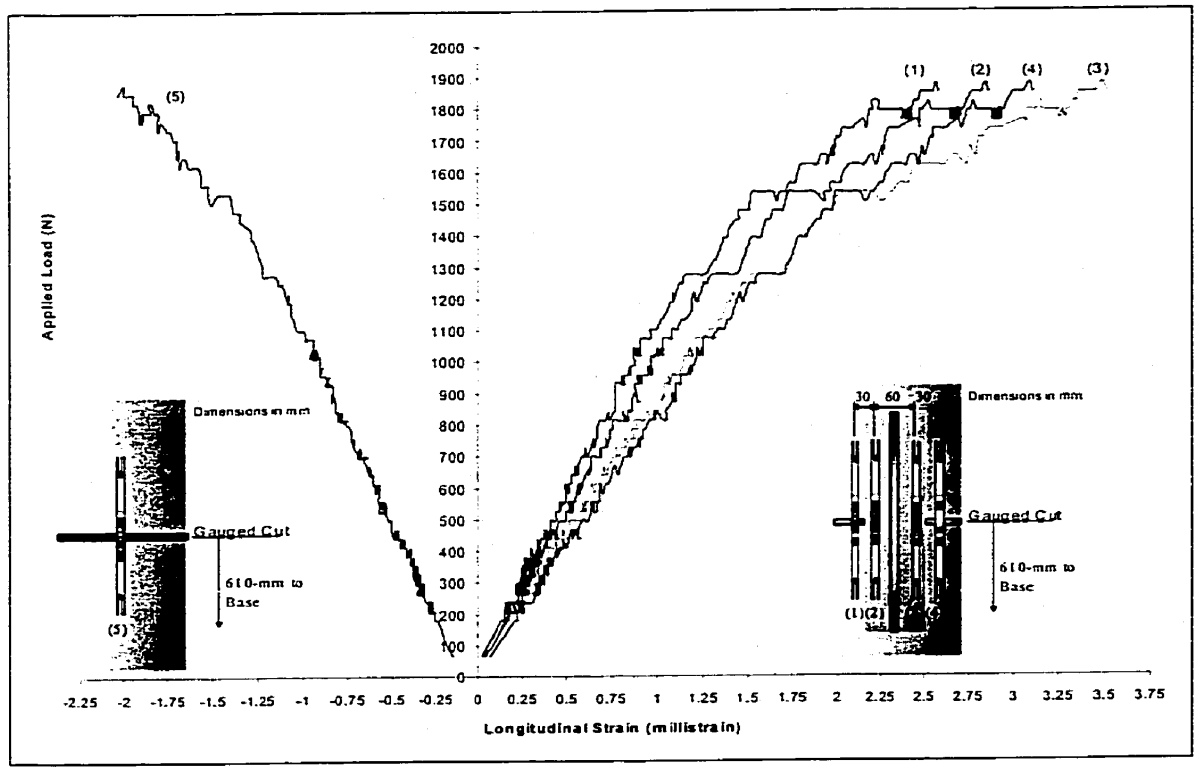

Figure 4.9 - Load- Longitudinal Strain curve for specimen P2-305-2

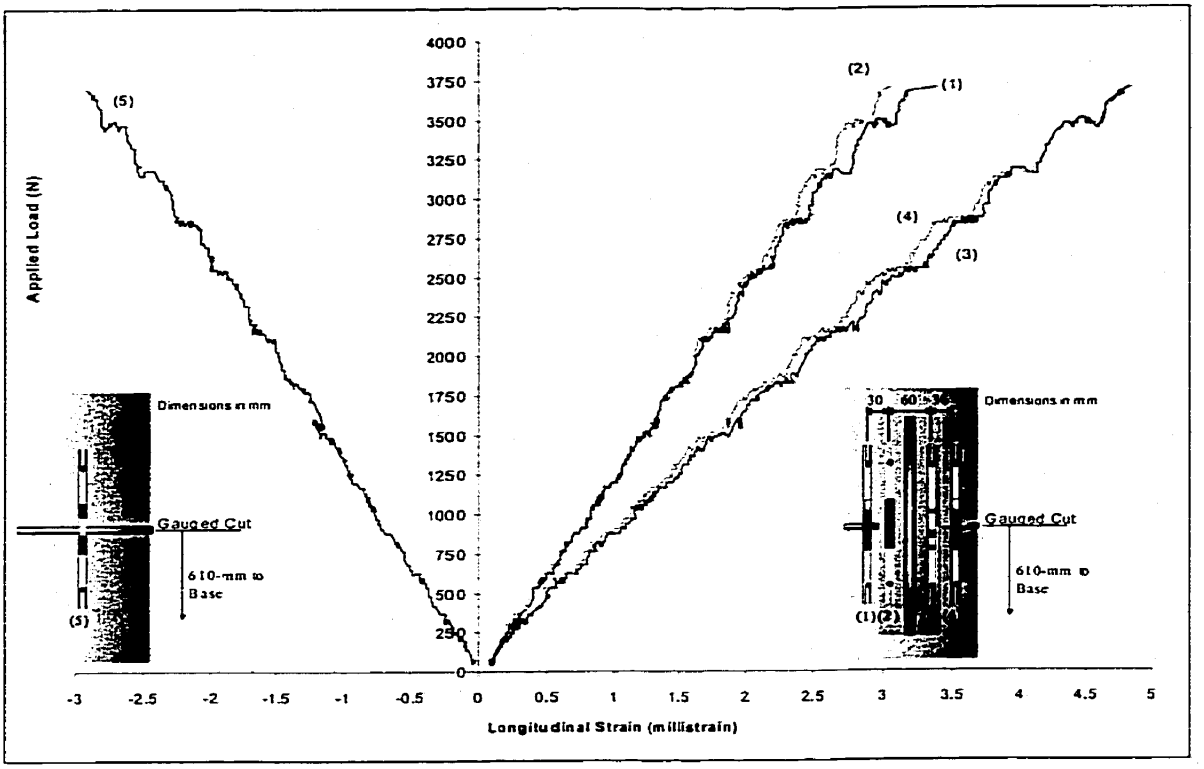

Figure 4.10- Load- Longitudinal Strain curve for specimen P2-305-3

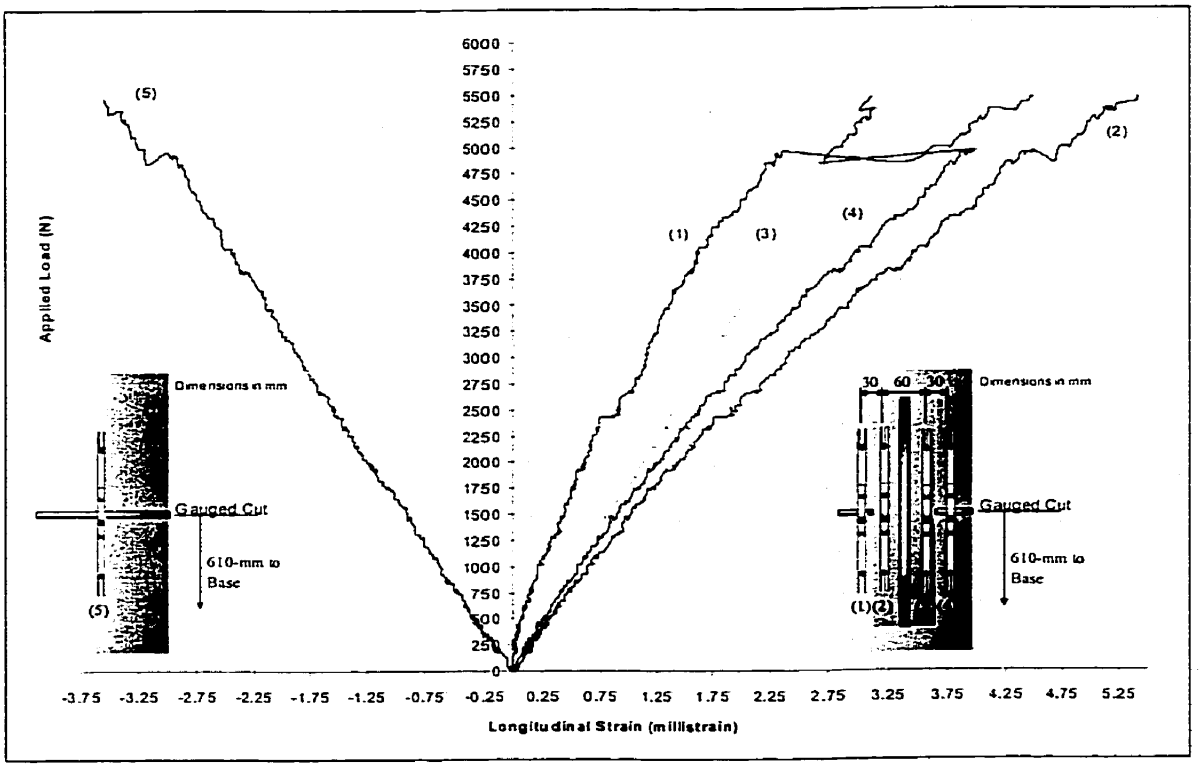

Figure 4.11 - Load- Longitudinal Strain curve for specimen P2-406-1

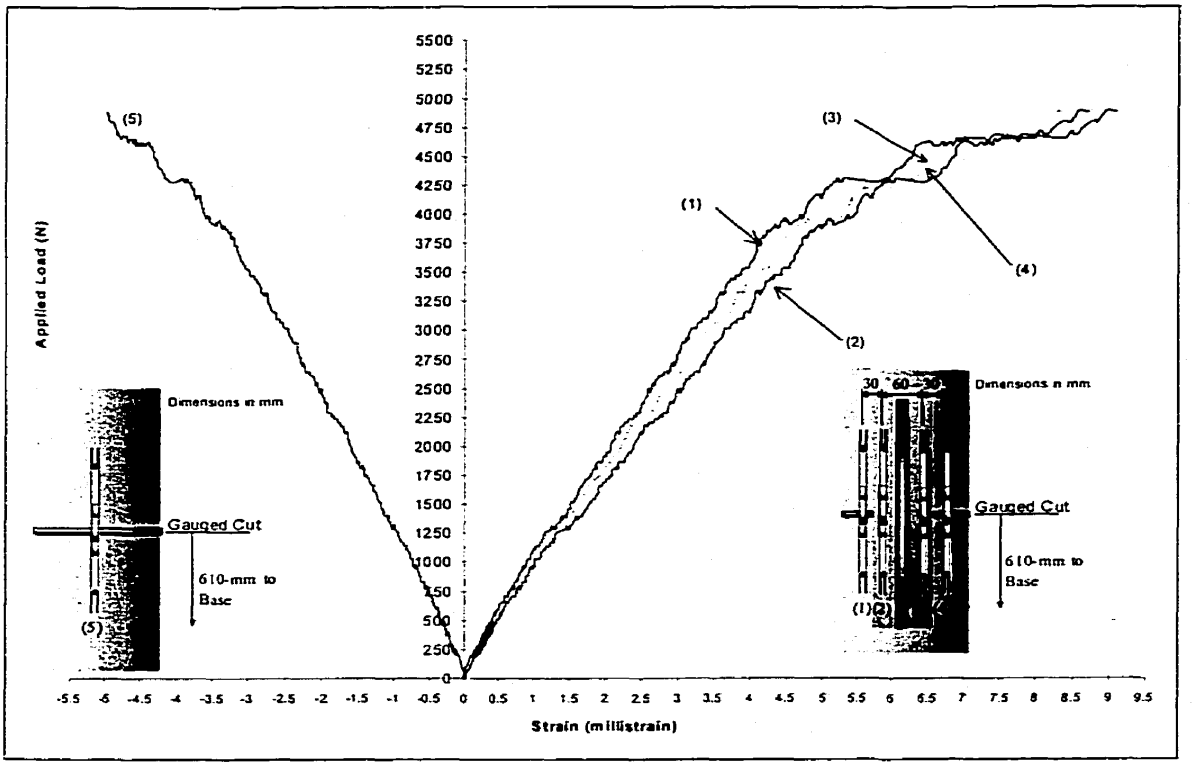

Figure 4.12- Load- Longitudinal Strain curve for specimen P2-406-2

Table 4.4 - Strains at Failure for Phase II specimens

see Figures 3.18 and 3.19 for gauge location

Specimen	Spline Length (mm)	Strain at Failure(10^{-3}) (gauge #2)	Strain at Failure(10^{-3}) (gauge #3)	Strain at Failure(10^{-3}) (gauge #5)	Strain at Failure(10^{-3}) (gauge #4)	Strain at Failure(10^{-3}) (gauge #1)
P2-203-1	203	0.18	0.81	-2.38	2.73	2.96
P2-254-1	254	3.54	4.57	-2.72	4.37	4.58
P2-305-1	305	2.92	4.18	-1.93	4.01	3.47
P2-305-2	305	2.84	3.49	-1.99	2.57	3.09
P2-305-3	305	3.05	4.82	-2.91	3.38	4.84
P2-406-1	406	5.42	1.81	-3.54	4.48	3.11
P2-406-2	406	9.09	8.38	-4.99	8.69	8.42

The bond between the splines and the wood in Phase II specimens performed adequately. From the strain profiles shown in Figures 4.6, 4.8 and 4.11, it can be

seen that specimens P2-305-1, P2-203-1, and P2-406-1 showed very little strain transfer from the flanges of the splines to the surface of the pole. The strain measured in the flanges of the FRP splines does not fit well with the strains measured in the wood. However, the strain profiles for specimens P2-254-1, P2-305-2, P2-305-3 and P2-406-2 strain profiles showed complete bonding of the flanges to the surface of the pole. The strain measured in the flanges fits very well with those measured in the wood. However, when comparing the ultimate loads of the individual specimens with the ultimate loads of specimens of similar spline lengths, it is seen that poles P2-305-1 and P2-406-1 performed better than their counterparts P2-305-2, P2-305-3 and P2-406-2. Upon investigating the cut-off sections, it was observed that the specimens that achieved good strain transfer between the flanges of the FRP spline and the surface of the pole had complete bonding between the two surfaces. However, those specimens that exhibited very little strain transfer between the flanges of the spline and the surface of the wood pole, had achieved complete bonding along the length of the groove, but not along the flanges where several voids were detected. A typical flange void is shown in Figure 4.13. From these investigations, the bonding of the spline web in the groove is more important than the bonding of the spline flanges to the pole. Although better strain transfer was observed when the bond was complete between the flange of the spline and the pole as higher capacities were recorded when the full bonding in the grooves was observed. Based on the results from Phase II, the 305-mm and 406-mm splines would be most effective in the repair of wooden poles.

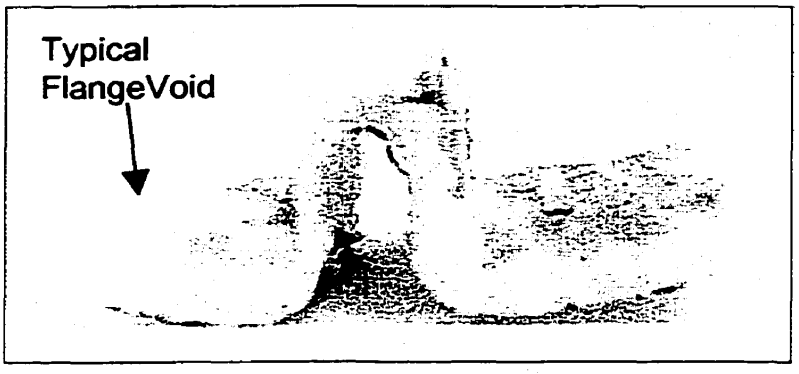

Figure 4.13 – Typical void in flange of spline after testing.

4.4 PHASE III POLES

4.4.1 Load Deflection Characteristics

In Phase III, two different spline lengths were tested based on the basis of the results from Phase II. In these specimens, 305-mm and 406-mm long splines were used. Two pole specimens were reinforced with 305-mm splines and confined by wrapping the repaired section with bi-directional tape. One pole was wrapped with two layers of tape and one was wrapped with four layers. Four poles were repaired using 405-mm splines. Two were confined in the same manner as the specimens with 305-mm splines. The remaining two specimens were reinforced with two splines with 405-mm long splines bonded to the pole using the fibre/resin interface described in Chapter 3. The type of specimens and their reinforcement schemes are listed in Table 4.5. The test results along with the ultimate loads predicted by the CSA 015-90 standard are listed in Table 4.6.

Table 4.5 – Reinforcement type of Phase III specimens.

Specimen	Spline Length (mm)	# Layers of Circumferential Wrap	Bond Type
P3-2-305-1	305	2	1
P3-4-305-2	305	4	1
P3-2-406-1	406	3	1
P3-4-406-2	406	4	1
P3-4-406-3	406	4	2
P3-4-406-4	406	4	2

(1) Bond consisted of thickened epoxy applied directly to spling and wood.
(2) Bond consisted of a fibre-resin interface next to the wood, and thickened epoxy between the fibre-resin interface and spline

Table 4.6 – Test results from Phase III.

Specimen	Ultimate Failure Load (N)	Deflection at Failure Load (mm)	Initial Failure Load (N)	Strength Prediction Based of CAN/CSA-015-90 (N)
P3-2-305-1	5620	272	4700	6940
P3-4-305-2	4490	63	4490	5460
P3-2-406-1	7000	271	7080	7210
P3-4-406-2	14190	275	14190	5020
P3-4-406-3	7953	279	7204	8670
P3-4-406-4	9430	254	7910	7490

The behavior of the specimens reinforced with 305-mm long splines was quite different than that of the specimens reinforced with 406-mm long splines. Thus, the results from the two cases are discussed separately below.

4.4.2 Poles Reinforced with 305-mm Splines

The load-deflection curves for the poles reinforced with the 305-mm splines is shown in Figure 4.14. The results indicate that the additional confinement in specimen P3-4-305-2 resulted in an increase in the stiffness of that pole.

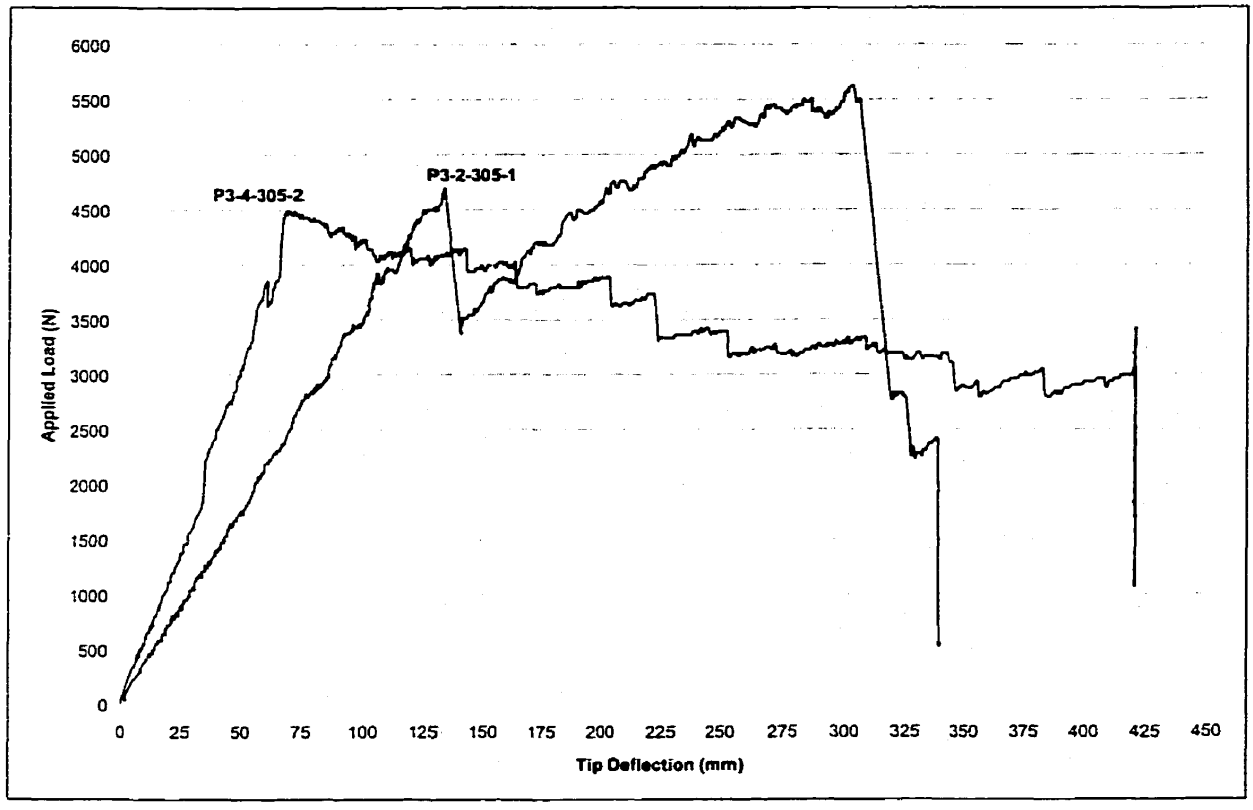

Figure 4.14 - Load-deflection curves for Phase III specimens.

Specimen P3-2-305-1, which was reinforced with the same size splines but with half the number of layers of circumferential wraps suffered an initial de-bonding of the spline from the pole at a load of 4500-N followed by shear failure through the center of the pole. The stiffness of this specimen was relatively linear until de-bonding took place. The specimen was able to sustain additional loading, but at reduced stiffness, until the bi-directional confinement wrap ruptured. The rupture started at the location of the gauged cut and worked its way up along the length of the spline until complete failure occurred. The Figure 4.15(a) shows the onset of rupture and Figure 4.15(b) shows the complete rupture of the jacket.

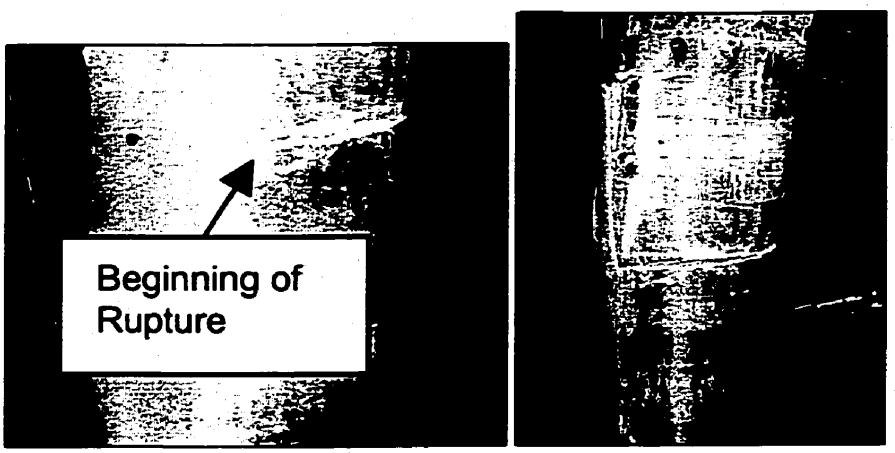

(a) (b)

Figure 4.15 - Rupture in P3-2-305-1

Specimen P3-4-305-2 failed through a combination of rupture of the FRP jacket, debonding of the spline from the pole and shear failure of the pole starting at the base of the gauged cut. The stiffness of the pole was reasonably constant until failure. At 3750-N, a drop in the load was recorded due to the debonding of the spline form the pole. The failure of specimen P3-4-305-2 is shown in Figures 4.16(a), (b) and Figure 4.17.

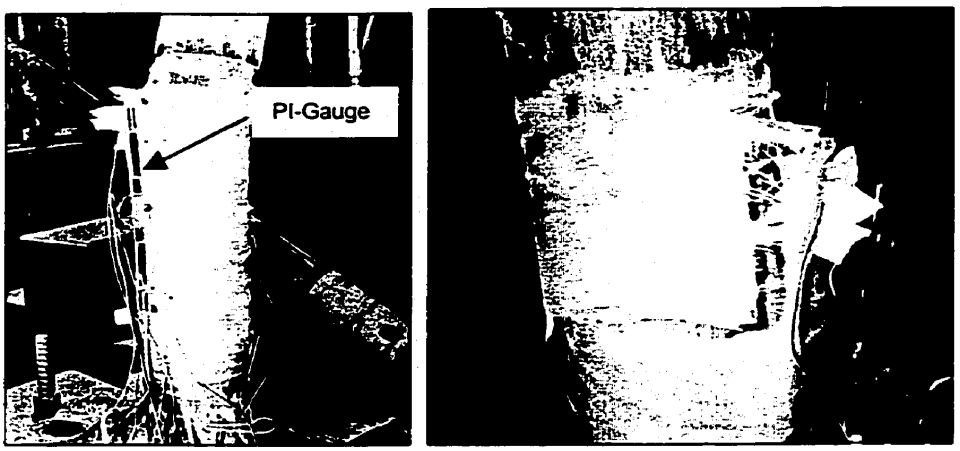

(a) (b)

Figure 4.16 – Failure in specimen P3-4-305-2

Figure 4.17 – Specimen P3-4-305-2 after testing.

On further examination of the failure zone, it was found that the spline was very poorly bonded in specimen P3-4-305-2. The resin had run out from under the spline before curing, indicating that the epoxy did not have enough viscosity to promote proper bonding, as shown in Figure 4.18.

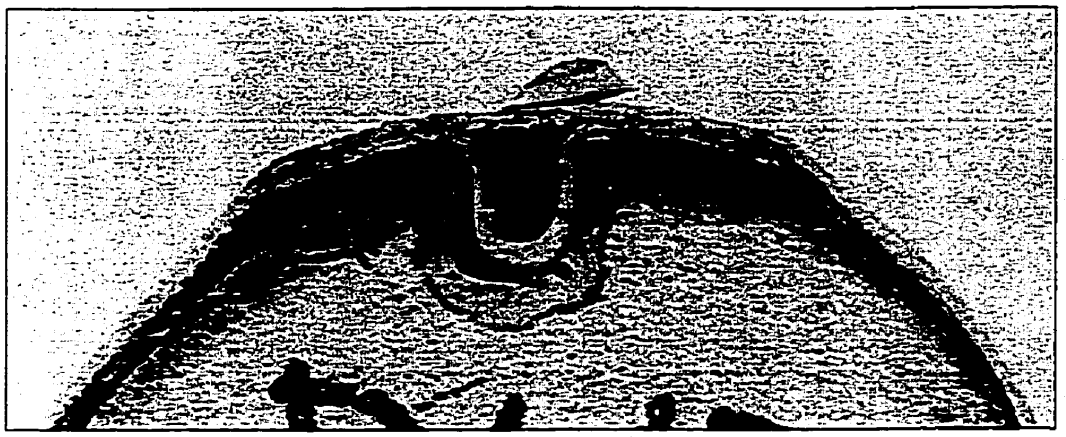

Figure 4.18 – Poor bond in specimen P3-4-305-2.

The confining action of the jacket was responsible for transferring the majority of the bending stresses to the spline. The poor bonding was also evident from the fact that the PI-gauge attached to the spline remained fixed to the pole for the duration of the test. In all other tests in which PI-gauges were used, the PI-gauges separated from the specimen at the point of debonding, as shown in Figure 4.16. Additionally, in all other specimens, additional load carrying capacity was realized after debonding of the spline. This was not the case with specimen P3-4-305-2 where the specimen reached 4490-N and continued to deflect through a decreasing load, as shown in Figure 4.14 until it failed at 3000-N.

4.4.3 Poles Reinforced with 406 mm Splines

The Load-Deflection curves for the specimens reinforced with the 406 mm splines are shown in Figure 4.19. It is evident from these plots that the additional confinement increased the stiffness of the poles.

4.3.2 Strain Distribution and Bond Performance

In Phase II, the strain in the wood was monitored at three locations, and the strain in the FRP spline was monitored in two locations. All strains were measured using PI-gauges with a gauge length of 200-mm, as was shown in Figures 3.18 and 3.19. Strains are plotted in Figures 4.7 through 4.13. The strains at failure are listed in Table 4.4. The majority of the poles were characterized by long helical cracks along the length of the pole. With the application of a load, these cracks were forced to close, and the pole twisted about their longitudinal axes. The twisting produced additional strains resulting in a non-linear load-strain diagram. In comparing the load-strain curves to the load-deflection curves, an increase in strain without an increase in deflection indicates twisting of the pole. An increase in strain with a comparable increase in deflection indicates either shear failure in the pole or debonding of the spline.

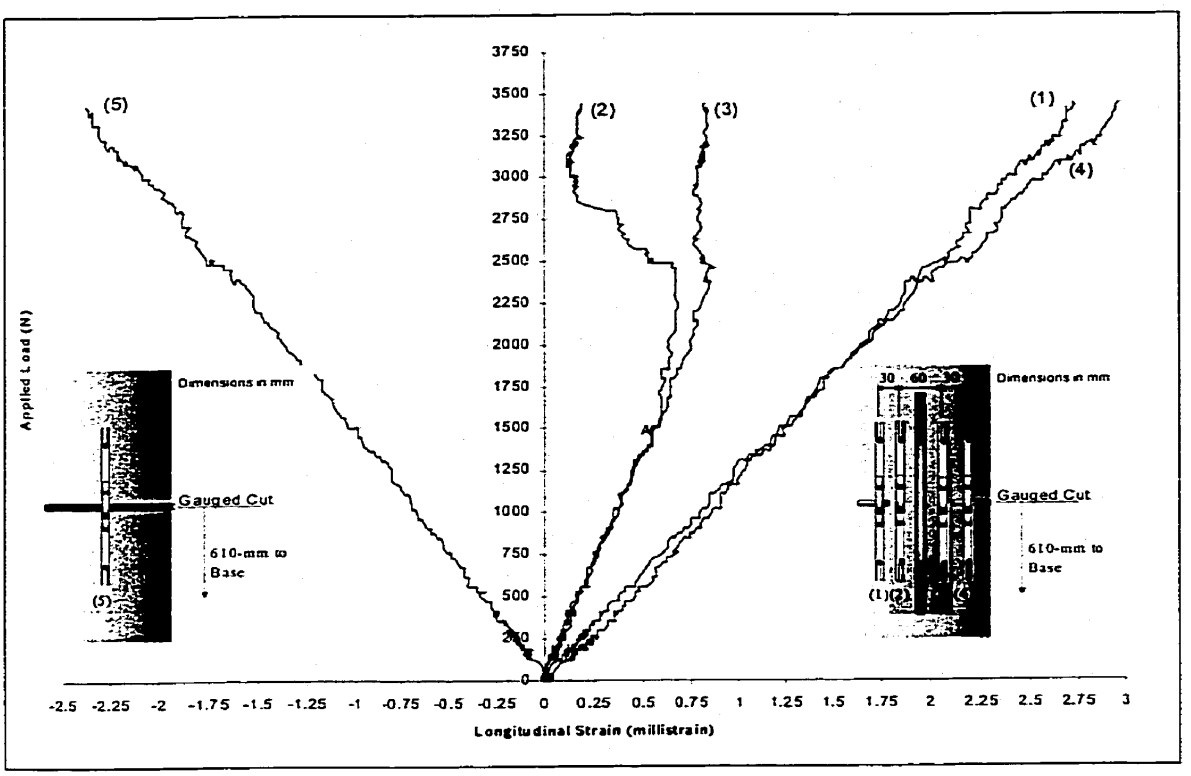

Figure 4.6 – Load-Longitudinal Strain curves for specimen P2-203-1

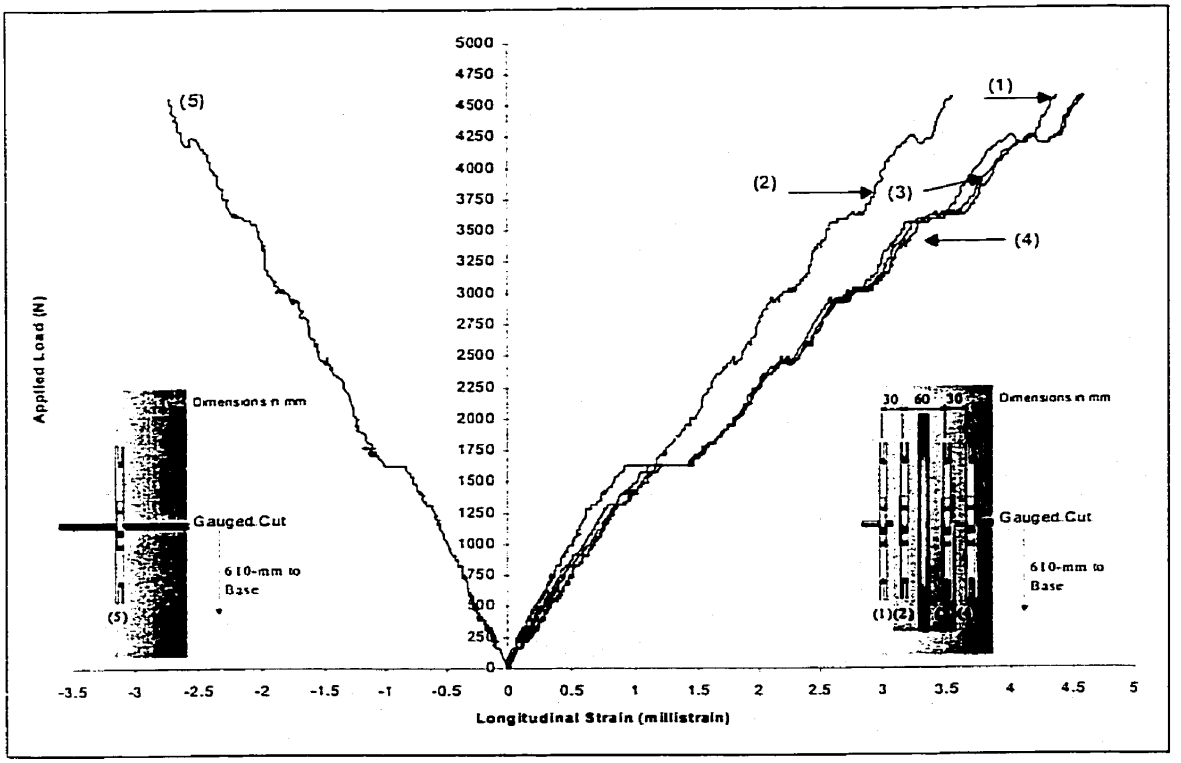

Figure 4.7 - Load- Longitudinal strain curve for specimen P2-254-1

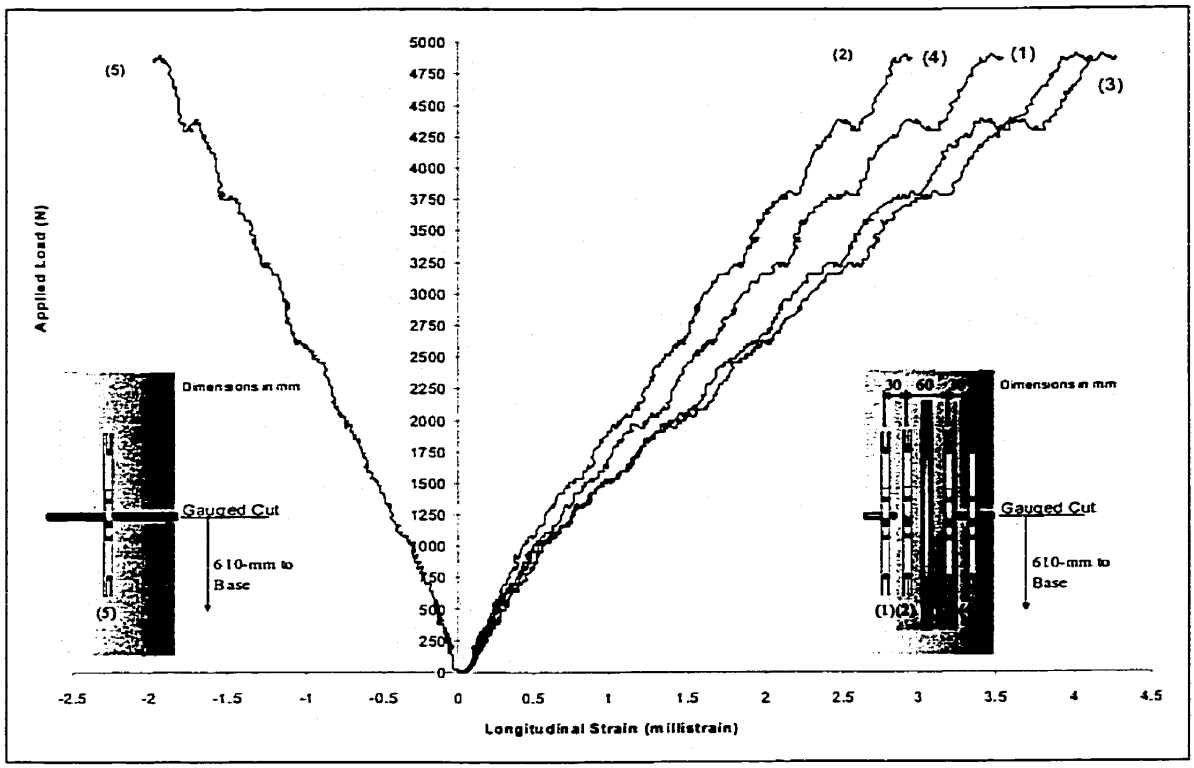

Figure 4.8 - Load-Longitudinal Strain curve for specimen P2-305-1

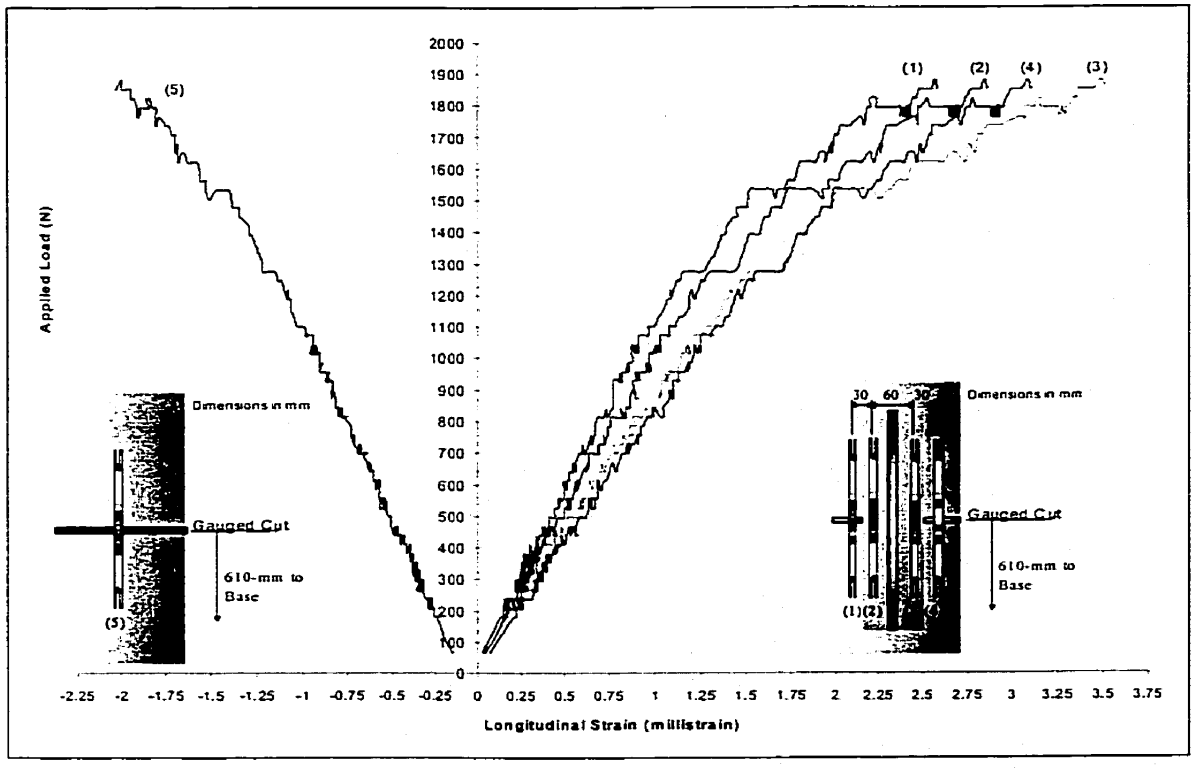

Figure 4.9 - Load- Longitudinal Strain curve for specimen P2-305-2

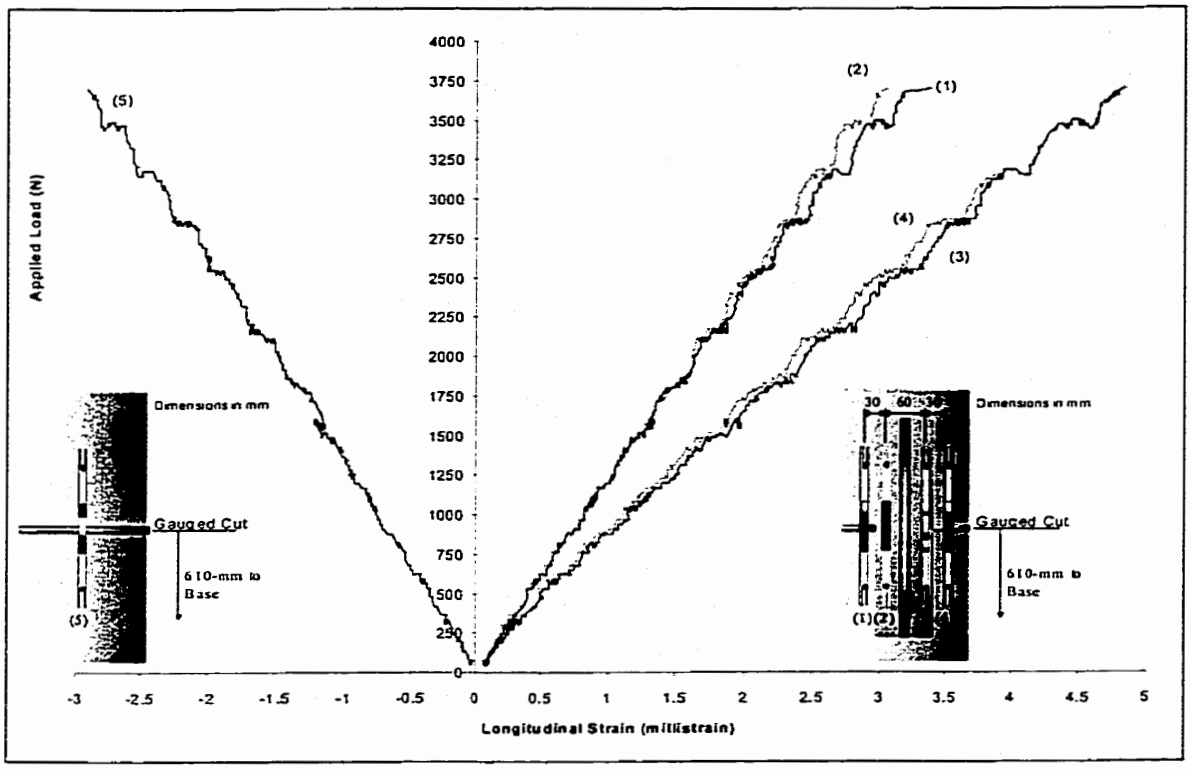

Figure 4.10- Load- Longitudinal Strain curve for specimen P2-305-3

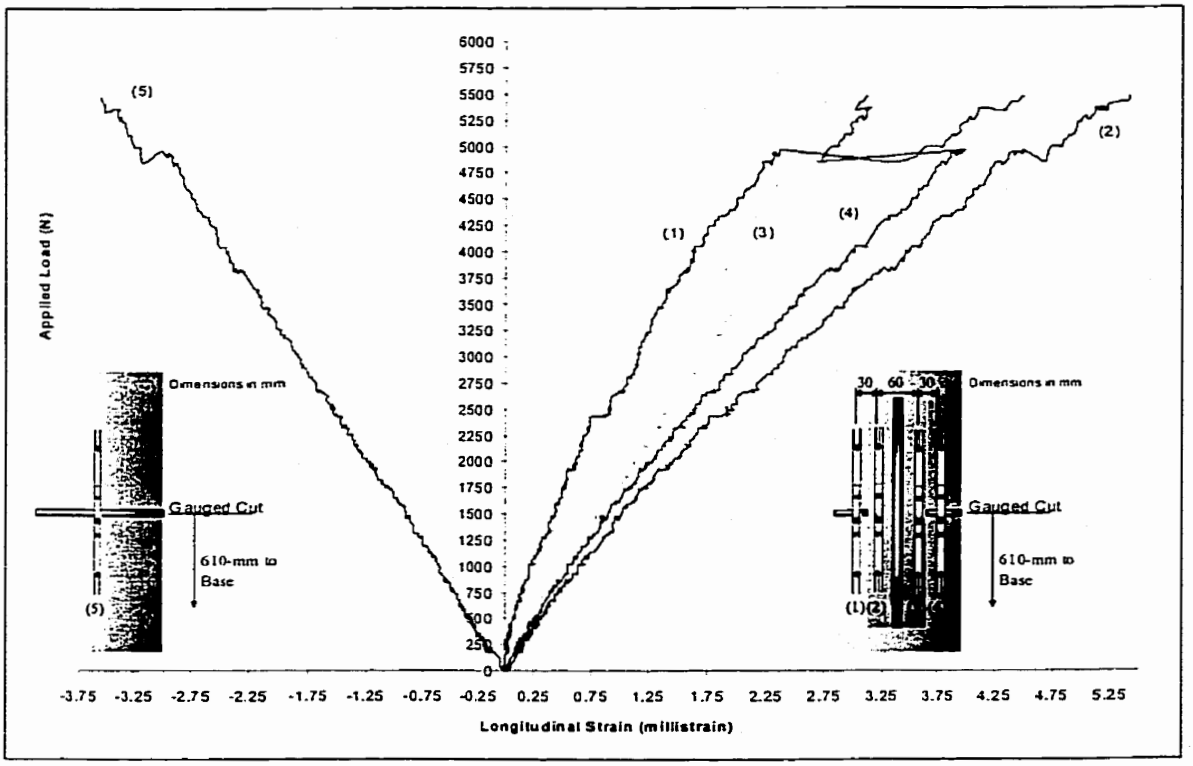

Figure 4.11 - Load- Longitudinal Strain curve for specimen P2-406-1

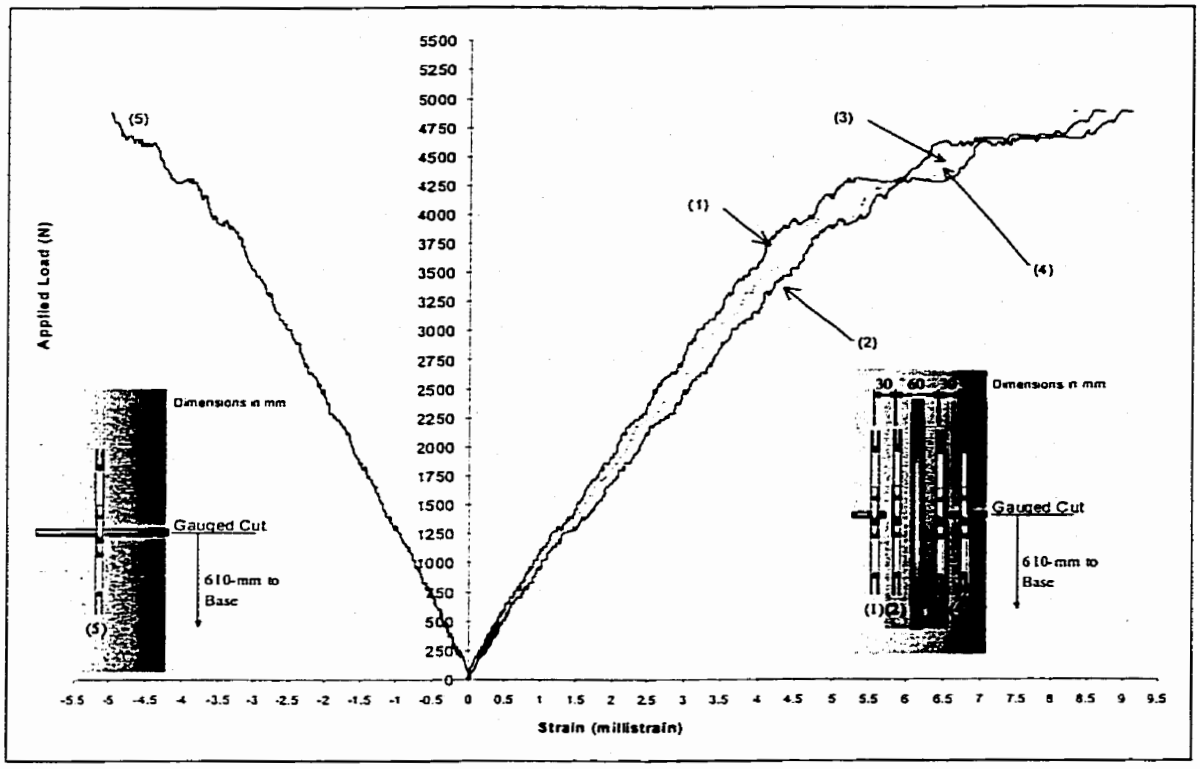

Figure 4.12- Load- Longitudinal Strain curve for specimen P2-406-2

Table 4.4 - Strains at Failure for Phase II specimens

see Figures 3.18 and 3.19 for gauge location

Specimen	Spline Length (mm)	Strain at Failure(10^{-3}) (gauge #2)	Strain at Failure(10^{-3}) (gauge #3)	Strain at Failure(10^{-3}) (gauge #5)	Strain at Failure(10^{-3}) (gauge #4)	Strain at Failure(10^{-3}) (gauge #1)
P2-203-1	203	0.18	0.81	-2.38	2.73	2.96
P2-254-1	254	3.54	4.57	-2.72	4.37	4.58
P2-305-1	305	2.92	4.18	-1.93	4.01	3.47
P2-305-2	305	2.84	3.49	-1.99	2.57	3.09
P2-305-3	305	3.05	4.82	-2.91	3.38	4.84
P2-406-1	406	5.42	1.81	-3.54	4.48	3.11
P2-406-2	406	9.09	8.38	-4.99	8.69	8.42

The bond between the splines and the wood in Phase II specimens performed adequately. From the strain profiles shown in Figures 4.6, 4.8 and 4.11, it can be

seen that specimens P2-305-1, P2-203-1, and P2-406-1 showed very little strain transfer from the flanges of the splines to the surface of the pole. The strain measured in the flanges of the FRP splines does not fit well with the strains measured in the wood. However, the strain profiles for specimens P2-254-1, P2-305-2, P2-305-3 and P2-406-2 strain profiles showed complete bonding of the flanges to the surface of the pole. The strain measured in the flanges fits very well with those measured in the wood. However, when comparing the ultimate loads of the individual specimens with the ultimate loads of specimens of similar spline lengths, it is seen that poles P2-305-1 and P2-406-1 performed better than their counterparts P2-305-2, P2-305-3 and P2-406-2. Upon investigating the cut-off sections, it was observed that the specimens that achieved good strain transfer between the flanges of the FRP spline and the surface of the pole had complete bonding between the two surfaces. However, those specimens that exhibited very little strain transfer between the flanges of the spline and the surface of the wood pole, had achieved complete bonding along the length of the groove, but not along the flanges where several voids were detected. A typical flange void is shown in Figure 4.13. From these investigations, the bonding of the spline web in the groove is more important than the bonding of the spline flanges to the pole. Although better strain transfer was observed when the bond was complete between the flange of the spline and the pole as higher capacities were recorded when the full bonding in the grooves was observed. Based on the results from Phase II, the 305-mm and 406-mm splines would be most effective in the repair of wooden poles.

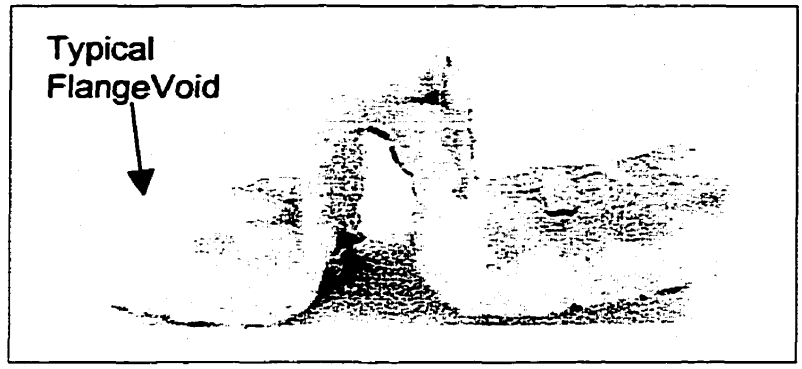

Figure 4.13 – Typical void in flange of spline after testing.

4.4 PHASE III POLES

4.4.1 Load Deflection Characteristics

In Phase III, two different spline lengths were tested based on the basis of the results from Phase II. In these specimens, 305-mm and 406-mm long splines were used. Two pole specimens were reinforced with 305-mm splines and confined by wrapping the repaired section with bi-directional tape. One pole was wrapped with two layers of tape and one was wrapped with four layers. Four poles were repaired using 405-mm splines. Two were confined in the same manner as the specimens with 305-mm splines. The remaining two specimens were reinforced with two splines with 405-mm long splines bonded to the pole using the fibre/resin interface described in Chapter 3. The type of specimens and their reinforcement schemes are listed in Table 4.5. The test results along with the ultimate loads predicted by the CSA 015-90 standard are listed in Table 4.6.

Table 4.5 – Reinforcement type of Phase III specimens.

Specimen	Spline Length (mm)	# Layers of Circumferential Wrap	Bond Type
P3-2-305-1	305	2	1
P3-4-305-2	305	4	1
P3-2-406-1	406	3	1
P3-4-406-2	406	4	1
P3-4-406-3	406	4	2
P3-4-406-4	406	4	2

(1) Bond consisted of thickened epoxy applied directly to spling and wood.
(2) Bond consisted of a fibre-resin interface next to the wood, and thickened epoxy between the fibre-resin interface and spline

Table 4.6 – Test results from Phase III.

Specimen	Ultimate Failure Load (N)	Deflection at Failure Load (mm)	Initial Failure Load (N)	Strength Prediction Based of CAN/CSA-015-90 (N)
P3-2-305-1	5620	272	4700	6940
P3-4-305-2	4490	63	4490	5460
P3-2-406-1	7000	271	7080	7210
P3-4-406-2	14190	275	14190	5020
P3-4-406-3	7953	279	7204	8670
P3-4-406-4	9430	254	7910	7490

The behavior of the specimens reinforced with 305-mm long splines was quite different than that of the specimens reinforced with 406-mm long splines. Thus, the results from the two cases are discussed separately below.

4.4.2 Poles Reinforced with 305-mm Splines

The load-deflection curves for the poles reinforced with the 305-mm splines is shown in Figure 4.14. The results indicate that the additional confinement in specimen P3-4-305-2 resulted in an increase in the stiffness of that pole.

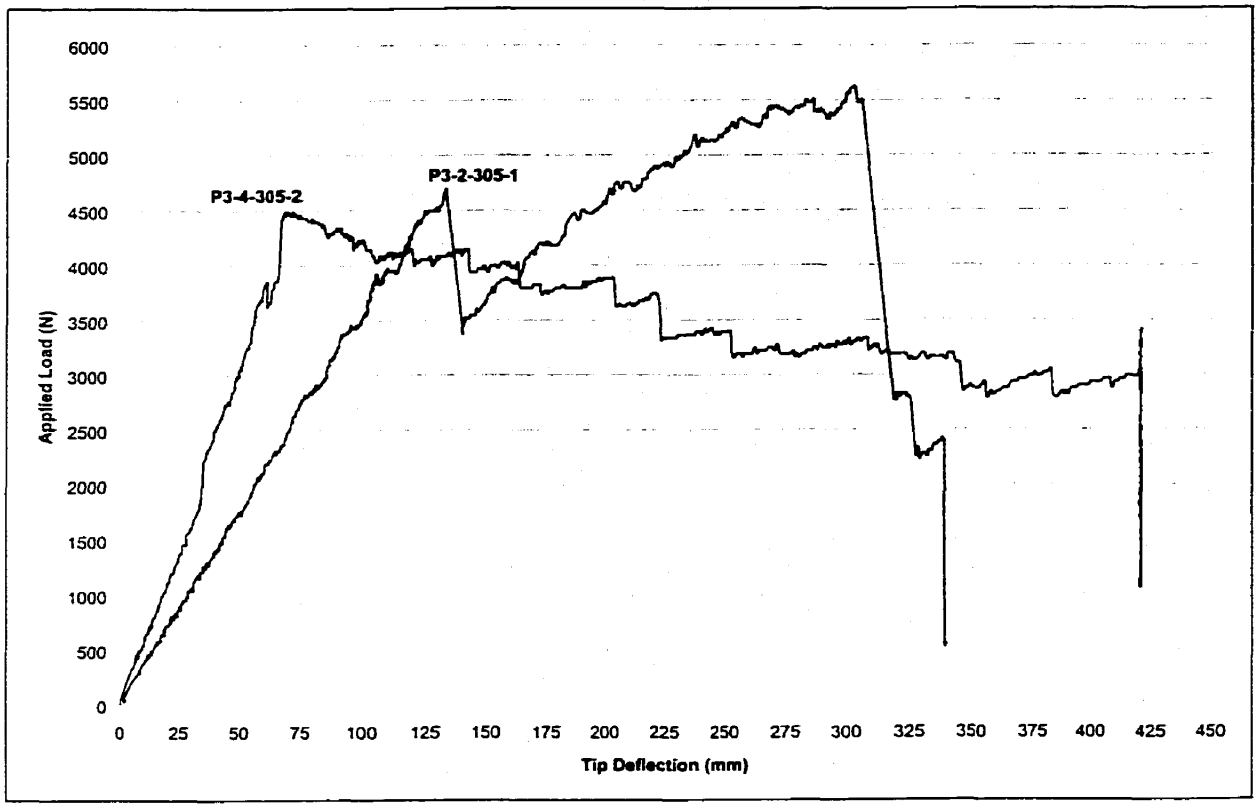

Figure 4.14 - Load-deflection curves for Phase III specimens.

Specimen P3-2-305-1, which was reinforced with the same size splines but with half the number of layers of circumferential wraps suffered an initial de-bonding of the spline from the pole at a load of 4500-N followed by shear failure through the center of the pole. The stiffness of this specimen was relatively linear until de-bonding took place. The specimen was able to sustain additional loading, but at reduced stiffness, until the bi-directional confinement wrap ruptured. The rupture started at the location of the gauged cut and worked its way up along the length of the spline until complete failure occurred. The Figure 4.15(a) shows the onset of rupture and Figure 4.15(b) shows the complete rupture of the jacket.

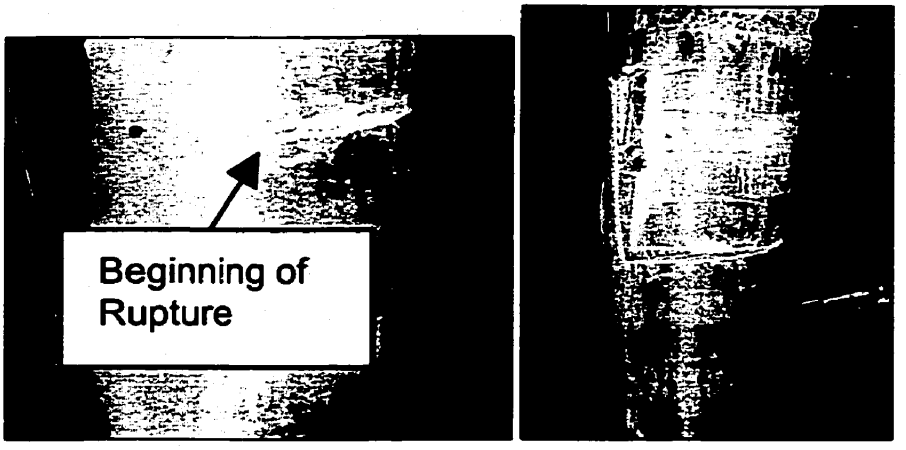

(a) *(b)*

Figure 4.15 - Rupture in P3-2-305-1

Specimen P3-4-305-2 failed through a combination of rupture of the FRP jacket, debonding of the spline from the pole and shear failure of the pole starting at the base of the gauged cut. The stiffness of the pole was reasonably constant until failure. At 3750-N, a drop in the load was recorded due to the debonding of the spline form the pole. The failure of specimen P3-4-305-2 is shown in Figures 4.16(a), (b) and Figure 4.17.

(a) *(b)*

Figure 4.16 – Failure in specimen P3-4-305-2

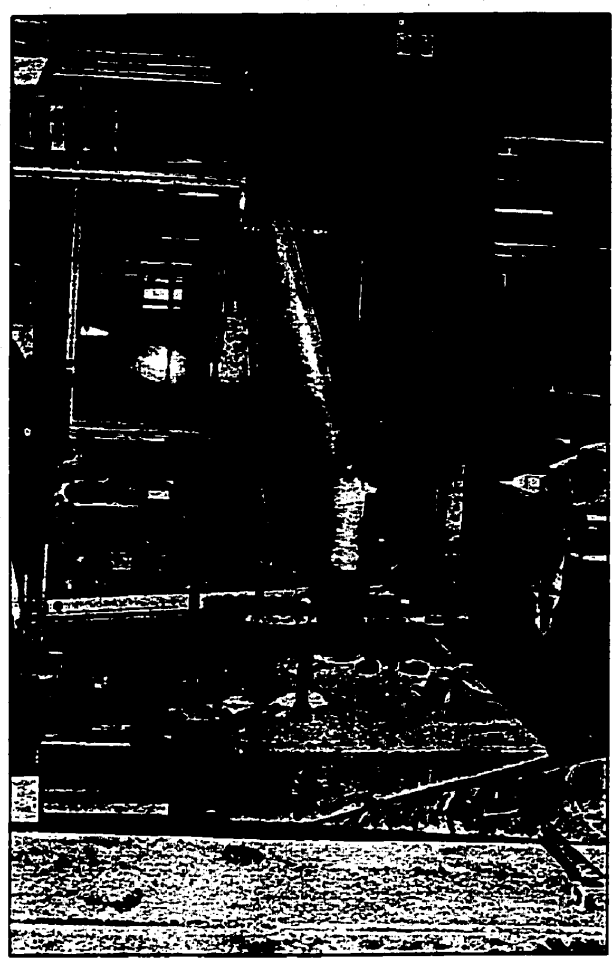

Figure 4.17 – Specimen P3-4-305-2 after testing.

On further examination of the failure zone, it was found that the spline was very poorly bonded in specimen P3-4-305-2. The resin had run out from under the spline before curing, indicating that the epoxy did not have enough viscosity to promote proper bonding, as shown in Figure 4.18.

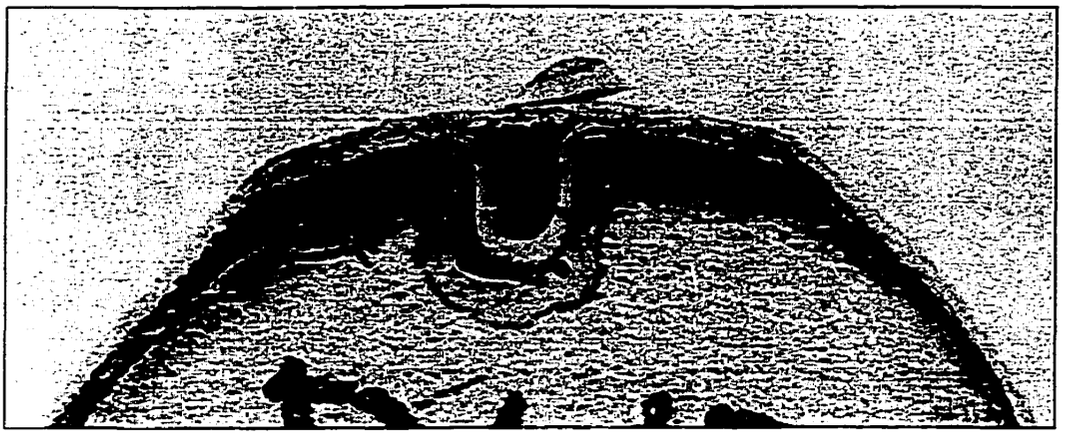

Figure 4.18 – Poor bond in specimen P3-4-305-2.

The confining action of the jacket was responsible for transferring the majority of the bending stresses to the spline. The poor bonding was also evident from the fact that the PI-gauge attached to the spline remained fixed to the pole for the duration of the test. In all other tests in which PI-gauges were used, the PI-gauges separated from the specimen at the point of debonding, as shown in Figure 4.16. Additionally, in all other specimens, additional load carrying capacity was realized after debonding of the spline. This was not the case with specimen P3-4-305-2 where the specimen reached 4490-N and continued to deflect through a decreasing load, as shown in Figure 4.14 until it failed at 3000-N.

4.4.3 Poles Reinforced with 406 mm Splines

The Load-Deflection curves for the specimens reinforced with the 406 mm splines are shown in Figure 4.19. It is evident from these plots that the additional confinement increased the stiffness of the poles.

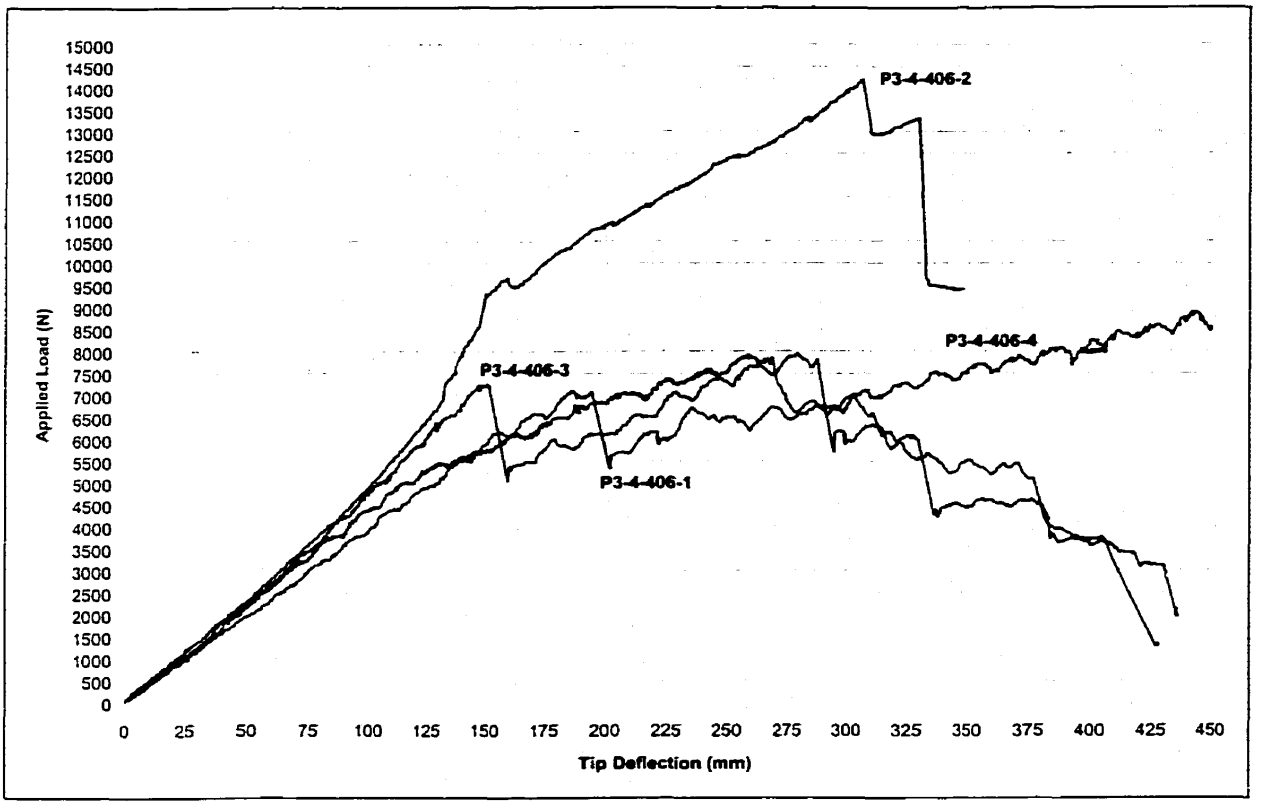

Figure 4.19 – Load-deflection curves for Phase III poles

Pole P3-2-406-1 failed through a combination of debonding of the spline from the pole and shear. The specimen was able to resist additional loading but at a lower stiffness until the bi-directional confinement wrap ruptured. The rupture started at the location of the gauged cut and worked its way up along the length of the spline until complete failure occurred, in a manner very similar to that observed in specimen P3-2-305-1, as shown in Figure 4.20.

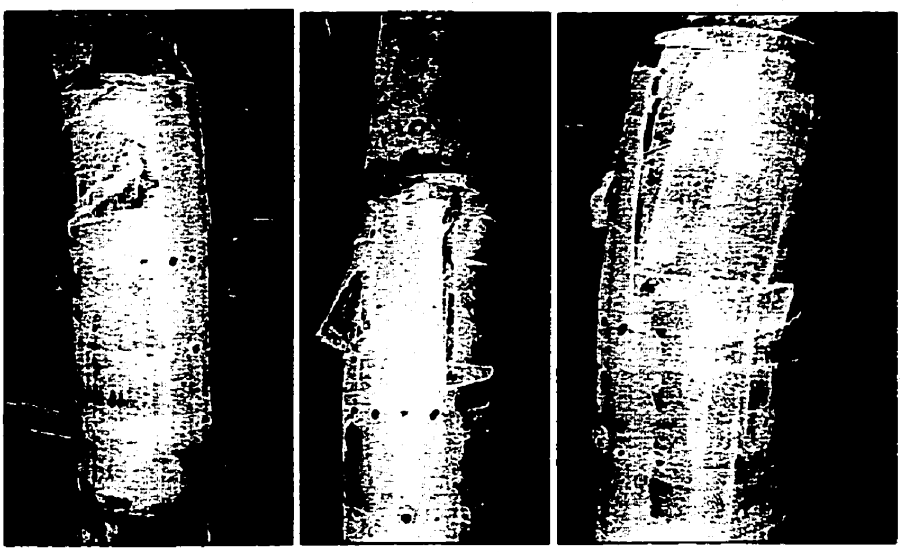

(a) (b) (c)

Figure 4.20 – Specimen P3-2-406-1 after failure

An examination of the cross-section after failure revealed that the spline was not bonded properly to the pole and that a shear crack was present, as shown in Figure 4.21.

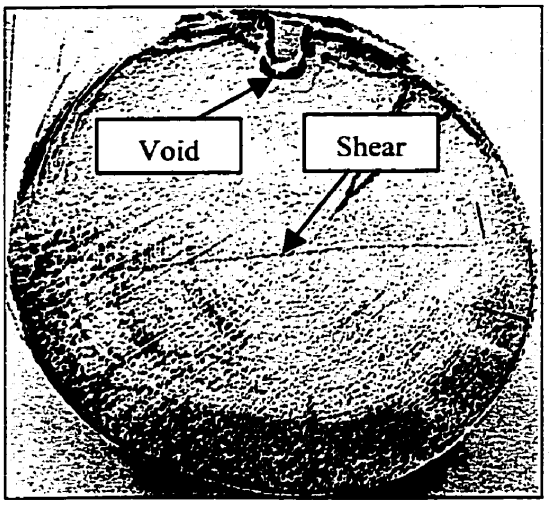

Figure 4.21 – Cross-section of specimen P3-2-406-1 after failure.

Specimen P316-2-2 failed in tension at the base between the repaired zone and the testing base. This pole had an odd geometry because it was tapered at both the top and the bottom. This specimen achieved the highest load capacity among all specimens tested, including the control poles. No debonding of the spline was observed.

Figure 4.22 – Specimen P3-4-406-2 after failure.

Specimen P3-4-406-3 failed initially on the compression side near the base, as shown in Figure 4.23(a). This failure was followed by shear failure of the wood at the base of the spline, as shown in Figure 4.23(b). No debonding of the spline was recorded for pole P3-4-406-3. Further examination of the cross section after failure revealed that the bond was uniform and developed well enough to cause shear failure in the wood at the base of the spline, as shown Figure 4.24. As in

previous specimens, a shear crack was observed projecting from the base of the gauged cut, although not as prominent as in previous experiments.

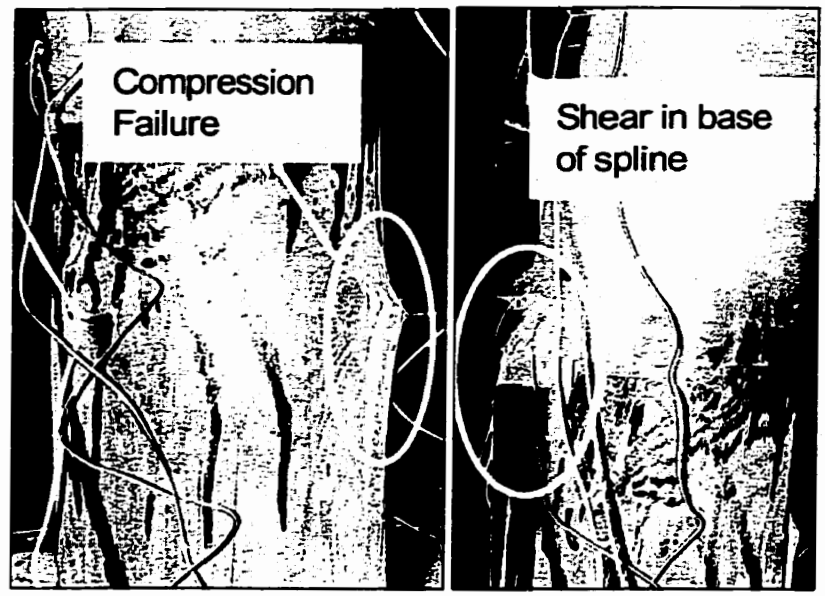

Figure 4.23 – Specimen P3-4-406-3 after failure.

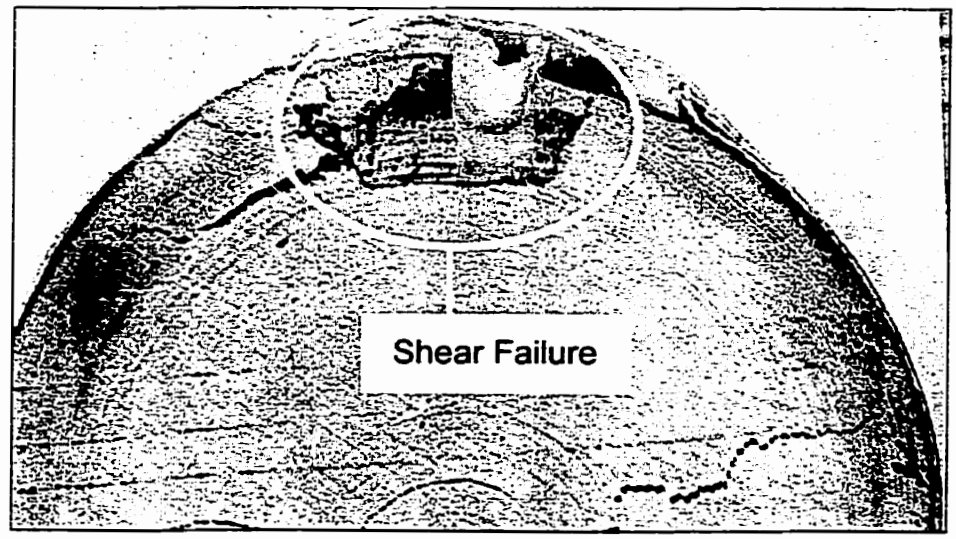

Figure 4.24 – Cross-section of specimen P3-4-406-3 after failure.

Specimen P3-4-406-4 failed mainly through shear failure along the centerline starting at the base of the gauged cut causing splitting the pole on both sides of the cut. Some tension failure at the base was also observed. The spline reinforcement remained bonded to the pole for the duration of the test. Some localized debonding of one of the flanges and the wrap were observed above the gauged cut, as shown in Figure 4.25. Upon further investigation of the specimen after failure, it was found that the specimen split into two parts, each sliding with respect to the other, as shown in Figure 4.26. The cross-sections revealed a very good bond between the spline and the pole, as shown in Figure 4.25. The small drops shown in the load-deflection curve of Figure 4.19 are due to cracking of the wood.

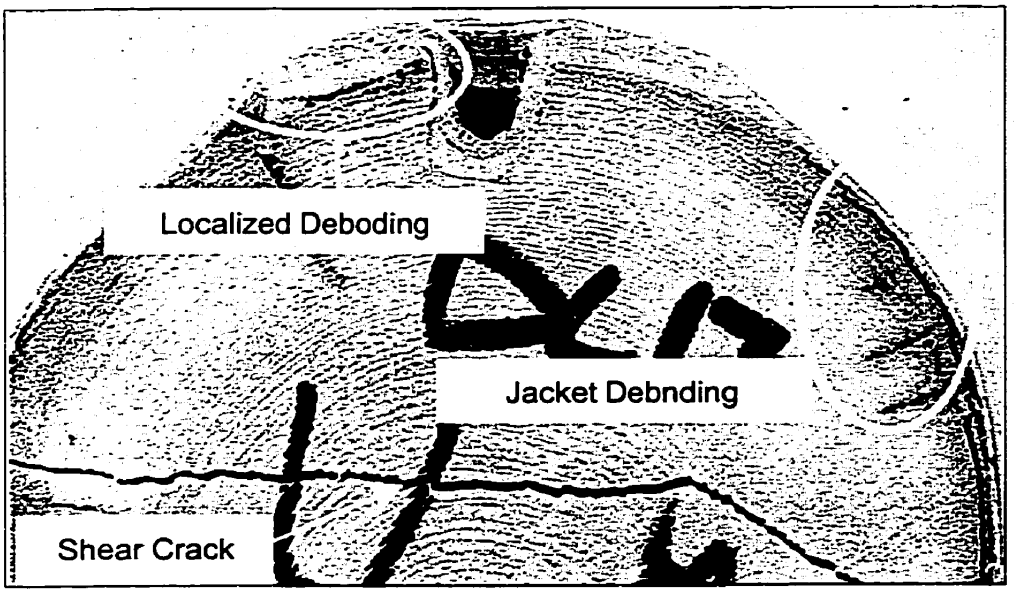

Figure 4.25 - Bond in specimen P3-4-406-4

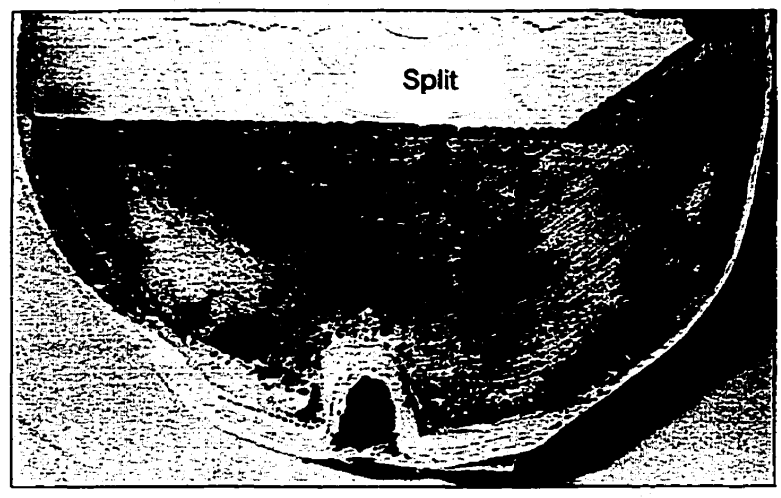

Figure 4.26 - Specimen P3-4-406-4 after testing.

4.4.4 Strain Characteristics of Phase III

The strain in specimen P3-2-305-1 was monitored at six locations using 200 mm PI-gauges as was shown in Figure 3.23 and 3.24. The load- strain curves are shown in Figure 4.27. Unfortunately, when the spline separated from the pole, the PI-gauges were also detached from the pole, so continuous monitoring of the strain was not possible for this specimen. However, the strains before the spline separated are comparable to the strains recorded in Phase II for Poles P2-305-1 and P2-305-2, indicating that the FRP jacket did not enhance the bond of the spline to the pole. Rather, it was the confining action provided by the jacket that contributed to the increased strength.

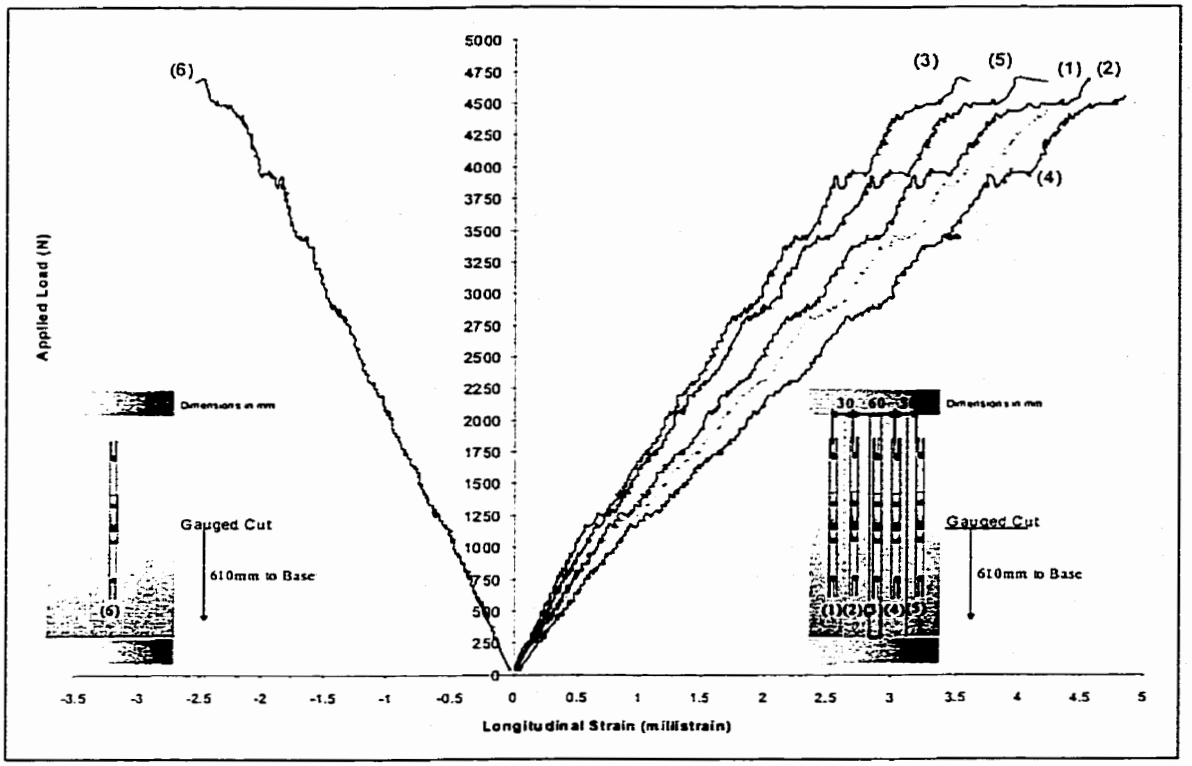

Figure 4.27 –Load-Longitudinal Strain curve for specimen P3-2-305-1

In specimen P3-4-305-2 strain gauges were used to measure the longitudinal and transverse strains in the FRP, as well as a 200 mm PI-gauge, as shown in Figure 3.25 and 3.26. The load-strain curves are shown in Figure 4.28 and Figure 4.29. A noticeable drop in the strains is observed with the addition of additional confinement layers. The highest strain was recorded over the gauged cut.

The load-longitudinal strain curves shown in Figure 4.28 indicate a slight decrease in strain at a load of 3750-N for specimen P3-4-305-2. The load-transverse strain curve, exhibit a rapid increase in the transverse strains indicating that the upper portion of the spline had completely debonded from the

pole, and began to bear fully against the jacket. The longitudinal strain recorded directly over the gauged cut when the spline debonded was 2.1-millistrain. After debonding the transverse strain in the FRP jacket increased to 3.5 millistrain before rupturing.

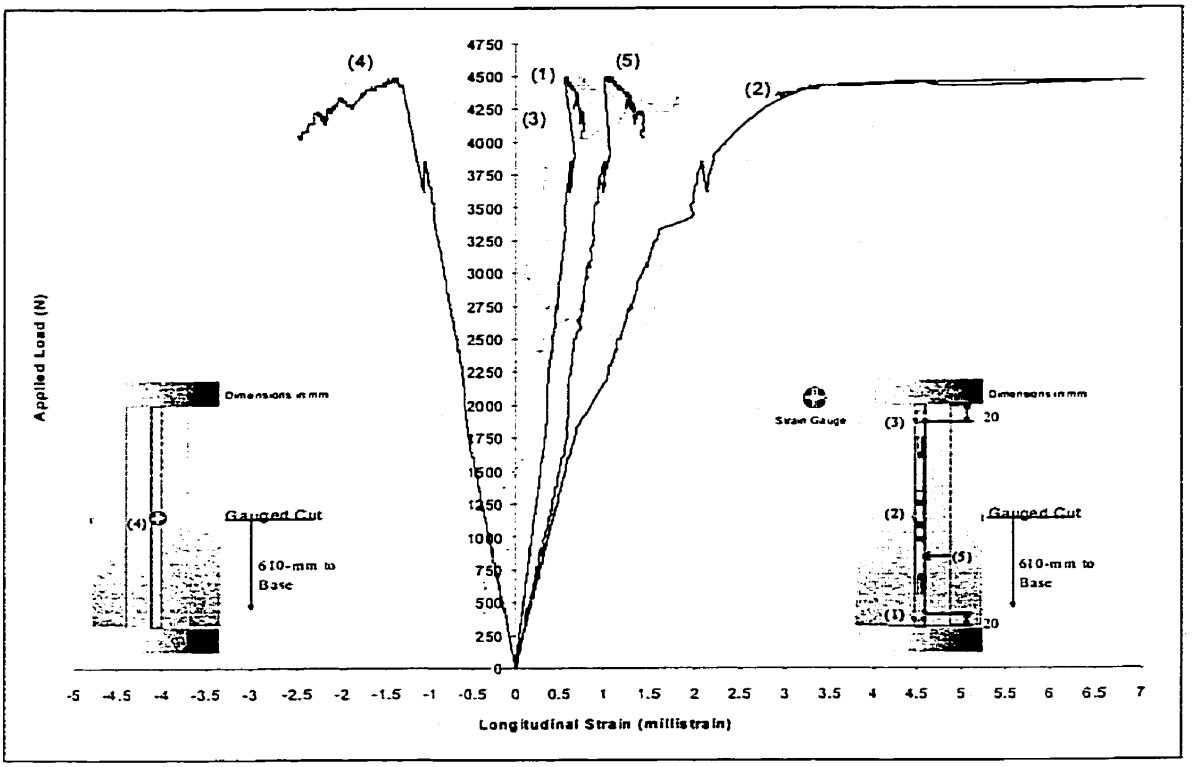

Figure 4.28 – Load-Longitudinal Strain curves for specimen P3-4-305-2

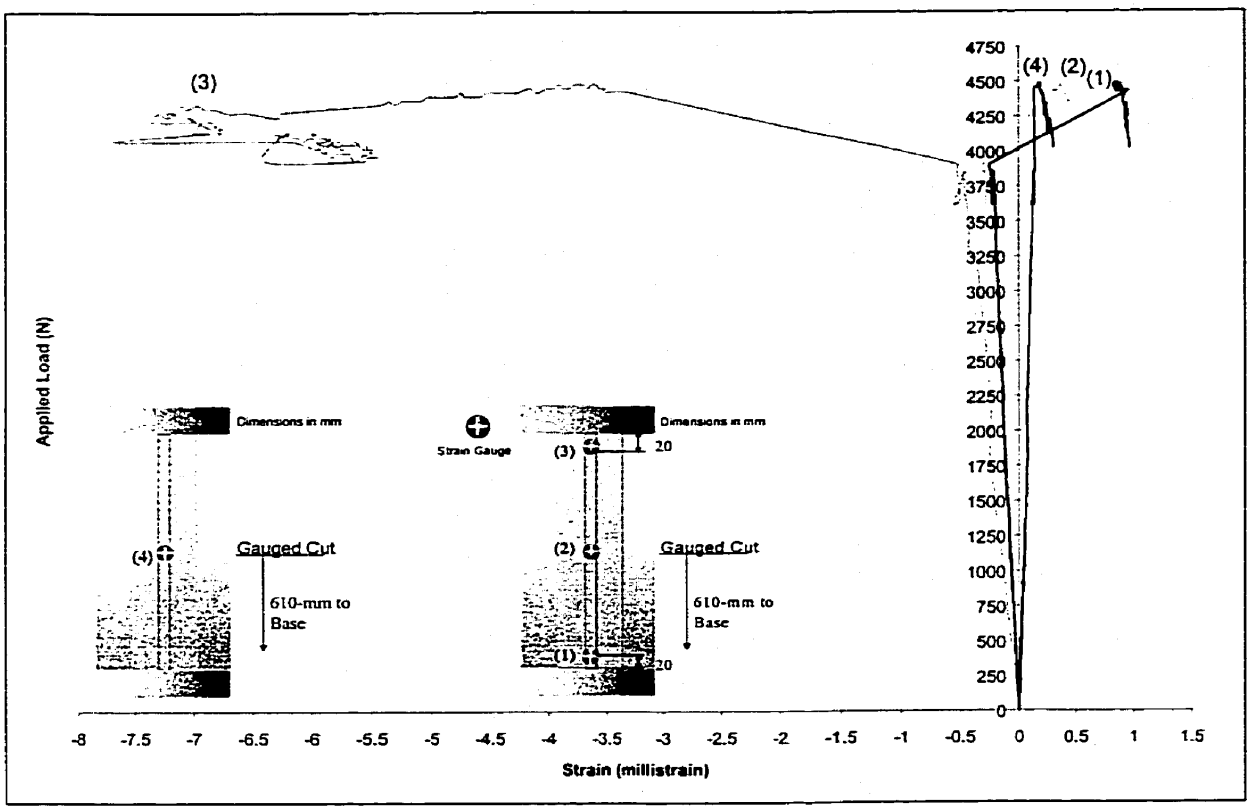

Figure 4.29 – Load-Transverse Strain curves for specimen P3-4-305-2

Specimen P3-2-406-1 failed in a manner similar to P3-2-305-1, beginning with debonding of the spline and followed by rupture of the composite jacket. The instrumentation for this specimen is shown in Figure 3.25 and 3.26. As in the case of specimen P3-2-305-1, the PI-gauges separated from the pole when the splines debonded and so continuous monitoring of the strains was not possible. In addition, one of the gauges did not function and was not included in the discussion of the results. It is interesting to note that the maximum strains in this specimen when debonding occurred are similar to those obtained in specimen P2-406-2. These strains and loads are considerably higher than those recorded

in the specimens reinforced with the 305-mm splines, indicating that the 405-mm splines provided increased capacity.

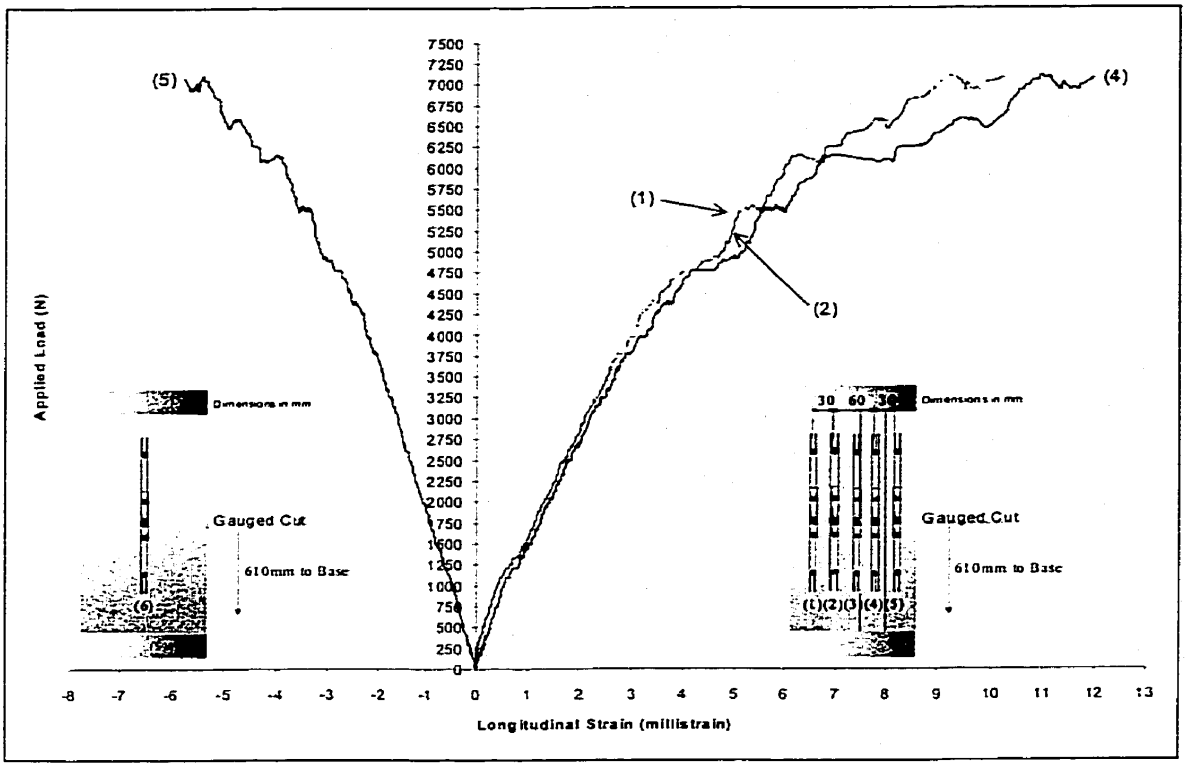

Figure 4.30 - Load - longitudinal strain curve for specimen P3-2-406-1

Specimen P3-4-406-2 failed at the base at a considerably higher load than the other specimens. This specimen achieved an ultimate load of 14190-N. No debonding of the spline was evident. From the load-longitudinal strain curves, shown in Figure 4.31, it was observed that there was a significant drop in strain at a load of 8500-N. There was only a minor change in the stiffness of the specimen at that level, as shown in the load-deflection curve, Figure 4.19. The load-longitudinal strain curve for specimen P3-4-406-2, as shown in Figure 4.31, shows a reverse in the strains recorded at this load. These results indicate that

the specimen failed mainly due to torsional effects induced by helical cracks in the pole

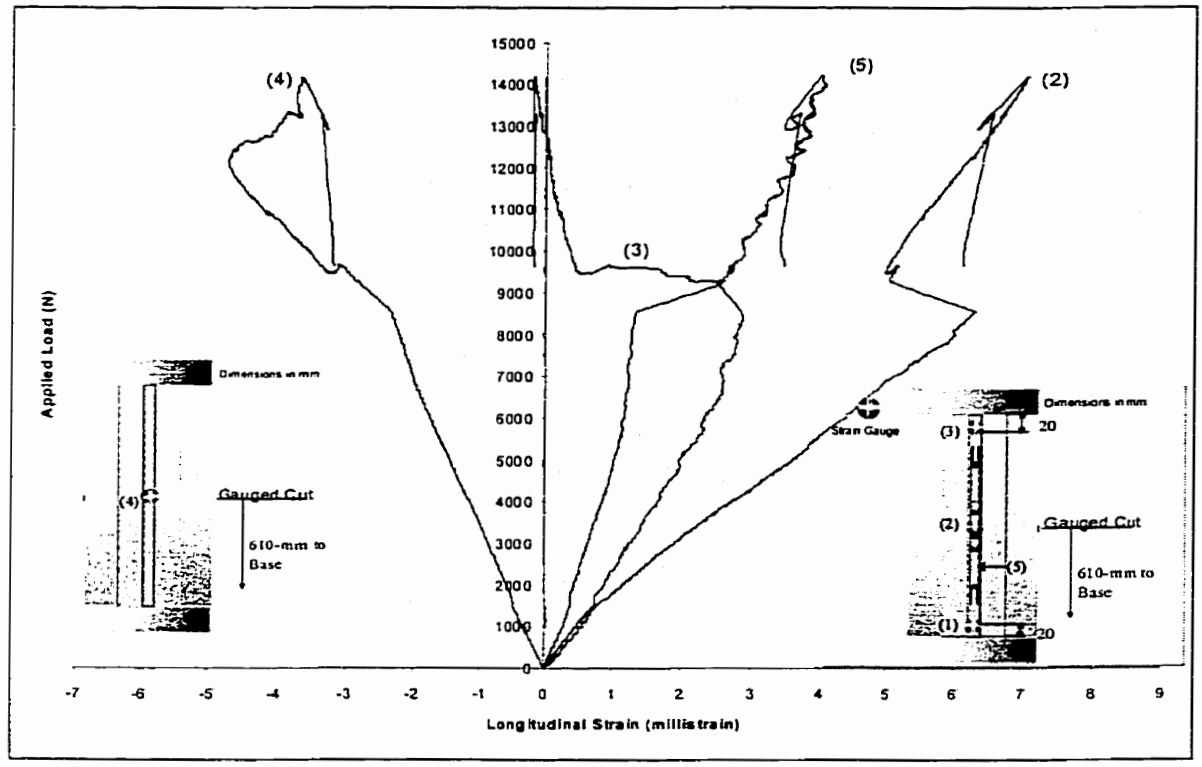

Figure 4.31 - Load – longitudinal strain curve for specimen P3-4-406-2

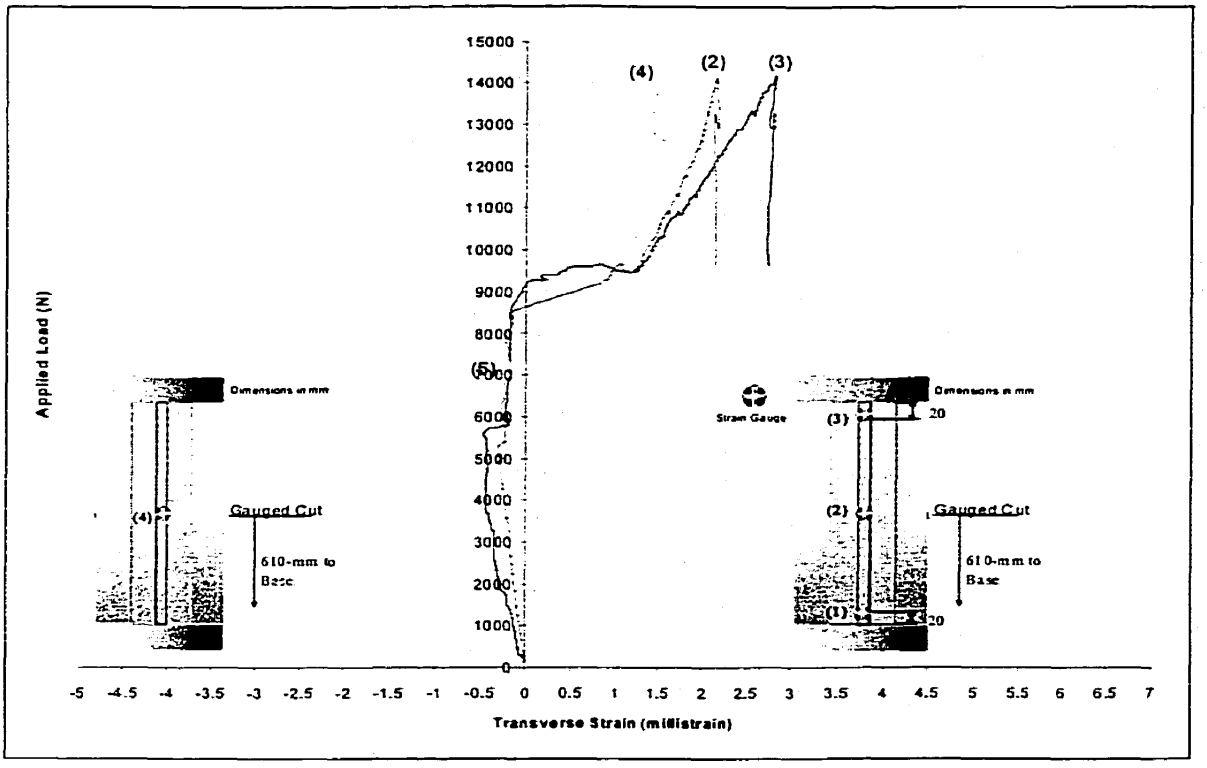

Figure 4.32 - Load - transverse strain curve for specimen P3-4-406-2

Specimens P3-4-406-3 and P3-4-406-4 were tested to determine the effect of saturating the groove with epoxy prior to placing the spline. As described in Chapter 3, this involved the placement of a wet layer of fabric in the groove. The load-deflection curves show that this technique was successful, as only some localized debonding occurred in specimens P3-4-406-3 and P3-4-406-4.

In specimen P3-4-406-3, the bond was developed well enough to cause failure in the wood due to shear, as shown in Figure 4.24. The highest strain, 13.5-millistrain, was recorded at the base of the spline, which is consistent with the shear failure in the wood at the base of the spline, as shown in Figure 4.33. The strain recorded with the PI-gauge is comparable to the strains measured in

specimen P3-2-406-1. The load-transverse strain curve for specimen P3-4-406-3 is shown in Figure 4.34. From these plots, it is observed that the spline remained attached to the pole, as no sharp increase in transverse strain was recorded, indicating the spline was bearing against the jacket.

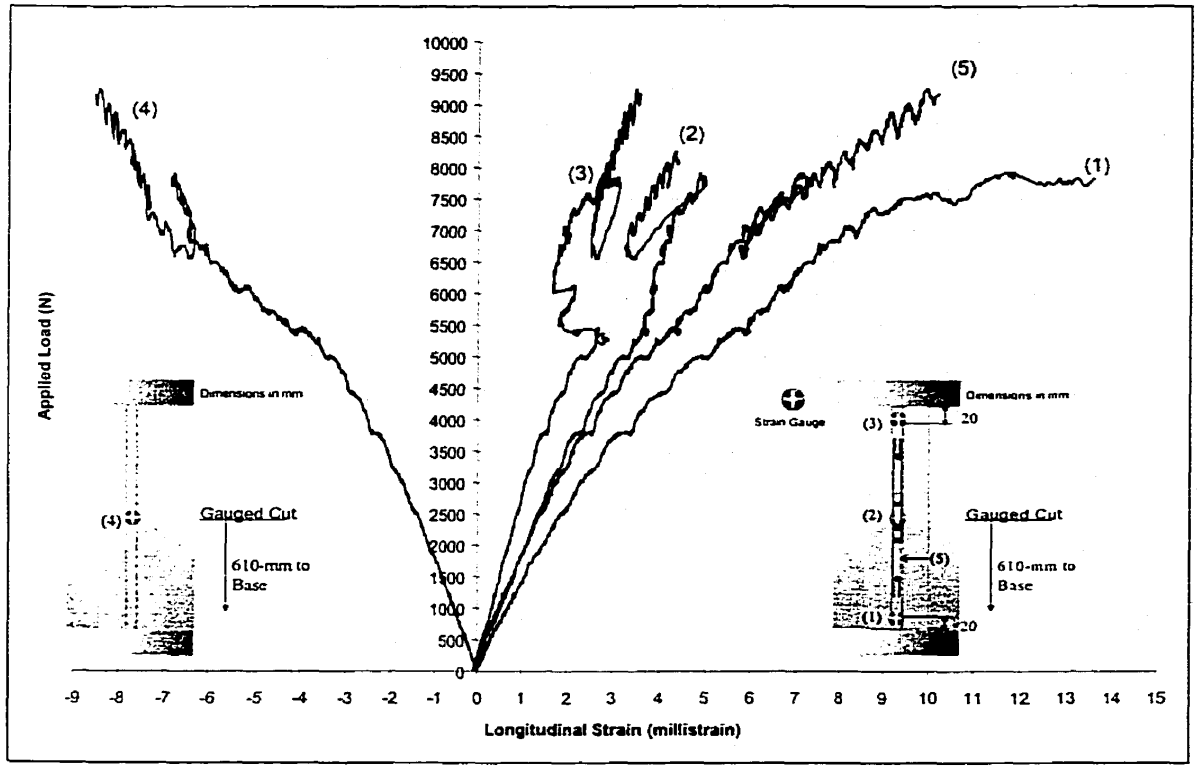

Figure 4.33 - Load - longitudinal strain curve for specimen P3-4-406-3

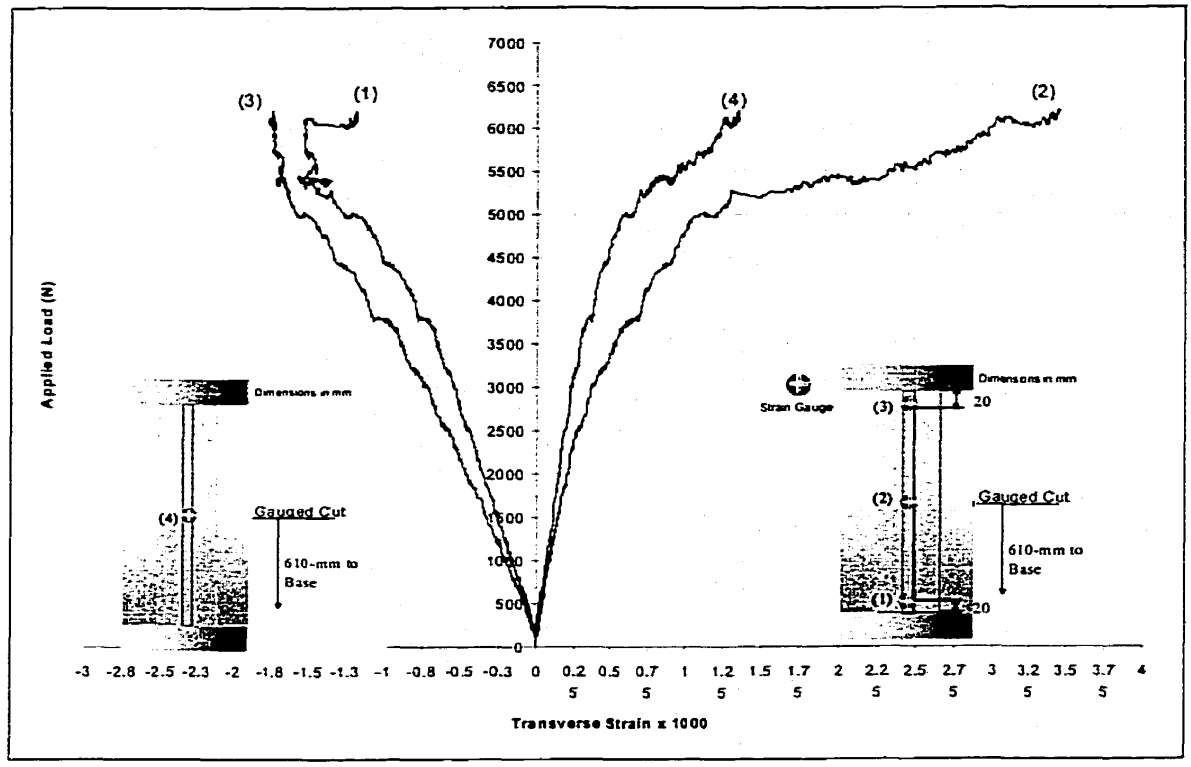

Figure 4.34 - Load – transverse strain curve for specimen P3-4-406-3

The load-longitudinal strain curve for specimen P3-4-406-4 is shown in Figure 4.35, and the load-transverse strain curve is shown in Figure 4.36. The load-transverse strain curve shows a reasonably linear increase until localized debonding, as described previously, occurred. Additionally, because the majority of the spline was still attached to the pole, the spline did not bear against the jacket, as was the case with previous tests. Instead, the strain was transferred to the jacket at the location of the cut, as indicated by the increase in the transverse strain at this point.

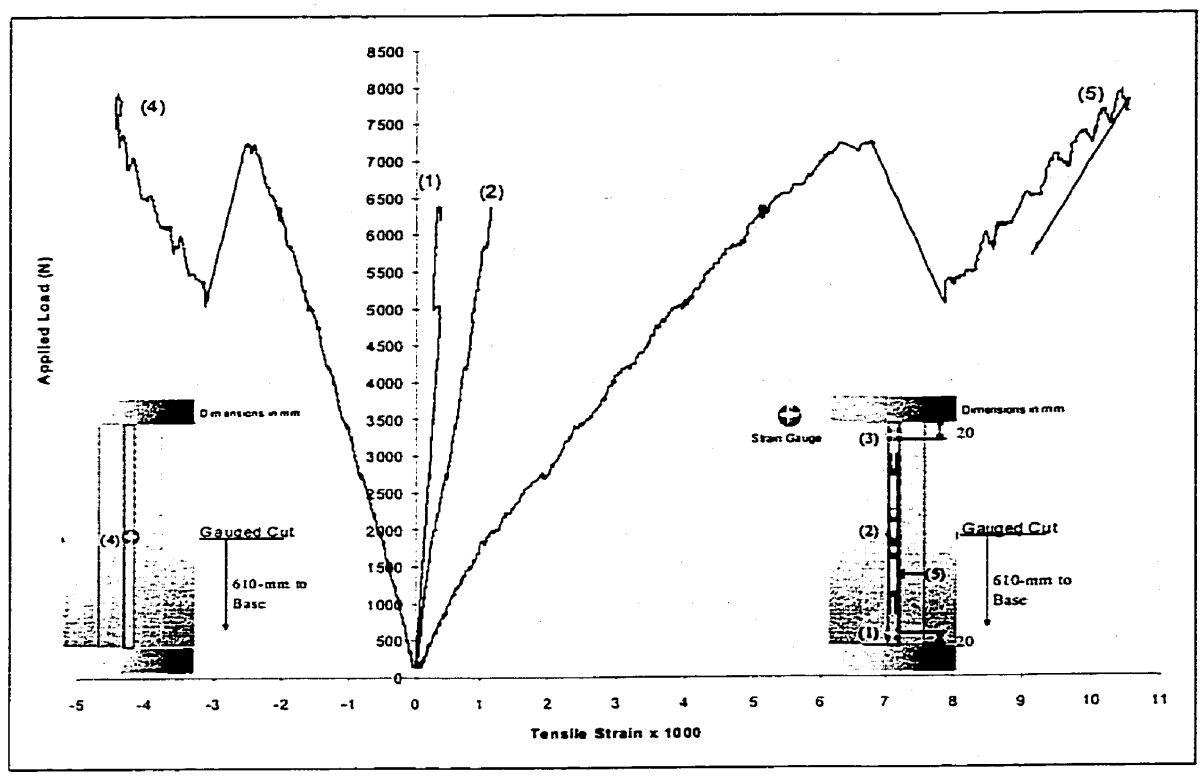

Figure 4.35 – Load - longitudinal strain curve for specimen P3-4-406-4

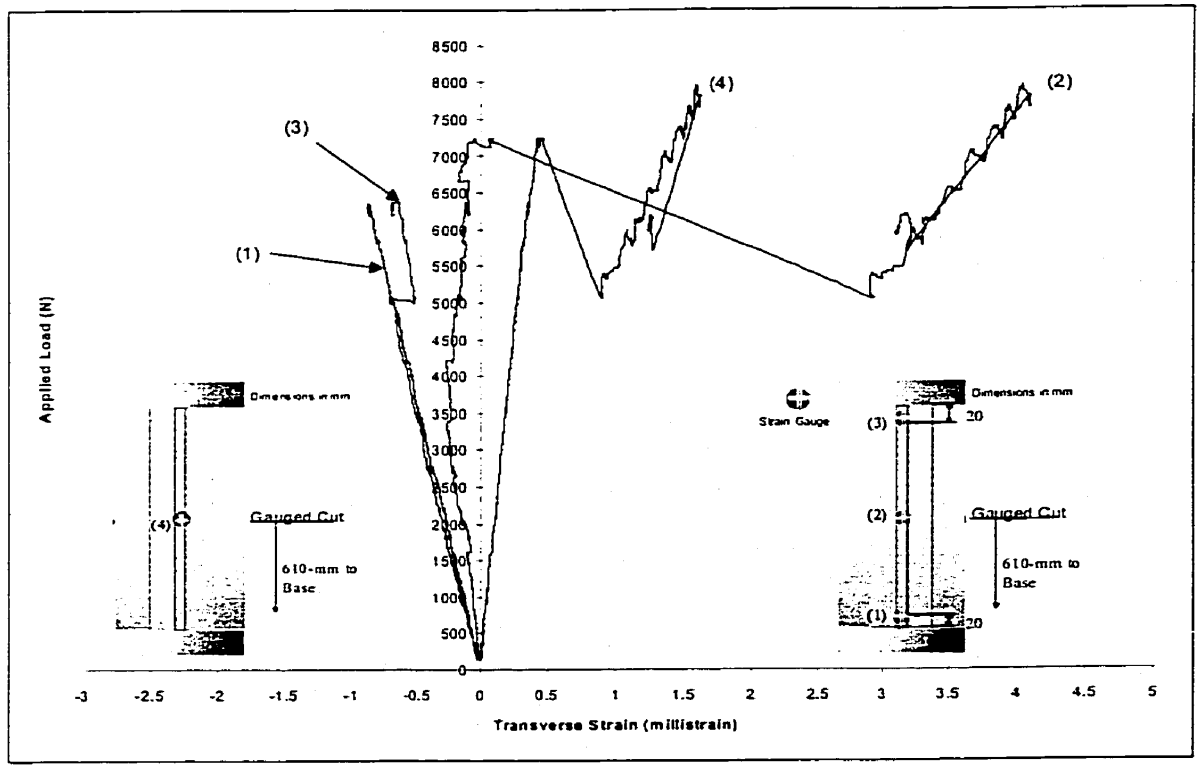

Figure 4.36 – Load -transverse strain curve for specimen P3-4-406-4

4.5 PHASE IV POLES

4.5.1 Load-Deflection Characteristics

Seven specimens fabricated using the methods described in Chapter 3 were tested to failure to evaluate the proposed repair technique. All of the specimens tested, with the exception of P4-1, were able to attain the load capacity predicted by the CSA standard, CSA-015-90, as indicated in Figure 4.37. The CSA standard predicted load was approximately 6300-N for a Jack-pine pole of similar geometric properties of the specimens tested in Phase IV. The load-deflection behavior of the Phase IV specimens was similar to that of the control poles shown in Figure 4.6. In both cases, there is almost a linear relationship between load and deflection until failure. This indicates that the repaired poles behaved like the solid wood poles and that the repair technique was successful allowing the poles to reach their ultimate load-carrying capacity.

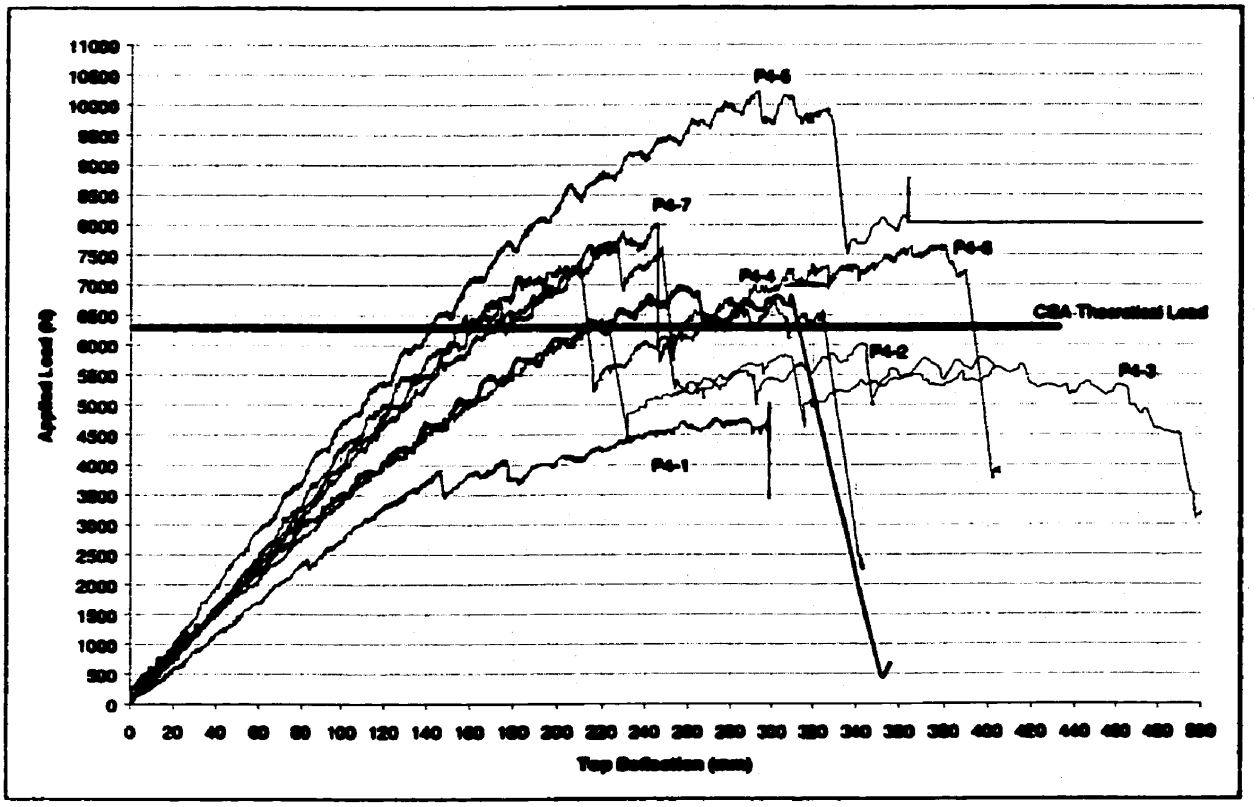

Figure 4.37 - Load-deflection curves for Phase IV poles

Specimen P4-1 failed by splitting of the wood and debonding of the spline. Failure was initiated by an eccentric loading condition that was brought on by the alignment keys. As discussed in Chapter 3, this specimen was repaired in the vertical position and additional alignment keys were added to prevent rotation of the pole during surface preparation of the pole. These keys were placed off center and during loading they created areas of high stress and caused failure of the pole. In subsequent tests, only one alignment key placed through the center of the pole was used. A cross-section view of specimen P4-1 is shown in Figure 4.40.

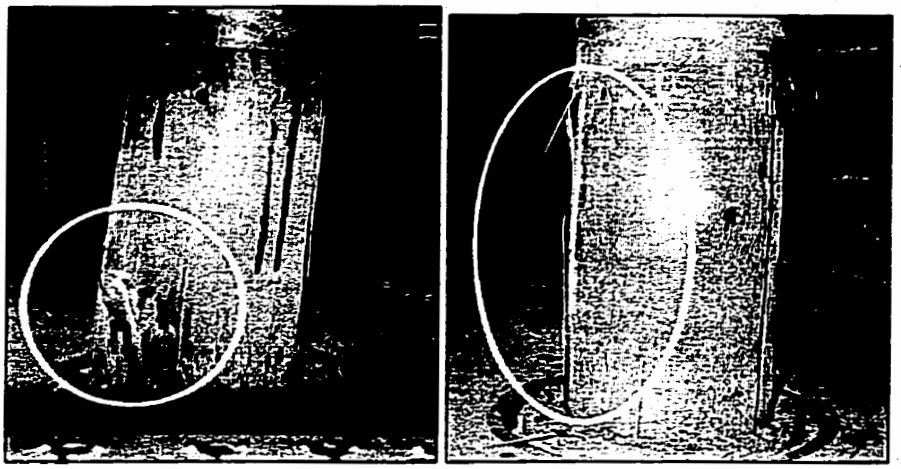

Figure 4.38 - Typical failure near the base for Phase IV specimens.

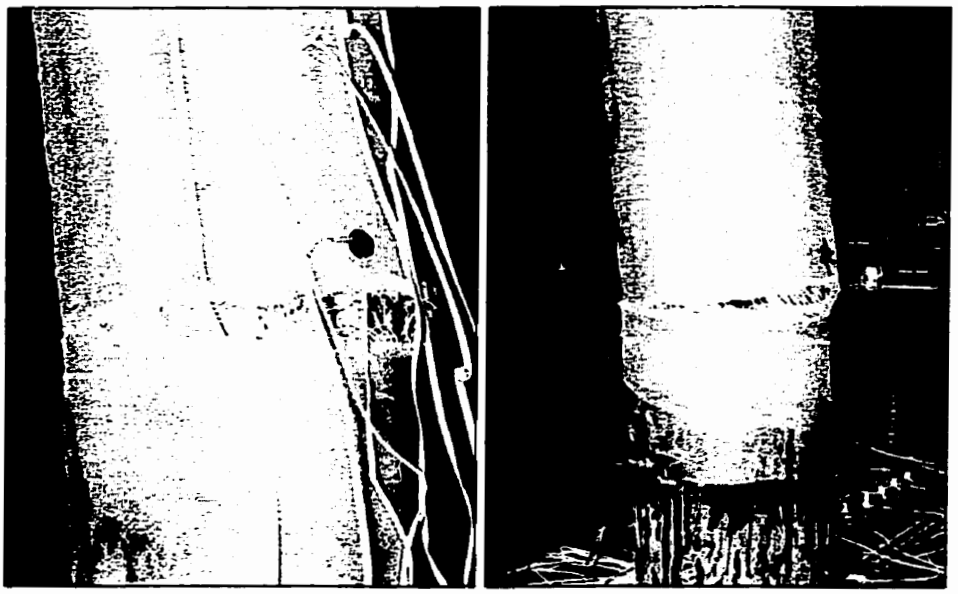

Figure 4.39 – Typical FRP rupture in specimens 4-1 and 4-2.

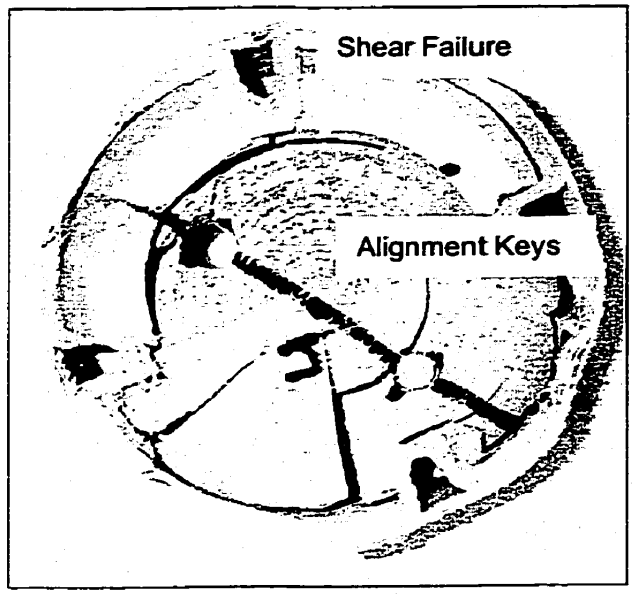

Figure 4.40 – P4-1 cross-section

In specimen P4-2 only one alignment key was used. This specimen failed in a combination of shear within the rehabilitated area and rupture of the FRP jacket. This latter failure was caused by the high hoop-stress concentration generated at the base of the spline. This shear failure was confined within the wrap until the wrap ruptured at the base of the groove. This rupture was shown in Figure 4.39. Some local debonding at the base of the spline was observed, but no separation of the splines from the rest of the pole was detected. The shear failure in the pole at the base of the groove is shown in Figure 4.41.

In order to facilitate the transfer of the shear stresses from the base of the spline to the base of the pole, a shear transfer layer was added, as described in Chapter 3. The specimens that were reinforced with the additional shear transfer

layer failed through tension at the base of the pole, outside the repaired section of the pole.

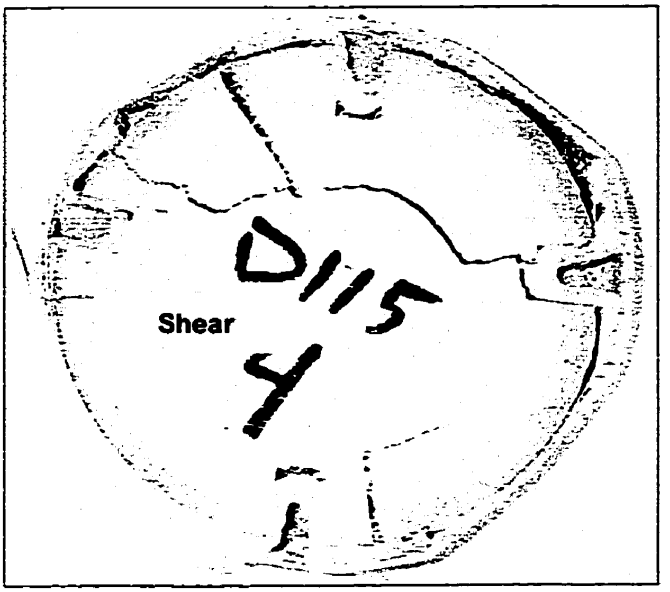

Figure 4.41 - Shear failure in P4-2

Using Equations 2.1 and 2.2, and the ground line circumference of the poles tested in Phase IV, the modulus of elasticity (MOE) and modulus of rupture (MOR) at ground line were calculated. These results are summarized in Table 4.7. Specimens P4-1 and P4-2 were excluded from this table, because their reinforcement type was different from other five specimens. Comparing Table 4.7 with the calculated values shown in Table 3.5, it is evident that all repaired specimens met or exceeded their original classification with the exception of pole P4-7. The MOE of specimen P4-7 was considerably lower than that of the other poles tested in this phase, indicating the presence of cracks along the length of the pole. It is possible that these cracks had a major influence on the behavior of the specimens.

Table 4.7 – Phase IV summary.

Pole Number	Failure Load (N)	Deflection at Failure Load (mm)	MOR (MPa)	MOE (MPa)	Class
P4-3	6430	220	51	7989	6
P4-4	6970	257	52	7423	6
P4-5	10140	289	70	8284	5
P4-6	7700	225	48	6900	6
P4-7	8000	245	43	5341	6
Average Values	*7848*	*247*	*53*	*7187*	*6*
Standard Deviation	*1421*	*28*	*10*	*1030*	

The average ultimate loads and deflections at failure for the control specimens are shown in Table 4.1 as 8460 ± 910-N and 226 ± 30-mm (7% to 10 % of pole height), respectively. Comparing these values with the average ultimate load (7848 ± 1421-N) and deflections (8% to 10% of pole height) from Table 4.7, it is seen that the repair was successful in restoring the strength and stiffness of the poles. The average calculated MOR and MOE are shown in the same Table 4.1 52.1 ± 5.6-MPa and 7790 ± 1453-MPa, respectively. Comparing these values with the values corresponding to Phase IV specimens, it is evident that that the rehabilitated poles behave like the control poles tested in Phase I.

4.5.2 Strain

The National Electric Safety Committee (IEEE,1997) gives the design modulus of elasticity for jack-pine poles as 8400 MPa. The strain and stress in the pole can be obtained from the following relationships:

$$\varepsilon_{ult} = \frac{\sigma_{ult}}{MOE}. \qquad \textit{Equation 4.1}$$

$$\sigma_{ult} = \frac{P_{ult} \cdot L}{S_{pole}} \qquad \textit{Equation 4.2}$$

Where

ε_{ult} = longitudinal strain in the jack-pine Pole at failure;

σ_{ult} = stress in the jack-pine Pole at failure;

MOE = modulus of elasticity;

P_{ult} =ultimate failure load;

L = distance from loading point;

S_{pole} = section modulus of pole about the axis of bending.

Substituting Equation 4.2 into Equation 4.1 yields;

$$\varepsilon_{ult} = \frac{P_{ult} \cdot L}{S_{pole} \cdot MOE} \qquad \textit{Equation 4.3}$$

By using the MOE recommended by NESC of 8400-MPA, and Equation 4.3, strain criteria can be developed and compared to the actual strains in the rehabilitate pole. Using the measured top and bottom diameters of each pole, the angle of taper was calculated for each pole. Using the angle of taper, the diameter of the pole and the section modulus at any section of a solid wood pole can be calculated. In the specimens tested in Phase IV, the strains were measured at four common points. Calculating the section modulus at these locations and using the MOE obtained from the NESC design guidelines, the design strains were determined. Because the diameter of the poles changes very little over the length of the repaired section, an average section modulus was computed based on the calculated diameters. These strains are plotted,

along with the experimental strains in Figures 4.42 to 4.48. The maximum load computed according to the CSA standard is also shown in these figures.

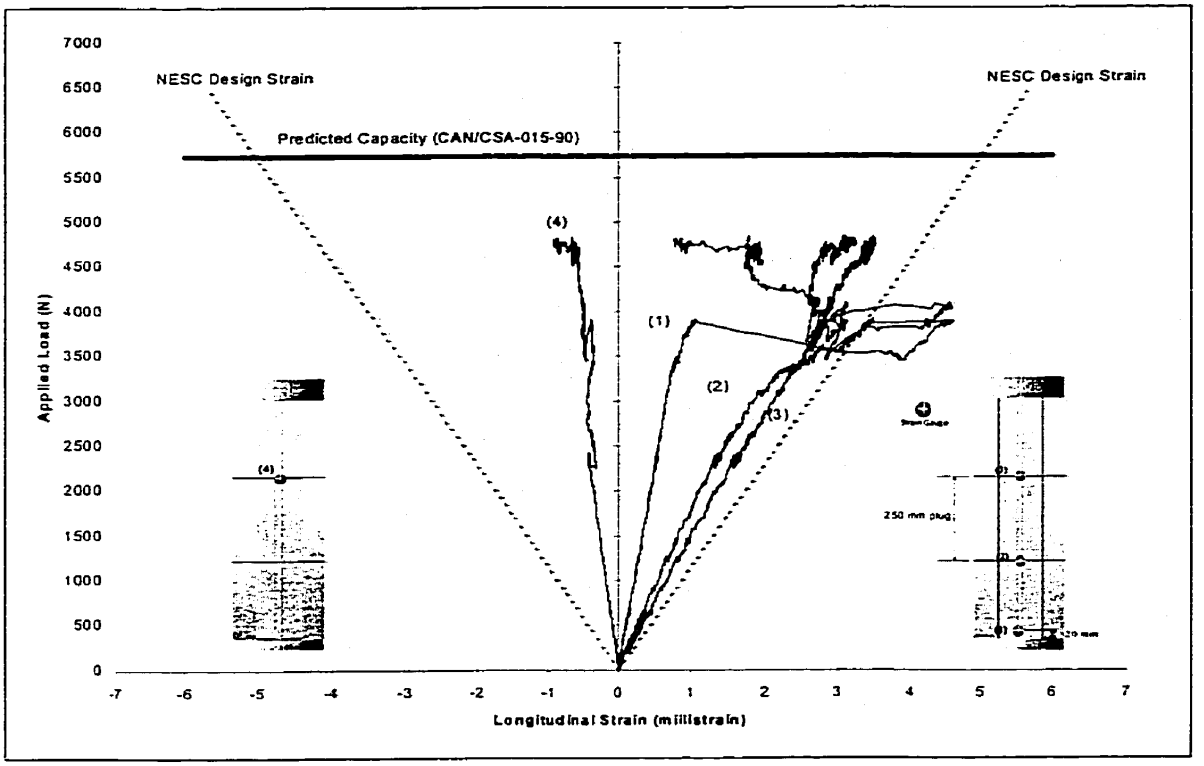

Figure 4.42 – Load - Longitudinal strain curve for P4-1

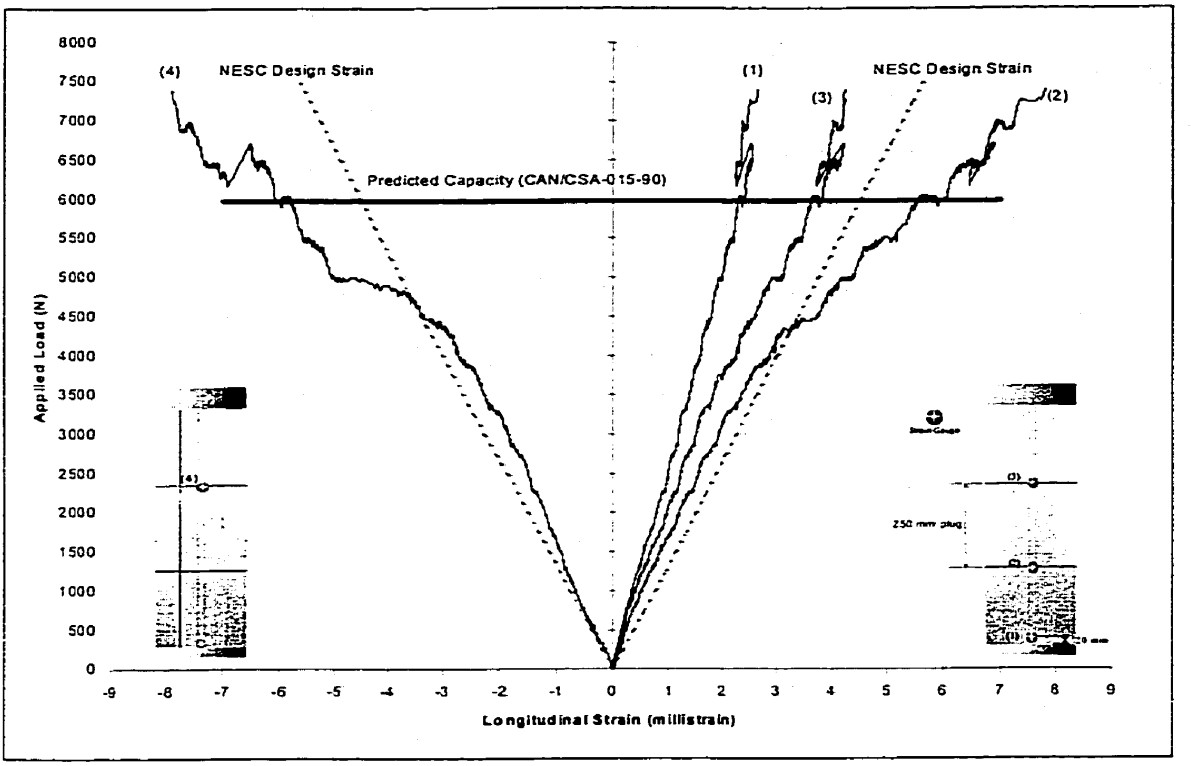

Figure 4.43– Load - Longitudinal strain curve for P4-2

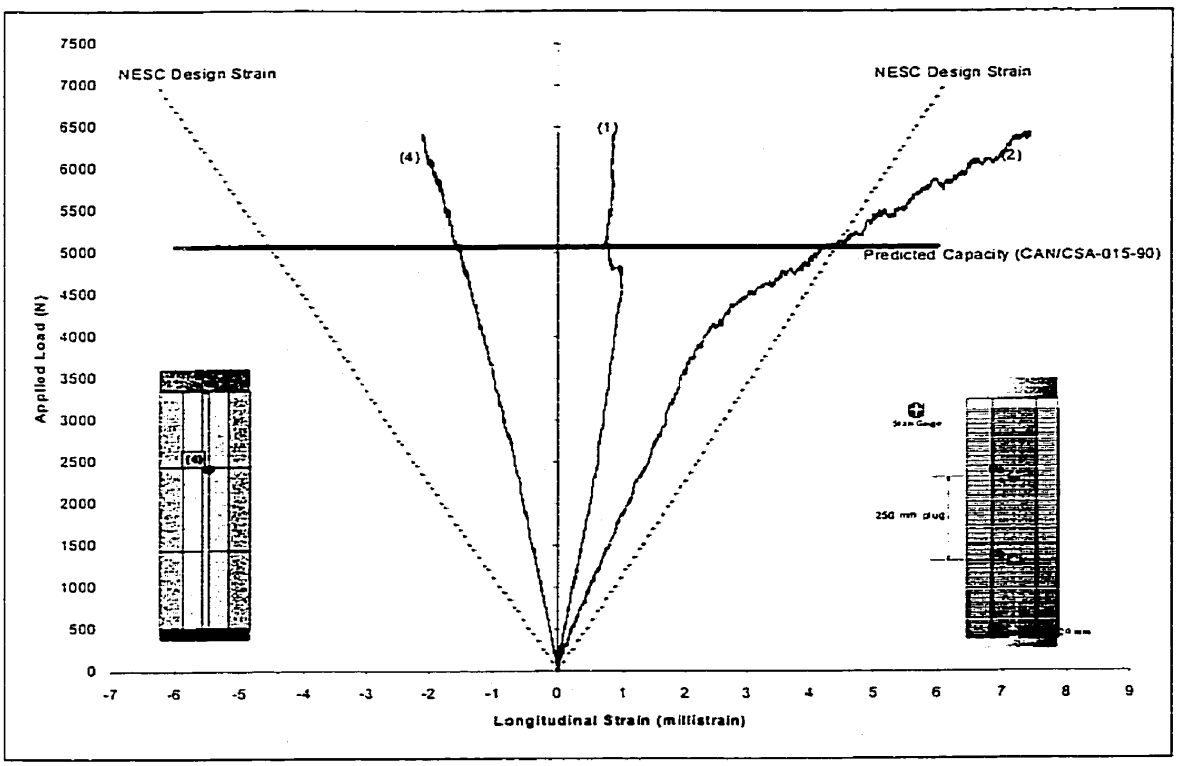

Figure 4.44– Load - Longitudinal strain curve for P4-3

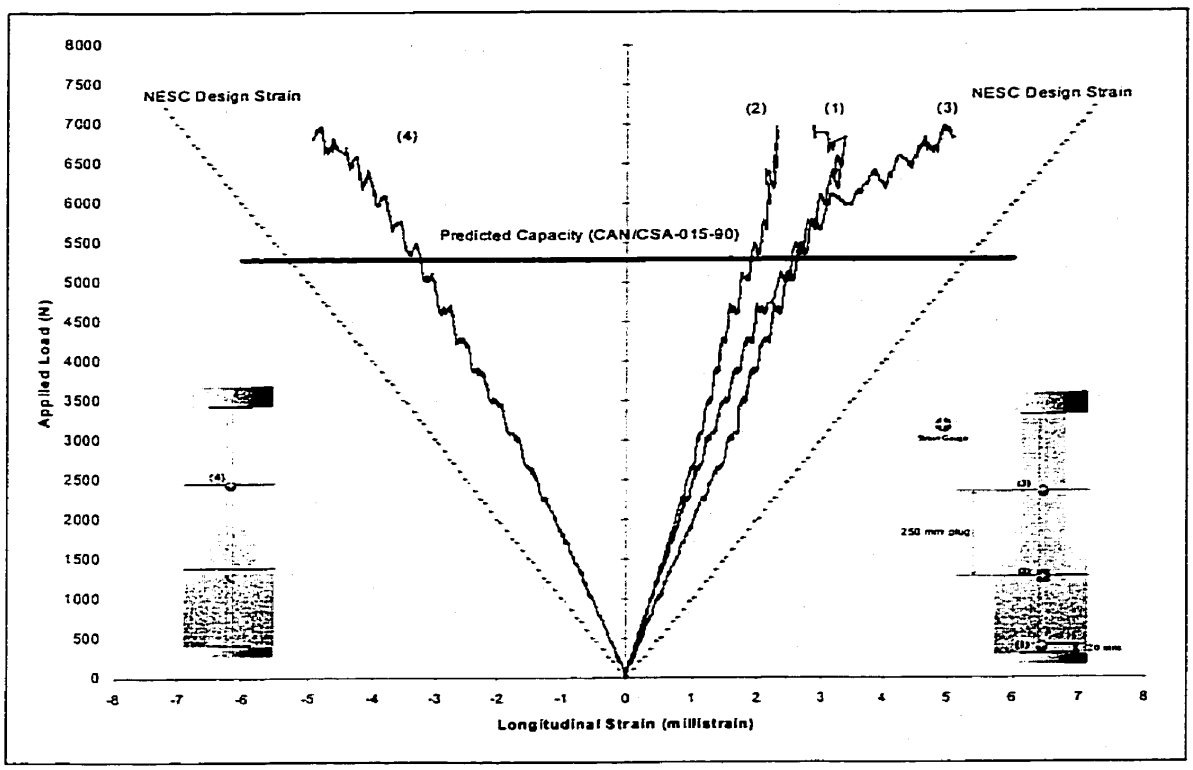

Figure 4.45– Load - Longitudinal strain curve for P4-4

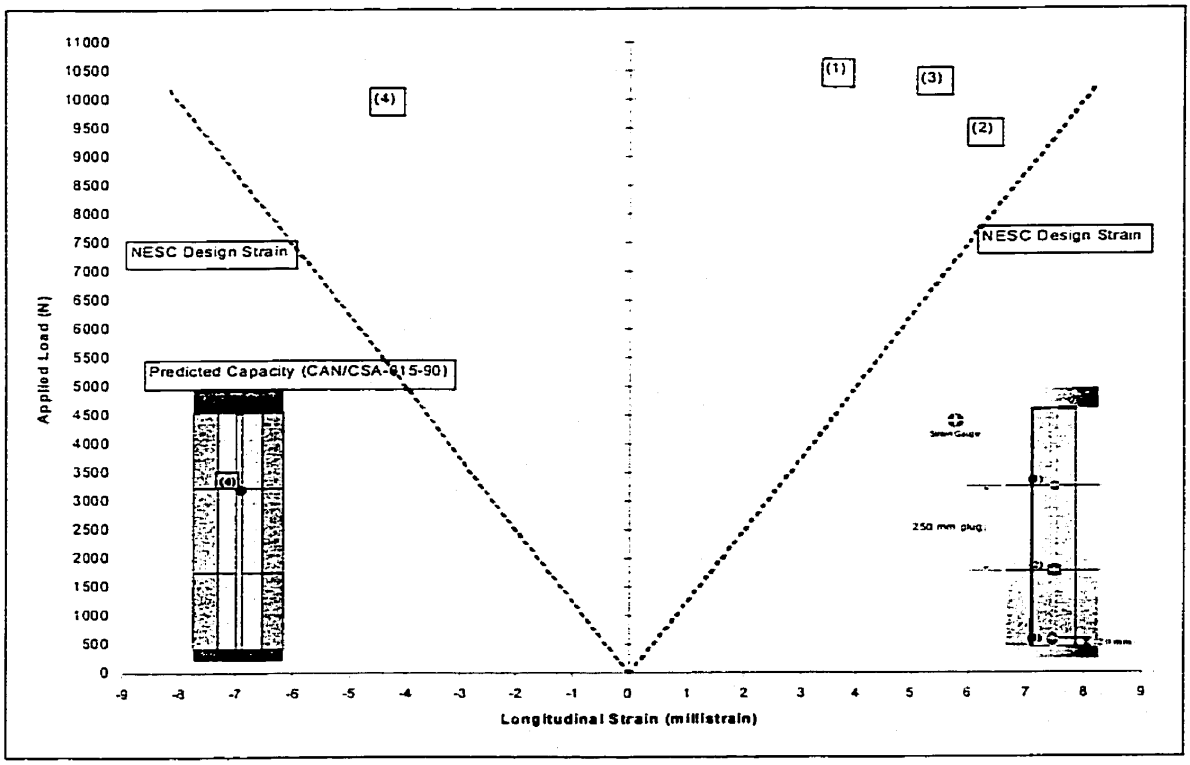

Figure 4.46– Load - Longitudinal strain curve for P4-5

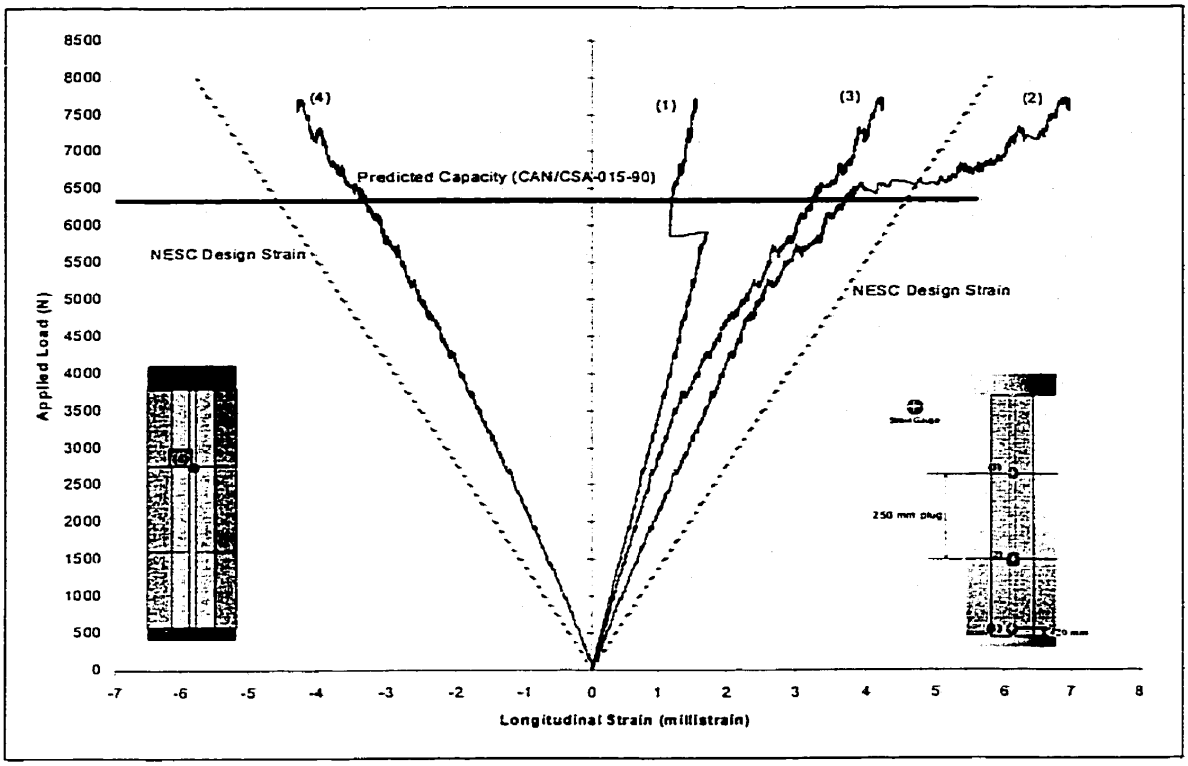

Figure 4.47– Load - Longitudinal strain curve for P4-6

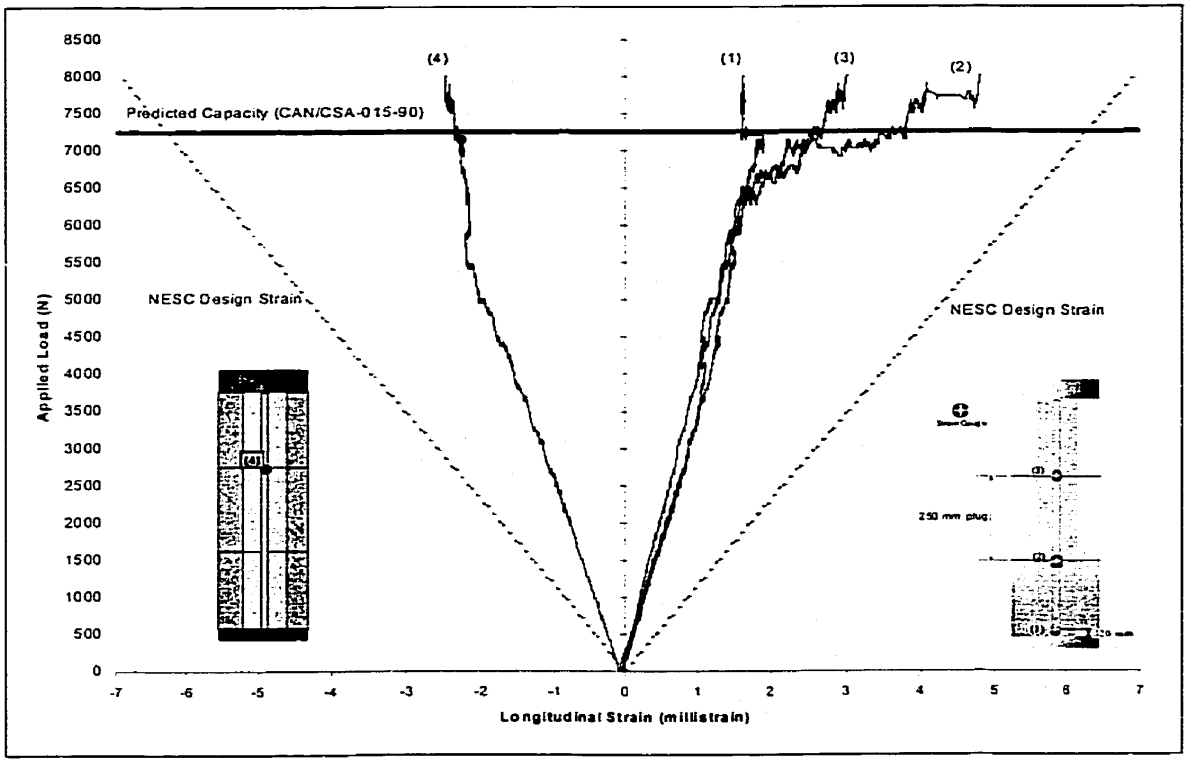

Figure 4.48– Load - Longitudinal strain curve for P4-7

One strain gauge in specimen P4-2 was damaged during testing. From the load-longitudinal strain profiles shown in Figures 4.42 to 4.48, the results indicated that the highest strains were located at the top and bottom of the wood stub. This was expected, as the FRP repair is transferring all of the tensile stresses at this location. The strains measured on the compressive side shows a reasonably linear strain profile, indicating that the neutral axis is in the geometric center of the pole and that plane sections remain plane through bending. Any non-linearity can be attributed to the alignment keys used to repair the specimens, as they were not placed in the geometric center of the pole.

In order to reduce the stress concentration at the base of the spline, a shear transfer layer was applied as described in Chapter 3. This layer was effective in reducing the stresses at the base of the spline. This is evident as the failure was forced into the base of the spline.

In analyzing the load-transverse strains, it became apparent that after testing the first two specimens, P4-1 and P4-2, additional confinement was required. In these specimens, jackets began to rupture almost immediately after the splines separated from the wood and began bearing against the circumferential wrap. The jacket was re-designed to resist twice the maximum strains in the splines. This would force the failure to occur in the splines, instead of the jacket. Additionally, it was observed that wider sheets of FRP were easier to handle and were able to be wrapped much tighter around the pole. Therefore, in subsequent

specimens, for every longitudinal layer of FRP used to make the splines, two layers of FRP confinement were used. As discussed in Chapter 3, the splines were made with two layers of FRP thus the confinement jacket was made with four layers of FRP sheets. The load-transverse strain plots corresponding to specimens reinforced with this technique are shown in Figures 4.49 to 4.55.

According to the data shown in Figure 4.50, specimen P4-2 experienced a sharp increase in strain in the confinement jacket at the base of the spline. At a load of 6700-N, there was a slight drop in strain at the base of the spline (gauge 1). A change in the load-strain curve at the base of the stub indicates some local internal failure within the repair zone that caused the spline to bear against the jacket. However, the additional confinement prevented the failure of the pole. None of the Poles failed in the confining jacket.

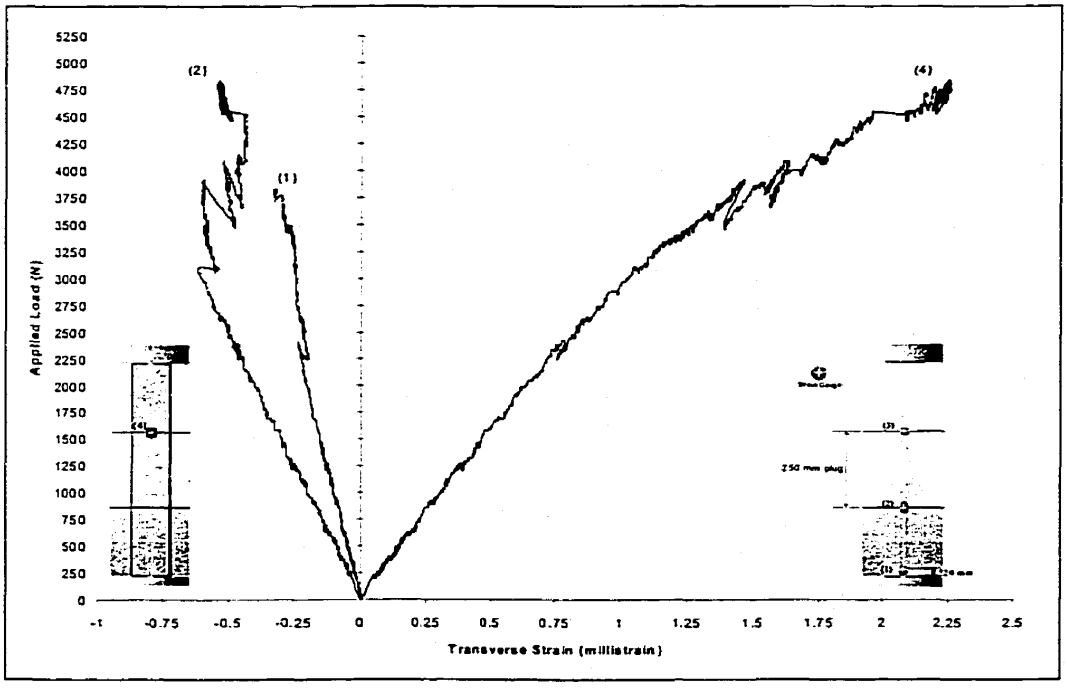

Figure 4.49 – Load-transverse strain curves for P4-1

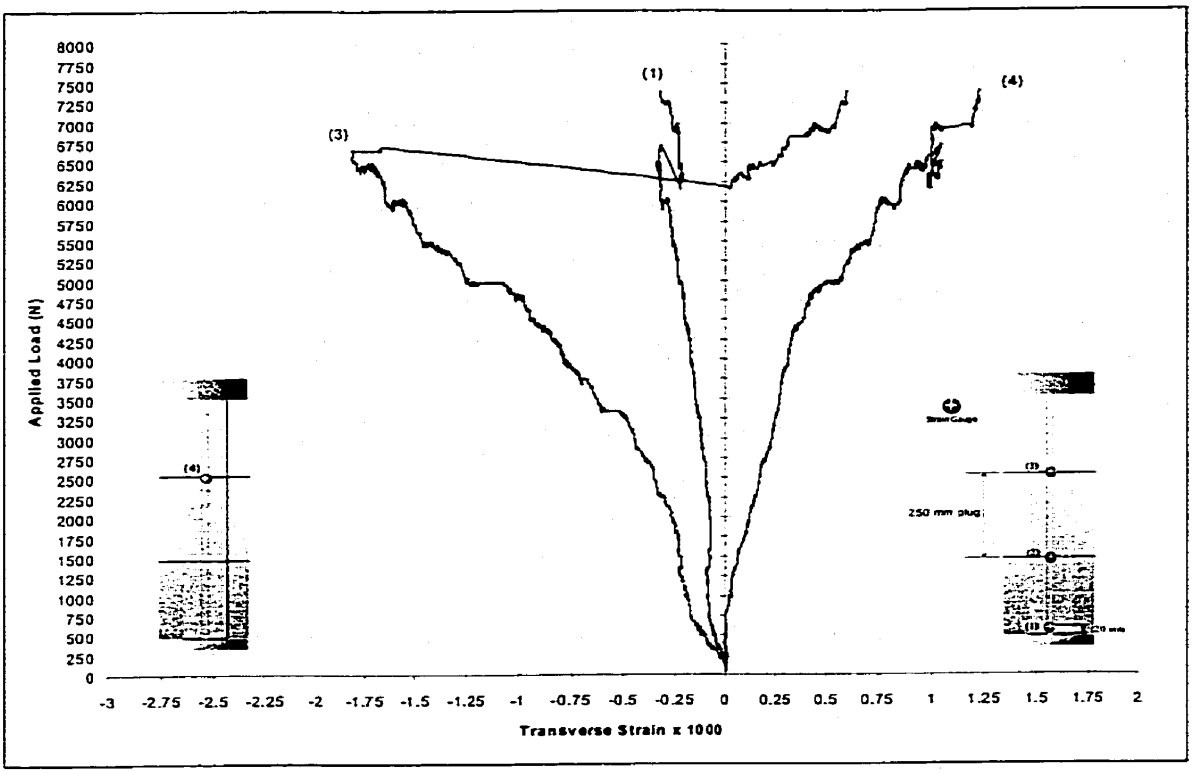

Figure 4.50 – Load-transverse strain curves for P4-2

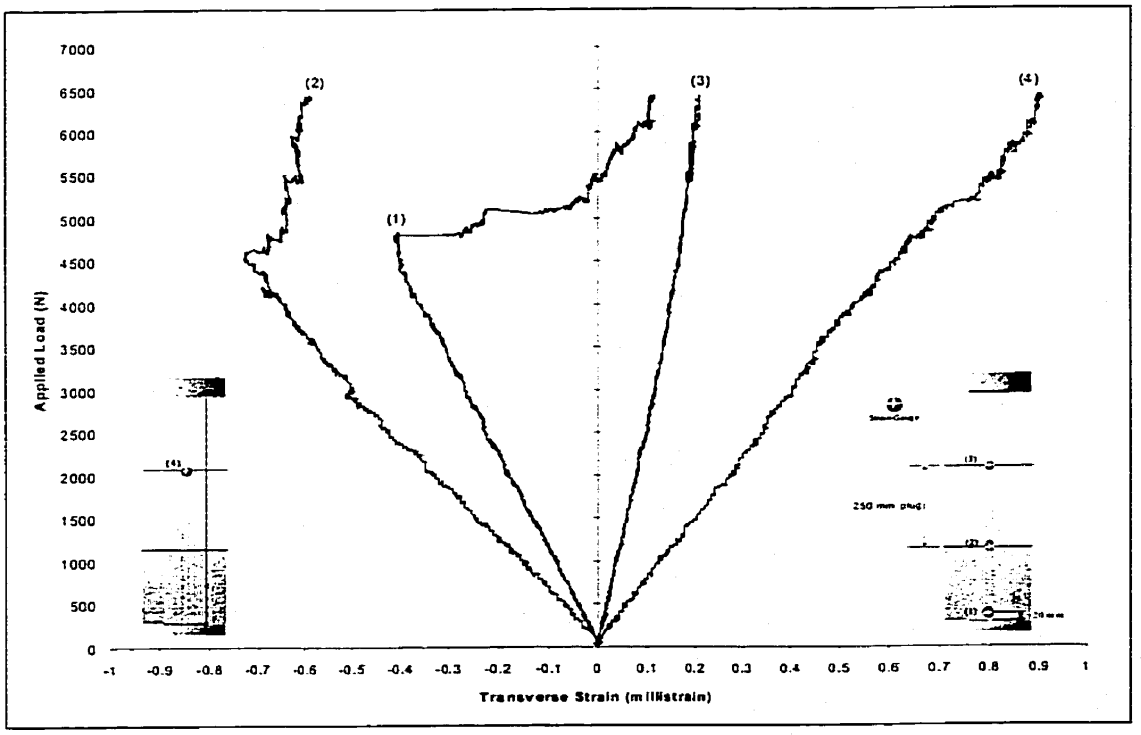

Figure 4.51 – Load-transverse strain curves for P4-3

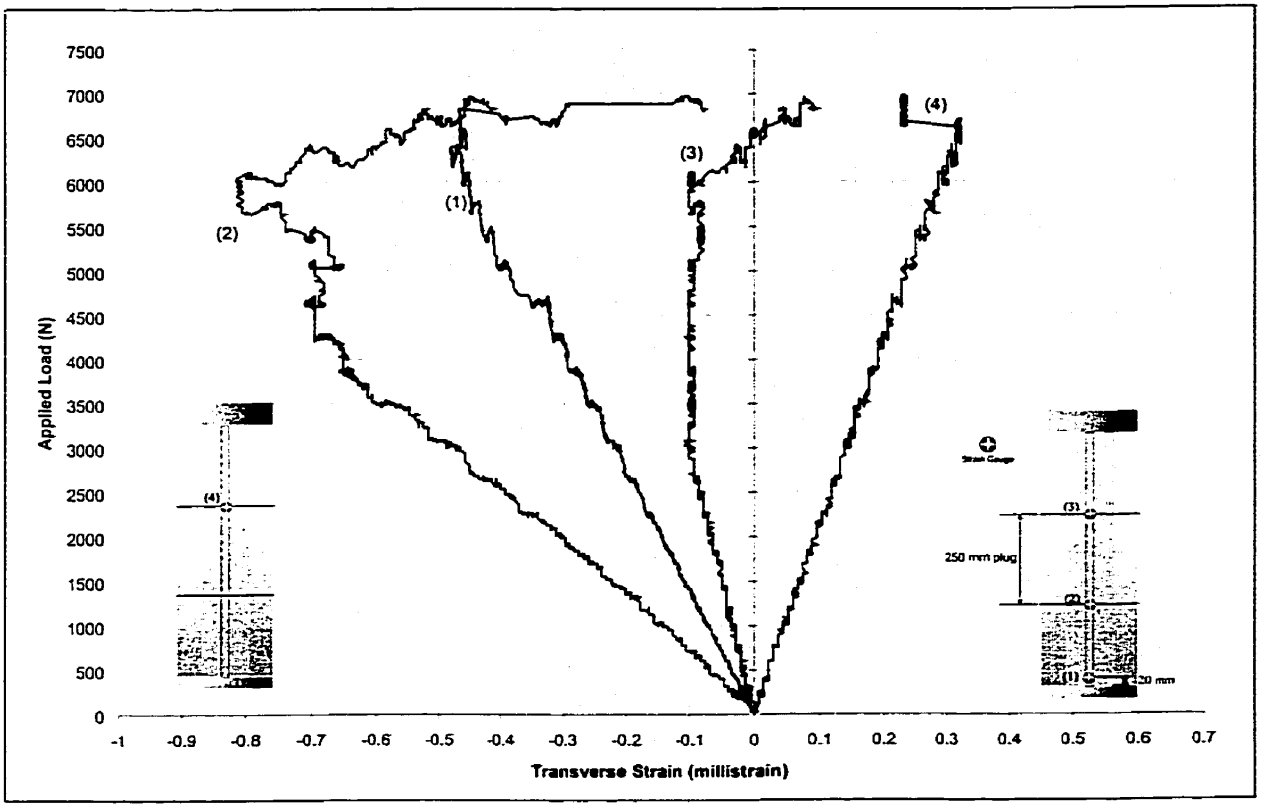

Figure 4.52 – Load-transverse strain curves for P4-4

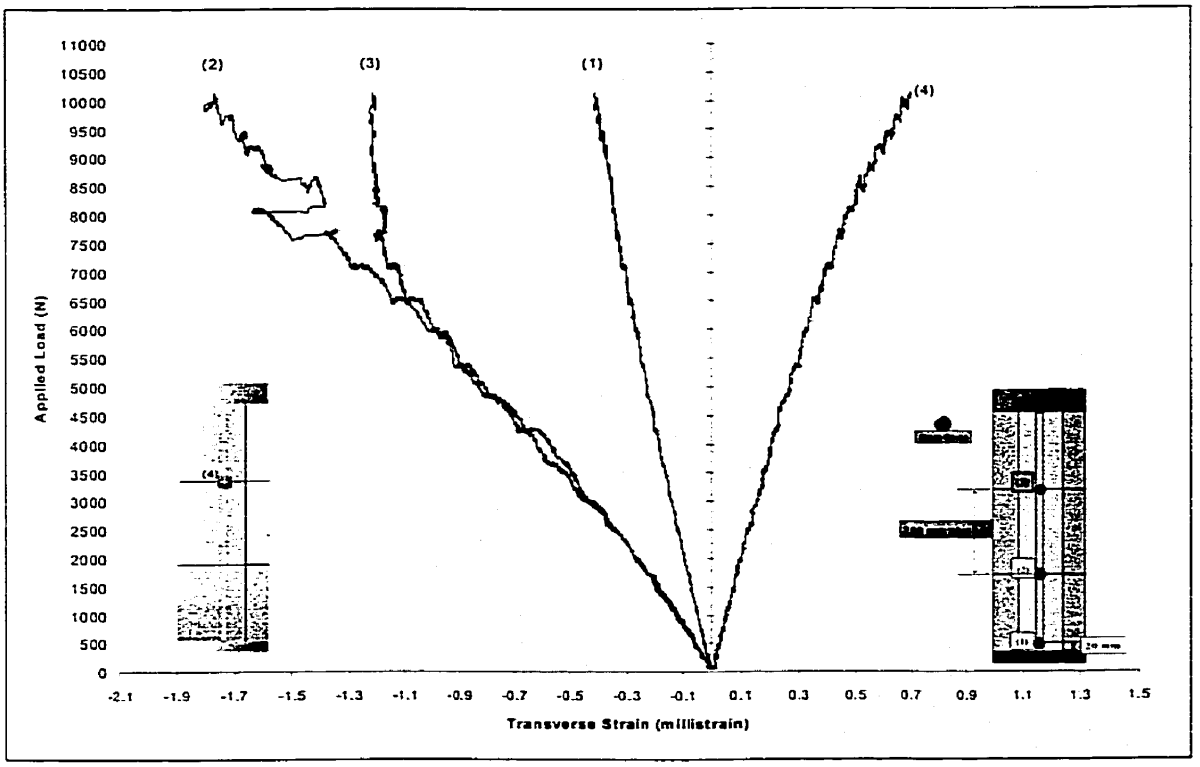

Figure 4.53 – Load-transverse strain curves for P4-5

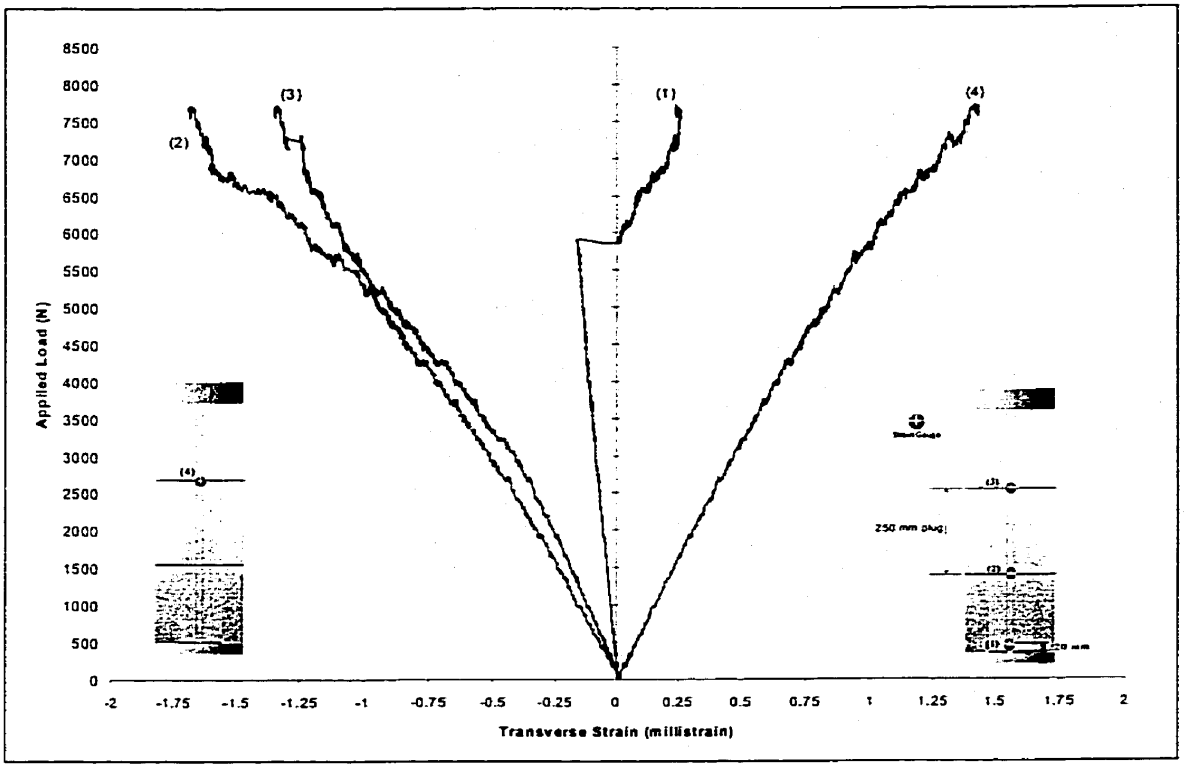

Figure 4.54 – Load-transverse strain curves for P4-6

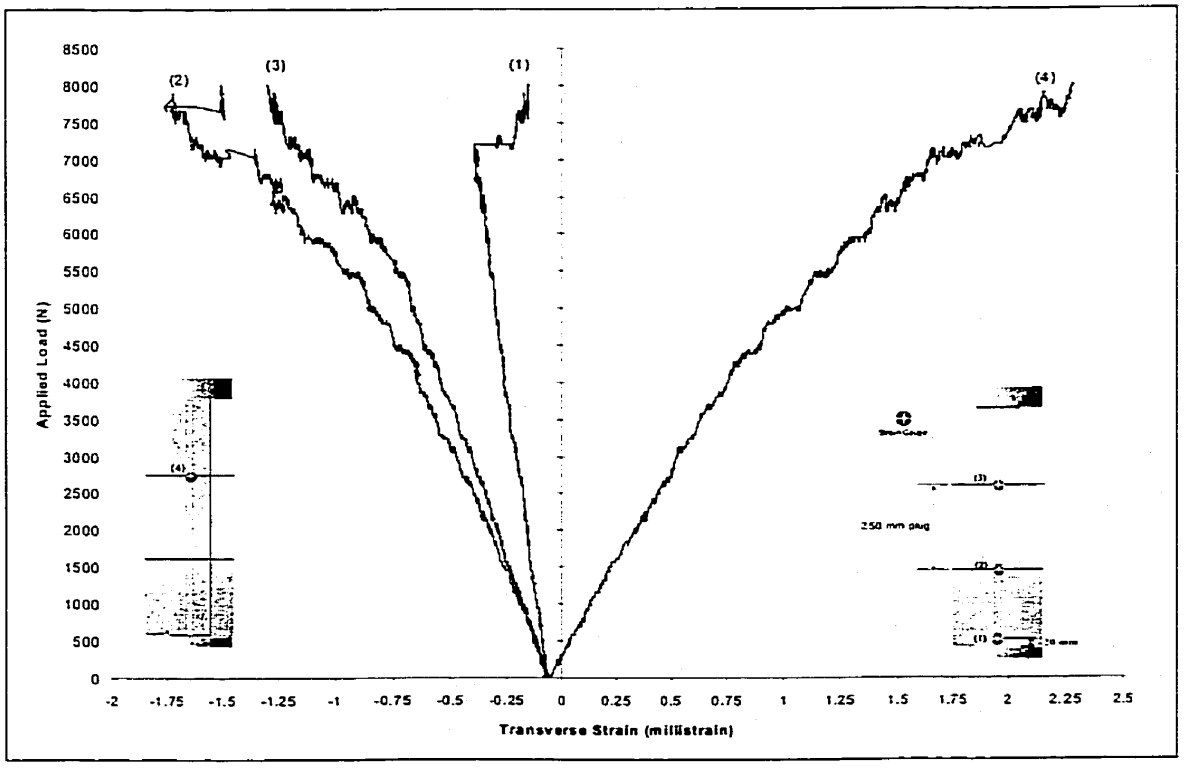

Figure 4.55 – Load-transverse strain curves for P4-7

4.6 MATERIAL CHARACTERIZATION

In order to determine the mechanical properties of the FRP materials, several tests were conducted according to current ASTM standards using test coupons described in Chapter 3.

4.6.1 Longitudinal Tension

Typical Stress-strain curves obtained from six tension coupons are shown in Figure 4.56. Strain readings were taken from strain gauges attached to the coupons. As the strain gauges had only limited ranges, they failed before the coupons ultimately failed. The coupons were tested to failure and the ultimate loads were recorded. Based on these loads, the ultimate stress for each coupon was computed. These ultimate stresses are listed in Table 4.8. The modulus of elasticity for the tension coupons was calculated from the linear portion of the stress-strain curves.

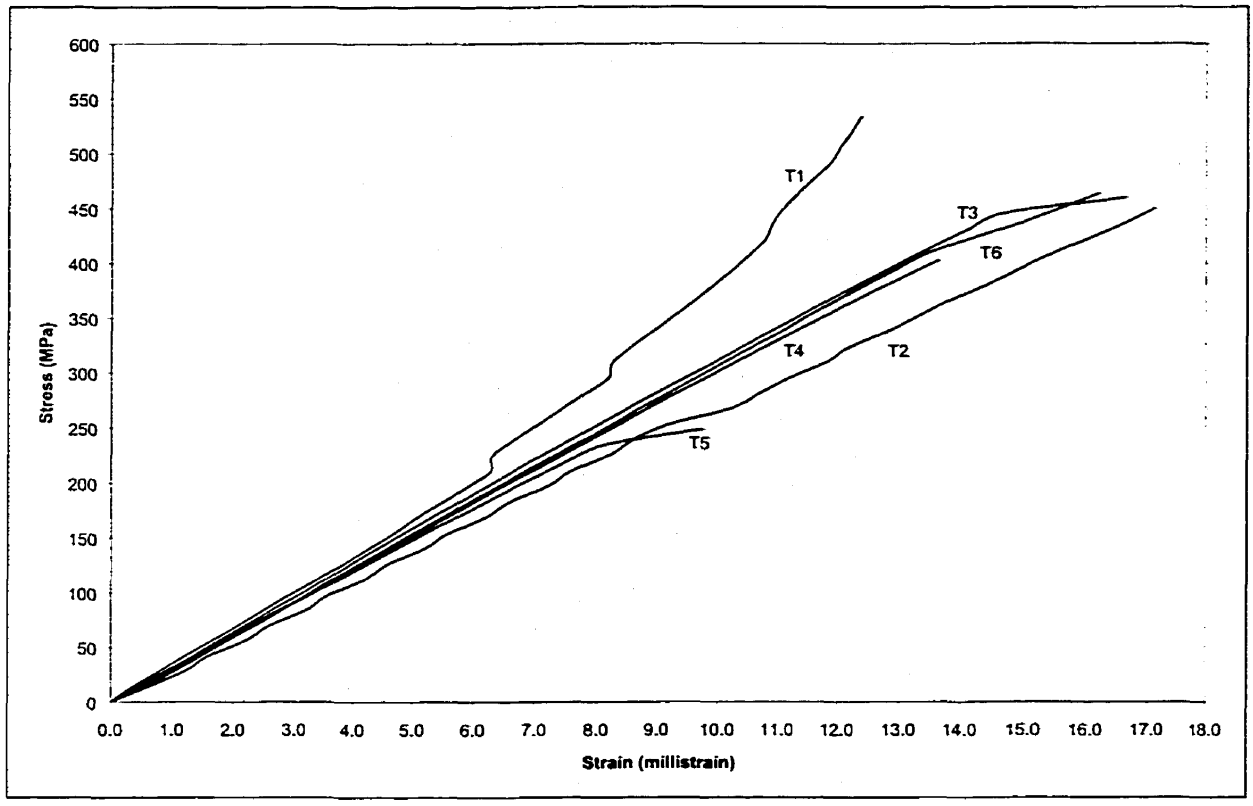

Figure 4.56 - Stress-strain curves for tension coupons

Table 4.8 – Summary of tension coupon tests.

Coupon	Area (mm^2)	Pult (N)	Modulus (GPa)	Fult (MPa)
T1	31.78	18750	36	590
T2	31.67	19570	28	618
T3	30.98	18615	32	601
T4	31.6	19350	30	612
T5	32.26	18800	29	583
T6	31.78	21100	36	664
Average	*31.7*	*19364*	*31.0*	*611*
Standard Deviation	*0.46*	*417*	*3*	*15*

The results from the tension coupons are lower than those obtained from the manufacturer data and the volume fractions reported in the Section 3.3.6. The calculated values for MOE and the ultimate stress are 30.57-MPa and 611-MPa

respectively. The manufacturers values for MOE and the ultimate stress are 34.34-MPa and 1580-MPa respectively. The difference in material properties between those obtained through testing and those obtained from published data is typical of any fabrication involving FRP. The physical properties given by the fibre suppliers are those of the fibres prior to any fabrication process. During fabrication, fibres will fracture and fewer fibres will be available to transfer load. Also, within a specific cross-sectional area, the fibre volume may vary and fewer fibres may be present to resist the load. A large number of coupons are required to develop very precise values for MOE and ultimate stress.

4.6.2 Compressive Properties

Stress-strain curves for the compression coupons are shown in Figure 4.57. The coupons were tested to failure and the ultimate loads were recorded. The modulus of elasticity for each tested coupon was calculated using the linear segment of the stress-strain curve. Coupon C1 was not placed properly into the test fixture and the results are unreliable. This coupon was not included in the analysis of the results. The ultimate stress was calculated using the measured cross-sectional area of the coupons and the ultimate load recorded during testing. The results are summarized in Table 4.9.

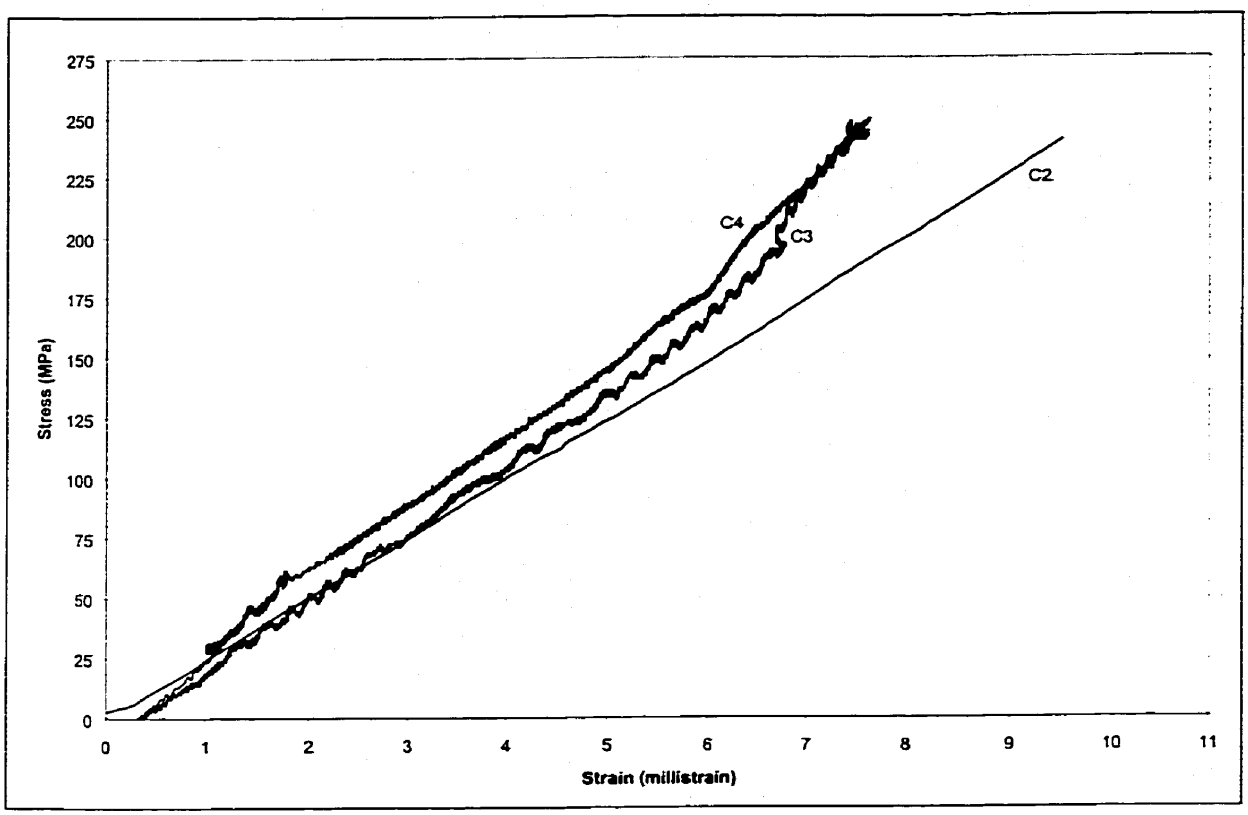

Figure 4.57 - Longitudinal Compressive Stress-Strain curve

Table 4.9 - Summary of compression coupon tests

Coupon	Area (mm^2)	Fult (MPa)	Modulus (GPa)
C2	16.29	333	25
C3	15.77	266	29
C4	15.9	257	30
Average	*16*	*285*	*28*
Standard Deviation	*0.3*	*42*	*3*

The test results indicate that the modulus of elasticity of the compression coupons are comparable to the MOE for the tension coupons, as expected. Also, as expected, the ultimate tensile stress is much higher than the ultimate

compressive stress as composites tend to be weaker in compression due to buckling of the fibres.

4.6.3 Shear Properties

The stress-strain curves for the shear coupons are shown in Figure 4.58. Strain gauges recorded strain until failure in coupons S1, S2, S3 and S5. However, in coupon S4, the strain gauge reached its limit before the coupon. The ultimate load of this coupon was recorded and was used to obtain the ultimate shear stress. The shear modulus for the tested coupons was calculated from the linear segment of the stress-strain curves. The ultimate shear stress was calculated using the measured shear areas of the coupons and the ultimate load attained. The results are summarized in Table 4.10. It can be seen that the measured modulus is considerably higher than that supplied by the manufacturer and the ultimate strength is considerably lower than the manufacturers strength value. This can possibly be attributed to the test method used to measure the strain.

Table 4.10 – Summary of shear coupons.

Coupon	Area (mm^2)	Pult (N)	Modulus (GPa)	Fult (MPa)
S1	64.52	3474	10.6	53.8
S2	70.32	3741	8.4	53.2
S3	59.84	1917	13.8	32.0
S4	59.84	3749	11.2	62.7
S5	64.52	2647	12.81	41.0
Average	*63.8*	*3105.6*	*11.4*	*48.6*
Standard Deviation	*4.33*	*802.57*	*2.09*	*12.02*

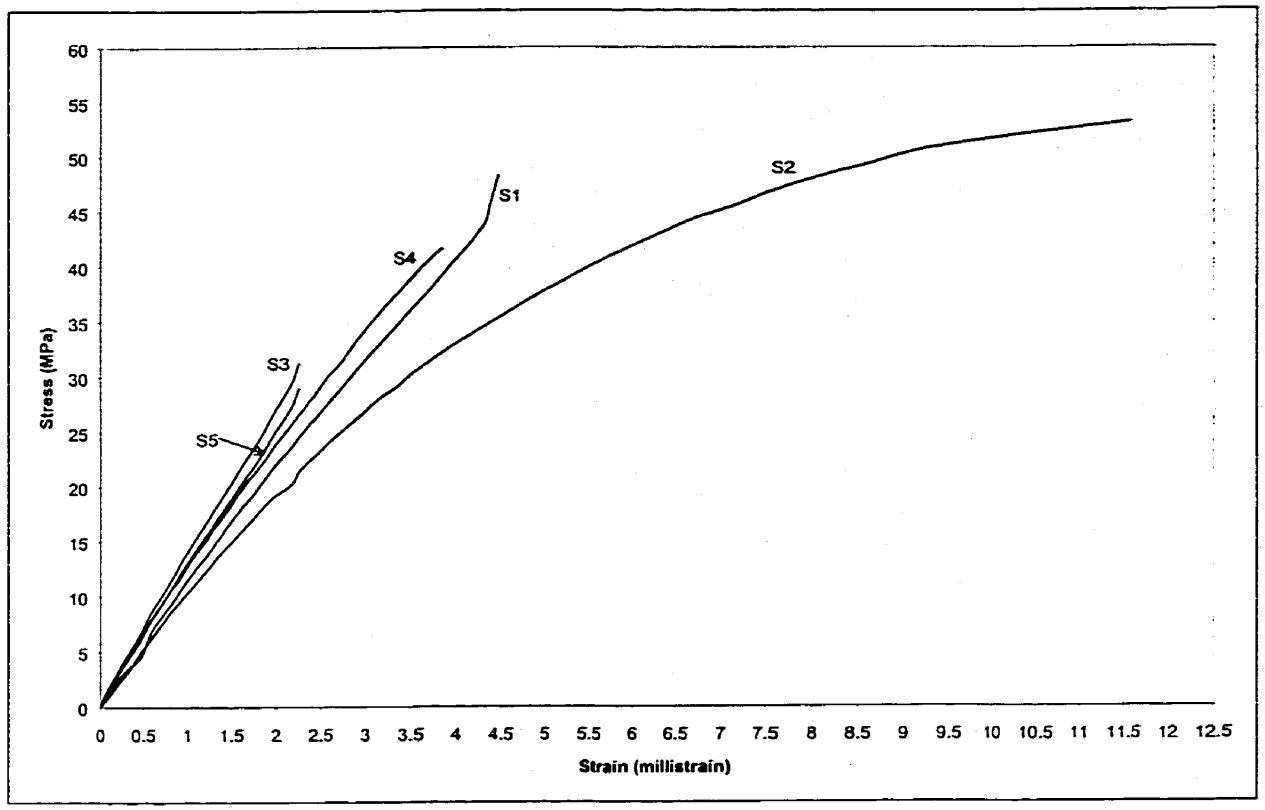

Figure 4.58 – Shear stress-strain curve.

CHAPTER 5

DEVELOPMENT OF ANALYTICAL MODELS AND DESIGN GUIDELINES

5.1 INTRODUCTION

Modeling the behavior of wooden poles is a complicated problem as imperfections in the wood, such as cracks and knots, become initiators of failure. It is, therefore, difficult to simulate defects in the pole. The development of such a model was outside the scope of the present study. In the present study, a finite element model was developed capable of simulating a rehabilitation scenario for a perfect pole; i.e., on without defects. Fortunately, the proposed FRP system must resist loads that a "perfect" pole would resist, so the assumption of a "perfect" pole is acceptable. In addition to the finite element model, a simplified design method was also developed. The ANSYS software program was used to develop the finite element model. The simplified design model was based on traditional stress analysis techniques. The results obtained from the finite

element model and the simplified design model are compared in this chapter to the experimental results. The two theoretical models are discussed below.

5.2 FINITE ELEMENT MODELING

The finite element technique uses a finite number of defined elements whose displacement behavior is described by a fixed number of degrees of freedom to predict the structural behavior of structures.

5.2.1 Element Selection

As two distinct materials, wood and FRP, are involved in the repair of wood poles, two different elements were required to model the structure accurately. To model the FRP jacket and splines, an eight-node quadrilateral layered shell element was selected as shown in Figure 5.1

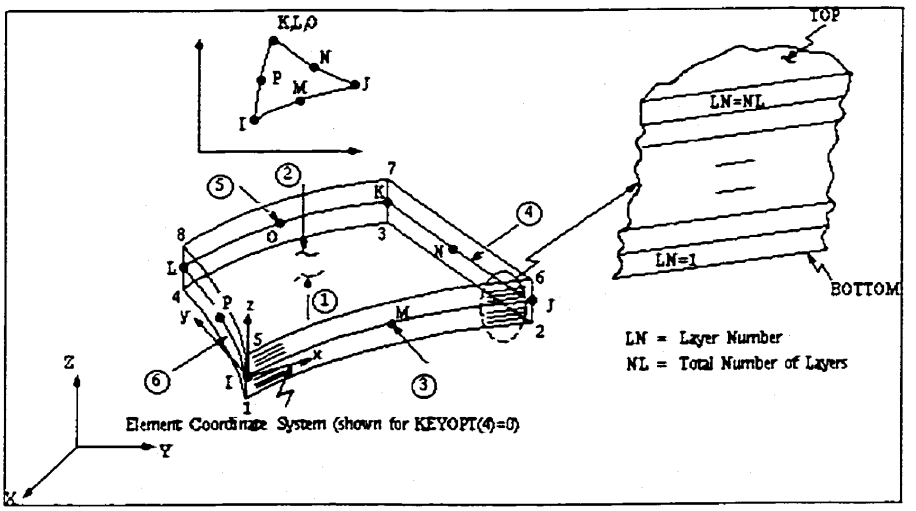

Figure 5.1 - Layered quadrilateral shell element (ANSYS, 1995)

This element, which is designated by ANSYS as SHELL99, is a 100-layer structural solid. The element has six degrees of freedom at each node, translations in the nodal x, y, and z directions, and rotations about the nodal x, y, and z-axes. This element was chosen mainly because of its ability to be meshed over an area, as will be discussed further in subsequent sections. The material properties are defined for this element in terms of the principal axes of the element. Using a single lamina for reference, the element coordinate system defines the axis running parallel to the fibres is designated as x, the axis running perpendicular to the fibres is designated as y, and the axis running through the thickness of the element is designated as z.

In order to model wood, a simple structural brick element could be used. To account for the "FRP" element bonded to the wood element, a structural brick element with mid-side nodes was required in order to couple to the mid-side nodes present on the 8 node quadrilateral element used to model the FRP. This technique was used by Becque (2000) to model concrete columns confined by FRP. Due to this requirement, the model became computationally large and required significant computing time. Additionally, because of the complicated shape of the physical model of the repaired pole, the element had to be able to handle irregular shapes with the same degree of accuracy. In order to meet these requirements, a 20-node structural solid element was used, as shown in Figure 5.2. This element is described by ANSYS as having the ability to model irregular shapes and being well suited to modeling curved boundaries (ANSYS,

1997). This element has three degrees of freedom, and translation in the x, y and z directions. Material properties are defined orthotropically for this element.

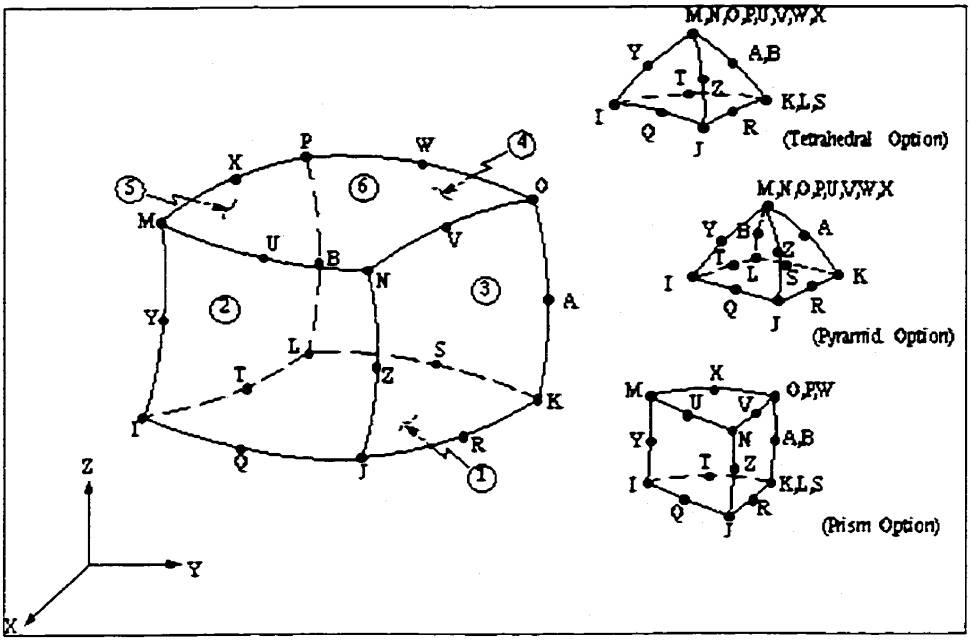

Figure 5.2 - Solid 20-node structural solid (ANSYS,1995)

5.2.2 Modeling of a Wood Pole

As wood is a material with considerable variability in material properties, a model was developed that could predict the behavior of the whole wood pole. As shown in Figure 5.3 the pole was modeled using 20-node brick elements and average cross-sectional properties obtained in Phase One. The material properties used were obtained from "Trial-Use Design Guide for Wood Transmission Structures" published by IEEE. For jack-pine poles, the MOE was taken as 8400-MPa and the density as 635-kg/m^3. Although wood's material properties are directional with respect to the grain, the properties were assumed to be homogeneous as described by IEEE. The base of the pole was assumed

to be perfectly fixed and the section of the wood pole confined by the concrete base in the experimental program was ignored in the analysis. A lateral load was applied at the tip of the pole in 500 N increments to a maximum load of 10,000 N, in order to obtain a load-time response of the model. The ANSYS input file for the wood pole model is given in Appendix C. The pole is modeled in the global coordinate system with the load being applied perpendicular to the z-axis.

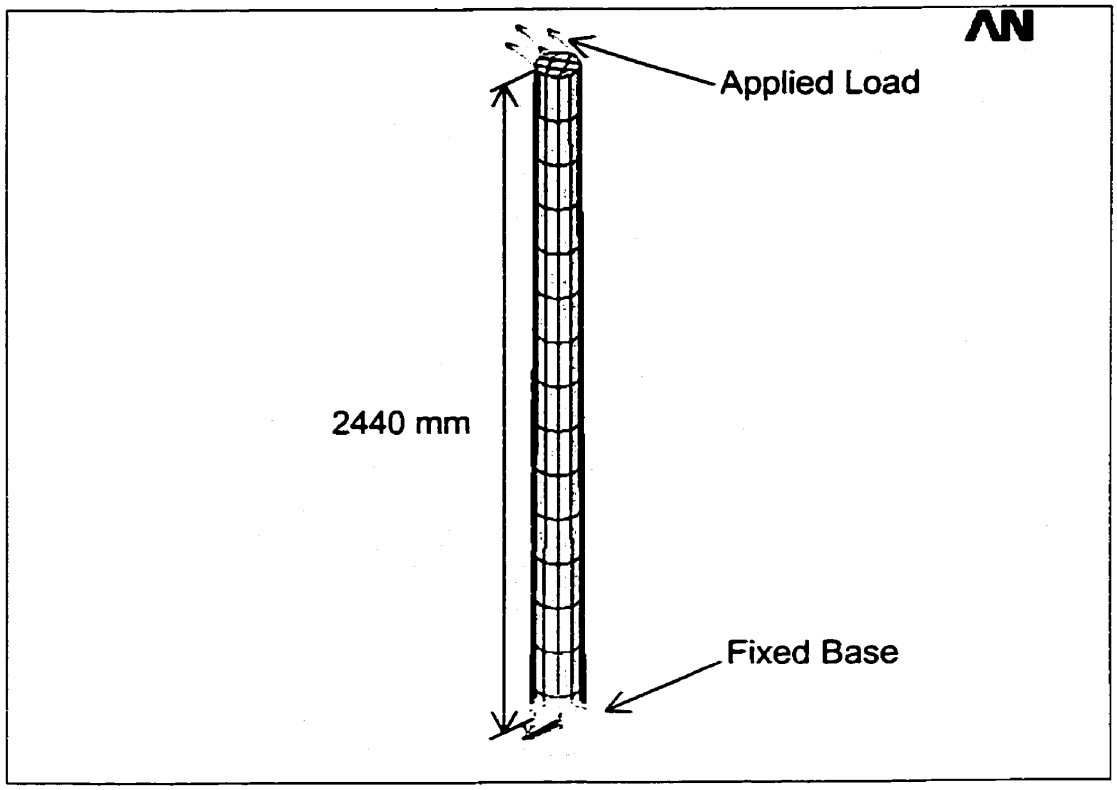

Figure 5.3 - ANSYS model of control pole.

5.2.3 Modeling of the Repaired Pole

Since the finite element model was to be used as a design tool, its geometric boundaries were defined as variables that could be readily changed to handle

different pole sizes. The user defined geometric boundaries are represented in Figure 5.4. The ANSYS input file for a repaired pole is given in Appendix D.

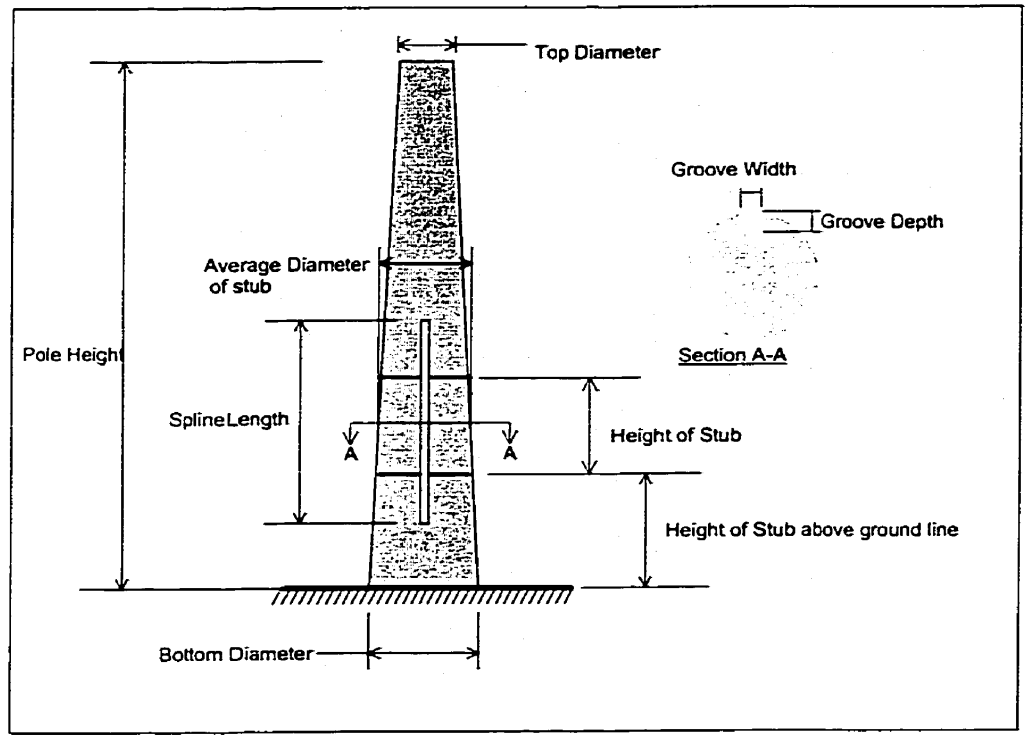

Figure 5.4 - Model inputs for repaired pole

The model was constructed from solid elements and boolean operations of adding and subtracting volumes were used in order to get an approximate shape. Due to the limitations of the ANSYS program with complex, curved shapes, the repaired section of the pole had to be modeled with a constant cross section. The ANSYS program could not model and mesh the grooves adequately on a tapered surface. Indicated in Figure 5.4, an average diameter was assumed throughout the repair region. Due to the curved and tapered nature of the sections, the entire wood pole had to be assembled using individual discrete volumes which when meshed, ensured continuity between the elements.

To model the interface between the plug and the pole, a thin gap was assumed at these locations. These gaps were sized so that the FRP spline would provide the entire bending resistance required in the pole. The model used is shown in Figure 5.5.

The FRP splines and jacket were modeled using shell elements meshed over brick elements representing the machined pole. The jacket and its cross-section are shown in Figure 5.6. The cross section is not an exact representation of the actual pole; however, it is considered an adequate approximation for the study. Figure 5.7 shows an exploded view of the repair.

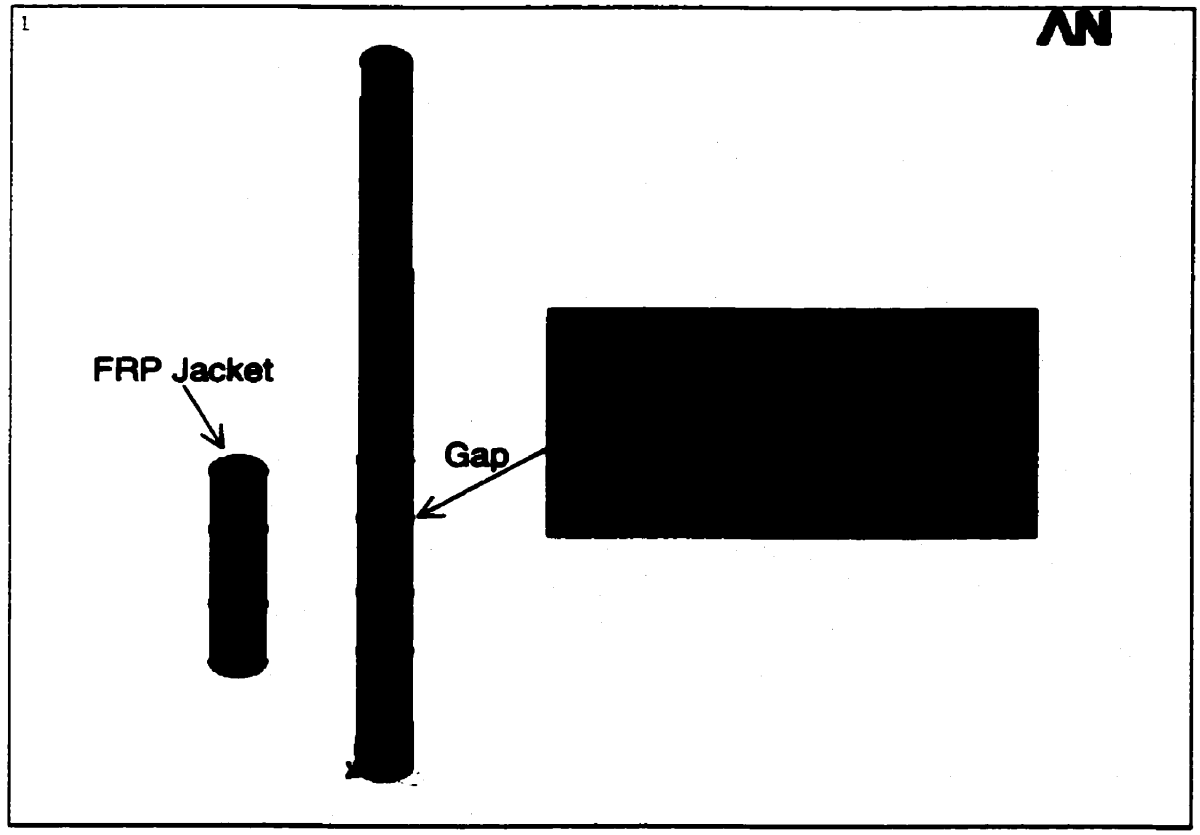

Figure 5.5 - Pole model

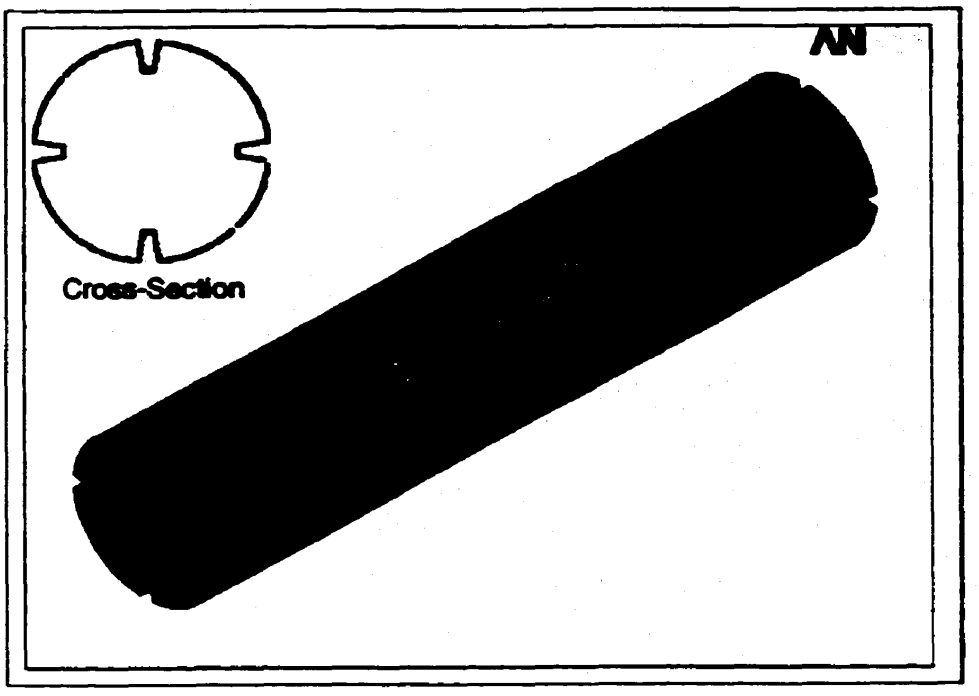

Figure 5.6 - FRP Jacket

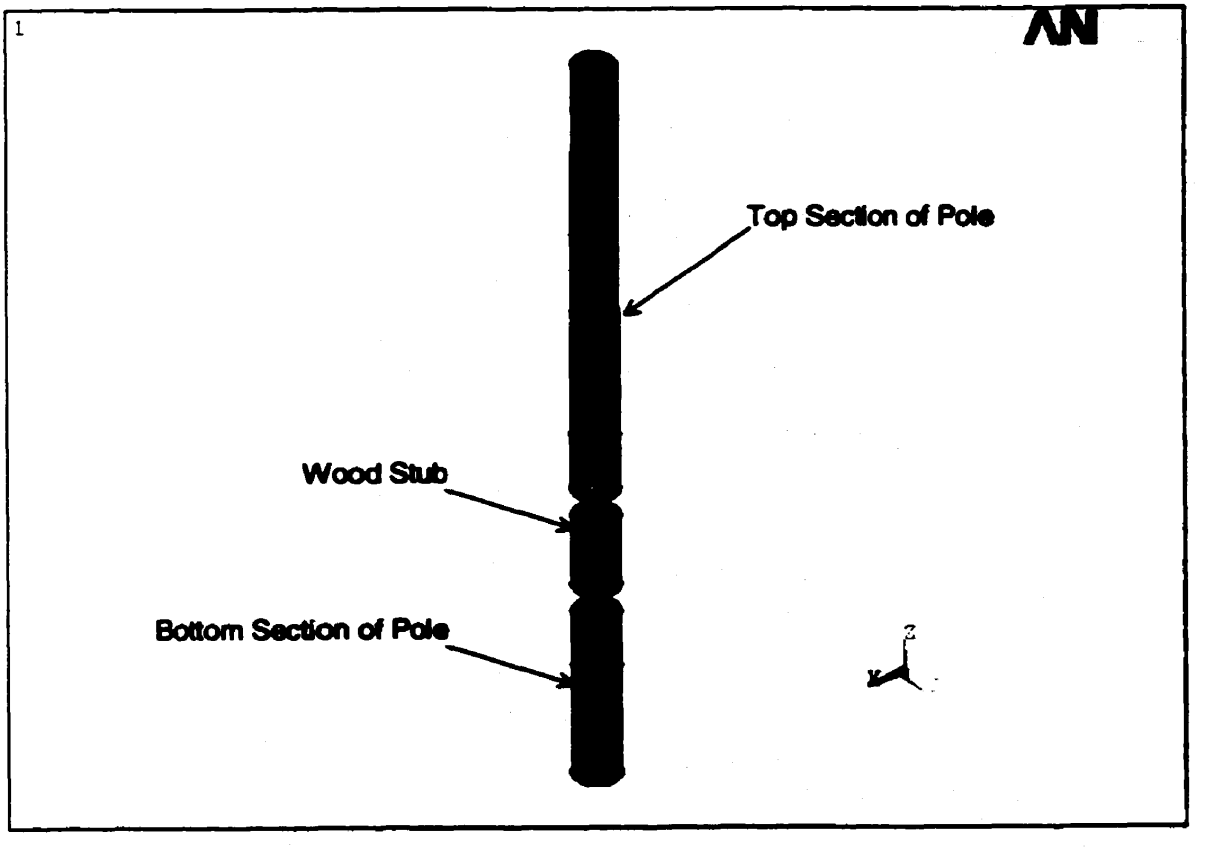

Figure 5.7- Exploded view of pole

To model the pole, an ordered mesh was required to facilitate the coupling of the nodes between the solid brick elements representing the wood pole and the shell elements representing the FRP repair material. Since the pole was curved, tight control of the mesh was required. In total, 448 elements were used to model the FRP repair material, and 1652 elements were used to model the wood pole. The mesh is shown in Figure 5.8.

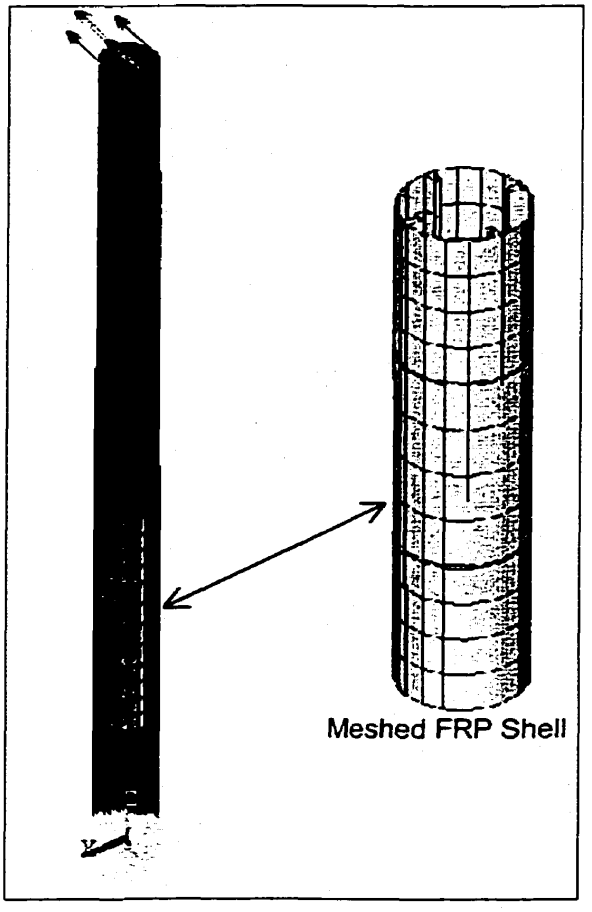

Figure 5.8 – Discretization of Pole

The material properties of the FRP used in the finite element model were those obtained in the experimental program. Since no test data were available for the

transverse modulus of elasticity of the FRP lamina, it was, conservatively, taken as that of the West System epoxy resin.

5.3 FINITE ELEMENT RESULTS

5.3.1 Control Poles

The control poles tested in Phase I were modeled using the previously described finite element model. The load-deflection curve obtained from the finite element model is compared with the load-deflection curves obtained from the experimental results in Figure 5.9.

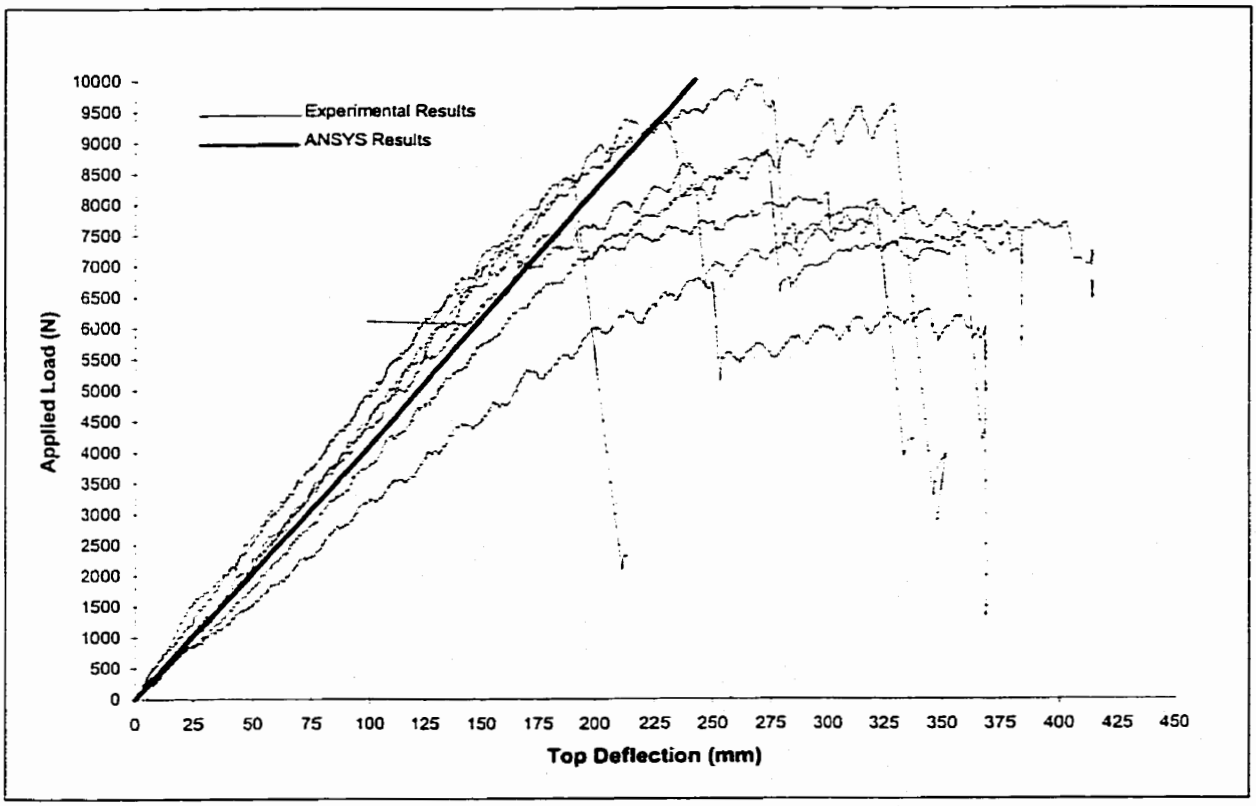

Figure 5.9 - Load-deflection curve for ANSYS control poles

The results shown in Figure 5.9 indicate that the finite element model gives a good prediction of the structural behavior of the wood poles tested in Phase I. The deflected shape of the pole at 6500 N, the load predicted by the CSA Standard as the ultimate load for a pole of the same dimensions, is shown in Figure 5.10.

The longitudinal stresses in the z-direction of the pole at 6500 N are shown in Figure 5.11. The maximum theoretical stress in the modeled pole is 47.35 MPa. The maximum stress determined according to CSA is 44 Mpa, indicating that the model can be used to accurately predict stresses.

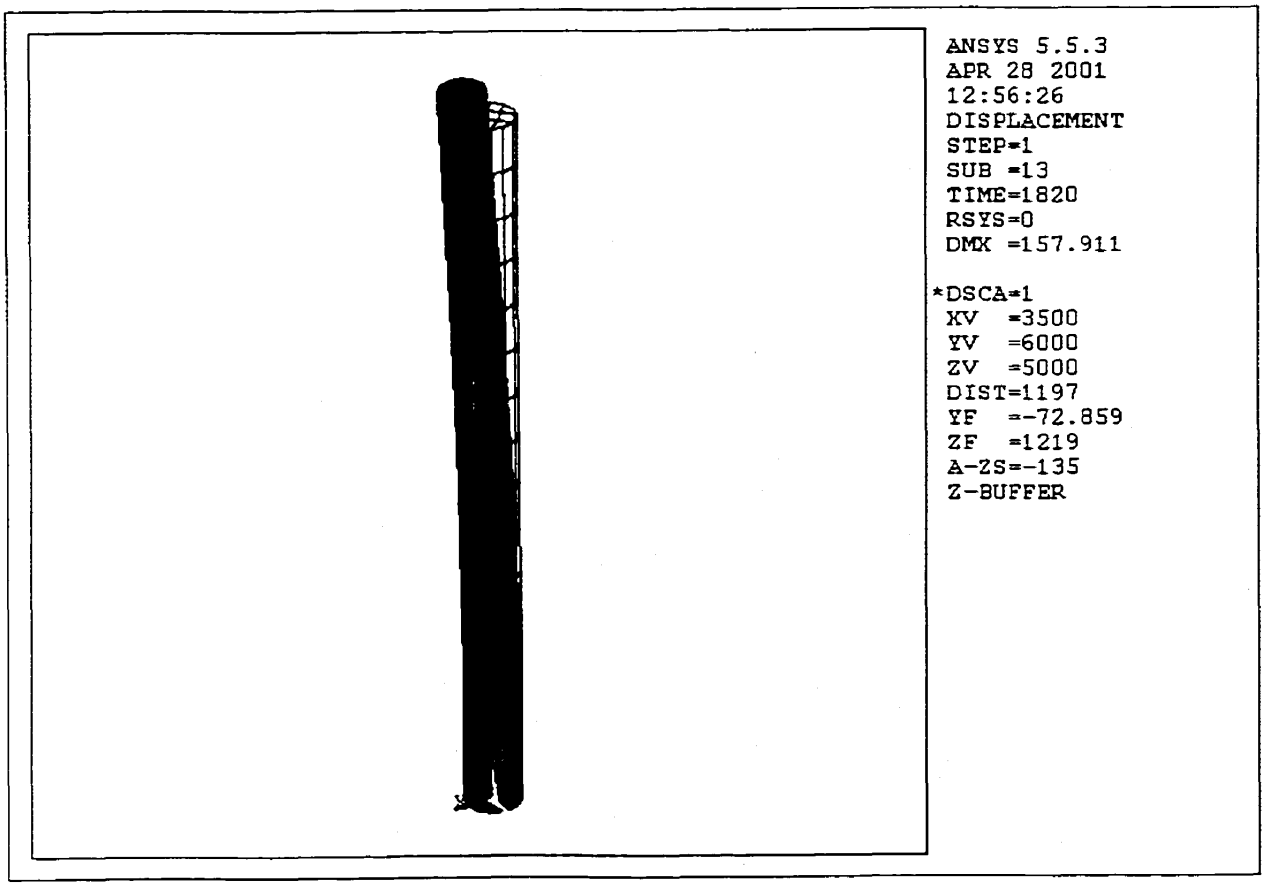

Figure 5.10 – Deflected pole

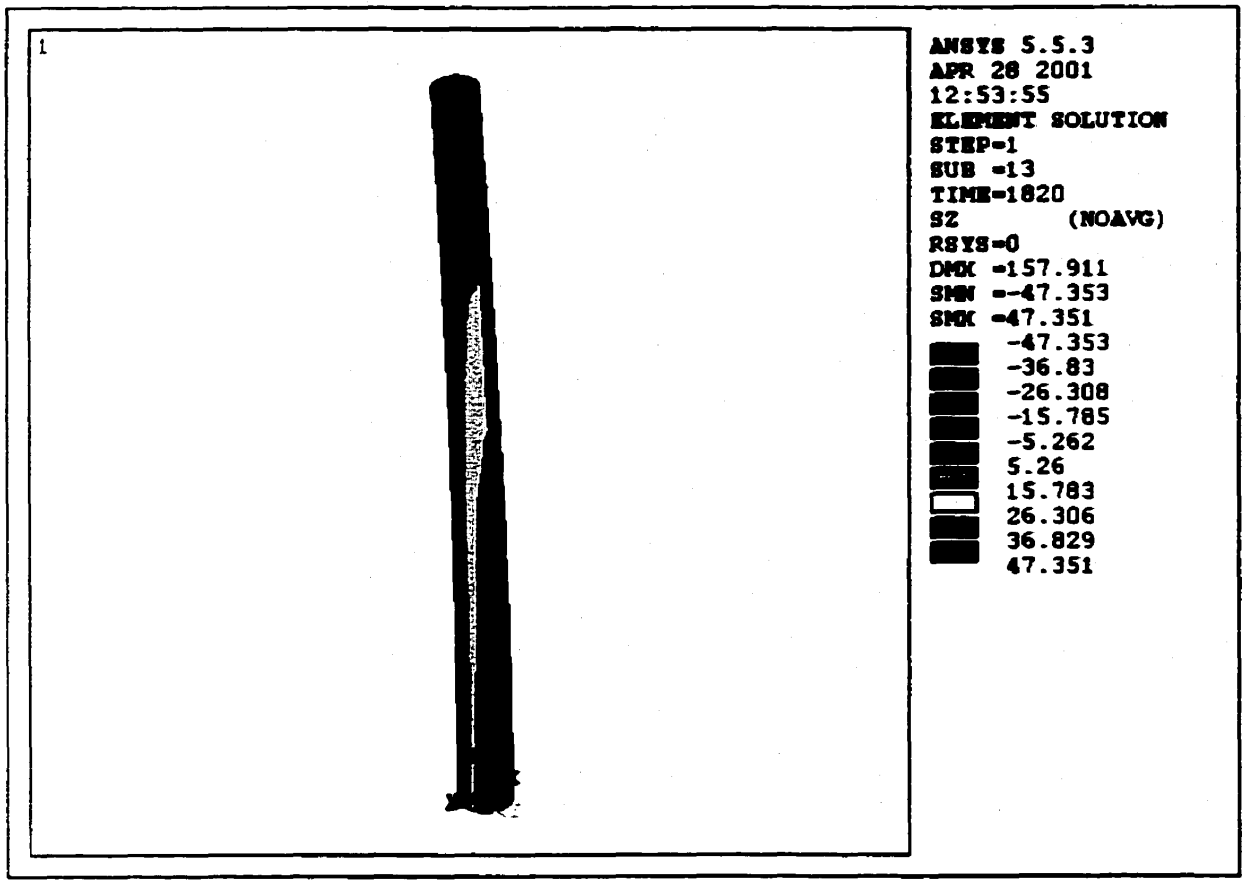

Figure 5.11 - Finite Element solution of control pole

5.3.2 Repaired Poles

The repaired poles were modeled, as described in Section 5.2.3, using the average cross sectional properties of the poles tested in Phase IV of the experimental program. A modulus of elasticity of 8400 MPa, as reported by IEEE, was used in the analysis for jack-pine poles. The load-deflection curves obtained through the finite element analysis are shown along with the load-deflection curves obtained from the Phase IV tests are shown in Figure 5.12.

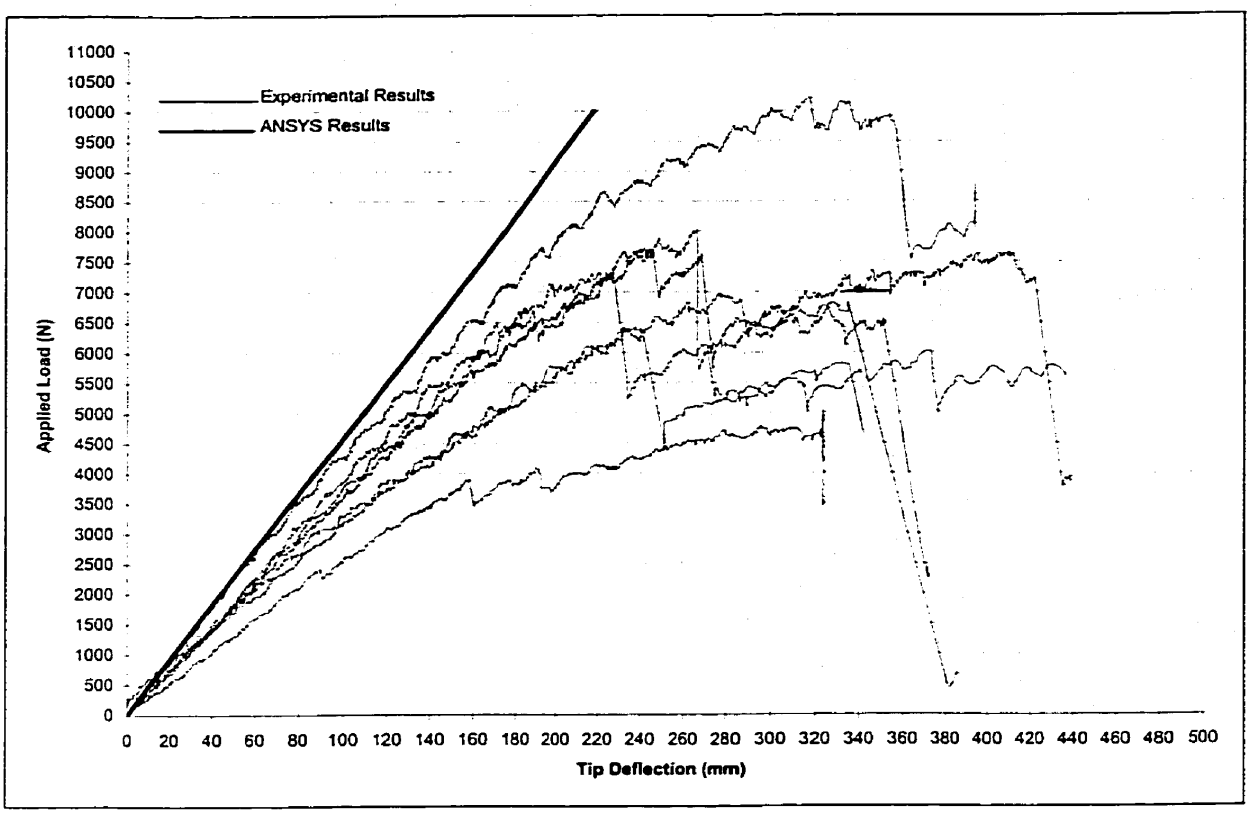

Figure 5.12 - Load-deflection curves for ANSYS repaired poles

From the plots, it can be seen that ANSYS predicts that the repaired pole will be stiffer than those in the experimental program. This is due to the lack of modeling of defects in the finite element model such as voids in the bond and defects in the pole.

The longitudinal stresses in the z- direction due to lateral load of 6500 N are shown in Figure 5.13. The maximum theoretical stress is 394 MPa, a value that is considerably higher than seen in the control pole. The point of maximum stress is located in the FRP repair region, and more specifically, in the spline and at the base of the plug. This location is shown in Figures 5.13 and 5.14.

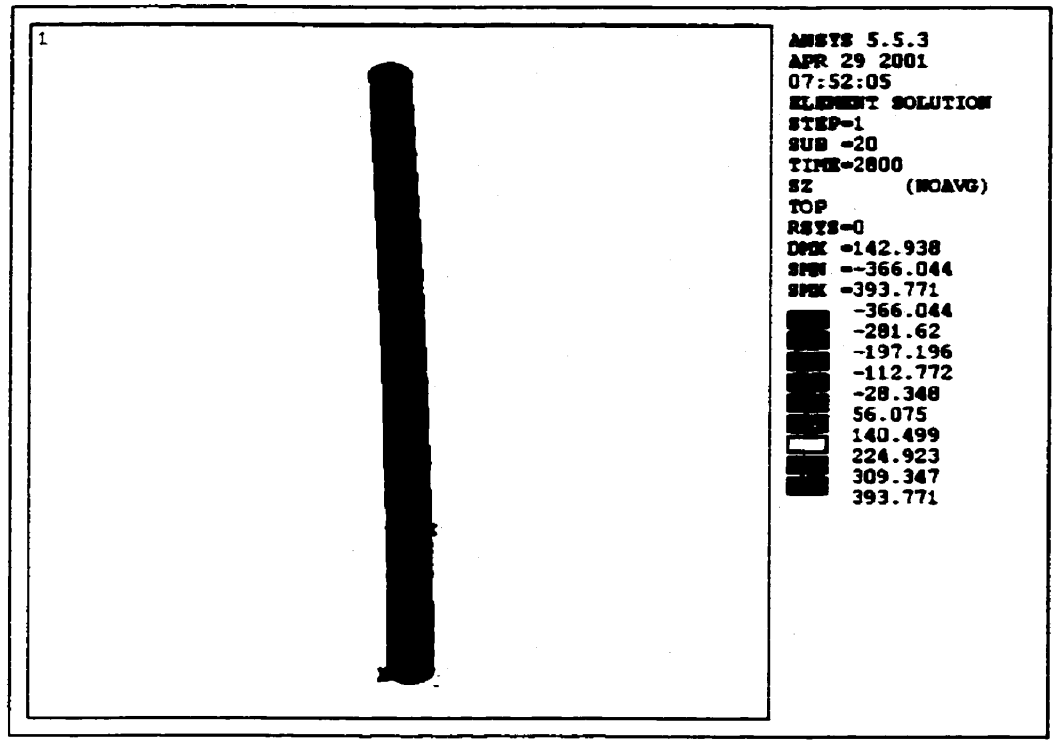

Figure 5.13 – Stress in z-direction in repaired pole

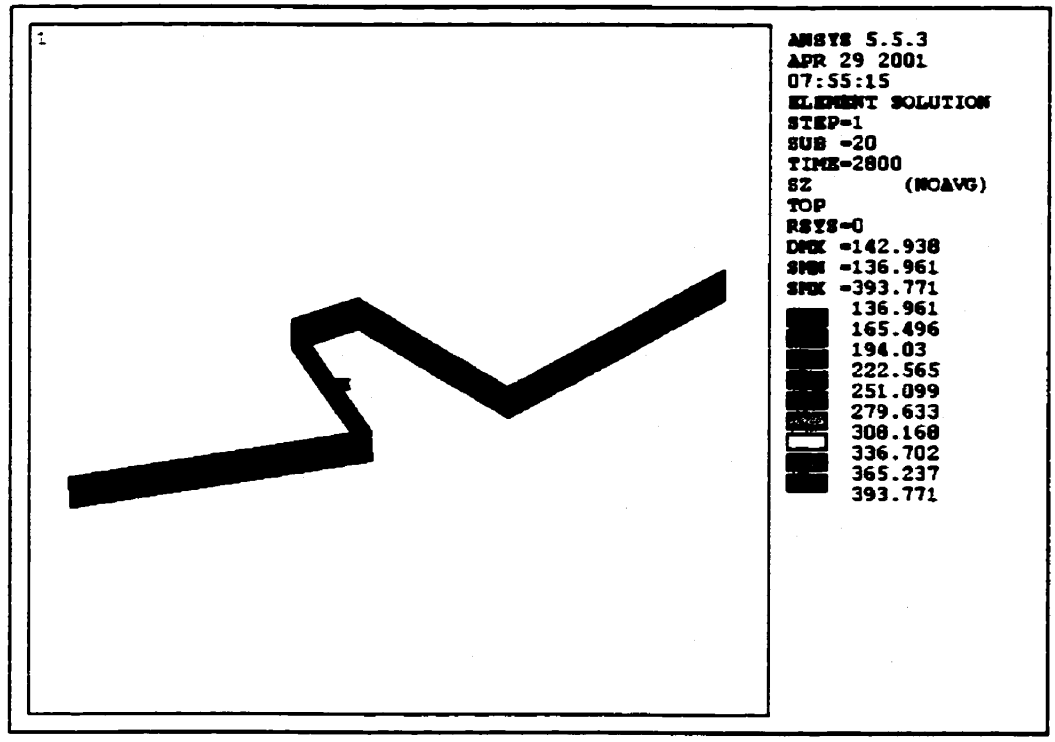

Figure 5.14 – Maximum stress in spline.

This value is a good approximation as the full tensile bending stress is transferred at this location from the plug to the butt of the pole. Using traditional stress analysis techniques and assuming that the splines resist the full bending, the average stress in the spline at a location 610-mm above the ground line is 388-MPa. This is computed in Appendix E. The theoretical stresses are lower than the value of 610-MPa recorded in the testing program. This indicates that the capacity of the FRP system surpasses the bending moment capacity required by the CSA Standard for new poles. Using the ultimate strength of each FRP spline, the bending capacity of four symmetrically placed FRP splines would be 18710 N-m. Using the distance between the applied load and the base of the plug of 1830-mm, it can be shown that the splines can resist a maximum applied load of 10000 N. None of the poles tested in this study had a failure load higher than this, implying that wood failure rather than FRP failure would govern. This was confirmed in the tests of Phase IV.

In order to evaluate the model further, the strains recorded in the testing program were compared with the strains obtained through the finite element analysis. Longitudinal strains were examined at four locations using the finite element model. These locations correspond to the locations of the strain gauges in the Phase IV specimens. The theoretical transverse strains at two locations were compared with the experimental transverse strains. The results are shown in Figures 5.15 through 5.20.

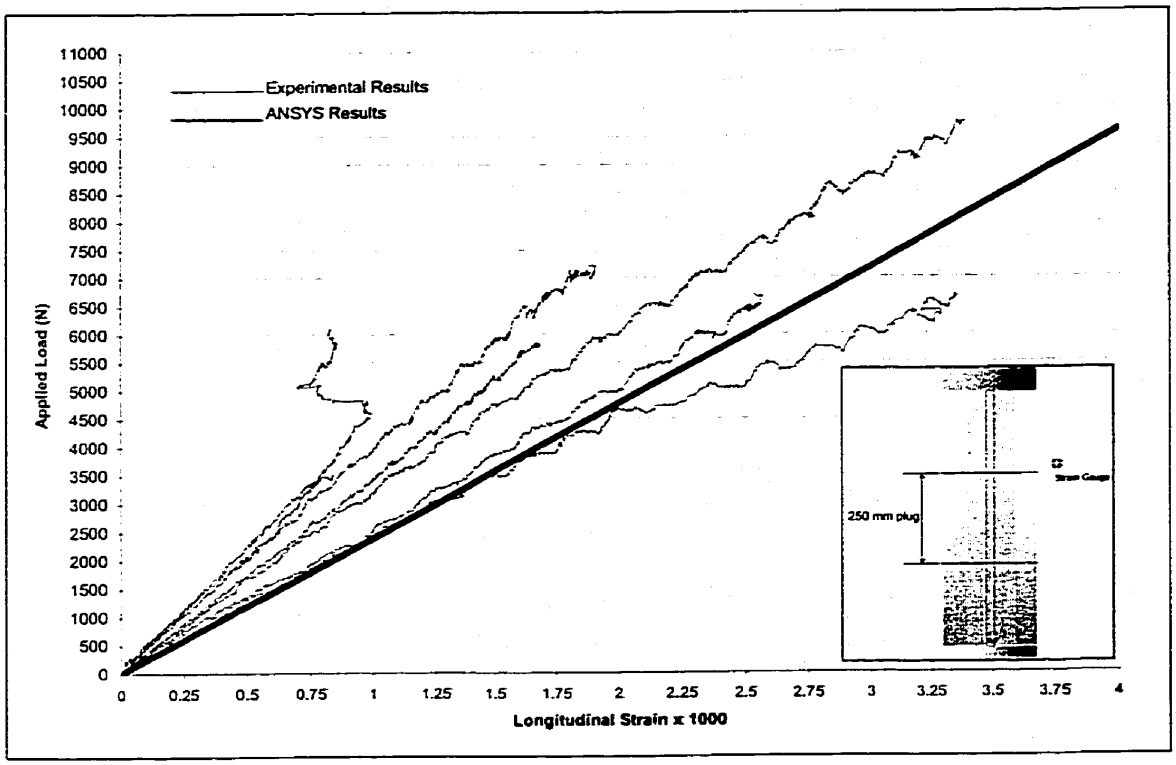

Figure 5.15 – Load – Longitudinal Strain comparison at base of spline.

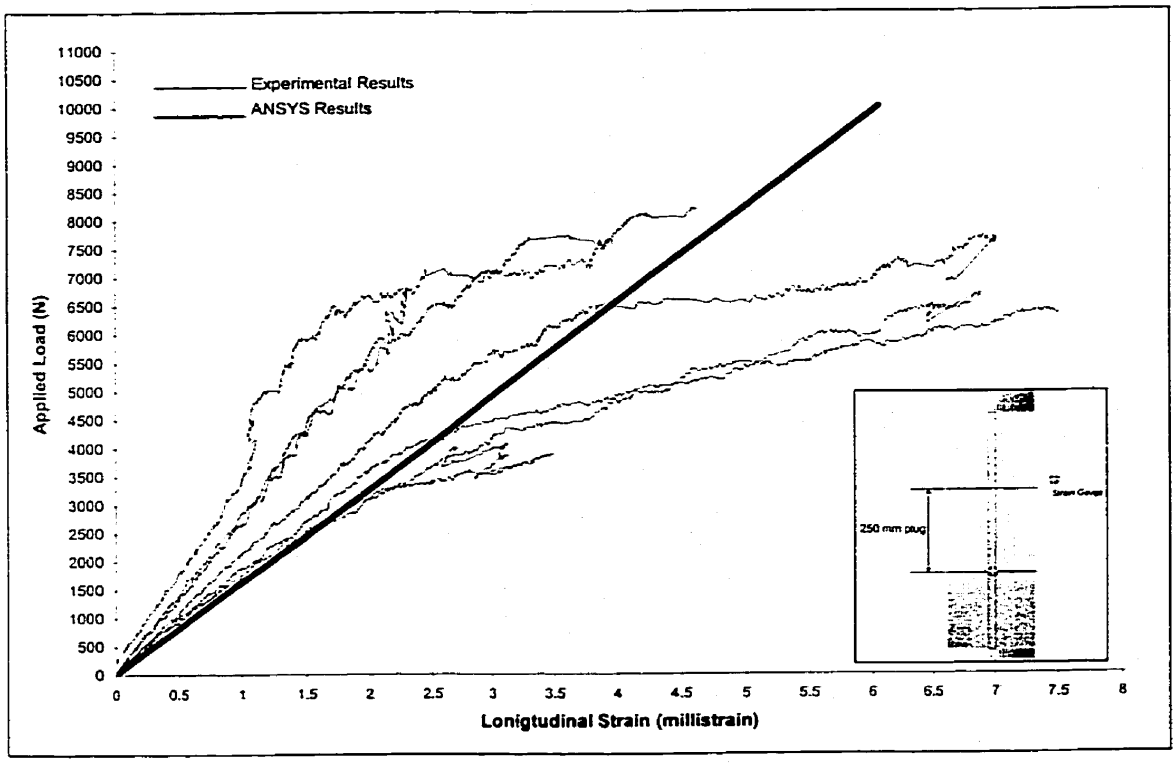

Figure 5.16 - Load – Longitudinal Strain comparison at base of stub.

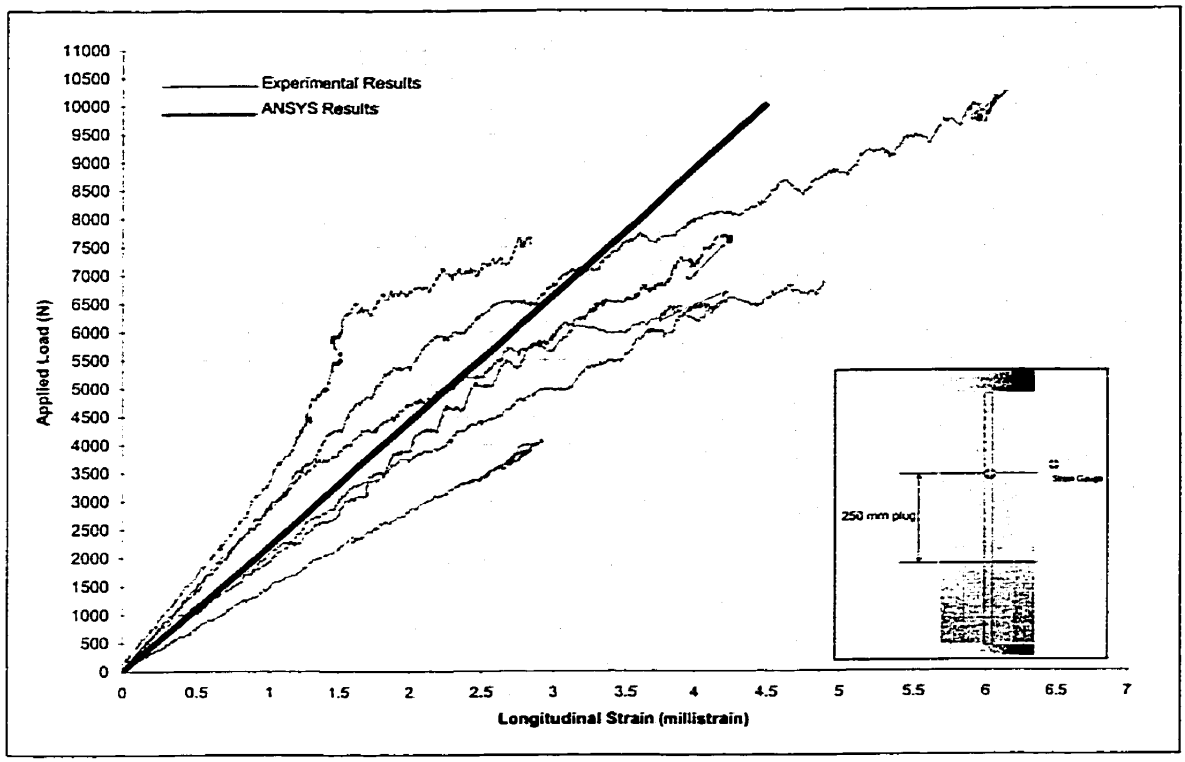

Figure 5.17 - Load – Longitudinal Strain comparison at top of stub.

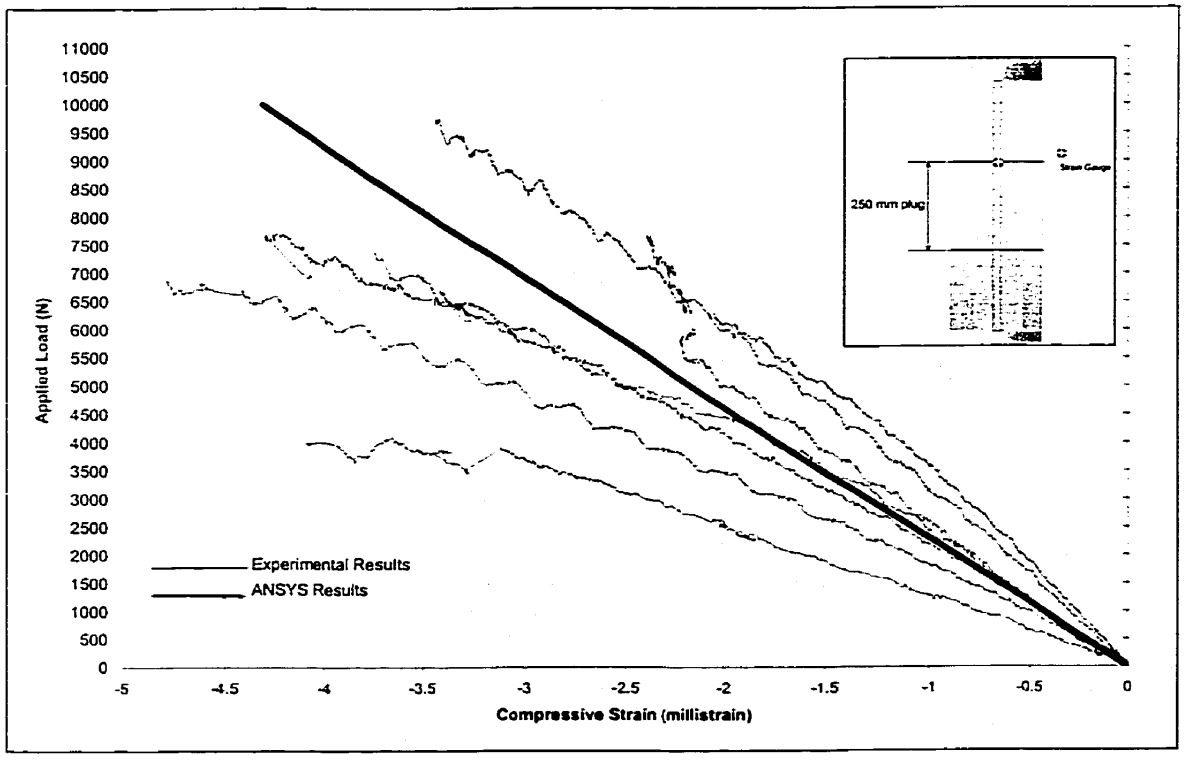

Figure 5.18 - Load –Compressive Strain comparison.

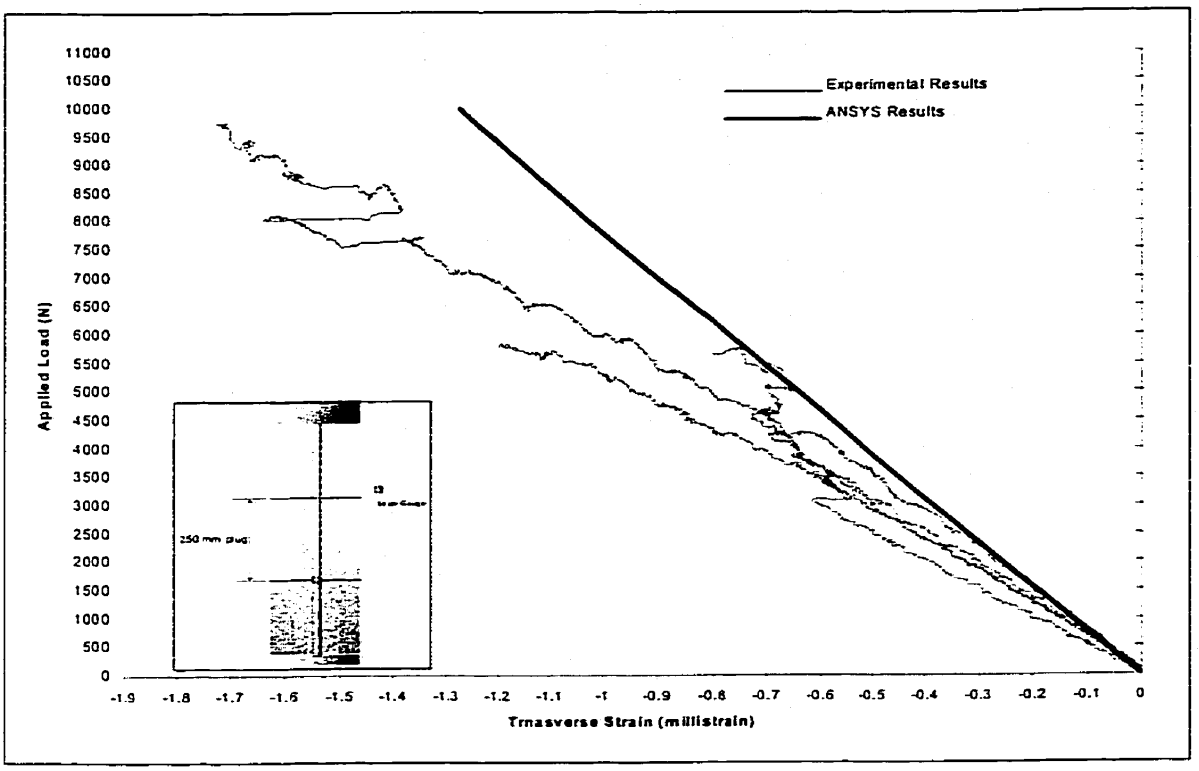

Figure 5.19 - Load –Transverse Strain comparison.

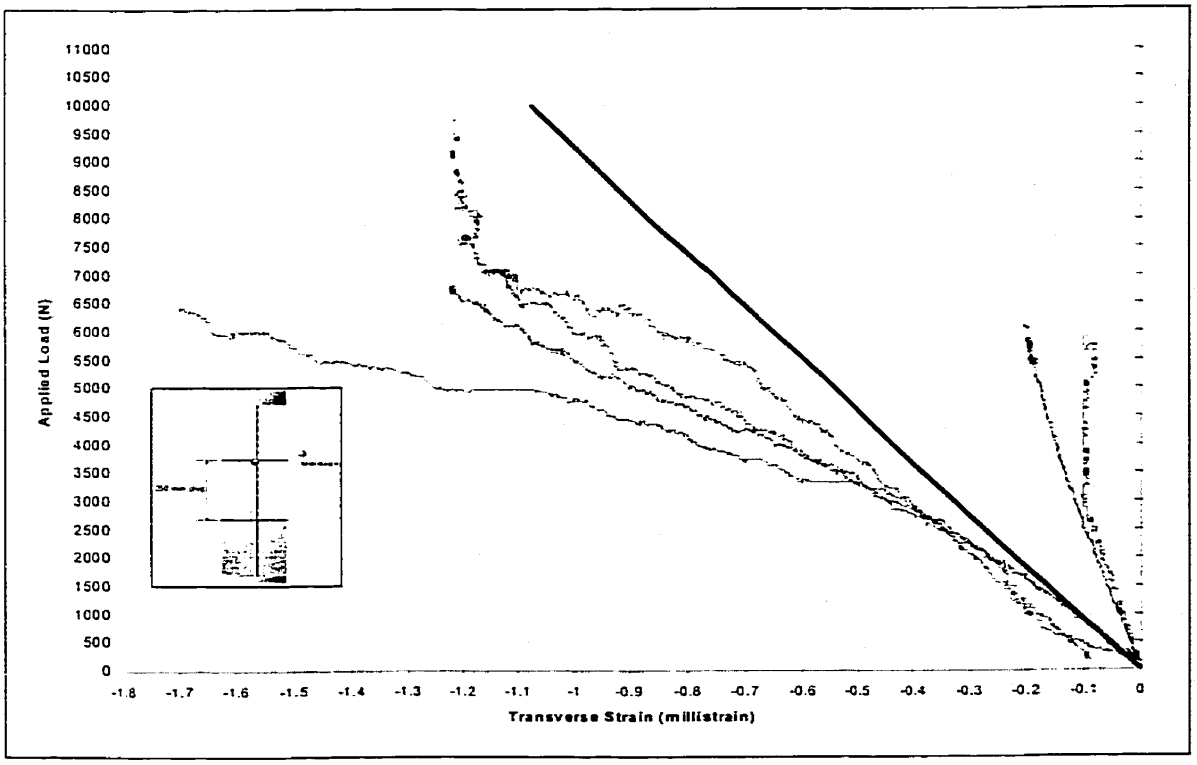

Figure 5.20 - Load –Transverse Strain comparison.

From the plots, it is seen that the finite element model can be used to accurately predict the strains in the FRP repaired poles.

5.4 DESIGN EQUATIONS

As seen in the literature, such as the Trial-Use Design Guide for Wood Transmission Structures by IEEE (IEEE,1991)n a very conservative design approach is used for wood poles. This conservative approach will be used in formulating equations for designing with the FRP materials for repairing wood poles.

5.4.1 Design of FRP Splines for Bending

In order to ensure that the FRP repair materials have adequate strength capacity to resist the applied load, it was assumed that only the FRP splines would provide the bending resistance in the repaired region. Additionally, as the design is fully symmetric in the plane of its cross section, a conservative approach to designing FRP splines was to assume that two splines will resist all of the bending in the pole. Only the required area of the FRP spline will be determined, and no consideration of the shape of the spline would be given. Although the reinforcement was designed without consideration to its shape, the advantage of the shape of the spline used in this thesis is that the centroid of the spline would be further from the axis of bending of the pole than the simplified round reinforcement, effectively increasing the bending section modulus of the splines.

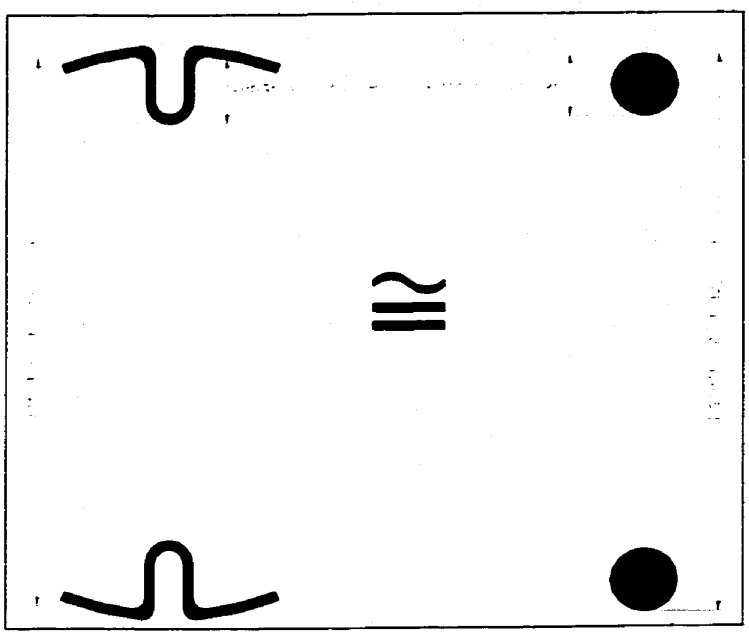

Figure 5.21 - Spline properties

The first assumption for the design equations was made realizing that the moment of inertia of the reinforcement about its own axis is negligible. From this assumption, the moment of inertia of the FRP splines was assumed to be;

$$I_{FRP} = 2 \cdot A_{FRP} \cdot d^2 \qquad \textit{Equation 5.1}$$

Where

I_{FRP} = moment of inertia of the FRP spline;

A_{FRP} = cross sectional area of the FRP spline;

d = distance of centroid of reinforcement from center of pole.

Additionally, because the inertia of the round reinforcement is only slightly smaller than that of the flanged section, the reinforcement can be assumed to be round for design purposes.

In order to be a satisfactory design, the repaired section must resist all of the bending stress incurred by the pole. The maximum stress occurs at the ground line for a wood pole is given by Equation 2.2 as

$$MOR = \frac{32\pi^2 P_{ult}(L-\delta_L)}{C^3} \qquad \textit{Equation 2.2}$$

Since,

$$M_{pole} = P_{ult}(L-\delta_L) \qquad \textit{Equation 5.2}$$

$$M_{pole} = \frac{MOR \cdot C^3}{32 \cdot \pi^2} \qquad \textit{Equation 5.3}$$

where;

M_{pole} = ultimate bending moment in pole.

The ultimate bending stress in the splines can be found using the following equations;

$$M_{FRP} = \frac{I_{FRP} \cdot \sigma_{FRP}}{d} \qquad \textit{Equation 5.4}$$

where;

M_{FRP} = moment capacity of spline;

σ_{FRP} = ultimate strength of FRP used in splines.

Realizing that the moment capacity of the splines must equal the applied moment in the pole, the required area of FRP can be determined combining Equations 2.2, 5.1, 5.3 and 5.4;

$$A_{FRP} = \frac{MOR}{\sigma_{FRP}} \cdot \frac{C^3}{64 \cdot \pi^2 \cdot d} \qquad \textit{Equation 5.5}$$

where;

C = circumference of the pole at groundline.

5.4.2 Development Length of Spline

As the FRP material is considerably stronger than wood, the wood will fail before the FRP ruptures in tension. Therefore, the development length of the FRP spline was designed assuming that the bond between the FRP and the wood was stronger than the shear capacity of the wood. In developing an approximate design approach, it was assumed that the spline was bonded only along the sides and the base of the groove. The bond along the flanges was ignored. This is a reasonable assumption since voids were present in the repair region. The applied tensile force acting parallel to the spline was computed based the free-body diagram in Figure 5.22.

$$T = \frac{P_{ult} \cdot h_{load}}{d_{\phi}} \qquad \textit{Equation 5.6}$$

where;

d_{ϕ} = average diameter of pole at repair location;

h_{load} = height of applied load measured from base of stub.

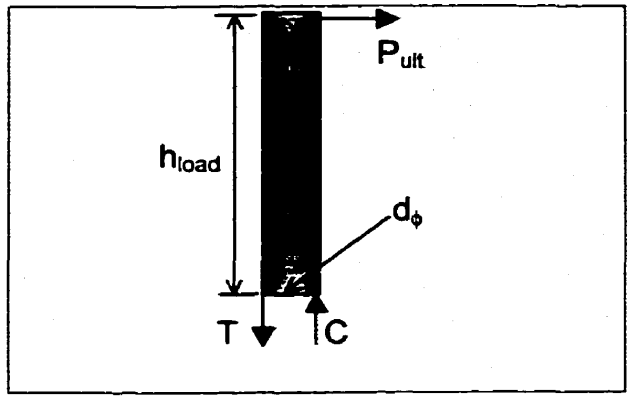

Figure 5.22 – Free-body diagram for spline development length

Additionally;

$$A_{dl} = (2 \cdot b + w) \cdot l_{spline} \qquad \textit{Equation 5.7}$$

where;

A_{dl} = bond development area required;

b = depth of groove;

w = width of groove;

l_{spline} = development length of spline.

Again assuming that the wood will fail in shear before the bond between the FRP and wood fails;

$$T = \tau_{wood} \cdot A_{dl} \qquad \textit{Equation 5.8}$$

where;

τ_{wood} = maximum allowable shear stress in wood (MPa).

Combining Equations 5.8 and 5.7 gives;

$$l_{spline} = \frac{P_{ult} \cdot h_{load}}{\tau_{wood} \cdot (2 \cdot b + w) \cdot d_{\phi}} \qquad \textit{Equation 5.9}$$

The length, l_{spline} in Equation 5.9 accounts only for the length of the spline required prior to the addition of the stub. With the addition of the stub, this length increased by the height of the stub as follows;

$$l_{spline} = \frac{P_{ult} \cdot h_{load}}{\tau_{wood} \cdot (2 \cdot b + w) \cdot d_{\phi}} + S_H \qquad \textit{Equation 5.10}$$

Where;

S_H = Stub Height.

5.4.3 Confinement Wrap

In order to confine the FRP splines, the conservative approach, also used by Tyfos Fibrewrap, is to apply two circumferential layers for every one longitudinal layer. Using this approach, the wrap would be designed to resist twice the ultimate load of the FRP. This is much more than is required, but this layer must also protect the splines from the environment. As the maximum stresses would occur below the plug, the stresses at this level were used to design the required thickness of the FRP layer. By calculating the sum of the areas of the FRP splines, the area can be represented by the circumference of the pole. As this

design deals with four splines, the longitudinal FRP thickness per unit of circumference can be determined by;

$$t_{FRP} = \frac{4 \cdot A_{FRP}}{C} \qquad \text{Equation 5.11}$$

Doubling this value gives the required thickness of the FRP jacket;

$$t_{jacket} = \frac{8 \cdot A_{FRP}}{C} \qquad \text{Equation 5.12}$$

The jacket is applied over the entire length of the repaired area.

In designing the shear transfer layer, the stresses must be transferred from the base of the splines to the base of the pole. The shear transfer layer needs to be orientated in the same direction as the splines. In order to ensure uniform stress transfer, one half of the shear transfer layer is applied on the spline, while the other half is applied to the pole. The required thickness of the shear transfer layer can be the same thickness as the FRP splines. To determine the length of the shear transfer layer, the surface area of the shear transfer layer must be large enough so that the wood on the surface of the pole would not fail in shear. In order to maintain a smooth shear transition zone, the base of the spline was chamfered to 45^0. The assumption of how the shear stress would be transferred to the pole is shown in Figure 5.23. The length over which this transfer would take place is;

$$l_{shear} = \frac{P_{ult} \cdot h_{load}}{\tau_{wood} \cdot w_s \cdot d_\phi} \qquad \text{Equation 5.13}$$

where;

l_{shear} = length of the shear layer;

w_s = total width of spline.

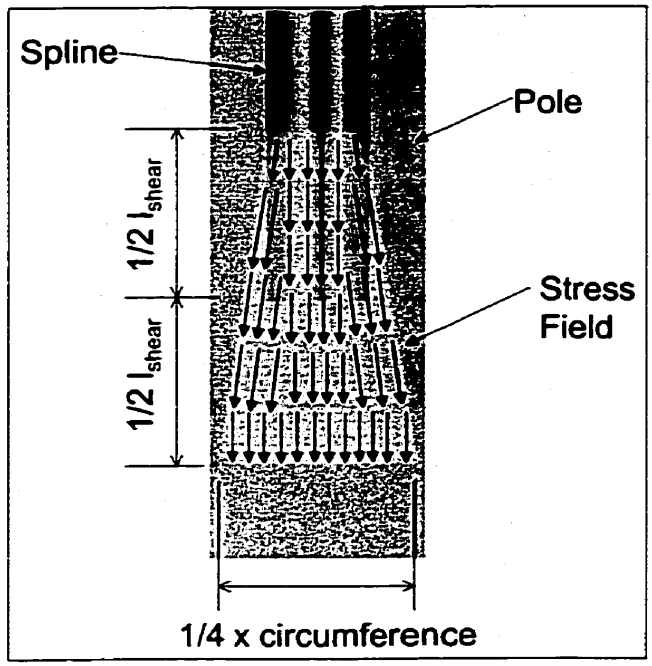

Figure 5.23 – Shear transfer

A detailed example of the design equations is given in Appendix F.

CHAPTER 6

SUMMARY AND CONCLUSIONS

6.1 SUMMARY

A total of 27 3050-mm jack-pine poles were tested to failure to determine the effectiveness of using FRP to restore wooden utility poles. The poles were tested in four distinct phases. In the first phase, seven poles were tested to failure to determine the material properties of the 3050-mm poles. Based on the results from the first phase, the following conclusions were made;

1. The poles tested had an average ultimate capacity of 8500-N, giving the tested poles an average class 5 rating. Using the CSA standard for wood poles, the average predicted ultimate capacity of the poles was 6500-N, a class 7 rating.
2. The average calculated modulus of elasticity (MOE) for the poles tested in Phase I is 7790 MPa. IEEE gives the MOE for design of pole structures using jack-pine poles as 8400 MPa. IEEE gives a coefficient of variation on this

value of 20%, indicating that the tested poles fall within the predicted range for MOE.

3. All poles failed through tension failure at the base.
4. The average calculated modulus of rupture at the base of the pole was 52.6 MPa.

The objective of the second phase was to determine the required length of reinforcement needed to restore the tension side of the pole after a 2-mm gauged cut located 610-mm from the ground line halfway through the cross-section and reinforced with varying lengths of FRP reinforcement. Based on the results of the second phase, the following conclusions were made;

1. The 203-mm and 254-mm splines were not long enough to develop the required bond between the spline and the pole. These reinforcement lengths obtained 46% and 56% of the predicted capacity of the poles.
2. The resin used in bonding the splines to the wood must have enough viscosity to ensure that the resin is uniformly distributed between the pole and spline as the resin cures.
3. The 305-mm and 406-mm splines had enough bond capacity to cause local wood failure between the pole and the spline. These reinforcement lengths obtained 58% and 66% of the predicted capacity of the poles.

4. A fully developed bond between the FRP spline and the groove in the wood pole has a greater bond capacity than a fully developed bond between the flanges of the spline and the surface of the pole.

The third phase involved confining selected spline reinforcement used in the second phase, and to further develop the bond between the wood pole and FRP spline. From this phase of the program it was concluded that;

1. Adding a confinement increased the load carrying capacity of the FRP repair. The poles reinforced with the 305-mm long splines saw an average capacity increase over the Phase II specimens reinforced with 305-mm splines of 45%. The poles reinforced with the 406-mm long splines saw an average capacity increase over the Phase II specimens reinforced with 406-mm splines of 77%.
2. Adding an FRP interface layer in the bond between the spline and the pole increased bond performance and forced the failure into the wood.
3. The fully bonded poles failed in shear at the base of the spline.

In the fourth phase of the project, the wood poles were repaired and tested using the proposed method. From this phase the following conclusions were drawn;

1. In order to provide alignment of the pole sections during repair, only one alignment key should be used for each interface to prevent premature failure.

2. To avoid the high stress concentration at the base of the spline, the base of the spline must be chamfered to 45^0 and a shear transfer layer must be added.
3. Fully rehabilitated poles were able to exceed the "at installation" capacities indicated by the CSA Standard, exceeding the 67% of "at installation" capacity required for a restored Grade B utility pole.
4. No separation of the stub from the rest of the pole was observed in fully restored poles, indicating that the bond between the pole and the FRP-spline had an anchoring capacity greater that the bending capacity of the pole.

Finite element models and approximate equations were developed to predict the structural performance of the FRP-restored wood utility poles. Using the developed finite element models and equations, the following conclusions were drawn;

1. The finite element model accurately predicted the load-deflection characteristics of a solid jack-pine pole within the range of variability typical with wood structures.
2. The theoretical maximum stress at ground line in the modeled pole was 47-MPa at the average CSA predicted capacity of 6500-N of the Phase I poles. This compares well with the ultimate predicted ground line stress (MOR) of 44-MPa.

3. The finite element model indicated that the FRP-restored pole was slightly stiffer than the poles in Phase IV of the experimental program. This is acceptable, as the FRP-repair was designed to resist loads for perfect poles.
4. The finite element model indicated that the maximum stress in a repaired pole occurs at the base of the stub, in the spline at a value of 394-MPa. This compares well with the maximum stress obtained in the repaired pole using traditional strength of materials giving a maximum stress of 388-MPa.
5. The longitudinal strains measured in the FRP-repaired poles in Phase IV of the experimental program were accurately predicted using the finite element model.
6. The transverse strains measured in the FRP-repaired poles in Phase IV of the experimental program were accurately predicted at the base and at the top of the wood stub on the tension side of the pole using the finite element model.
7. The simplified equations were evaluated through comparison with the experimental data and could, thus, be used as a first stage toward the design of a complete repair system for wood poles. A more detailed analysis, however, is recommended

6.2 RECOMMENDATIONS FOR FUTURE RESEARCH

In order to fully develop this FRP restoration system for wood utility poles, further research is recommended in the following areas:

1. Further development of field manufacturing techniques to ensure quick and safe implementation.
2. Investigation of different spline configurations.
3. Evaluation of the FRP repair system under cyclic and dynamic loading.
4. Full-scale testing on different species of wood poles.
5. Investigate long-term bond performance in a variety of environmental conditions.
6. Complete parametric studies on various pole sizes and classes using the developed finite element models.
7. Develop pole-climbing techniques for repaired poles.

REFERENCES

1. Adams, S.F., and Tang, R.C., "Applications of Reinforced Plastics for Laminated Transmission Poles," *Forest Products Journal*, Vol. 23, No. 10, October 1972, pp. 42-46.

2. Alden, H. A., "Softwoods of North America", *United States Department of Agriculture General Technical Report FPL-GTR-102*, September 1997

3. American Wood Preservers, American Wood Preservers Web Page, www.APWI.org, 2001.

4. American National Standards Institue, Standard 0.51-1992, American National Standard for Wood Poles - Specifications and Dimensions, developed by Accredited Standards Committee on Specifications for Wood Poles O5, 1992.

5. American Society For Testing and Materials, "D 1036-99, Standard Test Methods of Static Tests of Wooden Poles," developed by ASTM Subcommittee D07.04, 1999.

6. American Society For Testing and Materials, "D 3039, Standard Test Methods for Tensile Properties of Polymer Matrix Composite Materials", developed by ASTM Subcomitee D30.04, 2000.

7. American Society For Testing and Materials , "D 3410, Standard Test Method for Compressive Properties of Polymer Matrix Composite Materials with Unsupported Gage Section by Shear Loading", developed by ASTM Subcomitee D30.04, 1995.

8. ANSYS, "ANSYS User Manual, Revision 5.2", ANSYS Inc., 1995.

9. Ararwal, B.D., "Analysis and Performance of Fiber Composites", Wiley, 1980.

10. Ashour, A.F., El-Refaie, S.A., and Garrity, S.W., "Flexural Capacity of Reinforced Concrete Beams Strength with External Plates," *Structural Faults and Repairs 99*, 1999.

11. Becque, J., "Analytical Modelling of Concrete Columns Confined by FRP," M.Sc. Thesis, University of Manitoba, Winnipeg, Manitoba, Feb. 2000

12. Bingell, N.G, "Cost Saving Benefits of Wood Structure Maintenance," *Proceedings of the IEEE International Conference on Transmission and*

Distribution Construction and Live Line Maintenance, 1995 Columbus, OH, pp. 11-16.

13. Canadian Standards Association (CSA), "Wood Utility Poles and Reinforcing Stubs (CAN/CSA-015-90)," 1990, Rexdale, Ontario.

14. Chareswood Do-it Center, "jack-pine MSDS Sheet," Fax Transmittal, May, 2000.

15. Cheng, J.J., R and Dorey, A.B., "The Behavior of GFRP Glued Laminated Timber Beams," *Proceedings in Advanced Composite Materials in Bridges and Structures*, ACMBS II MMEL-BADRY, 1996, Montreal, pp. 787-794.

16. Daniel, I.M., and Ishai, O., "Engineering Mechanics of Composite Materials," Oxford University Press, New York, 1994.

17. Davalos, J.F., Qiao, P, and Zipfel, M.G., "Feasibility Study of GFRP-Reinforced Wood Railroad Crosstie," *Journal of Composites for Construction*, Vol. 3, No. 2, May, 1999, pp.92-99

18. Department of Defense, "MIL-HDBK-17-3 Volume 3, Materials Usage, Design, and Analysis", 1997.

19. Editor, "Lift that Pole - Avoid an Outage," *Electrical World*, Spetember/October 2000, pp. 20-21

20. Engineering Data Management, Inc., "Full-Scale Destuctive Tests of TYFOS Fibrwrap System for Wood Pole Restoration", Report to Fyfe Co., July 1995.

21. Funk & Wanglis, "Canadian College Dictionary", Fitzhenry and Whiteside, Markham, 1989

22. Fyfe, "Tyfo System for Wood," Product Brochure, 1999

23. Gentile, C., "Flexural Strengthening of Timber Bridges Using FRP", M.Sc. Thesis, University of Manitoba, Winnipeg, Manitoba January 2000.

24. Goodman, J.R. and Stewart, A.H., "Wood Pole Management – Utility Case Studies", *IEEE Transactions on Power Delivery*, Vol. 5, No. 1, January 1990, pp. 422-425

25. Gougen, "West System Epoxy Physical Properties", Gougen Brothers Inc. Web Page, www.westsystem.com, February 2001

26. Green, D. W., Winandy, J. E., and Kretschmann, D. E., "Mechanical Properties of Wood", *U.S. Department of Agriculture General Technical Report FPL-GTR-113*, 1999

27. Hayes, W., "Extending Wood Pole Life: Solving a $5-billion/year Program," *Electrical World*, Febuary, 1986, pp. 41-47.

28. Hosain, M. U., Marzouk, H. M., and Neis, V. V., "Built-up Utility Poles Using Prairie Timber," *Forest Products Journal*, Vol. 28, No.11, November 1978, pp 49-54.

29. IEEE Standard 751 "Trial Design Guide for Wood Transmission Structures," developed by the Wood Structure Working Group of the Towers, Poles, and Conductors Subcommittee, 1991.

30. IEEE Standard C2-1997 "National Electrical Safety Code," developed by Accreditted Standards Committee C2-1997, 1997.

31. Johns, K.C. and Lacroix, S., "Composite Reinforcement of Timber in Bending", *Accepted for publication in the Canadian Journal of Civil Engineering*, 2000.

32. Laminated Wood Systems, Inc., "Field Installation Manual for PRF and PRH Systems," P.O. Box 386, Seward, NE 68434

33. Laminated Systems, "Phaseraiser Product", Laminated Wood Systems Inc Web Page, http://www.lwsinc.com/phasermain.html, December 2000.

34. Lacovara, Bob, "What Exactly are Composites? Do we take the Definition for Granted?", Composite Fabricators Web Page, www.cfa-hq.org, 2001

35. Mallick, P.K., "Fiber-Reinforced Composites: Materials, Manufacturing and Design," Dekker, 1993

36. Manitoba Hydro, "Representative Recycling Projects from 1996/97", Manitoba Hydro Web Page, http://www.hydro.mb.ca, April 2001

37. Marshall, A.C., "Composite Basics - 5," Marshall Consulting, 1998

38. Osmose, "Product Literature", Osmose Wood Preserving Co. of America, Inc Web Pag., www.osmose.com, December 2000.

39. Plevris, N., and Triantafillou, T.C., "FRP-Reinforced Wood as Structural Material," *Journal of Materials in Civil Engineering*, Vol. 4, No. 3 August, 1992, pp. 300-317

40. Richardson, T., "Composites: A Design Guiude", Industrial Press, 1987.

41. Schwartz, M, "Composite Materials, Volume 2; Processing, Fabrication, and Applications," Prentice Hall, New Jersey, 1997.

42. SPI Composites Institute, "Extending Utility Pole Life," *FRP Composites in Construction Applications: A profile in Progress*, 1995, pp.47-48.

APPENDIX A

MOMENT CAPACITY OF SPLINE AND JACK-PINE POLE

A requirement for the FRP spline used to reinforce the wood poles was that one spline had moment capacity, approximately, equivalent to the poles tested in the experimental program. Assuming elastic behavior;

$$M_{pole} = MOR \cdot S_{pole} \qquad \textit{Equation A.1}$$

where;

M_{pole} = ultimate bending moment in pole;

S_{pole} = section modulus of pole;

MOR = modulus of rupture of pole.

For round sections;

$$S_{pole} = \frac{C^3}{32 \cdot \pi^2} \qquad \textit{Equation A.2}$$

Where;

C = circumference of pole at ground line;

Combining Equation A.1 and A.2 gives;

$$M_{pole} = \frac{MOR \cdot C^3}{32 \cdot \pi^2} \qquad \textit{Equation A.3}$$

The poles were ordered with a butt-circumference 480-mm, which will be taken as the circumference at the ground line. Using the Modulus of Rupture given by the CSA standard of 44-MPa, and Equation A.3, the ultimate moment capacity of the jack-pine poles used in the experimental program is 15.41-kN-m.

The moment of inertia of the splines about center of the pole was found to 1.16×10^4 mm^4. This is shown in Figure A.1. The maximum stress used for the spline was 1.08-Gpa, which is the generic E-Glass/Epoxy value obtained from Daniel and Ishai's text Engineering Mechanics of Composite Materials. This value was multiplied by .8 to reflect any uncertainty in the ultimate stress in the actual FRP material giving a maximum stress of 864 MPa. The distance of the centroid (y_{cgs}) of the spline from center of the pole was found to be 70.99-mm. Using the following equation;

$$M_{FRP} = \frac{I_{FRP} \cdot \sigma_{FRP}}{y_{cgs}} \qquad \textit{Equation A.3}$$

where;

M_{FRP} = moment capacity of FRP spline;

I_{FRP} = moment of inertia of FRP spline;

σ_{FRP} = ultimate strength of FRP splines,

y_{cgs} = centroid of FRP spline.

the moment capacity of the spline is calculated to be 14.15-kN-m.

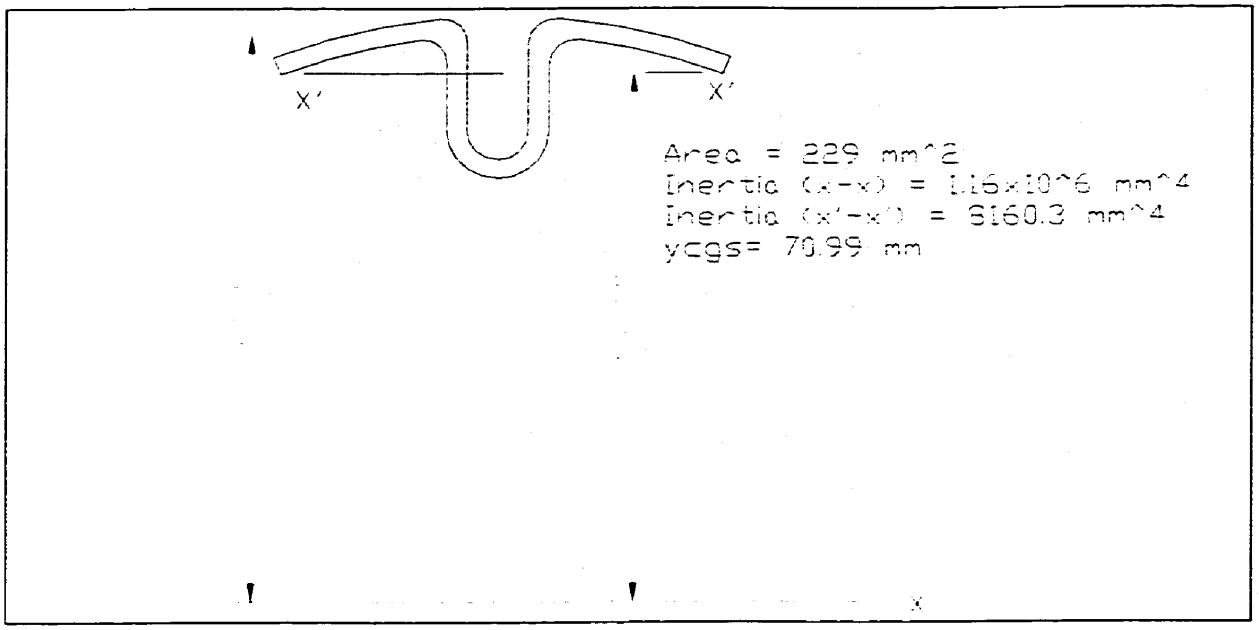

Figure A.1 – Centroid of Spline

APPENDIX B

MANUFACTURERS DATA FOR EPOXY RESIN (GOUGEN, 1999)

Test specimens cured at room temperature for two weeks, unless otherwise noted. Typical values; not to be construed as specifications. Neat epoxy specimens *(i.e.*, containing no fillers or fiber reinforcements) were used for testing.

Property	105/205	105/206	105/207	105/209
Mix Ratio by weight*	5.07:1	5.0:1	3.4:1	3.56:1
Mix Viscosity @ 72°F (cPs)	975	725	775	725
Pot Life of 100 g @ 72°F (min.)	12	21.5	26.4	51
Specific Gravity of Cured Resin	1.180	1.180	1.163	1.163
Hardness @ 1 day (Shore D)	80	80	78	70
Hardness @ 2 weeks (Shore D)	83	83	82	82
Compression Yield @ 1 day (PSI)	10,120	7,990	6,014	1,226
Compression Yield @ 2 weeks (PSI)	11,418	11,500	10,838	10,027
Tensile Strength (PSI)	7,846	7,320	7,509	7,338
Tensile Elongation (%)	3.4	4.5	3.4	3.5
Tensile Modulus (PSI)	4.08E+05	4.60E+05	4.10E+05	4.30E+05
Flexural Strength (PSI)	14,112	11,810	13,016	12,600
Flexural Modulus (PSI)	4.61E+05	4.50E+05	5.14E+05	4.28E+05
Heat Deflection Temperature (°F)	118	123	118	116
Onset of Tg by DSC (°F)	129	126	123	121
Ultimate Tg by DSC (°F)	142	139	137	134
Izod Impact, notched (ft-lbs/in)	0.93	0.54	1.27	1.10

Typical values; not to be construed as specifications. Neat epoxy specimens, *i.e.*, containing no fillers or fiber reinforcements, were used for testing.

APPENDIX C

ANSYS INPUT FILE FOR CONTROL POLE

```
/BATCH
/com,ansys, revision 5.4
/prep7
/show,x11
/pbc,f,1
/pbc,u,1
/nerr,5,100000000
/pnum,kp,0
/pnum,line,1
/pnum,area,1
/pnum,volume,1
/view,1,3500,6000,5000
/Repair of Wood Pole
!
!-----------------------------------------------------------------
!
!       CONSTANTS
!
!
!       POLE PROPERTIES
!
top_dia=131          !DIAMETER AT TOP OF POLE MM
bot_dia=154          !DIAMETER AT GROUND LINE OF POLE MM
top=2438             !HEIGHT OF POLE ABOVE GROUNDLINE
load=10000           !APPLIED LOAD AT TOP OF POLE IN MM
!
!
!       WOOD POLE MATERIAL PROPERTIES
!
!
et,1,95
!
mp,ex,1,8400
mp,ey,1,8400
mp,ez,1,8400
mp,dens,1,6.25E-7
!
!
!       GENERATE CENTER LINES FOR SECTIONS
```

```
!
!
k,1,0,0,0
k,2,0,0,top

!
l,1,2
!
k,3,bot_dia/2,0,0
k,4,top_dia/2,0,top
l,3,4
arotat,2,,,,,,1,2
al,7,9,11,13
al,6,12,10,8
va,1,2,3,4,5,6
!
lsel,all
vsel,all
vmesh,all
vsel,all
!
nsel,s,loc,z,0,0
d,all,all,0,0
nsel,all
esel,all
!nsel,s,loc,z,2794
ksel,s,kp,,4,10,2
fk,all,fy,-LOAD/4
nsel,all
esel,all
wsort,all,0,max
cpintf,all
save
!
save
/solu
antype,static
nlgeom,on
autots,on
sstif,on
nsubst,20,500,20,on
nropt,auto
neqit,30
cnvtol,f,,0.01,,1
cnvtol,u,,0.04,,0
nsel,all
```

```
time,2800
allsel, all
outres,,all
lswrite,1
lssolve,1
solve
save
finish
/solu
```

APPENDIX D

ANSYS INPUT FILE FOR REPAIRED POLES

```
/BATCH
/com,ansys, revision 5.4
/prep7
/show,x11
/pbc,f,1
/pbc,u,1
/nerr,5,100000000
/pnum,kp,0
/pnum,line,1
/pnum,area,1
/pnum,volume,1
/view,1,3500,6000,5000
/Repair of Wood Pole
!
!-----------------------------------------------------------------
!
!       CONSTANTS
!
!
tool_rad=6
top_dia=131
bot_dia=149
mid_dia=145
plug=254
top=2438.4
bott=600
num_ribs=4
rib=660
Spl_Dpth=19.5
Spl_Wdth=12.7
Spl_Rad=152.4
gap=3
over=(rib-plug)/2-gap
t=3
!
!
!       GENERATE CENTER LINES FOR SECTIONS
!
!
```

```
k,1,0,0,0
k,2,0,0,bott-over
k,3,0,0,bott
k,4,0,0,bott+gap
k,5,0,0,bott+plug+gap
k,6,0,0,bott+plug+2*gap
k,7,0,0,bott+plug+2*gap+over
k,8,0,0,top
!
l,1,2
l,2,3
l,3,4
l,4,5
l,5,6
l,6,7
l,7,8
!
!
!       GENERATE TAPERED TOP & BOTTOM PLUG
!
!
k,9,bot_dia/2,0,0
k,10,mid_dia/2,0,bott-over
k,11,mid_dia/2,0,bott+plug+2*gap+over
k,12,top_dia/2,0,top
l,9,10
arotat,8,,,,,,1,2
al,12,14,16,18
al,13,15,17,19
va,1,2,3,4,5,6
l,11,12
arotat,20,,,,,,7,8
al,29,27,25,31
al,26,28,30,24
!
va,7,8,9,10,11,12
!
!       GENERATE CONSTANT CROSS SECTION PLUG SECTION
!
vdrag,6,,,,,,2
vdrag,12,,,,,,6
vdrag,17,,,,,,3
vdrag,27,,,,,,4
vdrag,32,,,,,,5
!
!       GENERATE RIBS
```

```
!
k,45,mid_dia/2,Spl_Wdth/2,-bott
k,46,mid_dia/2,-Spl_Wdth/2,-bott
k,47,mid_dia/2-Spl_Dpth,-tool_rad/2,-bott
k,48,mid_dia/2-Spl_Dpth,tool_rad/2,-bott
!circle,47,tool_rad/2,48
l,47,48
l,45,46
l,45,48
l,46,47
al,72,74,73,75
k,53,mid_dia/2,Spl_Wdth/2,-bott-rib
l,45,53
vdrag,38,,,,,,76
k,59,mid_dia/2,0,-bott-rib/2
vsel,s,volu,,8,,0
local,11,1,0,0,0,0,0,0
vgen,num_ribs,all,,,,360/num_ribs,,,1
local,11,0,0,0,0,0,0,0
*do,vo,8,8+num_ribs-1,1
        vsel,a,volu,,vo,,0
*enddo
vgen,2,all,,,,,2*bott+plug+2*gap+over
vsel,all
vdele,8,8+num_ribs-1,,1
*do,v,8+num_ribs,8+2*num_ribs-1,1
        *do,jon,3,8,1
                vsbv,jon,v,,delete,keep
        *enddo
*enddo
vdele,8+num_ribs,8+2*num_ribs-1,,1
!
!
numstr,line,700
numstr,area,700
circle,2,mid_dia/2-Spl_Dpth+1,1
al,700,701,702,703
vdrag,700,,,,,,2
vdrag,705,,,,,,3
vdrag,710,,,,,,4
vdrag,715,,,,,,5
vdrag,720,,,,,,6
vsbv,4,8,,delete,keep
vsbv,6,9,,delete,keep
vsbv,7,10,,delete,keep
vsbv,3,11,,delete,keep
```

```
vsbv,5,12,,delete,keep
!
vdele,8,12,,1
numstr,line,950
l,224,213
l,213,218
l,218,221
l,221,224
al,950,951,952,953
l,226,212
l,212,216
l,216,220
l,220,226
al,954,955,956,957
aovlap,700,701
al,772,966,962
al,746,965,958
al,959,968,756
al,969,961,762
vdrag,700,,,,,,2
vdrag,701,,,,,,2
vdrag,702,,,,,,2
vdrag,703,,,,,,2
vdrag,704,,,,,,2
vdrag,705,,,,,,2
vdrag,706,,,,,,2
vdrag,707,,,,,,2
vdrag,708,,,,,,2
!
vdrag,712,,,,,,3
vdrag,826,,,,,,3
vdrag,849,,,,,,3
vdrag,836,,,,,,3
vdrag,845,,,,,,3
vdrag,721,,,,,,3
vdrag,716,,,,,,3
vdrag,831,,,,,,3
vdrag,841,,,,,,3
!
vdrag,853,,,,,,4
vdrag,885,,,,,,4
vdrag,880,,,,,,4
vdrag,876,,,,,,4
vdrag,871,,,,,,4
vdrag,867,,,,,,4
vdrag,862,,,,,,4
```

```
vdrag,858,,,,,,4
vdrag,890,,,,,,4
!
vdrag,926,,,,,,5
vdrag,921,,,,,,5
vdrag,917,,,,,,5
vdrag,912,,,,,,5
vdrag,908,,,,,,5
vdrag,903,,,,,,5
vdrag,899,,,,,,5
vdrag,894,,,,,,5
vdrag,931,,,,,,5
!
vdrag,967,,,,,,6
vdrag,936,,,,,,6
vdrag,940,,,,,,6
vdrag,945,,,,,,6
vdrag,949,,,,,,6
vdrag,954,,,,,,6
vdrag,958,,,,,,6
vdrag,963,,,,,,6
vdrag,972,,,,,,6
!
vdele,1,2,1,1

l,38,139
l,39,165
l,40,189
l,46,48
al,768,953,761,1286
al,760,956,752,1289
al,771,954,744,1287
al,951,745,1288,755
asel,s,loc,z,bott-over,bott-over
!
!csys,1
!vdrag,all,,,,,,1
vext,all,,,0,0,-bott+over,bot_dia/mid_dia
!
!csys,0
!
asel,all
lsel,all
a,37,113,329,77
a,161,185,55,52
a,136,186,195,193
```

```
a,170,78,135,27
asel,s,loc,z,bott+plug+2*gap+over,bott+plug+2*gap+over
vext,all,,,0,0,top-(bott+plug+2*gap+over),top_dia/mid_dia
asel,all
vsel,all
!
lsel,s,length,,0,spl_dpth*bot_dia/mid_dia
lesize,all,,,1
lsel,all
lsel,s,length,,spl_dpth*bot_dia/mid_dia,top
lesize,all,,,4
lsel,all
!lsel,s,length,,bott-over,bott-over
!lesize,all,,,6
!lsel,all
!
vsel,all
et,1,99,,0,0,0,1,3
keyopt,1,11,2
r,1,2,0
rmore,
rmore,1,90,1.5,1,90,1.5
!
r,2,2,0
rmore,
rmore,1,0,1.5,1,0,1.5
!
r,3,4,0
rmore,
rmore,1,90,1.5,1,90,1.5
rmore,1,0,1.5,1,0,1.5
!
et,2,95
!
et,3,95
!
mp,ex,1,11400
mp,ey,1,11400
mp,ez,1,30570
mp,gxy,1,11600
mp,gyz,1,11600
mp,gxy,1,11600
mp,prxy,1,.3
mp,pryz,1,.3
mp,prxz,1,.3
mp,nuxy,1,.02
```

```
mp,nuyz,1,.02
mp,nuxz,1,.02
!
mp,ex,2,8400
mp,ey,2,8400
mp,ez,2,8400
mp,dens,2,6.25e-7
!
mp,ex,3,100
mp,ey,3,100
mp,ez,3,100
mp,dens,3,625e-16
!
vsel,s,loc,z,bott+plug+2*gap,bott+plug+2*gap
vsel,a,loc,z,bott+gap,bott+gap
VATT,3,1,3,0
vsel,all
vsel,u,loc,z,bott+plug+2*gap,bott+plug+2*gap
vsel,u,loc,z,bott+gap,bott+gap
vatt,2,1,2,0
!
mshkey,1
mshape,0,3d
vsel,all
asel,all
vmesh,all
vsel,all
!
asel,s,area,,35
asel,a,area,,34
asel,a,area,,24
asel,a,area,,28
asel,a,area,,738
asel,a,area,,833
asel,a,area,,13
asel,a,area,,16
asel,a,area,,38
asel,a,area,,15
asel,a,area,,754
asel,a,area,,881
asel,a,area,,764
asel,a,area,,762
asel,a,area,,857
asel,a,area,,748
asel,a,area,,749
asel,a,area,,864
```

asel,a,area,,758
asel,a,area,,759
asel,a,area,,873
asel,a,area,,753
asel,a,area,,32
asel,a,area,,25
asel,a,area,,19
asel,a,area,,20
asel,a,area,,773
asel,a,area,,914
asel,a,area,,769
asel,a,area,,768
asel,a,area,,905
asel,a,area,,784
asel,a,area,,782
asel,a,area,,895
asel,a,area,,779
asel,a,area,,776
asel,a,area,,925
asel,a,area,,774
asel,a,area,,17
asel,a,area,,18
asel,a,area,,23
asel,a,area,,30
asel,a,area,,798
asel,a,area,,959
asel,a,area,,804
asel,a,area,,793
asel,a,area,,951
asel,a,area,,799
asel,a,area,,789
asel,a,area,,942
asel,a,area,,794
asel,a,area,,802
asel,a,area,,935
asel,a,area,,788
asel,a,area,,27
asel,a,area,,29
asel,a,area,,39
asel,a,area,,33
asel,a,area,,818
asel,a,area,,987
asel,a,area,,823
asel,a,area,,807
asel,a,area,,980
asel,a,area,,819

```
asel,a,area,,812
asel,a,area,,1004
asel,a,area,,809
asel,a,area,,824
asel,a,area,,996
asel,a,area,,744
asel,a,area,,739
asel,a,area,,728
asel,a,area,,741
asel,a,area,,827
asel,a,area,,731
asel,a,area,,725
asel,a,area,,734
asel,a,area,,729
asel,a,area,,718
asel,a,area,,814
aatt,1,1,1
amesh,all
!
esel,all
esel,s,elem,,1983,1986
esel,a,elem,,1903,1906
esel,a,elem,,1951
esel,a,elem,,1830
esel,a,elem,,1887,1890
esel,a,elem,,1863,1866
esel,a,elem,,1818
esel,a,elem,,2019
esel,a,elem,,1999,2006
!
esel,a,elem,,2023,2026
esel,a,elem,,1870
esel,a,elem,,1947,1950
esel,a,elem,,1831
esel,a,elem,,1967,1970
esel,a,elem,,1835,1838
esel,a,elem,,1822
esel,a,elem,,1823
esel,a,elem,,1883,1886
esel,a,elem,,1919,1922
!
esel,a,elem,,1987,1990
esel,a,elem,,1931,1934
esel,a,elem,,1815
esel,a,elem,,1826
esel,a,elem,,1851,1854
```

```
esel,a,elem,,1847,1850
esel,a,elem,,1827
esel,a,elem,,1834
esel,a,elem,,1971,1974
esel,a,elem,,2035,2038
!
esel,a,elem,,2015,2018
esel,a,elem,,1871,1874
esel,a,elem,,1819
esel,a,elem,,2022
esel,a,elem,,1899,1902
esel,a,elem,,1955,1958
esel,a,elem,,1867
esel,a,elem,,1954
esel,a,elem,,1915,1918
esel,a,elem,,1935,1938
emodif,all,real,3
!
!
numstr,area,4000
a,37,113,114,41
a,134,114,34,127
a,127,34,117,119
a,119,117,29,42
a,29,42,38,139
a,52,55,56,54
a,56,54,33,69
a,33,69,62,25
a,62,25,32,49
a,32,49,48,46
asel,all
asel,s,area,,4000,4004
arsym,y,all
!
asel,all
asel,s,area,,4005,4009
!
arsym,x,all
lsel,all
asel,all
asel,s,area,,4000,4019
!
lsel,s,length,,0,spl_dpth*bot_dia/mid_dia
lesize,all,,,1
lsel,all
lsel,s,length,,spl_dpth*bot_dia/mid_dia,top
```

```
lesize,all,,,4
lsel,all
!
aatt,1,2,1
amesh,all
!
esel,all
esel,s,elem,,1975,1982
esel,a,elem,,1828,1829
esel,a,elem,,1855,1862
esel,a,elem,,1816,1817
esel,a,elem,,1991,1998
!
esel,a,elem,,1939,1946
esel,a,elem,,1868,1869
esel,a,elem,,1959,1966
esel,a,elem,,1820,1821
esel,a,elem,,1875,1882
!
esel,a,elem,,1907,1914
esel,a,elem,,1952,1953
esel,a,elem,,1891,1898
esel,a,elem,,2020,2021
esel,a,elem,,2007,2014
!
esel,a,elem,,2027,2034
esel,a,elem,,1832,1833
esel,a,elem,,1839,1846
esel,a,elem,,1824,1825
esel,a,elem,,1923,1930
emodif,all,real,2
!
vsel,s,loc,z,bott+gap,bott
vsel,a,loc,z,bott+plug+gap,bott+plug+2*gap
vclear,all
vdele,all
vsel,all
nsel,s,loc,z,0,0
d,all,all,0,0
nsel,all
esel,all
ksel,s,kp,,356,366,2
ksel,a,kp,,369,370,1
fk,all,fy,-1250
ksel,all
nsel,all
```

```
esel,all
wsort,all,0,max
cpintf,all
save
!
save
/solu
antype,static
nlgeom,on
autots,on
sstif,on
nsubst,20,500,20,on
nropt,auto
neqit,30
cnvtol,f,,0.01,,1
cnvtol,u,,0.04,,0
nsel,all
time,2800
allsel, all
outres,,all
lswrite,1
lssolve,1
save
finish
/solu
```

APPENDIX E

THEORITICAL STRESS IN SPLINES

The spline system used in the experimental program, and shown in Figure E.1 has the following physical properties;

Area:	916.2179 mm
Centroid:	X: 0.0000, Y: 0.0000
Moments of inertia:	X: 2.41×10^6 mm^4
	Y: 2.41×10^6 mm^4

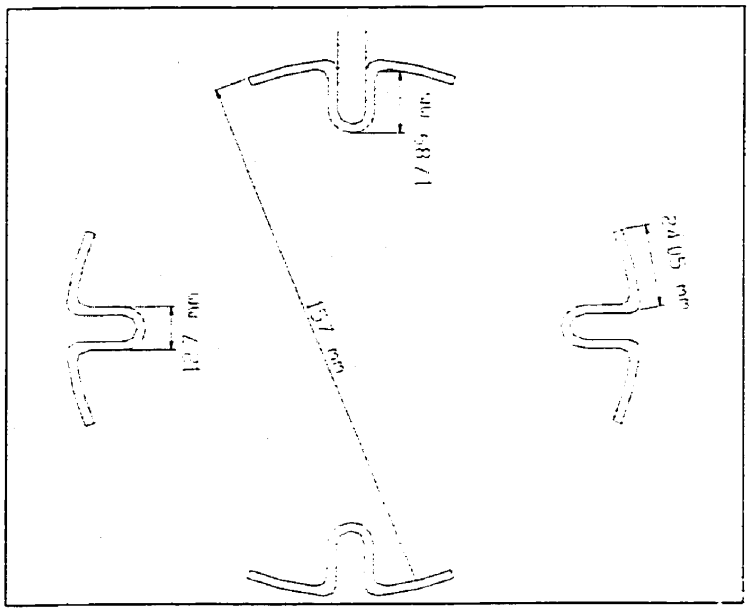

Figure E.1 – Symmetric FRP spline system.

Using traditional stress analysis, an applied load of 6500-N, and a distance from the load of 1830-mm the maximum stress in the splines shown in Figure E.1 is 388-MPa.

APPENDIX F

DESIGN EXAMPLE

The pole used in this example has dimensions similar to the poles used in the experimental program. The pole is an air-dried jack-pine pole, and using CSA-015-90, the maximum horizontal load for this class 5 pole is;

$$P_{applied} = 8500 \text{ N}$$

From equation 5.5 the required area of FRP can be determined using,

$$A_{FRP} = \frac{MOR}{\sigma_{FRP}} \cdot \frac{C^3}{64 \cdot \pi^2 \cdot d} \qquad \textit{Equation D.1}$$

with:

L = 1838 mm;

MOR = 44 Mpa;

σ_{FRP} = 610 MPa (from material tests)

C = 465 mm;

d = 70 mm

Which yields;

$$A_{FRP} = 164 \text{ mm}^2.$$

The splines used in the experimental program had an area of 229 mm^2. It would be impossible to obtain an area of 164 mm^2 as one layer of FRP has a cross-sectional area of 114.5 mm^2, so two layers were used with an area of 229 mm^2.

Using Equation 5.10, the length of the spline can be determined;

$$l_{spline} = \frac{P_{ult} \cdot h_{load}}{\tau_{wood} \cdot (2 \cdot b + w) \cdot d_{\phi}} + S_H \qquad \textit{Equation D.2}$$

with;

d_ϕ = 145 mm

b = 19 mm

w = 13 mm

Plug Height = 250 mm

τ_{wood} = 5.17 MPa. (Alden, 1997)

Which gives;

L_{spline} = 660 mm

The length of the spline used in the experimental program was 660 mm.

The confinement wrap was designed using;

$$t_{jacket} = \frac{8 \cdot A_{FRP}}{C} \qquad \textit{Equation D.3}$$

t_{jacket} = 4 mm

The thickness of the jacket was 4 mm.

The length of the shear transfer layer was determined using Equation ;

$$l_{shear} = \frac{P_{app}}{\tau_{wood} \cdot w} \qquad \textit{Equation D.4}$$

$$l_{shear} = 268 \text{ mm}$$

The length of the shear transfer layer used in the experimental program was 254 mm.